Deciphering X chromosome architecture during mouse preimplantation development

Noémie Ranisavljevic

NNT : 2017SACLS546

Deciphering X chromosome architecture during mouse preimplantation development

Thèse de doctorat de l'Université Paris-Saclay

préparée à Université Paris Sud

École doctorale N° 577 Structure et dynamique des systèmes vivants

Spécialité de doctorat : Sciences de la vie et de la santé

Thèse présentée et soutenue à l'Institut Curie - Paris, le 14 décembre 2017, par

Noémie Ranisavljevic

Composition du Jury :

Pr. Pierre Capy	Professeur à l'Université Paris Saclay	Président
Dr. Nathalie Beaujean	Directrice de recherche à l'Institut SBRI	Rapportrice
Pr. Wouter de Laat	Professeur à l'Université de Utrecht	Rapporteur
Dr. Bernard de Massy	Directeur de recherche à l'IGH	Examinateur
Dr. Daan Noordermeer	Directeur de recherche à l'I2BC	Examinateur
Pr. Edith Heard	Professeure au Collège de France	Directrice de thèse
Pr. Catherine Patrat	Professeure à l'Université Paris VII	Directrice de thèse

Nothing in life is to be feared, it is only to be understood.
Now is the time to understand more, so that we may fear less.

Marie Curie

TABLE OF CONTENTS

Summary

3D folding of the genome is thought to play an important role in gene regulation. Recently, a new era in our understanding of genome organization has been opened up thanks to the plethora of new techniques enabling interactions between loci to be captured and sequenced in depth. Several layers of chromosome organization have been identified. In particular topologically associating domains (TADs) have been uncovered as a level of folding at the megabase scale. TADs represent preferential cis-interactions within domains across chromosomes and are thought to sometimes operate as regulatory units in coordinating gene expression. Although TADs are largely constant during cellular differentiation and are conserved between man and mouse, drastic changes in conformation can occur in some biological processes such as X-chromosome inactivation (XCI). XCI achieves dosage compensation in mammalian females, be rendering one X chromosome silent. The conformation of the inactive X is strikingly different from its active counterpart: with a global loss of local structure and formation of two large domains. The aim of my PhD was to explore genome architecture - and more specifically X-chromosome structure after fertilization - when the newly formed embryo reprograms its chromatin toward totipotency, and activates its own genome. In mouse, this structural and functional reorganization coincides with the onset of imprinted XCI in female embryos. Using two complementary techniques, 3D DNA FISH with super resolution microscopy and allele-specific, single-cell HiC, I examined the dynamics of genome reorganization in mouse pre-implantation embryos during and after genome activation. I also characterized the structural changes of the paternal X chromosome while it is inactivated. This study describes the conformation dynamics of the genome in the early embryo and in particular of the X chromosome as it undergoes XCI, thus contributing to our understanding of the intricate interplay between structure and function at the onset of development.

Lay summary

How is the nucleus organized is a longstanding question. Recently, new molecular techniques have demonstrated that the genome is partitioned into domains of preferential interactions termed 'Topologically Associating Domains'. The TADs are well preserved through evolution and differentiation; they may play a crucial role in enabling coordinated gene regulation. What about during early development, when the embryo needs to reprogram its nucleus to become totipotent and to activate its own genome? Shortly after fertilization, the X chromosome also initiates X inactivation in female to achieve dosage compensation. X chromosome partitioning is strikingly different in its active or inactive form in differentiated cells. Thanks to molecular biology techniques and high-resolution microscopy, I describe here the dynamics of genome organization, and especially the X chromosome structure, during mouse pre implantation embryo.

Résumé en français

La structure tridimensionnelle du génome semble avoir un rôle important dans la régulation de l'expression des gènes. Récemment, l'essor de nouvelles et nombreuses techniques permettant de capturer et séquencer les interactions entre différentes régions du génome (voire du génome entier) a révolutionné notre vision de l'organisation du génome. Plusieurs niveaux d'organisation ont été décrits et plus particulièrement les TADs (Topologically Associating Domains) à l'échelle du mégabase. Ces derniers représentent des domaines d'interactions préférentielles au sein du chromosome à l'échelle du mégabase et pourraient opérer en tant qu'unité régulatrice de l'expression des gènes contenus dans ces domaines. Bien qu'ils soient très conservés, par exemple entre l'homme et la souris, mais également au cours de la différentiation, des modifications majeures de conformation ont lieu lors de certains évènements tels que l'inactivation du chromosome X. Ce phénomène épigénétique permet la compensation de dose chez les femelles mammifères, où l'un des deux chromosomes X est rendu silencieux. La structure du X inactif est extrêmement différente de celle du X actif avec une perte globale de la structure locale en TADs et la formation de deux larges domaines, appelés mégadomaines. L'objectif de ma thèse a été d'explorer l'architecture du génome après la fécondation, et plus particulièrement la structure du chromosome X, au moment où l'embryon nouvellement formé reprogramme sa chromatine, devient totipotent et active son propre génome. Chez la souris, cette réorganisation structurelle et fonctionnelle coïncide avec l'inactivation soumise à l'empreinte du chromosome X chez les femelles. Grâce à deux techniques complémentaires, le DNA FISH 3D avec imagerie à haute résolution et le HiC sur cellule unique et allèle-spécifique, j'ai décrit la dynamique de la ré-organisation du génome en embryon pré implantatoire, à cette période d'activation du génome embryonnaire. Par ailleurs, j'ai caractérisé les changements de structure du chromosome X paternel au cours de son inactivation. Cette étude détaille la dynamique spatio-temporelle du génome, et plus spécifiquement du chromosome X au cours de son inactivation, dans l'embryon précoce et élargit ainsi notre compréhension du lien entre la structure et la régulation transcriptionnelle au cours des premières étapes du développement embryonnaire suivant la fécondation.

Résumé vulgarisé grand public

L'organisation du noyau est depuis longtemps une question brûlante. Récemment, des techniques moléculaires couplées au séquençage ont permis de décrire une compartimentalisation du génome en domaines d'interactions préférentielles ("Topologically Associating Domains", TADs). Ces TADs, conservés au cours de l'évolution et de la différenciation, semblent avoir un rôle essentiel dans la régulation de l'expression des gènes. Qu'en est-il au cours du développement précoce, moment clé où l'embryon reprogramme son noyau pour devenir totipotent et active son propre génome? Cette période est également marquée par l'inactivation de l'un des chromosomes X dans l'embryon femelle. Or l'architecture du X inactif est différente de celle du X actif dans les cellules somatiques. Par des techniques moléculaires et d'imagerie à haute résolution, je décris ici la dynamique de l'organisation du génome, et du chromosome X en particulier, au cours du développement pré implantatoire de la souris.

Acknowledgments

I am incredibly grateful to Nathalie Beaujean and Wouter de Laat for agreeing to examine my thesis.

Besides, I would like to express my very great appreciation to each member of my jury: Claire Vourc'h, Bernard de Massy, Daan Noordermeer, Pierre Capy. I would like to offer my special thanks to my *directrices de thèse* Edith Heard and Catherine Patrat for their guidance during my PhD.

Un immense merci à Katia, pour ta patience, ton dévouement et ton soutien, dans la rédaction de cette thèse mais aussi tout au long de ces trois années. Si, si, "delighted" était un mot juste. :) Merci de m'avoir coachée malgré tes a priori sur les MD ;)

Thank you Takashi for your help in setting up scHiC protocol for embryos (with its difficult beginnings!!) and for all the work achieved since then! Thank you Csilla for your precious analysis, and for your time in the final rush to prepare the last results for this thesis! Thank you Peter Fraser for your collaboration: it was a great opportunity to join this project!

Merci Tristan pour toutes ces heures passées à l'OMX, pour ta patience quand le signal était vraiment faiblard, pour ton emploi du temps que tu étirais pour tout faire passer dans les temps.

Merci Maud pour tes cours accélérés de dissociation de single cells et tes nombreux conseils en tant qu'experte Cast! Merci Julian pour ta compagnie à l'animalerie et pour tes bons soins pour cette colonie de Cast tatillon.

Merci aux collègues et amis du "corner of the lab" pour les discussions (scientifiques et moins scientifiques!): Rafael pour ta disponibilité et ton amitié infaillibles, Jan pour tes conseils pleins de sagesse et Chris qui sait t'inviter dans notre coin de labo pour notre plus grand plaisir, avec toujours de quoi régaler nos estomacs et de quoi enrichir notre vocabulaire!

Merci Lucile pour ton soutien fidèle, même aux pires heures de la nuit!

Merci Aurélie pour tes coups de pouce de pro du R et autres trucs et astuces de bioinfos. Merci Laurène pour ta disponibilité malgré tes "tout doux listes" à rallonge!

Merci Julie pour tes conseils, notamment pour les DNA FISH à la dérive.

Thanks Joke for suggesting this 3C JC: it helped me a lot! (and thanks to all 3C JC members!!! I've learned a lot with you!!)

Merci à tout le Heard lab pour la place que vous m'avez faite dans l'équipe, pour la gentillesse et l'attention de chacun. Merci à l'unité de BDD pour ce cadre de travail plaisant dont j'ai profité pendant 3 ans.

Merci à l'équipe d'animalerie pour votre expérience et votre professionalisme! Merci à l'équipe imagerie, tout particulièrement à Olivier Leroy pour tes macros à toute épreuve!

Merci à la Fondation de la recherche médicale de m'avoir financée pendant 3 ans.

Merci aux grands-mères nounous qui ont assuré le quotidien pendant 2 mois pour me permettre de travailler sans relâche.

Merci à Eliott et Mia d'avoir attendu patiemment que je termine de rédiger ce manuscript pour être plus disponible.

Merci à Guillaume pour ta patience et ton soutien moral et logistique, tout particulièrement lors de la dernière ligne droite de la rédaction.

Abbreviations

1C	1-cell stage (zygote)
2C	2-cell stage
4C	4-cell stage
8C	8-cell stage
16C	16-cell stage (morula)
32C	32-cell stage (early blastocyst)
64C	64-cell stage (blastocyst)
E3.5, E4.5...	Embryonic day 3.5, 4.5...
3C	Chromosome conformation capture
4C	Chromosome conformation capture-on-chip
5C	Chromosome conformation capture carbon copy
HiC	Chromosome conformation capture using High throughput sequencing
ATAC-seq	Assay for Transposase-Accessible Chromatin using sequencing
ChIPseq	Chromatin immuno-precipitation sequencing
CT	Chromosome territory
DamID	DNA adenine methyltransferase identification
DHS	DNase I hypersensitivity site
DNA	deoxyribonucleic acid
EGA	Embryonic genome activation (aka ZGA)
ESC	Embryonic stem cell
FISH	Fluorescent *in situ* hybridization
FRAP	Fluorescence recovery after photobleaching
H2AK119ub	Histone H2A Lysine 119 ubiquitinylation
H3K27ac	Histone 3 Lysine 27 acetylation
H3K27me3	Histone 3 Lysine 27 trimethylation
H3K4me3	Histone 3 Lysine 4 trimethylation
HERV-L	Human Endogenous RetroVirus-like
ICM	Inner cell mass
LAD	Lamina Associated Domain
LINE	Long Interspersed Nuclear Element
lnc RNA	long non-coding RNA
MII	metaphase II
MSCI	Meiotic Sex Chromosome Inactivation
MuERV-L	murine Endogenous RetroVirus-like
NGS	Next Generation Sequencing
NLB	Nucleolar Like Body
PN	pronucleus
PRC1	Polycomb repressive complex 1

PRC2	Polycomb repressive complex 2
RNA	Ribonucleic acid
RNA pol II	RNA-polymerase II
RNA seq	RNA-sequencing
RT PCR	reverse transcription polymerase chain reaction
scHiC	single cell HiC
SINE	Short Interspersed Nuclear Element
SNP	Single nucleotide polymorphism
TAD	Topologically Associating Domain
TE	Trophectoderm
TSS	Transcription Start Site
UCE	Ultra conserved element
Xa	active X-chromosome
Xi	inactive X-chromosome
XCI	X-chromosome inactivation
Xic	X-chromosome inactivation center
Xist	X-inactive specific transcript
Xm	maternal X-chromosome
Xp	paternal X-chromosome
ZGA	Zygotic genome activation (aka EGA)

INTRODUCTION

The eukaryotic genome is tightly packed in the nucleus and its meticulous spatial organization preserves its functionality, notably gene expression regulation. Thanks to combinatorial approaches based on microscopy and more recently chromosome conformation capture techniques, the folding of the genome has been extensively explored: several hierarchical layers of structure have been described and it appears that the most relevant as regards to transcription is the scale of topologically associating domains (TADs). While TAD organization is mostly constant through cell differentiation or in between mouse and human, it is deeply reshaped during X-chromosome inactivation (XCI). This highly regulated process results in silencing of most genes of one X-chromosome in female mammals, so as to achieve dosage compensation in between sexes. On one hand, random XCI takes place in mouse as the cell differentiates and is accompanied by a global loss of TAD structure: the inactive X-chromosome is mainly composed of two large blocks - termed mega-domains - and a few TADs organized around genes that resist XCI - termed escapees. On the other hand, after fertilization, while both X are active in female mouse embryos, paternally inherited X-chromosome undergoes XCI during preimplantation development. The structure of the inactive X in early development is unknown. Are the two X-chromosomes structurally different as imprinted XCI proceeds? What are the interplay and the kinetics of spatial and transcriptional reorganizations during imprinted XCI?

To contextualize the questions of my PhD, I will first depict in this introduction the process of XCI and more specifically imprinted XCI during mouse early development; I will then describe genome organization and its interplay with gene regulation, together with the characteristic organization of the inactive X-chromosome in differentiated cells.

It is well known that TADs are lost in the mitotic chromosome and rebuilt in each daughter cell. One intriguing question is whether TADs are conserved through meiosis and fertilization. In fact, shortly after fertilization, the newly formed embryo needs to reprogram toward totipotency the parental genomes inherited from two highly differentiated gametes. This implies drastic remodeling of chromatin and nuclear architecture, which is also concomitant with the transcriptional activation of the embryonic genome. Preimplantation development is thus a dynamic period of both structural and functional reorganization. Because of the fundamental role of TADs in shaping regulatory landscapes, a compelling question concerns their establishment in early development in link with the onset of embryonic transcription. How do structure and function articulate at the onset of development? In my introduction, I will thus next outline the dynamics of genome remodeling in preimplantation embryo taking place hand in hand with embryonic genome activation.

1. X-chromosome inactivation (XCI)

1.1 X-chromosome inactivation for dosage compensation in mammals

Male XY and female XX have unbalanced karyotypes, with a very small gene-poor (<200 genes) Y-chromosome in male versus a large gene-rich (>1000) X-chromosome in female. This difference in sex chromosomes can lead to an imbalance in gene products, and thus could impair multiple functions, notably during development (Takagi and Abe, 1990, Marahrens et al., 1997, Borensztein et al., 2017). To achieve dosage compensation between the sexes, several mechanisms have evolved (as discussed below, see 1.4.1). In her observation of the expression of X-linked coat color genes in female mice, Mary Lyon noticed variable mosaic coat color in females that were heterozygous and suggested in 1961 that one of the X-chromosomes must be genetically inactivated in female cells, that this inactivation occurs during early embryonic development and affects either the paternal or the maternal X (LYON, 1961). To provide direct evidence of random X-linked gene silencing and its stable inheritance in daughter cells, Davidson and colleagues examined single cells in a female who is heterozygous for an X-linked gene with a measurable effect (DAVIDSON et al., 1963). To this end, they cultured *in vitro* fibroblasts from human female heterozygous for glucose-6-phosphate dehydrogenase (G6PDH) electrophoretic variants. Whereas the electrophoretic bands of both types are visible at the population level, subsequent isolation of single cell clones indicates that only one or other of the two variants is expressed. This early experiment outlined, at least for the G6PDH locus, gene silencing resulting from X-chromosome inactivation.

X-chromosome inactivation (XCI) is a highly regulated process involving the differential treatment of two homologous chromosomes within the same nucleus. It is a striking model for the study of epigenetic mechanisms as it concerns the stable but reversible silencing of a whole chromosome throughout the individual lifetime. It is also a classic example of facultative heterochromatin on a chromosome-wide scale.

1.2 XCI steps and mechanisms in mouse

XCI occurs in two waves during mouse development. A first wave is found during the early cleavage stages and concerns only the paternal X chromosome; this is reversed in the inner cell mass of the blastocyst, and this is followed by a second wave of random XCI in cells of epiblast (the embryonic lineage). Embryonic stem cells (ESC), that are derived from blastocysts and can be cultured and differentiated *in vitro*, are a powerful tool to dissect the

mechanisms regulating this process. XCI is often considered to occur in three steps (Disteche and Berletch, 2015): initiation, spreading and maintenance, although the events occur in a continuum (Figure 1).

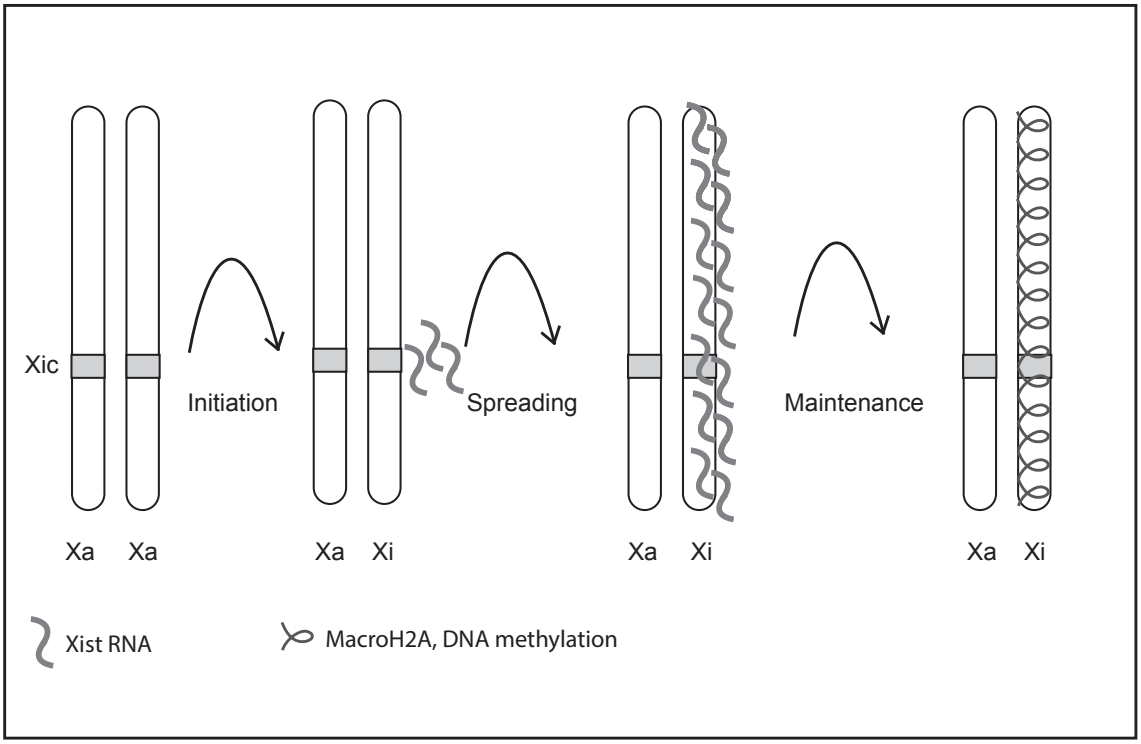

Figure 1 - Three steps of XCI

1.2.1 XCI initiation

The *X-inactivation center* triggers XCI by up-regulating long non coding *Xist* RNA from only one X-chromosome. This monoallelic expression is tightly regulated.

1.2.1.a X-inactivation center (Xic)

'One would therefore not expect all points on the X to act independently with regards to inactivation. There might be some center or centres from which the inactivation spreads.'

(Lyon, 1964)

Thanks to the analysis of multiple autosomal-X-chromosome translocations and rearrangements, in mouse and in human, the region responsible for orchestrating the initiation of X-chromosome inactivation was progressively determined (Rastan, 1983, Rastan and Robertson, 1985, Brown et al., 1991b). This "*X inactivation center*" (*Xic*) was defined as

the minimal genetic region necessary and sufficient to trigger XCI (Rastan and Brown, 1990). The exact extent of the *Xic* region and the sequences responsible for orchestrating this process are still being unraveled, but several elements from the *Xic* have been clearly established for their fundamental role in XCI (Galupa and Heard, 2015).

1.2.1.b A key molecule : Xist long non coding RNA

Within the *Xic*, the *Xist* gene (for *X-inactive specific transcript*) was discovered almost by chance in 1990 (Brown et al., 1991a, Brockdorff et al., 1991, Borsani et al., 1991) to play a key role in the initiation of XCI. This gene encodes a long non coding (lnc) RNA that is up regulated specifically in female cells and expressed from one X only (Augui et al., 2011). Its Xist lnc RNA coats the future inactive X-chromosome *in cis*, forming a cloud detectable by RNA FISH (Clemson et al., 1996) (Fluorescent In Situ Hybridization targeting RiboNucleic Acid molecules - this technique uses complementary and fluorescently labeled probes to detect and localize specific RNA molecules in fixed cells). Xist coating triggers X-chromosome silencing through a cascade of molecular changes in chromatin composition at the chromosome scale (see 1.2.2).

Xist is conserved across placental mammals, though not in marsupials and monotremes whether other mechanisms trigger dosage compensations (Grant et al., 2012, Deakin et al., 2009). It is poorly conserved at the sequence level overall, except for several unique repeats, the most conserved of which is the A-repeat (Nesterova et al., 2001) that is involved in gene silencing. Indeed mutant ESCs lacking the A-repeat recapitulate Xist coating but not transcriptional repression (Wutz et al., 2002). Recent studies identified the protein factors that bind to the Xist A-repeat and these have been shown to be involved in triggering gene repression (Pinheiro and Heard, 2017). Three main proteomic screens (Chu et al., 2015, Minajigi et al., 2015, McHugh et al., 2015) were conducted using three different techniques and converged remarkably on common factors. Among them, SPEN (for “Split-ends”, originally identified in *Drosophila* (Wiellette et al., 1999), and also known as SHARP or MINT) is an RNA-binding protein involved in transcriptional repression. It binds directly to the Xist A-repeat required for Xist-mediated gene silencing (Chu et al., 2015). It has been suggested that SPEN recruits the SMRT (Silencing Mediator for Retinoid or Thyroid-hormone receptors) deacetylase complex responsible for the deacetylation of histones via HDAC3 (Histone deacetylase 3), leading to transcriptional silencing of X-linked genes (McHugh et al., 2015). Xist also interacts with HNRNPU (Heterogeneous Nuclear RiboNucleoProtein U, also known as SAF-A), a nuclear matrix protein that is crucial for the Xist coating onto the Xi (Hasegawa et al., 2010). Discovering new players in XCI extend our understanding of Xist-mediated gene silencing.

1.2.1.c Regulators in XCI

The developmentally regulated, monoallelic and X-chromosome dosage sensitive expression of *Xist* is ensured by several cis and trans regulators. The cis-regulators are elements located in the *Xic*, which spans several hundred kilobases based on the genetic and cytogenetic studies cited earlier. Amongst the known *Xist* cis-acting regulators in mice, *Tsix* is the repressive antisense transcript which overlaps with the *Xist* gene (Lee and Lu, 1999, Lee et al., 1999). Amongst the trans-acting factors, these include negative regulators such as the pluripotency factors (Oct4, Nanog, Sox2, Rex1) that repress *Xist* both directly and indirectly (for example via *Tsix*) and positive regulators, such as RLIM/RNF12, which is an XX dosage sensitive regulator of *Xist (*Galupa and Heard, 2015*)*.

RNF12 is an E3 ubiquitin ligase and is thought to target the REX1 protein, a direct *Xist* repressor, for degradation when present at high enough doses (Gontan et al., 2012, Jonkers et al., 2009). Indeed, *Rnf12* is an X-linked gene that lies in the *Xic* region. When present at a double dose in XX ESC cells or in XY cells with a *Rnf12* transgene, it can trigger *Xist* expression. However, heterozygous mutant *Rnf12*+/- ESCs and mice, harbouring only one copy of the gene, can still trigger XCI, implying that there must be additional regulators of Xist.

1.2.2 XCI spreading

XCI is a dynamic process operating at different levels including gene silencing, chromatin modifications and chromosome reorganization.

1.2.2.a Xist RNA spreading

Once Xist is monoallelically up-regulated, how the RNA then spreads across the X-chromosome from its site of production in order to ensure subsequent silencing is still not totally clear. It has been proposed to be either a two-step process, initially targeting gene-rich regions before extending to gene-poor regions (Simon et al., 2013) or rather to exploit 3D conformation of the X-chromosome to define “Xist entry sites” (Engreitz et al., 2013). Moreover, some experiments with autosomal Xist transgenes raised the hypothesis that there might be sequences on the X-chromosome, termed “way stations”, to enhance Xist spreading and chromosome silencing (Gartler and Riggs, 1983). Indeed when *Xist* transgenes are located on autosomes, autosomal silencing is less efficient than silencing of the X-chromosome (reviewed in (Gartler and Riggs, 1983). Similarly, in earlier studies involving X/autosome translocations, where the X included the *Xic*, the translocated

autosome regions were less efficiently silenced compared to the X-chromosome segment (reviewed in (Gartler and Riggs, 1983). Mary Lyon suggested that one explanation for this could be that repetitive elements such as LINE-1 (for Long Interspersed Nuclear Elements) which are rather enriched on the X-chromosome compared to autosomes (Boyle et al., 1990, Waterston et al., 2002), may behave as "way stations" and facilitate local propagation of silencing (Lyon, 2006). Indeed, it has been proposed that Xist-mediated gene silencing in an autosomal context seems to be enhanced by the proximity and the general density of L1 (Chow et al., 2010).

1.2.2.b Gene silencing and chromatin modifications

The earliest event observed during the course of XCI is the exclusion of the transcription machinery (RNA polymerase II and its partners) from the Xist RNA-coated-X-chromosome (Chaumeil et al., 2006). This creates what appears to be a repressive compartment to which genes are progressively recruited as they are silenced: this compartment contains mainly repeat-rich regions that are the first to be silenced (Chaumeil et al., 2006, Clemson et al., 2006). Exclusion of the transcription machinery occurs before gene silencing is complete, suggesting that Xist RNA plays multiple roles, both at the nuclear organisation level and at the gene silencing and chromatin levels. In terms of chromatin changes, RNA Pol II depletion is followed by rapid loss of active marks: depletion of H3K4me3 within Xist RNA territories and deacetylation of H3K9 at least based on immunofluorescence studies (for review see (Cohen et al., 2005).

On the other hand, the repressive complexes such as the Polycomb complexes PRC1 and PRC2 are found enriched on the Xist RNA coated chromosome subsequently (Brockdorff, 2017)for review). Polycomb group proteins were first described in *Drosophila*; these chromatin remodelers act in an antagonistic manner with the Trithorax group to control spatial and temporal expression of Hox/homeotic genes during *Drosophila* embryonic development (Aranda et al., 2015) for review). The Polycomb complexes are involved in the maintenance of gene silencing in multiples organisms via alterations in chromatin structure and modifications such as monoubiquitination of histone H2A on lysine 119 (H2AK119ub, by PRC1) and trimethylation of histone H3 on lysine 27 (H3K27me3, by PRC2). The model for hierarchical PRC2 followed by PRC1 recruitment has been revisited with recent studies identifying PRC1 but not PRC2 members as Xist-interacting proteins (Chu et al., 2015, Minajigi et al., 2015). A study suggests that Xist-mediated PRC1 recruitment precedes indirect recruitment of PRC2 through Jarid2 (da Rocha et al., 2014). Indeed, Jarid2 may bind to PRC1-mediated H2AK119ub and thus represent an important intermediate between PRC2 and Xist during onset of XCI (Cooper et al., 2016). Nonetheless, Polycomb recruitment pathways and mechanisms appear to be complex and multiple.

In addition to these changes in chromatin, Xist RNA has also been reported to induce a global reorganisation of the X chromosome based on chromosome conformation capture technologies, with globally more random interactions, loss of TADs and formation of megadomains (Splinter et al., 2011, Deng et al., 2015, Giorgetti et al., 2016) (see below 2.3).

1.2.3 XCI maintenance

In order to lock XCI, a role has been proposed for several repressive modifications added to X-chromosome chromatin: for example H3K9me2 is enriched on the Xi (Heard et al., 2001), histones are globally deacetylated (Keohane et al., 1996, Chaumeil et al., 2002), histone H2A is replaced by macrohistone macro-H2A and DNA methylation is deposited on CpG islands (for review see (Gendrel and Heard, 2014)). The inactive X is gradually transformed into facultative heterochromatin and shifts to late replication timing (Takagi et al., 1982). Polycomb repressive complexes, PRC1 and PRC2 also seem to be involved in XCI maintenance: indeed, in Eed (Embryonic ectoderm development, a PRC2 member) knock-out mice, reactivation X-chromosome is observed in the extra-embryonic tissues. This suggests that Eed is implicated in the stable maintenance of imprinted X inactivation in extra-embryonic tissues (Wang et al., 2001). The role of PRC2 is less clear in the embryo-proper, as there may be redundancy with other epigenetic marks such as DNA methylation (not present in extra-embryonic tissues). Importantly, a recent study demonstrated a role for PRC1 upstream of PRC2 during random XCI (Almeida et al., 2017). The precise interplay of different Polycomb complexes, as well as other repressive epigenetic mechanisms in locking in the inactive state of the X chromosome is still being unravelled. However, once the X-chromosome is stably silenced, Xist RNA seems to be dispensable in XCI maintenance (Brown and Willard, 1994, Csankovszki et al., 1999, Wutz and Jaenisch, 2000). The inactive state of the X-chromosome is then epigenetically maintained and transmitted through cell division. However, Xist RNA together with DNA methylation and other epigenetic marks are thought to act synergistically for maintenance of the inactive state (Csankovszki et al., 2001).

Although most of the X chromosome is affected by X-chromosome inactivation, a number of genes can nevertheless **escape** from silencing (see (Carrel and Brown, 2017) for review). For instance, the shared region in between the X and the Y chromosomes - involved in X-Y pairing during meiosis (the pseudo-autosomal region, PAR) - contains genes that are present in two copies both in male and female cells: they therefore do not require dosage

compensation and are not silenced during XCI. Escapees appear to be more frequent in some species (human or marsupials) or some cell-types (mouse trophoblast giant cells). In the mouse, it was previously estimated that about 3% of X-linked genes escape XCI (Yang et al., 2010), while up to 15% of X-linked genes in human (Carrel and Willard, 2005) and most genes studied in marsupials escape to some extent (Deakin et al., 2009). More recent studies reveal higher frequencies of variable escapees in both mice and humans however (Carrel and Brown, 2017, Tukiainen et al., 2017). Some escapees are constitutive (i.e. Jarid1c) whereas some are tissue- or developmental stage-specific: facultative escapees (i.e. Mecp2, Huwe1) (Andergassen et al., 2017). These facultative escapees tend also to be variable from one individual to another. How these escapees can resist Xist RNA-mediated XCI to maintain or reinstate expression from the otherwise heterochromatic environment of the Xi is still unknown. Their distinctive spatial arrangement on the inactive X-chromosome will be discussed later (see 1.5.3 and 2.3.2).

1.3 XCI in mouse preimplantation embryos

As indicated above, XCI occurs in 2 waves during mouse development. The first wave of XCI takes place during preimplantation development and is subject to imprinting, with exclusive inactivation of the paternal X-chromosome (Xp). While the Xp is maintained inactive in the trophectoderm (TE) (Takagi and Sasaki, 1975, West et al., 1977), it is reactivated in the inner cell mass (ICM) of the blastocyst (Okamoto et al., 2004, Mak et al., 2004). This is where the second wave of inactivation occurs, in a random mode: it affects either the paternal (Xp) or maternal X (Xm) (Rastan, 1982, Takagi et al., 1982). Once inactivated, the same inactive X-chromosome (Xi) is maintained in each daughter cell, indicating epigenetic memory (Figure 2).

Imprinted XCI has been investigated at first thanks to RNA FISH and immunofluorescence studies mainly, owing to paucity of the material: only few cells per embryo are available during the early stages of development. More recently, RNA-sequencing - which gives access to the whole transcriptome even at a single-cell level (Tang et al., 2009) - unveils the dynamics of gene silencing and reactivation during preimplantation development (Borensztein et al., 2017); Borensztein, in press).

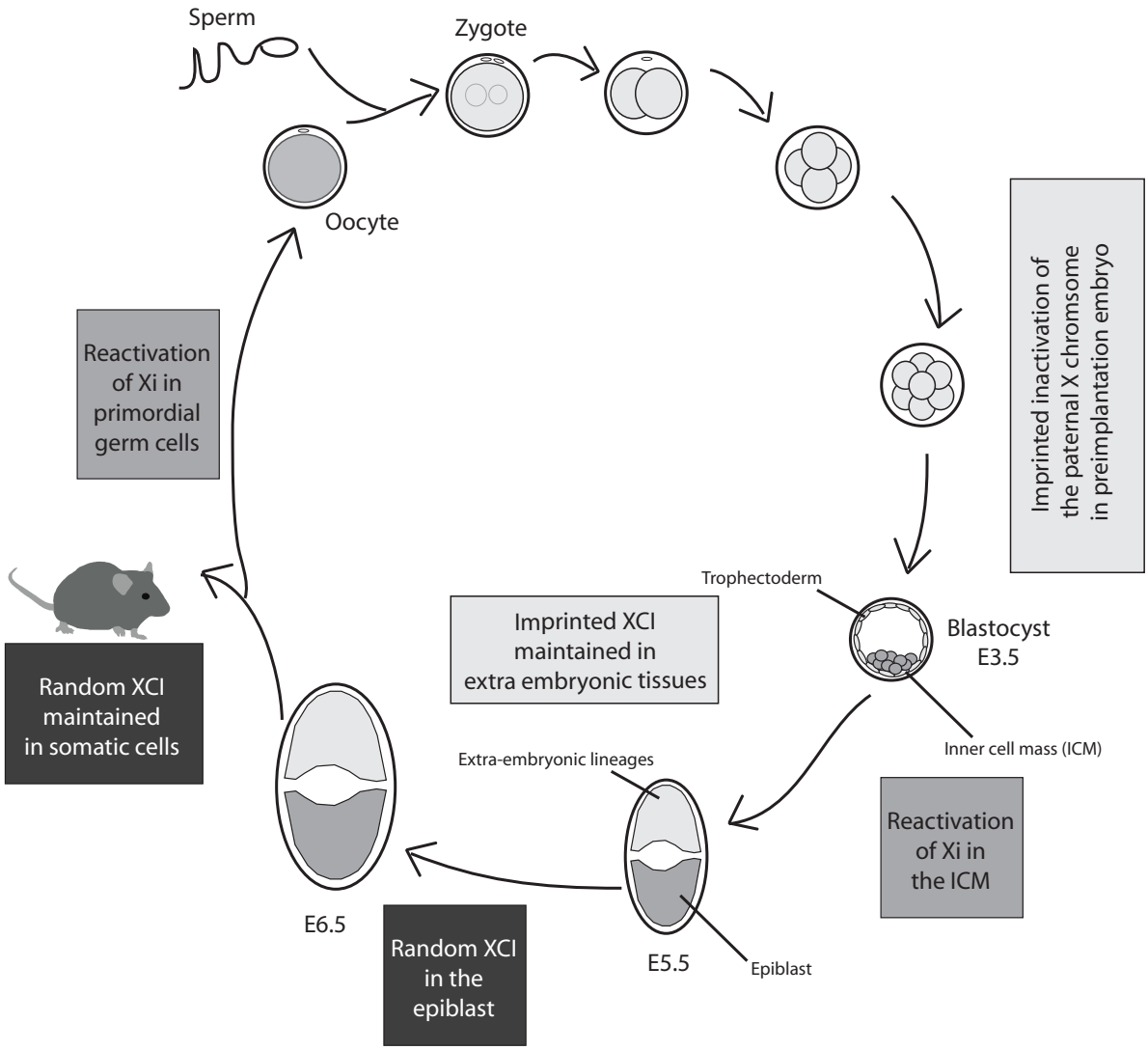

Figure 2 - Two waves of XCI in mouse (adapted from (Wutz, 2011)

1.3.1 XCI kinetics during preimplantation development

1.3.1.a Imprinted Xist expression in early embryo

Xist RNA is only expressed from the Xp, during the first wave of imprinted XCI (Kay et al., 1993). It might be detected by RNA FISH as early as the 2C stage in some blastomeres, as a punctate signal (Huynh and Lee, 2003, Okamoto et al., 2004). A single-cell RT-PCR (Reverse Transcription Polymerase Chain Reaction) analysis dissected the timing of *Xist* expression in detail and showed that *Xist* expression starts from the G2-phase of 2C stage in mouse female embryos, at the time of embryonic genome activation (Zuccotti et al., 2002). To define what determines the expression of *Xist* alleles in early embryo, *Xist* expression was studied on hybrid parthenogenetic and gynogenetic embryos (with only maternal chromosomes) and androgenetic embryos (with only paternal chromosomes). All paternal *Xist* alleles are expressed, whereas maternally inherited *Xist* is maintained silenced irrespective of the number of X-chromosomes. Thereby, *Xist* expression from the Xp is first by imprinted at cleavage stages; then at the morula stage, the imprint is somehow erased and monoallelic *Xist* expression is controlled by a counting mechanism with respect to chromosome number (Kay et al., 1994).

It was suggested that **Xp might arrive partially inactivated** after fertilization, due to a carry-over effect of meiotic sex-chromosome inactivation (MSCI) in the male germ line (Huynh and Lee, 2003, Namekawa et al., 2010). During spermatogenesis, homologous chromosomes pair to complete meiosis. The X and Y chromosomes are condensed and packed into a compact structure - the sex-body. MSCI is the epigenetic process of transcriptional silencing of the X and Y chromosomes in the male germ line and it was thus proposed that this leads to transcriptional pre-inactivation of the Xp, accounting for imprinted XCI. However, studies from our lab showed that both X chromosomes are fully active at early stage of development (zygote and 2-cell (2C) stage) - rather than being “pre-inactivated” (Okamoto et al., 2004, Patrat et al., 2009).

Furthermore, a study with mice carrying Xist transgenes located on autosomes demonstrated that MSCI is not essential for imprinted Xist expression and initiation of X-chromosome inactivation in mice (Okamoto et al., 2005). Indeed, autosomal Xist transgenes do not undergo MSCI in the male germ line as autosomes are able to pair during meiosis, but nevertheless, these autosomal Xist transgenes are still able to induce imprinted cis-activation when paternally inherited (Okamoto et al., 2005). Another hypothesis is that paternal Xist expression might be promoted in the male germ-line by the hemizygous (unpaired) state of the Xist region (Sun et al., 2015).

The basis for imprinted Xist expression is however, most likely to be due to robust repression of the maternal allele. Nuclear transplantation experiments have demonstrated that a maternal imprint is set on the Xm during oocyte growth. The maternal allele of Xist cannot be expressed and/or the maternal X chromosome are thus resistant to inactivation in the extraembryonic tissues (Tada et al., 2000). This is supported by the fact that maternally inherited autosomal Xist transgenes show no Xist expression in early embryos, unlike their paternally inherited counterparts (Okamoto et al., 2005). The exact nature of the Xist imprint is still unknown. It is believed to be independent of DNA methylation (Chiba et al., 2008) but might involve H3K9me3 maternal enrichment at the Xist promoter (Fukuda et al., 2014) and its subsequent condensation, along with a fine-tuning of Rnf12 dosage (Fukuda et al., 2016). Overexpression of Kdm4b (histone lysine demethylase) in mouse embryo causes H3K9me3 loss, chromatin decondensation and Xist expression from the maternal allele (Fukuda et al., 2016). Thus maternal Xist silencing might be maintained thanks to specific histone modifications laid down in the female germ line or zygote. Intriguingly, maternal H3K27me3 has recently been suggested to be involved in a DNA methylation-independent imprinting mechanism (Inoue et al., 2017). Whether this might account for Xist imprinting too remains to be seen.

1.3.1.b Kinetics of transcriptional inactivation and chromatin modification on Xist RNA-coated Xp in early development

Xist RNA coats in cis the X-chromosome: it accumulates on the Xp and is visualized by RNA FISH as it forms a cloud in all blastomeres from 4-cell (4C) stage, that is clearly smaller than at later stages when it resembles the Xist RNA coated X in somatic cells (Okamoto et al., 2004). The timing of onset of RNA pol II exclusion subsequent to Xist RNA-coating has been debated: Okamoto et al. suggested that RNA pol II exclusion can be seen at the 4C stage and is coincides with the Xist RNA domain in all blastomeres by the 32-cell stage (32C) (Okamoto et al., 2004). On the other hand, Namekawa et al. proposed that RNA pol II exclusion is already detectable from the 2C (Namekawa et al., 2010) and that this may correspond to the repetitive fraction of the X chromosome.

After Xist coating and RNA pol II exclusion, **Xp chromatin becomes progressively modified**, based on immunfluorescence combined wih Xist RNA FISH: at the 8C stage, loss of active marks (hypoacetylation of H3K9 and hypomethylation of H3K4) is observed and later, by the 16-cell (16C) stage, PRC2 members (Eed and Enx1/Ezh2) start accumulating over the Xist RNA domain, along with H3K27me3 mark deposited by PRC2. Accumulation of the histone H2A variant, macroH2A, also initiates by the 16C stage (Costanzi et al., 2000).

However, the heterochromatic mark H3K9 methylation appears later on, by the 32-cell stage (32C), suggesting that this mark may be independently deposited (Okamoto et al., 2004, Mak et al., 2004).

Although the early steps in imprinted and random XCI are similar, there are nevertheless some differences in the timing of chromatin modifications and gene silencing (see (Chow and Heard, 2009) for review) : random XCI appears to acquire additional epigenetic marks such as DNA methylation, which more stably lock in the inactive state. Indeed, the lack of DNA methylation on the Xp during early, imprinted XCI may facilitate the X-chromosome reactivation step which takes place in the ICM only a few cell cycles after imprinted XCI is complete. It could also explain the crucial role of Polycomb complexes in maintaining imprinted XCI (Wang et al., 2001)

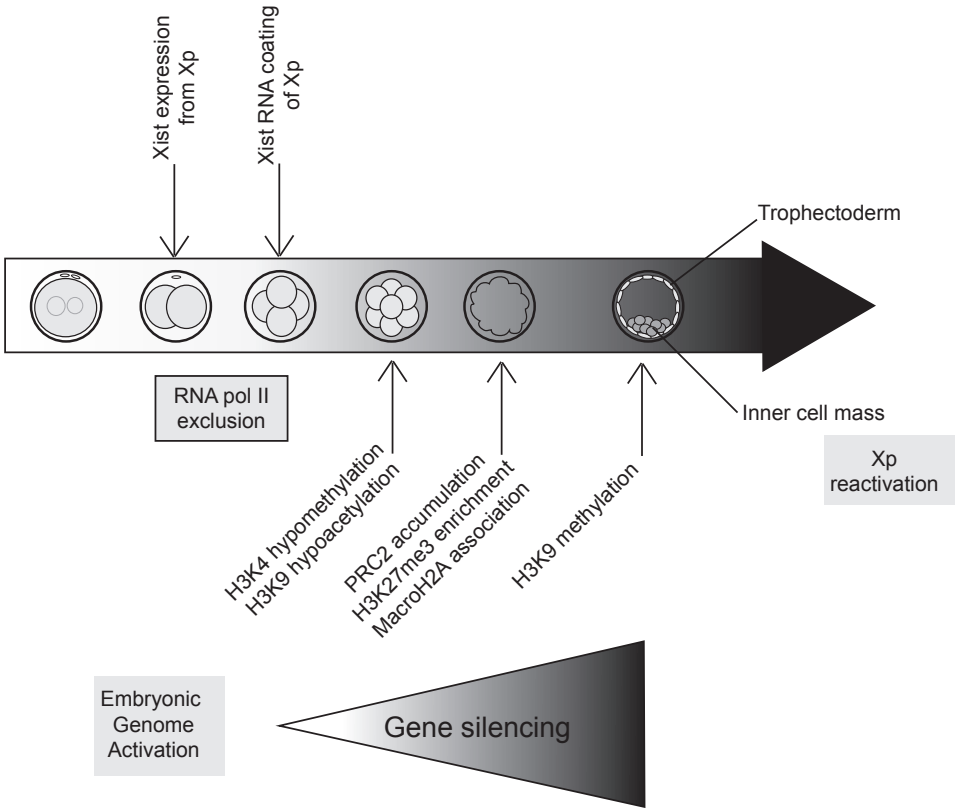

Figure 3 - Kinetics of transcription inactivation and chromatin modifications during imprinted XCI (adapted from (Okamoto et al., 2004)

1.3.2 Gene silencing during preimplantation development

Gene silencing is a progressive and sequential process. A two-step model has been proposed for imprinted XCI whereby repetitive element silencing occurs from the 2C stage in a Xist-independent manner, prior to genic silencing that requires Xist RNA (Namekawa et al.,

2010), although Okamoto and colleagues found silencing of repeats following Xist RNA coating at the 4-cell stage and the initiation of gene silencing also begins at this stage (Okamoto et al., 2004). Different kinetics of gene silencing have been described during XCI: genes can be categorized into different groups with respect to their timing of XCI (early-inactivated, mid-inactivated, late-inactivated genes or escapees) (Patrat, 2009; Borensztein, 2017). Based on single-cell RNAseq data, silencing initiates from the 4C (Deng, 2014) or 8C stage (Borensztein, 2017) and is complete by the blastocyst stage - with the exception of escapees.

1.3.2.a Is Xist mandatory?

Whether and how Xist RNA is necessary for XCI *in vivo* has been debated for a long time. Female mouse embryos carrying a paternally inherited *Xist* deletion are severely growth-retarded from E6.5 and die in early embryogenesis (Marahrens et al., 1997). In such mutants, XCI is not achieved in the extraembryonic tissues where both X-chromosomes are active whereas in the embryo proper, XCI is skewed: only the wild-type maternal X-chromosome is inactivated. Thereby, Xist RNA appears to be crucial for imprinted XCI to proceed properly in preimplantation embryo.

Past studies have suggested that *Xist* is not initially necessary for XCI in very early stages of embryonic development. In fact, it was reported that Xist RNA is dispensable for initiation of repeat silencing but essential for gene silencing during imprinted XCI (Namekawa et al., 2010). Another study reported that certain X-linked genes are efficiently silenced in early *Xist* knock-out female embryos but that their inactivation could not be maintained at day E6.5 in extraembryonic tissues (Kalantry et al., 2009). This suggested that imprinted XCI could initiate independently of Xist RNA for some genes and the authors proposed that Xist RNA was only essential to stabilize silencing on the Xp.

This report contrasted with findings, for example in ESCs where Xist is clearly essential for initiation of XCI (Wutz and Jaenisch, 2000). In a recent study, comparing RNAseq data from wild-type mouse female embryos and paternally inherited *Xist* mutant female embryos, it was found that Xist RNA is mandatory for XCI during early development. In *Xist* mutant female embryo, X-linked genes display higher expression compared to wild-type; and significant defects in dosage compensation at the blastocyst stage (Wang et al., 2016a, Borensztein et al., 2017). Moreover, in mutant female embryos lacking paternal *Xist*, the transcriptomic analysis highlighted aberrant autosomal transcription: some genes involved in extraembryonic tissue pathways such as *Sox17* are downregulated, several genes involved in pluripotency are overexpressed, and most of all *Rhox5* is highly overexpressed, which could explain in part subsequent defects in differentiation (Borensztein

et al., 2017). Thus, *Xist*-mediated accurate X-linked gene dosage-compensation is crucial for subsequent differentiation and development.

1.3.2.b Is there a silencing gradient along the X-chromosome?

The reasons why the kinetics of gene silencing differ from one gene to another are not clear. In one report, based on allele-specific semi-quantitative RT-PCR analysis of just 13 genes in hybrid female mouse embryos (morula stage), suggested that silencing along the X-chromosome was proposed to occur as a gradient of silencing, with the highest degree of silencing around the Xic, decreasing toward the telomeres with escapees more likely located in distal regions (Huynh and Lee, 2003).

However, subsequent studies did not confirm this finding, neither by RNA FISH (Patrat et al., 2009) nor by RNAseq (Deng et al., 2014, Borensztein et al., 2017). Although genes around the Xic are silenced earlier or tend to inactivate faster (Patrat et al., 2009), others are not and spreading of gene silencing is not a simple function of the distance to Xic (Patrat et al., 2009, Deng et al., 2014). Indeed, experiments that capture Xist RNA associated regions define the first regions to be associated in mESCs: Xist RNA entry sites (Engreitz et al., 2013). These Xist RNA entry sites are associated with the earliest inactivated genes (Borensztein et al., 2017). However, some late-silenced genes, or even escapees, also lie in their vicinity.

Hence, although spatial proximity to *Xist* might be involved in early silencing, this alone does not predict the silencing kinetics of X-linked genes. Whether silencing spreads locally from Xist-coated region to neighbouring sequences and whether local chromatin architecture impacts on silencing progression are still open questions.

1.3.3 Xp reactivation

Whereas Xp remains inactive in the trophectoderm (Takagi and Sasaki, 1975, West et al., 1977), it is reactivated in the ICM and undergoes random XCI from day E5.5 to E6.5 (Mohammed et al., 2017, Borensztein et al., 2017). Xp reactivation is associated with chromatin modifications. First, Xist RNA and PRC2 factors (such as Eed-Ezh2) dissociate rapidly from the inactive X. Loss of H3K27me3 occurs slightly later during X-chromosome reactivation in the ICM (Okamoto et al., 2004, Mak et al., 2004).

A recent study based on allele-specific single-cell RNA-seq, nascent RNA FISH and immunofluorescence (Borensztein, in press) has examined the kinetics of gene reactivation with respect to H3K27me3 kinetics (from published data, (Zheng et al., 2016)). This has

revealed that the timing of gene reactivation varies substantially from one gene to another. Interestingly, allele-specific single-cell RNAseq data from hybrid early embryos (Borensztein et al., 2017) was used to compare the kinetics of silencing and timing of reactivation and revealed that Xp reactivation timing does not mirror Xp-inactivation timing. On the contrary, initial enrichment in H3K27me3 anti-correlates with the speed of reactivation, - with late reactivated genes being more enriched for H3K27me3 on the paternal allele. This study also revealed that a first wave of reactivation takes place at day E3.5, before lineage segregation: a subset of genes initiates reactivation independently of Xist RNA and H3K27me3 loss; in other words, these genes are reactivated while X-chromosome is still coated by Xist RNA and enriched for H3K27me3. Many of them are “re-silenced” in the Primitive Endoderm cells. A second wave occurs at E4 in epiblast precursor cells: most X-linked genes are reactivated during this wave, and Xist RNA and H3K27me3 are lost. This second wave of Xp reactivation seems to be facilitated by an active H3K27 demethylation process, involving Utx/Kdm6a histone demethylase (Borensztein, in press). Thus, different mechanisms are involved during X-chromosome reactivation in the ICM. The factors engaged in this epigenomic reprogramming are not fully identified yet.

1.4 Differences in other species

1.4.1 Other models of dosage compensation

While in mammals XCI is the process used to achieve dosage compensation between the sexes, alternatives compensation mechanisms have evolved in different organisms including the nematode *Caernorhabditis elegans* and the fruitfly *Drosophila melanogaster* (see (Ferrari et al., 2014) for review). However, in all three models, the general mechanism is conserved: regulators of dosage compensation bind initially to nucleation sites and then spread in cis on the targeted X chromosome(s).

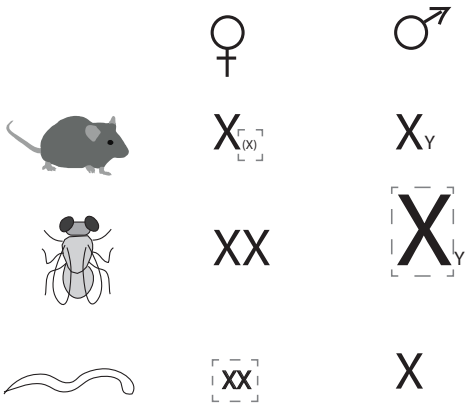

Figure 4 - Dosage compensation in between sexes in mouse, D.melanogaster and C.elegans

1.4.1.a C.elegans

In the nematode *Caenorhabditis elegans*, males harbour a single copy of chromosome X (X0 karyotype) while hermaphrodites have two X chromosomes (XX). XX individuals repress by 50% gene expression in both copies of the X (for review see (Meyer, 2010)), through a condensin-like complex named the DCC (Dosage Compensation Complex) that is loaded onto both X-chromosomes at specific sequences named the "recruitment elements on the X" (rex). It then spreads to "dependent on X" (dox) regions located in promoters of active genes to repress their expression (Csankovszki et al., 2004).

1.4.1.b Drosophila:

In the fruitfly *Drosophila melanogaster*, as in mammals, males have an heterologous pair of sex chromosomes (XY) while females have homologous sex chromosomes (XX). Compensation mechanism involves a two-fold upregulation of the male X-chromosome genes. Male specific MSL (for Male Specific Lethal) complex targets "high affinity sites" and then spreads to bind most active genes (Alekseyenko et al., 2008, Straub et al., 2008).

1.4.2 Different mechanisms of XCI in mammals

In marsupials, XCI is always imprinted with the paternal X being inactivated. Although marsupials clearly undergo the XCI process, they do not possess a Xist gene. Instead, a cis-acting noncoding RNA locus, *Rsx* (for *RNA on the silent X)*, has been proposed to fulfill the same function as *Xist* in marsupial species (Grant et al., 2012). Like Xist RNA, Rsx RNA is transcribed uniquely from the Xi, coating and Pask, 2016).

Monotremes on the other hand, harbour several copies of X chromosomes. In females, dosage compensation appears to be achieved through stochastic monoallelic expression of X-linked genes, rather than chromosome-wide silencing (Deakin et al., 2009).

1.4.3 Different kinetics for XCI in various mammal embryos

Among eutherians, the mouse embryo model is convenient and has extensively been used for XCI analysis in mammal embryo. Several studies achieved in other mammals have however reported very different kinetics and mechanisms of XCI in early embryos. As a matter of fact, imprinted XCI is not the rule in mammal embryos, *Xist* expression might not be mono-allelic and silencing is not necessarily achieved by the blastocyst stage. Below are the main findings about XCI in non-murine mammal embryos.

1.4.3.a Primate

In human and in rhesus monkey blastocysts, XCI is not imprinted: XIST is expressed from both X-chromosomes initially and the X-linked genes studied either by RNA FISH or by RT-PCR are bi-allelically expressed, both in the ICM and the TE (Okamoto et al., 2011, Tachibana et al., 2012). In human blastocysts, no specific enrichment of H3K27me3 is observed on the X-chromosome, suggesting that XCI has not properly initiated by the late blastocyst stage, despite the upregulation of XIST (Okamoto et al., 2011). However H3K27me3 enrichment is detected in some cells in Day8 blastocysts (Teklenburg et al., 2012). A recent study based on single-cell RNAseq in human embryos supports the idea that both X chromosomes are active in female human blastocysts and describes a female-specific partial down-regulation "dampening" of both X chromosomes (Petropoulos et al., 2016). Thus, in all three lineages, X-linked genes are bi-allelically expressed but are nevertheless progressively dose-compensated. This dampening of X expression occurs gradually, with a late compensation at the centromere and the distal q-arm (Petropoulos et al., 2016). The hypothesis of X dampening has recently been questioned (Moreira de Mello et al., 2017): after reanalysis of published RNAseq data from human embryos, using a different computational pipeline, the authors claim to find an increase of monoallelic X-linked gene expression from the 4C stage, indicating that XCI occurs in early human development. Timing and mechanisms involved in XCI during human early development are thus still open questions.

1.4.3.b Rabbit

In rabbit embryos, which from an evolutionary point of view are close relatives to rodents, Xist RNA expression patterns are rather different from mice. First, Xist expression starts from the 8C stage when embryonic genome activates. Xist is transiently expressed in male embryos. In females, Xist RNA accumulates first in trophectoderm cells and then in the ICM. Some cells transiently display a Xist RNA cloud on both Xs, implying that there is no imprinting: these blastomeres subsequently either reverse XCI on one X or stop proliferating. XCI hallmarks as mono-allelic expression and H3K27me3 enrichment are observed. Thus, although rabbits and mice are phylogenetically close, they have evolved very differently with respect to *Xist* regulation and the onset of XCI (Okamoto et al., 2011). In fact, taken together the data in eutherian mammals, for both imprinted and random XCI (in ESC) suggests that mice are rather the exception.

1.4.3.c Porcine

In porcine blastocyst, Xist expression is not imprinted. By the blastocyst stage, some genes likely achieve dosage compensation but XCI is not complete (Hwang et al., 2015).

1.4.3.d Bovine

In bovine embryo, Xist RNA is expressed (as assessed by RT-PCR) from 8C stage (Day 3 after fertilization) (De La Fuente et al., 1999). A study based on the allele-specific expression of the X-linked gene MAOA indicates that XCI is imprinted in the placenta with preferential silencing of the paternal X-chromosome (Xue et al., 2002). However, an RNAseq analysis on day-15 bovine female placenta indicates random XCI in bovine membranes (Chen et al., 2016c). XCI in bovine early development is not totally unraveled.

1.4.3.e Equine

Data from RNA-sequencing of placental tissue from reciprocal hybrids of horse and donkey are consistent with random XCI. XCI is very likely mediated by Xist as its expression correlates negatively with X-linked genes expression along the X-chromosome, similarly to what is well described in mouse (Wang et al., 2012).

While many features of XCI are conserved in mammals, there are marked differences in when and how X-inactivation is initiated during early embryonic development. While either X-chromosome is randomly inactivated in the somatic cells of eutherian mammals, XCI is

imprinted in marsupials and extra-embryonic tissues of most rodents. Identifying similarities and differences in X-inactivation among mammals may extend our understanding of not only the evolutionary but also the molecular aspects for the mechanism of X-inactivation.

1.5 Co-existence of an active and an inactive X in the same nucleus

During XCI, two homologous chromosomes in the same nucleus are treated very differently: these differences not only lie in the transcriptional and chromatin features of the Xi but also in the overall structure and organisation of the X-chromosome in the nucleus.

1.5.1 Barr body - The inactive X: an unusual heterochromatic structure

More than a decade before Mary Lyon suggested that X-chromosome inactivates (LYON, 1961), Murray Barr and his student Ewart George Bertram had described a well-stained body adjacent to the nucleolus and visible in female cat neurons but not in male cells (BARR and BERTRAM, 1949). They termed it “nucleolar satellite” and suggested that this second body could be derived from the “heterochromatin of the sex chromosomes” and that female cells would have a visible one as they had a double copy of the X-chromosome. It is ten years later that Ohno claimed that “only one of the two X-chromosomes in the female is observed to be heteropycnotic”: the sex chromatin is indeed formed by a single X-chromosome, the inactive X-chromosome (OHNO et al., 1959).

When Barr and Bertram described the “heterochromatin of sex chromosomes” (BARR and BERTRAM, 1949), they didn’t realize that they were already anticipating the dualist structure of the active and inactive X-chromosomes. The bright aspect of this Barr body with simple nuclear staining suggests that the inactive X-chromosome is more condensed than its active counterpart. For a long time, the hypothesis was that the series of epigenetic modifications associated with X-chromosome silencing would condense the Xi (Arney and Fisher, 2004). But is the facultative heterochromatin of the Xi simply a “more compact” organization and architecture? This assumption has been reconsidered after the X-paint experiments pursued by Bischoff et al. in 1993 on human amniotic cells (Bischoff et al., 1993). This analysis of the 3D morphology of the active and inactive Xs reveals similar volumes for both, arguing against a simple compaction of the inactive heterochromatic chromosome. Somehow, the Xa shows a more elongated structure (Bischoff et al., 1993). The 3D reconstruction of interphasic painted Xa and Xi territories corroborates this finding, and highlights differences in their shape and surface. Whereas the Xa has a flatter shape

and a larger and more irregular surface, the Xi territories have a smoother surface and rounder shape (Eils et al., 1996).

Thanks to electron microscopy, the Xi ultrastructure was more deeply analyzed (Rego et al., 2008). The facultative heterochromatin of Xi territory certainly differs from the euchromatin structure of the Xa but more surprisingly it is also distinct from constitutive heterochromatin. The Barr body is not a basic solid mass of chromatin but instead it contains tightly packed heterochromatin fibers with wide regions of interchromatin spaces between these packed structures (Rego et al., 2008). Another argument against a uniform compaction of the Barr body was obtained based on super-resolution microscopy (3D-SIM)(Smeets et al., 2014). While strong differences are found between the functional architecture of transcriptionally active chromosome territories and the Barr body, basic structural features of chromosome territory organization are conserved (Smeets et al., 2014).

Hence, diverse imaging approaches over the years have revealed the unique structure of the Xi: it is strikingly different from the Xa and seems more organized than a simple compact and condensed silent chromosome.

1.5.2 X-chromosome localisation in the nucleus

Global nuclear positioning is believed to correlate with gene activity: whereas late-replicating, gene poor regions of the genome are generally found at the nuclear periphery, early-replicating regions which are rich in active genes commonly occupy the center of the nucleus (Takizawa et al., 2008). Furthermore, heterochromatin preferentially associates with the nuclear periphery (Van de Vosse et al., 2011). Does the inactive X also have a preferential localisation in the nucleus?

Several studies reveal that the inactive X-chromosome is preferentially located at the nuclear membrane (Belmont et al., 1986, KLINGER, 1958, Rego et al., 2008) and/or at the periphery of the nucleolus (BARR and BERTRAM, 1949, Bourgeois et al., 1985, Rego et al., 2008). It has been proposed that the Xi localization to the perinucleolar compartment might maintain its silent state (BARR and BERTRAM, 1949, Zhang et al., 2007). Similarly, recruitment to the lamina through the lamin B receptor might play a role in chromosome-wide silencing by enabling Xist spreading to active genes across the X-chromosome (Chen et al., 2016a). However, recruitment to the nuclear periphery is not sufficient to trigger transcription silencing: indeed, male X and female active X-chromosomes are also seen at nuclear periphery (Borden and Manuelidis, 1988). The exact interplay between nuclear organization and XCI gene silencing is still being explored.

1.5.3 Spatial refolding of the Xi: Inner and outer layers for X-linked genes

Not only the XCI is associated with particular positioning at the scale of the nucleus, but also the inactive X is affected by a specific re-organization at the scale of the chromosome. As Xist RNA coats the X-chromosome, the lnc RNA creates a repressive compartment with RNA pol II exclusion and gene silencing (discussed above 1.2.2; (Chaumeil et al., 2006, Clemson et al., 2006). This silent Xist territory contains centromeric heterochromatin (Clemson et al., 2006) and repetitive elements that are the first to be silenced (Clemson et al., 2006, Chaumeil et al., 2006, Chow et al., 2010). In human lung fibroblasts, both in the active and inactive X, genes are reproducibly found at the periphery of the X-chromosome. In the Xi, they reproducibly border the Xist RNA territory, and this irrespective of their activity (Clemson et al., 2006).

However, unlike what is described in human differentiated somatic cells a reorganization of the X-chromosome has been observed during mESC differentiation and subsequent XCI: while transcribed genes are found at the periphery or outside the Xist RNA domain, silenced genes are relocated inside the Xist RNA domain (Chaumeil et al., 2006). Hence, escapees such as Jarid1c, are consistently placed at the outer layer of the Xi (Chaumeil et al., 2006, Deng et al., 2015). Similarly, during imprinted XCI in mouse embryo, silencing is substantially associated with the translocation of the corresponding genes into the Xist repressive compartment (Namekawa et al., 2010).

To test if translocation of X-linked genes is due to Xist RNA silencing or to chromatin modulation, gene positioning across X inactivation has been investigated in mutant ESC lacking the Xist A-repeat (that is responsible for the gene silencing function of Xist). When the A-repeat is deleted, RNA pol II is still excluded upon Xist coating and repetitive elements are still silenced, thereby creating the “repressive” Xist RNA territory. However, X-linked genes are not silenced and interestingly, they are not relocated into the silent, repetitive Xist RNA coated domain (Chaumeil et al., 2006). However, whether gene relocation into the repressive Xist compartment is a cause or a consequence of gene silencing still remains unsolved.

1.5.4 Role of repetitive elements in Xi chromosome folding

As discussed above (see 1.2.2) LINE-1 elements have been proposed to play a role in Xist RNA spreading, as “way stations” across X-chromosome (Lyon, 2006). Presence of LINE (both at the region scale (in other words, LINE density) and at the locus scale (in other

words, LINE proximity)) might determine the capacity of genes to relocate into the silent repetitive Xist RNA domain (Chow et al., 2010). While most repetitive elements are the first to be silenced and located in the inner compartment of Xi, a subpopulation of young active LINE-1 elements, however, is expressed during XCI. These L1 transcripts are initially clustered outside the Xist RNA domain and are found inside the repressive Xist compartment at a later stage (Chow et al., 2010). This unexpected LINE expression requires an heterochromatic environment, induced by Xist RNA (Chow et al., 2010). LINEs may thus participate to XCI by at least two means: first with silent LINEs contributing in the Xist-mediated heterochromatic compartment, and second with active LINEs involved in local propagation of XCI and gene attraction into this silent compartment (Figure 5).

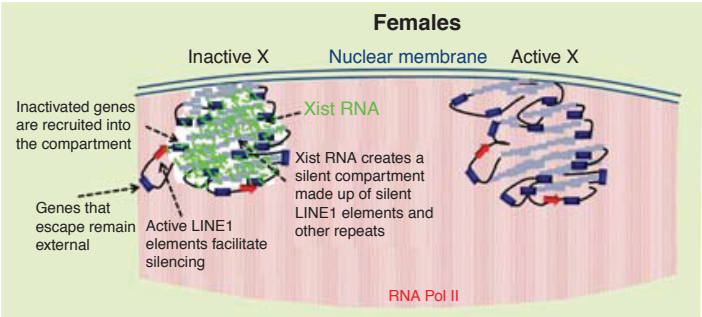

Figure 5 - Active and inactive X in the nucleus (as in (Chow et al., 2010))

In the above sections, I have described the extent to which X-chromosome inactivation is a highly dynamic process involving a cascade of molecular events and implying profound changes at several levels: chromatin modifications, gene silencing and nuclear position. These studies were limited either to microscopy techniques or to biochemical analysis of chromatin. More recent techniques have emerged for analyzing intrachromosomal architecture as well as the 3D structure of the genome. These approaches have shed new light onto global Xi reorganization upon Xist coating. In the next chapter, I will present the hierarchical organization of the genome, stressing the importance of domain formation and TADs in gene expression regulation as well as the unique conformation of the inactive X-chromosome.

2. Three-dimensional genome organization at the megabase scale

2.1 Different scales of genome folding

How is the whole genome - a chromatin fiber measuring about 2 to 3 meter in each human cell - packaged into such a small volume as the nucleus - measuring only a few microns in diameter? How might this level of high compaction preserve genomic functions, i.e. proper gene transcription, replication or DNA repair?

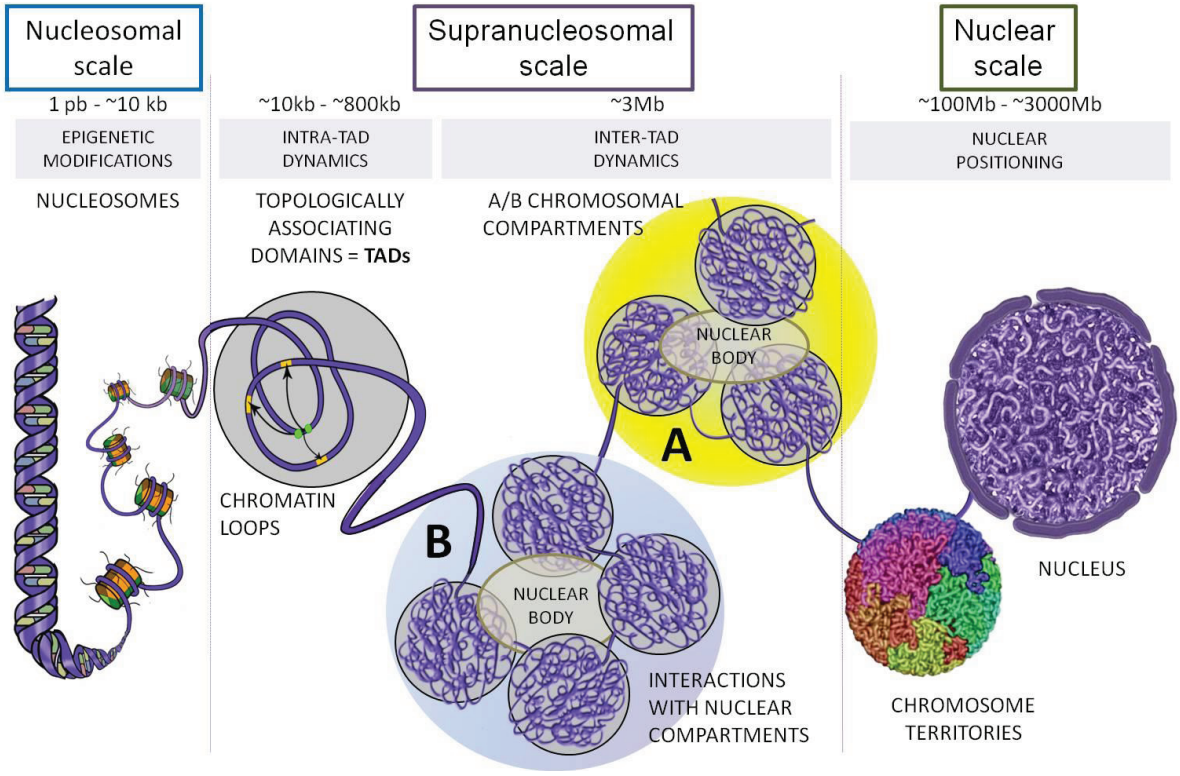

Figure 6 - Schematic representation of genome organization in mammals (as in (Ea et al., 2015))

Optical and electron microscopy observations revealed that the eukaryotic genome is divided in two types of chromatin: euchromatin - that is gene-rich, transcriptionally active and positioned at the center of the nucleus - and heterochromatin - that is gene-poor, more compact and likely to be transcriptionally silent and located at the nuclear periphery. Development of Chromosome Conformation Capture (3C) based technique and its association with Next-Generation Sequencing (NGS) (see Box 1 - Tools to explore 3D genome organization) extended our knowledge on genome organization at the megabase scale, between the nucleosomal scale and the nuclear scale (Figure 6). I will hereafter cover genome organization at the scale of chromosome territories, compartments and topologically associating domains (TADs).

Box 1 - Tools to explore 3D genome organization

Two different and complementary approaches have been extensively used to investigate chromosome structure and 3D genome organization: imaging tools and chromosome conformation capture (3C) and its derivatives (hereafter referred to as C-techniques). To answer my questions, I have taken advantage of both approaches during my PhD.

Imaging approach

Imaging tools enable direct visualization of a region of interest. Before the rise of C-techniques, DNA fluorescent in situ hybridization (DNA FISH) was the main method to study genome organization. DNA FISH involves fixation and permeabilization of cells, denaturation prior to hybridization of fluorescently labeled DNA probes. Fixation with formaldehyde and permeabilization with detergents such as Triton X-100 preserves the shape of the cells: 3D DNA FISH along with 3D microscopy acquisition are crucial for measuring accurate distances and exploring genome organization. Imaging tools have recently improved in two major limitations of FISH: first, resolution thanks to super-resolution microscopy (see (Ricci et al., 2017) for review) and molecular beacon short oligonucleotide probes (Ni et al., 2017); second coverage: while conventional FISH only targets a few loci at a time, multiplexed FISH method enables nowadays tracking of more than 30 loci simultaneously (Wang et al., 2016b).

C-techniques

Spatial organization can also be inferred from pairwise contact frequencies in the genome. C-techniques are biochemical assays that include fixation using a crosslinking agent to preserve genome structure inside the nucleus, followed by digestion of its chromatin with a restriction enzyme and religation of DNA fragments that are spatially close to each other (for review see (Schmitt et al., 2016b, Denker and de Laat, 2016)). This was called the "proximity ligation": it creates hybrid DNA particles between crosslinked restriction fragments whenever they are sufficiently close in the 3D space. A 3C library is then obtained and quantified by various methods described below. An interaction profile is retrieved, indicating probabilities of contacts for the studied region: spatial organization is hence estimated.

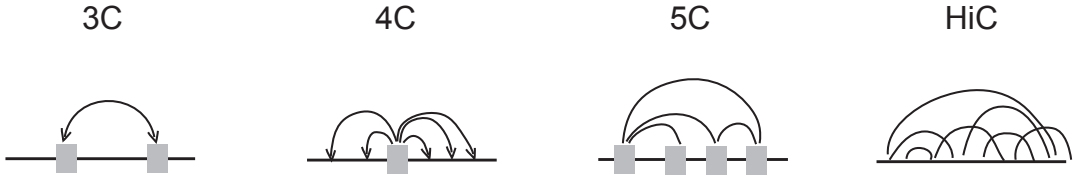

3C (one-vs-one) – investigates interactions between a single pair of genomic loci, using qPCR primers to quantify their ligation frequency in the 3C library.

4C (one-vs-all) – investigates interactions between one chosen locus (termed "viewpoint") and all other genomic loci. The 3C library undergoes a second digestion and ligation step, followed by an inverse PCR to amplify the sequences that have contacted our viewpoint. They will be further analyzed by sequencing.

5C (many-vs-many) – investigates all interactions within a region of interest (up to a few megabases). Oligos covering the region of interest and coupled to universal primers are hybridized to the 3C library, prior to ligation and amplification by multiplex PCR, followed by deep-sequencing to detect all interaction events.

Hi-C (all-vs-all) – investigates all interactions in the genome. Digested DNA fragments are labelled with biotin, and then ligated and sonicated. 3C library is enriched for ligation events by a streptavidin pulldown and deep-sequenced.

C-techniques assess contact frequencies in a population of cells by averaging chromosome conformation of millions of nuclei. **Single cell HiC** (scHiC) (Nagano et al., 2013) provides individual cell information: it outlines cell-to-cell variability and the dynamic of genome organization. ScHiC allows chromatin folding analysis in rare cell types. Somehow, it bridges current gaps between genomic sequencing approach and microscopy studies of chromosomes (Ulianov et al., 2017). Indeed, some studies outlined some discrepancy in between FISH and C-data sets: one example is the investigation of the HOXD cluster in mouse with 5C and FISH in different developmental and activity states, in wild-type and mutant models lacking some epigenetic regulators (Williamson et al., 2014).

Both DNA FISH and C-techniques explore the architecture of the genome: however, while FISH enables spatial distance or colocalization measurement, 3C-techniques report interaction frequencies in between loci that were "sufficiently close" at the time of fixation. But what is "sufficiently close"? One should hence be cautious when comparing images and C-data before inferring genome organization (Giorgetti and Heard, 2016, Fudenberg and Imakaev, 2017).

Advantages and limitations of imaging and C-techniques in genome exploration

Imaging	C techniques
Directly measure spatial distance or colocalization	Detect proximity events and their abundance. Not able to distinguish direct & indirect interaction (cross-linking)
Live imaging: movement	Fixed cells
Cell to cell variability	Population effect
Limited throughput	High throughput
Limited resolution	May be of high resolution
Limited genome coverage (region specific)	May be genome wide

Box 1 - Tools to explore 3D genome organization

2.1.1 Chromosome territories (CT)

Since the late 19th century, scientists have attempted to describe the nuclear structure and its chromosome organization. Carl Rabl was the first to postulate that each interphase chromosome would occupy a distinct nuclear domain (Rabl, 1885). A few years later, Theodor Boveri created the term “chromosome territory” while observing cytological images of chromosomes in early cleavage stages of fertilized eggs of the horse roundworm (Boveri, 1909). However it took about a hundred years for that model to be fully established in the scientific community and quite some technological advances to strengthen it (Cremer and Cremer, 2006).

Despite some cell-to-cell variability, CTs have preferential radial positioning in the nucleus that depends on gene density: i.e. human chromosome 18 (gene-poor) is found at the periphery whereas chromosome 19 (gene rich) is found at the center of the nucleus (Croft et al., 1999). Positioning also depends on chromosome size: larger chromosomes are found at the periphery whereas smaller ones are at the center (Cremer et al., 2001).

Although CT have been initially described in light of to microscopy studies, HiC data also supports this preferential chromosome segregation into the nucleus in CT: intrachromosomal contacts are much more frequent than interchromosomal contacts, even at distances greater than 200 Mb (Lieberman-Aiden et al., 2009). More recently, from haploïd single-cell HiC data, CT have been modeled from single cell datasets. This technique enables genome folding to be examined at a scale of less than 100 kb, and not only CT but also compartments and TADs can be modeled at single cell level (Stevens et al., 2017).

When one “zooms in” on genome organization, within CTs, chromosomes are partitioned into large compartments at the multi-megabase scale, containing either the active and open (A compartments) or inactive and closed chromatin (B compartments).

2.1.2 Compartments

When normalized contact matrix is extracted from a HiC dataset, it shows a plaid pattern with large blocks of enriched and depleted interactions: this suggests that each chromosome is divided into a succession of two types of compartments where contacts within each compartment are enriched whereas contacts across compartments are depleted (Lieberman-Aiden et al., 2009). Compartment A/B partitioning has mainly been inferred from

population data but is also detectable in individual cell, as shown in single-cell HiC modeling (Stevens et al., 2017) or in multiplexed FISH experiment (Wang et al., 2016b).

Principal component analysis partitions each chromosome into these two compartments, termed compartment A and B, based on first principal component (Lieberman-Aiden et al., 2009). When HiC dataset resolution is higher, more subcompartments can be distinguished, with specific pattern of histone modifications (Rao et al., 2014). The A compartments preferentially cluster with other A compartments throughout the genome, as do B compartments. Compartment A gathers early-replicating, gene-rich, transcriptionally active regions, with accessible chromatin and active chromatin marks (H3K36me3). In contrast, compartment B harbours late-replicating regions that coincide with Lamina-Associated Domains (LADs).

LADs are genomic regions that interact with the nuclear lamina (Pickersgill et al., 2006, Kind et al., 2015). They have been identified using the DamID (DNA adenine methyltransferase (Dam) identification) technology, in which Dam enzyme is fused to a nuclear protein, usually Lamin B1, and thus tethered to the nuclear envelope. Genomic regions that contact the nuclear protein are subsequently marked by adenine methylation: this modification can be mapped genome-wide (van Steensel and Henikoff, 2000). LADs are thought to help establishing the overall folding of the genome and to be involved in gene repression (see (van Steensel and Belmont, 2017) for review).

A/B compartment distribution is cell-specific and A/B compartment switching is observed during differentiation or in between different cell types (Dixon et al., 2015, Schmitt et al., 2016a). It is conserved through quiescence and senescence (Criscione et al., 2016). Thus, the partitioning of chromosomes into distinct A/B compartments and sub-compartments correlates well with cell type-specific gene expression and chromatin status of the genome. Indeed, A/B compartments identified by Hi-C can be estimated and reconstructed using various epigenetic data reflecting genome-wide DNA methylation or chromatin accessibility patterns (Fortin and Hansen, 2015).

2.1.3 Topologically Associating Domains (TADs)

2.1.3.a TADs are conserved through evolution and differentiation

The compartments at the multi-megabase scale can further be divided in sub-megabase domains: these domains of preferential interactions, termed Topologically Associating Domains (TADs), were first described in mouse and human (Dixon et al., 2012, Nora et al., 2012) (see Box 2 - TAD calling). An analysis of Xic region by 5C supports that

the active X-chromosome in male mouse ESC is also organized in TADs (Nora et al., 2012). TADs are conserved and have also been reported in non-mammalian genomes such as *Drosophila* (Sexton et al., 2012), *C.elegans* (Crane et al., 2015), and zebrafish (Woltering et al., 2014, Gómez-Marín et al., 2015). Some domains of preferential interactions have been characterized in *Schizosaccharomyces pombe* as “globules” (Mizuguchi et al., 2014) and in bacteria *Caulobacter crescentus* as “Chromatin Interaction Domains” (Le et al., 2013). In mouse ESC, the genome is partitioned into about 2 200 TADs, the size of which ranges from tens of kb up to 1 or 2 Mb, with an average of around 800 kb (Dixon et al., 2012).

Unlike A and B compartments that appear to switch between cell types, TAD structure is conserved through differentiation (Dixon et al., 2015). It is also preserved through male meiosis (Battulin et al., 2015, Jung et al., 2017) whereas at the packaging level sperm chromatin is very different from other cell types with protamines replacing histones. Although TAD partitioning appears to correlate with chromatin marks as suggested by studies that reconstructed contact frequency maps from epigenomic data (Chen et al., 2016b, Huang et al., 2015), TAD formation seems to be independent of chromatin modifications. In fact, TAD structure in chromatin modifier mutant mESC (such as G9a knock-out which lacks H3K9me2 or Eed knock-out which lacks H3K27me3) is not affected (Nora et al., 2012). Thus, whereas TADs and the large blocks of H3K27me3 and H3K9me2 on the X-chromosome highly overlap, impaired histone mark machinery does not disturb chromosome architecture.

Box 2 - TAD calling

Once HiC libraries are sequenced, computational analysis takes over bench work. The initial processing step for HiC data consists of mapping the reads to the corresponding reference genome and filtering of the mapped reads. Data are represented in contact maps. A contact map is a matrix with rows and columns representing non-overlapping 'bins' across the genome. Each entry in the matrix contains a count of read pairs that connect the corresponding bin pair in a Hi-C experiment. Contact map is subsequently normalized: several normalization or correction techniques have been developed. Then the actual analysis can start: significant long-range contacts may be extracted, 3D colocalization of regions or loci of interest can be tested, domains may be identified (or "called"), 3D models may be computed.

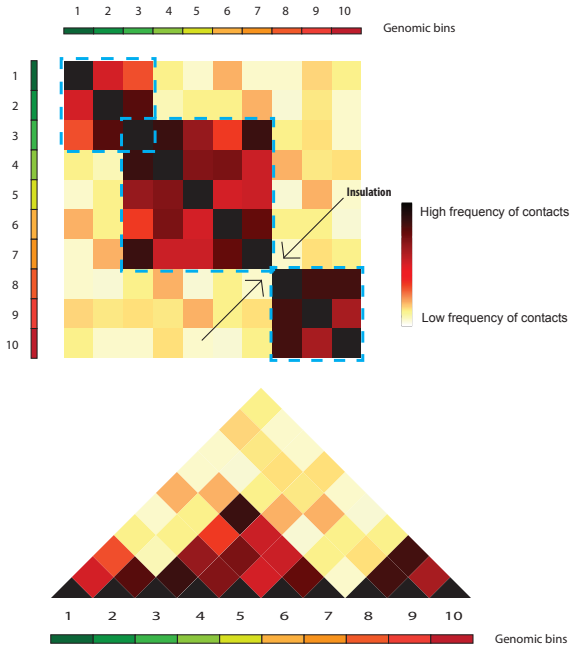

Scheme showing a HiC contact map (top panel): the genome is binned and read pairs are represented according to their count in each bin with a color code. The dark diagonal represents short-range contacts. Dark bin off-the diagonal represents long-range contact. Domains of preferential interactions are indicated with dashed outlines. Arrow indicates insulation in between domains. Contact maps are often represented with the diagonal horizontalized (bottom panel).

There are several approaches to call TADs. The two most common TAD calling techniques are the directionality index and the insulation score. For both techniques, two parameters are necessarily pre-determined: window (or bin) size and contact cutoff. The window size will determine the size of the identifiable TADs. The cutoff will strongly influence the sensitivity and specificity of TAD identification.

Directionality index

A TAD is a domain harbouring preferential interactions: it thus creates an imbalance between the upstream and downstream contacts of a region. Dixon et al. quantify this imbalance in a statistic named directionality index (DI) and use an Hidden Markov Model to determine the underlying bias state for each locus (upstream biased, downstream biased, none) (Dixon et al., 2012). These HMM state calls are used to infer domains as continuous stretches of downstream bias states followed by upstream bias states. Directionality index thus defines putative boundary in between two domains.

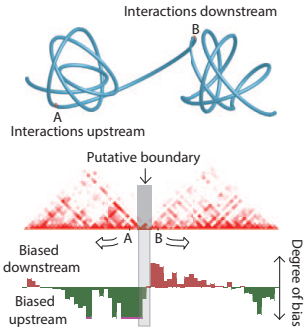

Scheme as in Dixon et al., 2012 illustrating topological domains and resulting directional bias.

Insulation score

To quantify TADs, Crane et al. assign an 'insulation score' to genomic bins along the chromosome (Crane et al., 2015). The score reflects the amount of interactions occurring across each bin. Minima of the insulation profile indicate regions of high insulation, in other words domain boundaries.

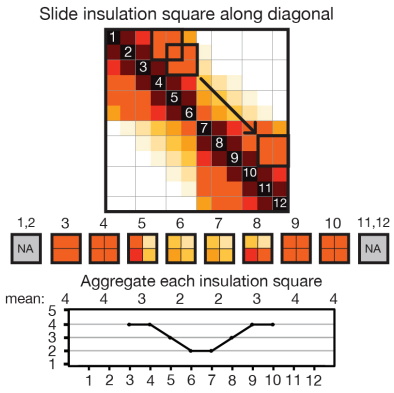

Scheme as in Crane, 2015. "A square is slid along each diagonal bin of the interaction matrix to aggregate the amount of interactions that occur across each bin (up to a specified distance upstream and downstream of the bin). Bins with a high insulation effect (for example, at a TAD boundary) have a low insulation score (as measured by the insulation square). Bins with low insulation or boundary activity (for example, in the middle of a TAD) have a high insulation score. Minima along the insulation profile are potential TAD boundaries."

Box 2 - TAD calling

2.1.3.b TADs are not conserved through cell cycle

A very recent study has suggested that TADs are not conserved through cell cycle (Naumova et al., 2013, Nagano et al., 2017): indeed TADs and compartments are erased during mitosis. There seems to be a universal cell-type and locus-invariant mitotic conformation for chromosome: unlike during interphase where chromosomes are folded into TADs, a homogenous folding state is observed during mitosis, lacking domains of preferential interactions.

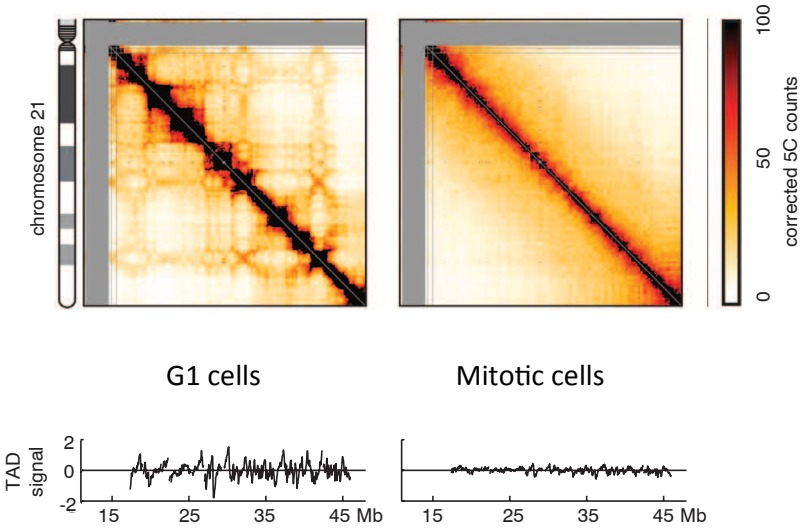

Figure 7 - Organization of chromosome 21 in G1 versus during mitosis: corrected 5C matrices of chromosome 21 for synchronized cell populations; TAD signal for each data set. (adapted from Naumova et al, 2013)

Mitotic chromosome displays a characteristic scale of cis-chromosomal contact distances that peaks between 2 and 12 Mb (Nagano et al., 2017). A recent single-cell HiC indicates that it is possible to phase cells along the cell cycle thanks to two major anchors: the distribution of short- and long-range interactions, characteristic of each step of the cell cycle, named “mitotic signature” and the analysis of time of replication with a “repli-score” (Nagano et al., 2017). If cells are represented comparing frequency of short-range contacts (less than 2Mb) to the frequency of mitotic-range contacts (between 2 and 12Mb), they form a singular circular pattern reminiscent of gradual chromosome remodeling across cell cycle (Figure 8a). For example, while mitotic cells have a high frequency of long-range contacts and low frequency of short-range contacts, G2 cells display a low frequency of long-range contacts and high frequency of short-range contacts.

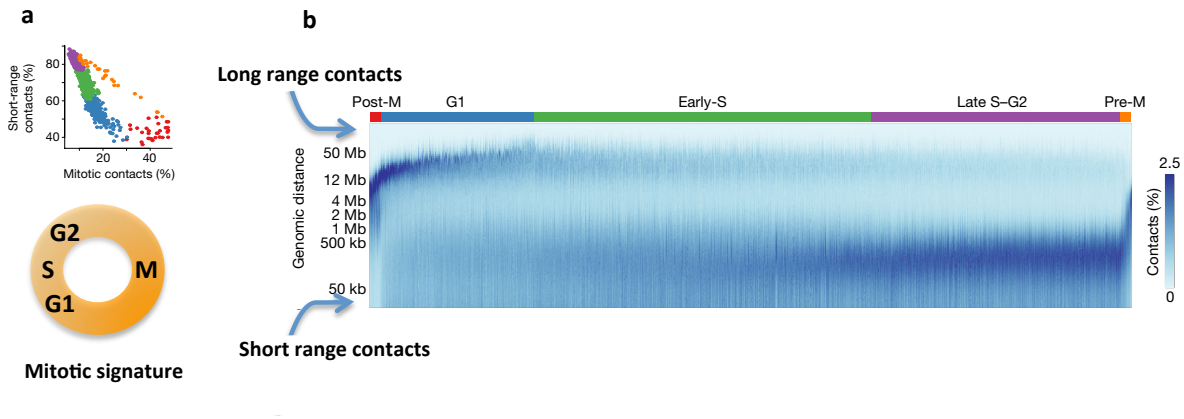

Figure 8 - a. Cell cycle phasing according to "mitotic signature" (schematic distribution of cell cycle on orange circle).

b. Single-cell contact decay profiles ordered by in silico inferred cell-cycle phasing, with approximate cell-cycle phases shown on top. Each column represents a single cell (adapted from Nagano et al., 2017)

The 'repli-score' is calculated for each cell based on the copy-number ratio of early-replicating regions (these regions are annotated in the mouse ENCODE (Stamatoyannopoulos et al., 2012)) to total coverage. For example, G1 cells have low repli-scores, whereas mid-S cells have very high repli-score. Once cells are classified into cell cycle stages thanks to the "mitotic signature", the repli-score is used to order the cells within those main categories. Cells are then represented and ordered according to their *in silico* inferred cell-cycle phasing (Figure 8b).

TAD insulation and A/B compartmentalization were found to be dynamic over the cell cycle: while no structure is detected during mitosis, TAD insulation is the strongest in G1 and compartmentalization in G2 (Nagano et al., 2017). Interestingly the genome is not stably folded at any point of the cell cycle. Consequently, it is not surprising to observe cell-to-cell variability in chromosome structure from single-cell HiC datasets (Nagano et al., 2013) or from predictive polymer modeling (Giorgetti et al., 2014).

2.1.3.c TAD boundaries and putative insulators

TAD boundaries have been found to be enriched for multiple elements such as gene promoters, housekeeping genes, active chromatin marks (H3K4me3), tRNA genes, short interspersed element (SINE) retrotransposons (Dixon et al., 2012).

They are also enriched for CTCF binding sites. This nuclear factor is a zinc-finger protein that binds to DNA at specific binding motif sequences. It is a well-known and conserved insulator that is broadly expressed. It was originally described in promoting

transcriptional insulation at the beta-globin cluster (Bell et al., 1999) and at the imprinted loci of Igf2 (Bell and Felsenfeld, 2000). It is nowadays viewed as a key player in genome organization (for review see (Phillips and Corces, 2009, Merkenschlager and Nora, 2016)). CTCF enrichment at boundaries suggests a decisive role for CTCF in boundary formation; however many CTCF sites aren't engaged in chromatin folding and number of TAD boundaries lack CTCF occupancy (Dixon et al., 2012).

CTCF depletion by knock-down in human cell line leads to modest genome organization disruption: intradomain interactions seem reduced while interdomain interactions increase (Zuin et al., 2014). But knock-down assays aren't efficient enough to completely deplete CTCF (knock down efficiency 80%, as observed by Western Blot). A recent study using the auxin-inducible degron system circumvents this limitation in mouse ESC (Nora et al., 2017): adding auxin to the culture medium depletes CTCF (CTCF becomes undetectable by Western Blot) and washing out auxin allows CTCF to accumulate back to initial levels. In this reversible system, TADs are lost upon CTCF depletion and restored when CTCF is rescued. Persistent CTCF depletion dramatically slows cell proliferation. CTCF is thus required for insulation of TADs and also for looping between CTCF target sites. Interestingly, it is not necessary for A/B compartment partitioning (Nora et al., 2017). Even non-dividing cells lose TAD structure upon CTCF depletion; however they don't recover their structure once CTCF is rescued. Therefore, cell division does not seem to be necessary to lose structure however it might be to gain it.

In addition, maternal depletion of CTCF is associated with transcriptional misregulation in CTCF-depleted oocytes, delayed meiotic maturation and decreased meiotic competence, some early mitotic defects from the 2C to 4C stage transition with a developmental delay that might be caused by defective embryonic genome activation. Most of CTCF-depleted embryos fail to reach the blastocyst stage (Wan et al., 2008). Therefore, CTCF appears to be a crucial factor *in vitro* to sustain cell viability and *in vivo* for proper development.

Cohesin complex is found overlapping with CTCF sites; this complex, is known to be involved in sister chromatin holding after DNA replication to allow proper chromatid segregation during cell division. It might be another candidate for chromosome folding (Parelho et al., 2008, Merkenschlager and Nora, 2016). WAPL, which promotes sister-chromatid resolution in mitotic prophase by releasing cohesin from chromatin, has also recently been suggested as a key-factor for genome architecture (Busslinger et al., 2017, Haarhuis et al., 2017).

2.1.3.d TADs emerge as a functionally privileged scale

TADs are commonly described as domains in which genomic loci interact preferentially with each other, rather than with regions belonging to different TADs. However this definition could also apply to most of the domains identified by the C-techniques at different scales: the compartments, the TADs, the sub-TADs or contact domains (Phillips-Cremins et al., 2013, Rao et al., 2014). Thus mammalian genome has nested hierarchical configurations in which larger domains encompass smaller ones. Domain identification substantially depends on the resolution of the C-data used and on the setting of the algorithm parameters used for domain characterization.

By applying a novel algorithm named CaTCH that identifies and stratifies topological domains from Hi-C maps, using a single parameter - reciprocal physical insulation- Zhan et al. demonstrate that no structurally privileged folding level exists. There is indeed a continuous spectrum of nested self-interacting domains. However, TADs appear as a functionally privileged scale where several functional properties are maximised (Zhan et al., 2017) such as active histone marks, CTCF clustering at boundaries (Dixon, 2012), transcriptional coregulation (Nora et al., 2012), enhancer-promoter optimal communication (Nora et al., 2013). Hence, TADs are not only a simple additional layer of genome folding but seem to be “the unit of chromosome organization” (Dixon et al., 2016).

2.2 TADs shaping regulatory landscapes

This functionally privileged scale is consistent with the fundamental role in shaping regulatory landscapes that TADs might play. They appear not only to co-regulate the genes within TADs but also to insulate the activity between neighboring TADs. This function is essential as shown in the following examples during development and in diseases.

2.2.1 TADs as transcriptional co-regulation units

Transcriptional co-regulation within TADs has been illustrated in the Xic region during ESC differentiation. Respective promoters of *Xist* and *Tsix* lie in two neighbouring TADs. Whereas the *Xist* promoter and its positive regulators are located in one TAD, the promoter of *Tsix* lies in another TAD (Nora et al., 2012). Coordinated gene expression has also been reported upon hormone-stimulation: in a breast cancer cell line, up to 20% of the TADs showed coordinated upregulation or downregulation of the majority of the genes therein upon steroid hormone exposition (Le Dily et al., 2014). Hence, expression profiles of genes located within the same TAD are correlated.

To assess how TADs confine regulatory networks in specific and large domains with specific gene expression profiles, Symmons and colleagues developed a powerful tool. They inserted a *LacZ* reporter construct at more than 1 000 loci across the genome in mice, the latter being driven by a weak promoter that would be under the control of endogenous regulatory elements. In their paper, they showed that the sensor emulated expression patterns of neighboring genes but only of genes contained in the same TAD as the reporter. Regulatory domains, defined as "as the largest possible interval containing multiple insertions with shared expression", are included within TADs (Symmons et al., 2014). To maintain properly this co-regulation network inside the TAD, efficient boundaries are mandatory: their disruption leads to ectopic expression (see 2.2.4 for examples).

2.2.2 TADs as long-range contact facilitators

TAD structure promotes contacts between cis-regulatory elements. An interesting example in the *Sonic hedgehog* (Shh) locus illustrates this function. Shh is expressed during vertebrate development in mouse posterior limb buds; the specific expression of Shh in the zone of polarizing activity, which establishes antero-posterior patterning of the developing limbs, is regulated by a long-range enhancer - named ZRS - about 1 Mb upstream of the *Shh* promoter (Lettice et al., 2003, Sagai et al., 2005). Several genetically engineered chromosomal rearrangements were achieved in the vicinity of the *Shh* locus, modifying distances between *Shh* promoter and its enhancer ZRS. Changing distances within *Shh* TAD has little effect on its expression and on correct limb development. In contrast, *Shh* TAD disruption prevents physical and regulatory interactions between *Shh* and its ZRS enhancer, leading to misexpression and abnormal limb formation. Reducing genomic distance can partially rescue disrupted long-range interactions (Symmons et al., 2016). Thus, TADs seem to facilitate the action of remote enhancers by reducing the effects of genomic distances; they promote distance-independent interactions, which would otherwise be too rare to trigger appropriate gene expression.

2.2.3 An example of regulatory TAD-switching during development

One example that has been extensively studied to understand and characterize the role of TADs is the *HoxD* cluster during development.

During embryonic development, precise spatial and temporal control of *Hox* cluster transcription is fundamental to achieve a proper patterning of the main body axis. Notably, *Hox* genes inside the cluster are positioned along the genomic sequence in an order that corresponds to their expression along the body axis. This sequential transcriptional strategy is termed collinearity (Noordermeer and Duboule, 2013).

HoxD cluster is also involved in the development of secondary axial structures, such as limbs (for review see(Lonfat and Duboule, 2015)). Two successive waves of *HoxD* gene transcription are required during early development of vertebrate limbs. The first wave (phase I) is required for the development of the proximal part of the limb: anterior and central *Hoxd* genes (from *Hoxd1* to *Hoxd11*) are sequentially expressed. Afterwards, the second phase (phase II), involving *Hoxd8* to *Hoxd13*, is necessary for the most distal limb segment. The tight control of *Hox* gene expression relies on multiple well conserved enhancer sequences (Lee, 2006), located outside the gene clusters, in the flanking gene deserts on both sides of the cluster (Montavon et al., 2011). They define a large 'regulatory landscape' (Spitz et al., 2003) (Figure 9).

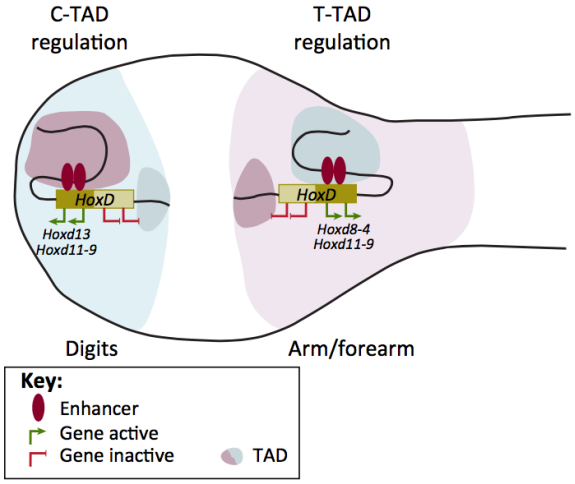

Figure 9 - HoxD cluster example illustrates spatio-temporal regulation over development (as in (Gonzalez-Sandoval and Gasser, 2016))

Regulation of early and late phases of transcription lies on a bipartite architecture of the region: the cluster is contained in two adjacent TADs, overlapping the boundary (Andrey et al., 2013). Regulatory elements for the phase I are located in the telomeric TAD whereas regulatory elements for the phase II are located in the centromeric TAD. Therefore, the early and late phases of Hoxd gene transcription in limb buds are controlled by two opposite

deserts flanking the cluster on either side and corresponding to two adjacent topological domains.

While genes in either extremity of the cluster interact preferentially with the TAD they are closer to, a subset of *Hoxd* genes mapping centrally into the cluster, at the border between domains, changes regulatory landscape and domain during development. While initially interacting with the telomeric domain, central *Hoxd* genes secondly switch toward centromeric domain regulatory elements (Andrey et al., 2013). This switch is associated with changes in spatial proximity as revealed by super-resolution DNA FISH and microscopy experiments (Fabre et al., 2015).

Thus the example of *HoxD* cluster through development outlines how TAD structure is dynamically involved in transcriptional regulation: switch of genes from one TAD to the other is accompanied by their expression modification.

2.2.4 Disrupted TAD structure and disease

As TAD structure seems to be essential to preserve correct promoter-enhancer interactions for appropriate gene regulation, its alteration may lead to ectopic interactions between regulatory elements and cause gene dysregulation. Some mutations or chromosome rearrangements may disrupt TAD boundaries and activate genes that would otherwise be silent. Some examples illustrating this pathophysiology are reported in **Table 1.**

Several cases of ectopic activation of oncogenes in link with structural changes have been described in cancer (Hnisz et al., 2016, Gröschel et al., 2014, Vicente-García et al., 2017). Besides, CTCF binding sites are frequently mutated in cancer (Katainen et al., 2015, Kaiser et al., 2016) or CTCF binding might be impaired due to aberrant hypermethylation of its binding sites (Flavahan et al., 2016).

Loss of TAD integrity is also involved in congenital diseases as illustrated *in vivo* with various structural variations in the *Epha4* TAD involved in polydactyly and limb malformation (Lupiáñez et al., 2015) or in *Sox9* region (Franke et al., 2016).

Misexpression of genes secondary to architecture remodelling has been reported in numerous pathologies such as cancer (for review see(Valton and Dekker, 2016)), congenital or degenerative diseases.

Table 1- 3D genome organization in disease and cancer

Paper	***Model***	***Locus or region of interest***	***Phenotype***	***Conclusion***
(Nora et al., 2012)	mESC (engineered)	*Xic*		Deleting boundary induces ectopic contacts and altered TAD organization.
(Symmons et al., 2016)	Mouse (engineered)	*Shh*	Limb malformation	Disruption of the TAD prevented physical and regulatory interactions between Shh and its limb enhancer, unless the genomic distance between the two was significantly reduced.
(Symmons et al., 2014)	Mouse (engineered)	Genome wide, hundreds of insertions of a regulatory sensor.		Enhancers distribute their activities along broad regions and not in a gene-centric manner, defining large regulatory domains that correlate well with the TADs.
(Tsujimura et al., 2015)	Mouse (engineered)	*Tfap2c* and *Bmp7*		Highligths TAD function in long range gene expression regulation. Redistribution of the interaction domains and misexpression upon chromosomal inversions.
(Franke et al., 2016)	Human and mouse (engineered)	*Sox9* (Sex reversal) and *Kcnj* (Cook syndrome)	Sex reversal, Cook syndrome	Genomic duplications can result in the formation of new chromatin domains (neo-TADs). Overlapping duplications that extended over the next boundary into the neighbouring TAD resulted in the formation of a new chromatin domain (neo-TAD) that was isolated from the rest of the genome (and thus had no phenotypic effect).
(Lupiáñez et al., 2015)	Human and mouse (engineered)	*EphA4*	Limb malformation	Disruptions of TADs lead to de novo enhancer-promoter interactions, misexpression and congenital malformations.
(Hnisz et al., 2016)	Human and mouse (engineered)	Multiples loci	Tcell acute lymphoblastic leukemia	Microdeletions eliminating the boundary sites of insulated neighborhoods containing prominent T-ALL proto-oncogenes. Perturbation of such boundaries in nonmalignant cells was sufficient to activate proto-oncogenes.
(Gröschel et al., 2014)	Human	*EVI1*	Acute Myeloid Leukemia	Chromosomal rearrangements (inv(3)/ t(3;3)) reposition a distal GATA2 enhancer to ectopically activate EVI1
(Vicente-García et al., 2017)	Human and mouse (engineered)	*PAX3* and *FOXO1*	Rhabdomyosarcoma	A translocation brings together the PAX3 and FOXO1 genes
(Northcott et al., 2014)	Human and mouse (engineered)	*GFI1* and *GFI1B*	Medulloblastoma	Somatic structural variants juxtapose GFI1 or GFI1B (oncogenes) coding sequences proximal to active enhancer or super-enhancers, instigating oncogenic activity ('enhancer hijacking').
(Weischenfeldt et al., 2017)	Human	*IRS4*, *SMARCA1* and *TERT*	Database encompassing 7,416 cancer genomes	Looking for pan-cancer candidate genes, in cis-regulatory element rearrangements mediating dysregulation in cancer
(Flavahan et al., 2016)	Human	*PDGFRA* (oncogene)	Glioma	Deficient TET enzymes cause hypermethylation at cohesin and CTCF binding sites: CTCF binding is thus impaired, TAD insulation is lost and gene activation is aberrant (oncogenes).

(Kaiser et al., 2016)	Human	Mutated CTCF binding sites	Database encompassing 11 tumor types	CTCF binding mutations and widespread breakdown of chromatin organization.
(Giorgio et al., 2015)	Human	*LMNB1*	Adult-onset demyelinating leukodystrophy (ADLD)	A large (~660 kb) heterozygous deletion that begins 66 kb upstream of the LMNB1 promoter eliminates a genome topological domain boundary. This allows normally forbidden interactions between at least three forebrain-directed enhancers and the LMNB1 promoter: thus LMNB1 is overexpressed.
(Ibn-Salem et al., 2014)	Human	Genome wide computational analysis	Human diseases	Enhancer adoption caused by deletions of regulatory boundaries may contribute to about 12% of CNV phenotypes.

Thus, TAD structure is an important functional layer of genome folding involved in regulatory landscape and which disruption may cause gene expression dysregulation and pathology. If TADs are globally conserved, through evolution or cell differentiation for instance, notable reorganization occurs during some biological processes such as mitosis. With regard to the X-chromosome, a tremendous architectural transformation takes place during X-chromosome inactivation.

2.3 New insight into the X structure thanks to C-techniques advent - The bipartite organization of the Xi

As previously discussed (see 1.5), simple cytological observations pointed at the dualist structure of the Xa and Xi. The advent of conformation capture techniques opened up new perspectives in the exploration of chromosome structure and verified the singularity of the silenced X-chromosome.

In order to explore the inactive X-chromosome's structure, two essential challenges have to be dealt with: first, one has to be able to distinguish in between the active and the inactive X-chromosomes. This implies use of a highly polymorphic model with a large number of single nucleotide variants (SNPs) to distinguish in between reads obtained from the paternal or maternal genome. Second, the sample that is studied needs to be clonal and to have stably inactivated either the paternal or the maternal X-chromosome.

The first molecular study that hinted at the differences in between Xa and Xi was an allele-specific 4C analysis in neural progenitor cells (NPCs) (Splinter et al., 2011). Unlike inactive regions in autosomes (B compartment (Lieberman-Aiden et al., 2009)) or on the active X-chromosome, silenced genes from the Xi are devoid of preferential contacts. In

addition, long-range interactions are not observed in the Xi contrary to the Xa. Furthermore, escapees gene tend to cluster in nuclear space. The Xi structure was thus suggested to be unique and more “random” - as the preferential interactions, detected on the Xa, were lost.

2.3.1 The Xi is organised into two large "mega-domains"

More recently, HiC studies confirmed this specific Xi architecture by analysing the whole X-chromosome in mouse, human and rhesus macaque (Rao et al., 2014, Minajigi et al., 2015, Deng et al., 2015, Giorgetti et al., 2016, Darrow et al., 2016). Unlike homologous autosomes that have highly similar high-order chromatin structure (Dixon et al., 2015, Deng et al., 2015), the Xi is extremely different from its active counterpart. While the active X displays TADs of regular size, the Xi is composed of two consecutive large domains separated by a hinge region containing repetitive DNA with a macrosatellite sequence named DXZ4. Using two sets of oligonucleotide probes located either on the same mega-domain or spanning the DXZ4 boundary (Figure 10), 3D DNA FISH investigation in mouse NPCs corroborates this finding at the single cell level (Giorgetti et al., 2016). Indeed, probes targeting regions from the same mega-domain show greater overlap on the Xi than on the Xa chromosome, whereas probes spanning the boundary show lower colocalization on the Xi chromosome. The inactive X is partitioned into two large domains (termed mega-domains or super domains), spatially distinct.

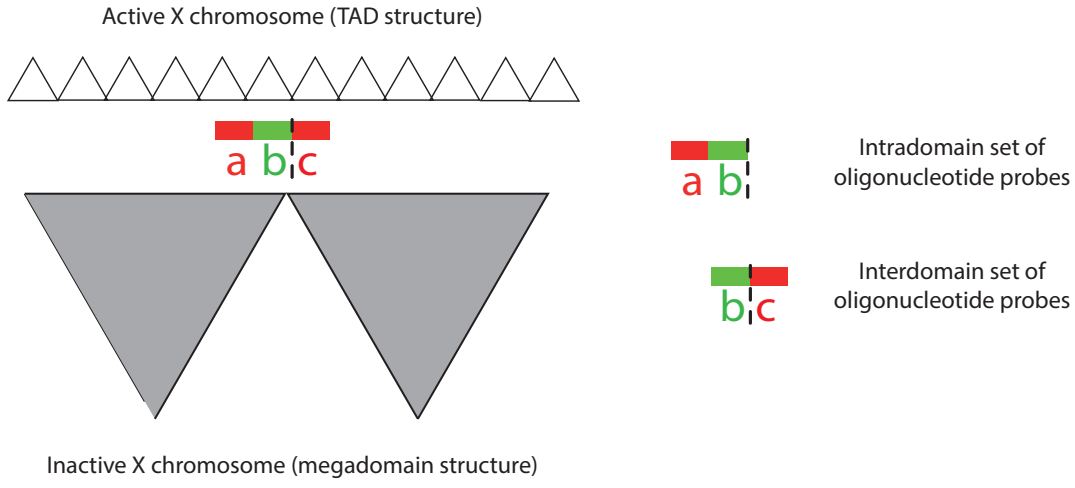

Figure 10 - DNA probes as used in Giorgetti et al., 2016 to explore Xi structure

2.3.1.a The DXZ4 boundary

When the DXZ4 macrosatellite was described for the first time in human, this X-chromosome-specific repetitive sequence was found to be highly methylated on the active X-chromosome and hypomethylated on the inactive X (Giacalone et al., 1992). It was hence used for sex determination, based on the difference of methylation pattern on the DXZ4 region (Naito et al., 1993). This region has been useful for sex-typing in forensic identification (Naito et al., 1994) but also for more surprising investigation: it was a helpful tool in Italy to determine gender of dried blood on a statue of the Virgin Mary (Palmirotta et al., 1998).

While on the active X-chromosome DXZ4 is organized into constitutive heterochromatin, it displays euchromatin marks on the overwise heterochromatic inactive X and is bound by CTCF (Chadwick, 2008). These peculiar features suggested that it could be involved in the process of X inactivation, long before the mega-domains were discovered.

Even though the bipartite structure of the Xi is not clearly observed by DNA FISH with X-paint, associating X-paint and a specific probe for Dxz4 in a female mouse cell line shows that Dxz4 preferentially localizes outside of the Xi (Deng et al., 2015). Moreover, the hinge region has been reported to present a NAD (Nucleolus Associated Domain): this region might be an anchor to the nucleolus for the inactive X (Deng et al., 2015).

2.3.1.b Differences in between mouse and primate

The bipartite organization of the Xi has been described in mouse, human and rhesus macaque. The macrosatellite DXZ4 is partially conserved through evolution (Rao et al., 2014, Deng et al., 2015, Darrow et al., 2016). However, the size of the mega-domains differs. In human, the two mega-domains on the Xi are of unequal size (115 Mb and 40 Mb) whereas in mouse they are closer in size (72 Mb and 94 Mb). Similarly, when comparing the syntenic gene content of the mega-domains in mouse and human, several inversions of genomic material are observed: loci included in one mouse mega-domain are found in distinct mega-domains in human (Deng et al., 2015).

2.3.2 Loss of TADs except at escapees

As suggested by previous 4C (Splinter et al., 2011) and 5C (Nora et al., 2012) studies, long-range contacts inside the TADs, at the sub-megabase scale, are lost on the Xi. The analysis of the whole chromosome by HiC reveals that Xi chromosome globally displays no TADs (Minajigi et al., 2015, Deng et al., 2015, Giorgetti et al., 2016) and might lose compartment partitioning in some cell lines (Giorgetti et al., 2016, Darrow et al., 2016).

However, a few residual TAD-like structures are detectable on the Xi. These Xi TAD-like structures are localized at hotspots of residual transcription and open chromatin (Giorgetti et al., 2016). They correspond to facultative and constitutive escapees. As previously shown (Splinter et al., 2011), escapees tend to contact each other, even across the DXZ4 boundary (Giorgetti et al., 2016). Facultative escapees are silenced in some of the clones: interestingly, when they are silenced, the TAD-like structure is lost (Giorgetti et al., 2016). Thus, unlike on the Xa and autosomes where TADs are present independently from transcriptional activity of their genes, appearance of TAD structures is intimately linked to gene expression on the Xi chromosome.

2.3.3 Xist RNA plays a role in Xi global reorganization

To investigate the importance of Xist RNA in the bipartite structure of the Xi, two types of experiments have been performed: either inducing Xist RNA in a male undifferentiated ESC line with an inducible promoter of *Xist* at its endogenous locus (with either a wild-type Xist RNA or a mutant Xist RNA lacking the A-repeat); or deletion of *Xist* in differentiated cells (MEFs or NPCs).

When Xist RNA is induced in male ESC, interactions frequencies increase along the X-chromosome and a physical insulation appears at the DXZ4 boundary. These changes are not observed with the Xist RNA lacking the A-repeat (which is efficient for chromosome coating and exclusion of RNA pol II but not for gene silencing) (Giorgetti et al., 2016). However, these modifications are mild compared to what is observed in the Xi in NPCs: TAD structure is unchanged, however interaction frequencies along the chromosome are increased and physical separation across the boundary is observed by FISH. This might be due, among others, to differences in Xi chromatin modifications on the recently Xist-coated Xi in ES cells comparable to that in stably differentiated NPCs.

When *Xist* is conditionally deleted (either in NPCs or in MEFs), loss of Xist RNA coating leads to a partial refolding of the X-chromosome in a structure more reminiscent of that of the Xa (Splinter et al., 2011), with restored TADs (Minajigi et al., 2015). Xist RNA is thus necessary for the maintenance of the Xi structure. However, Xist RNA is dispensable for the maintenance of gene silencing on the Xi in a somatic cell line where XCI is fully achieved (Csankovszki et al., 1999, Wutz and Jaenisch, 2000). Thereby, loss of structure occurs without change in expression. The mechanism of *Xist* regulating Xi organization has recently suggested to be repelling of cohesin binding at specific loci (Minajigi et al., 2015).

In short, during random XCI, the unique structure of the Xi is dependent on Xist RNA and on its A-repeat. Xi structure during imprinted XCI in mouse embryo development is still unknown. As discussed above (see 1.3.1.b), although most events are similar in between random and imprinted XCI, some differs. Furthermore, in the ICM, XCI is reversible as reactivation of the paternal X occurs a few cell divisions later. Many questions remain open: is Xist RNA coating sufficient to trigger Xi structural reorganization in mouse preimplantation development? Is X-linked gene silencing sufficient to induce loss of TAD and mega-domain formation on the imprinted Xi?

2.3.4 Is DXZ4 region involved in mega-domain formation?

To investigate the importance of the DXZ4 region in the bipartite structure of the Xi, a deletion around the DXZ4 macrosatellite was achieved in two different cell types: in female mouse ESCs, subsequently differentiated (Giorgetti et al., 2016) and in a female human somatic cell line (RPE1 cells) (Darrow et al., 2016).

Loss of the DXZ4 boundary region causes a mega-domain disruption (Darrow et al., 2016) or even a fusion of the two large domains (Giorgetti et al., 2016), and might influence the histone modification patterns on the Xi (Darrow et al., 2016). However, it has no effect on Xi transcription (Darrow et al., 2016), even though silencing of some facultative escapees is observed in some clones (Giorgetti et al., 2016).

The mechanism of DXZ4 regulating Xi organization may be that DXZ4 region acts like a hub or an anchor that brings about the formation of superdomains (Darrow et al., 2016). Besides, DXZ4 has been proposed to anchor the inactive X to the nucleolus (Deng et al., 2015).

In summary, both Xist repression and the DXZ4 element contribute to the formation of Xi-specific conformation (Figure 11).

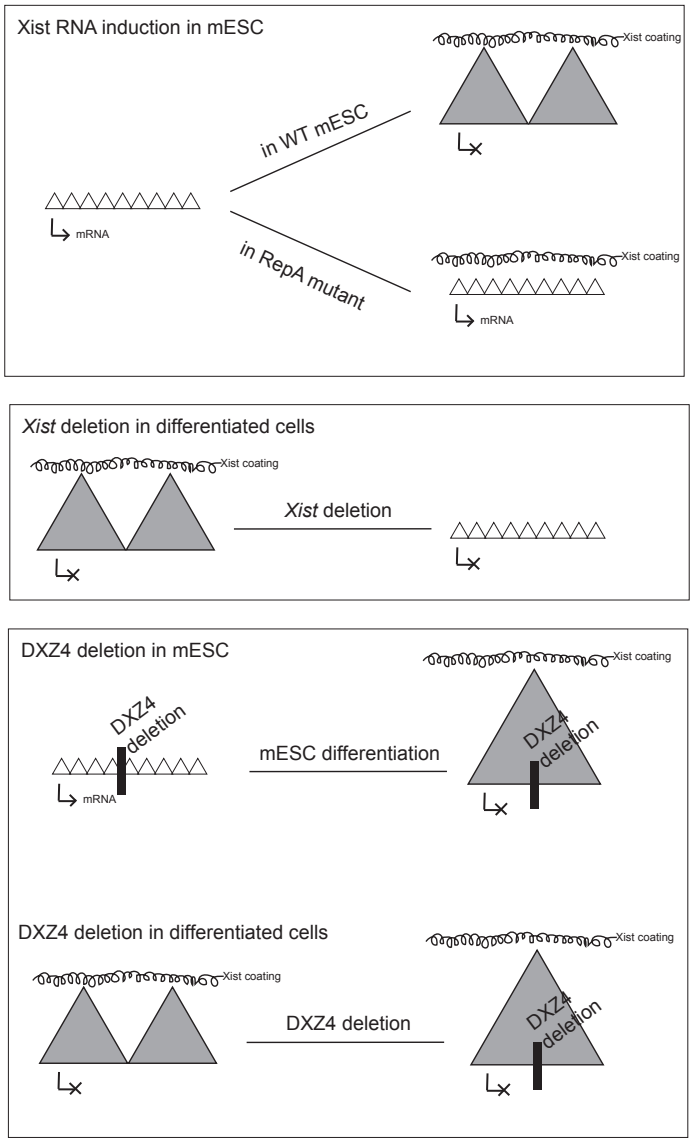

Figure 11 - Xist RNA and DXZ4 impact on Xi structure formation

Development of C-techniques has extended our understanding of genome architecture, highlighting nested hierarchical configurations from which TADs appear to be the most correlated to functional aspects such as regulatory landscapes. Disruption of TAD structure can eventually lead to gene misregulation and diseases. Albeit globally conserved, TAD structure is deeply refolded during random XCI. This dynamic process involves various events, including important chromatin modifications and gene silencing. Early preimplantation development is also a period of tremendous reorganization of the nucleus, its chromatin, and its transcription. How does the genome structure evolve during such reprogramming? When does this essential organization of the genome set up? Is it inherited from one generation to the other? Or is it reset after fertilization?

3. Genome organization in early embryo

At fertilization, two very specialized cells, the oocyte and the sperm, meet to give rise to a whole new individual. During preimplantation development, the newly fertilized egg - or zygote - needs to completely reprogram its inherited genome (or maybe one should say “genomes”) towards totipotency. The paternal genome inherited from sperm is strikingly different from its maternal counterpart as it is tightly condensed, packaged with protamines instead of histones (Braun, 2001). These are rapidly exchanged. Both parental genomes go through remarkably different programs of chromatin remodelling. Parental asymmetry is thus a feature of early embryonic genome.

Zygote proceeds to successive cell divisions, without cell growth (therefore termed “cleavages”), originally synchronous and thereafter asynchronous (Kelly et al., 1978, Johnson et al., 1986). Compaction subsequently occurs, reducing the space in between the blastomeres and increasing their surface area of contacts; divisions become asymmetrical and give rise to two populations, the ‘inside’ and ‘outside’ blastomeres. This segregation determines later distinct lineages of the embryo.

Hence, two differentiated and almost inactive gametes are converted into a transiently totipotent and soon transcriptionally active embryo. The zygote is a unique totipotent cell, which implies that it is proficient to contribute to all lineages in an organism. Pluripotency *per contra* refers to the competence of a single cell to differentiate into all three layers of the embryo but not into extra-embryonic tissues. Experimentally, totipotency has been tested by splitting the embryo into single blastomeres: blastomeres at the 2-cell (2C) stage in mice are also totipotent. Indeed “half-embryos” (obtained from single blastomeres of 2C stage embryos) develop normally and when transferred into recipients, they give rise to new individuals with normal phenotype and completely fertile (TARKOWSKI, 1959). On the contrary, “quarter-embryos” from 4-cell (4C) stage isolated blastomeres display an impaired development (TARKOWSKI, 1959). However single blastomeres at the 4C and 8-cell (8C) stages still manifest totipotency in aggregation chimaeras (Kelly, 1977). They may contribute to both embryonic and extra-embryonic tissues, but fail to support a viable conceptus because of reduced cell numbers at the blastocyst stage (Rossant, 1976). Experiment using transcription inhibitor in mouse embryos to investigate the timing and the link in between transcription and morphogenesis has suggested that transcription activation of embryonic genome is required for switching from totipotency to pluripotency (Kidder and McLachlin, 1985).

In point of fact, while the embryo undergoes transition from totipotency to pluripotency, developmental control is handed from maternally provided factors to the ones produced by the embryo itself: it is the maternal-to-zygotic transition (MZT). This transition is accompanied by broad remodelling of the embryonic genome.

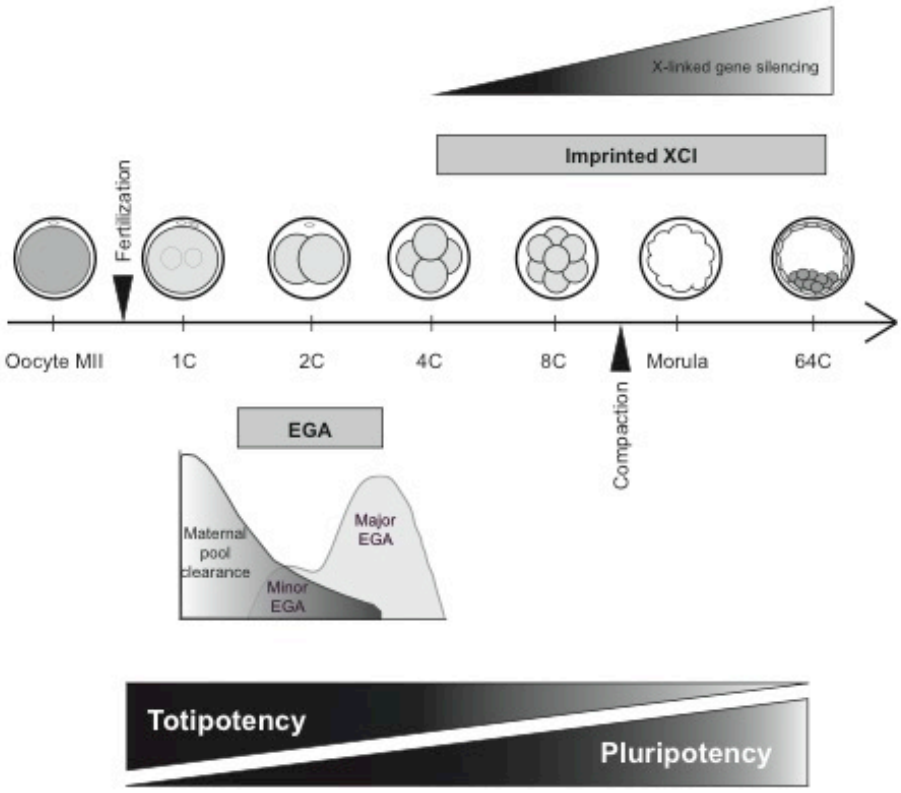

Figure 12 - Preimplantation development important time points and events

Therefore, the period of early development harbours a series of crucial events (Figure 12), leading the mammalian zygote to a fully grown blastocyst that is qualified for implantation and further development. Meanwhile, it has undergone its first differentiation that separates two lineages: the trophectoderm, that progresses to the placenta and the extra-embryonic tissues, and the inner cell mass that contains pluripotent cells which will give rise, *inter alia,* to the embryo proper. This implies a tremendous reorganization of the embryonic nucleus and genome, both at functional level with zygotic genome activation and at structural level with chromatin modifications and architecture remodelling.

In this chapter, I will first describe maternal-to-zygotic transition, enhancing features of early embryonic transcription; I will then detail the enormous reorganization occurring in the preimplantation nucleus and in its chromatin composition and structure.

3.1 Maternal-to-zygotic transition

Maternal-to-zygotic transition (MZT) starts right after fertilization and encompasses two parallel and complementary events (Tadros and Lipshitz, 2009): first the depletion in maternal mRNA pool, also termed maternal clearance; second, the initiation of embryonic transcription, usually referred as "Zygotic Genome Activation" (ZGA) (see for review (Lee et al., 2014, Jukam et al., 2017).

3.1.1 Maternal clearance

Depletion in maternal mRNA pool is triggered at fertilization. At the zygote and the 2C stage, as confirmed by single-cell RNA-seq data (Deng et al., 2014), mouse embryos contain mainly maternal RNA. Then, the maternal fraction progressively decreases to reach parity with paternal transcripts at 4C stage. Two forms of maternal mRNA clearance have been described: the maternal mode, relying on maternally provided factors and the zygotic mode depending on de novo transcription (Bashirullah et al., 1999). In mouse, the maternal mode is prominent and active shortly after fertilization (Pikó and Clegg, 1982). However, there is a second wave of clearance overlapping with the major ZGA (Deng et al., 2014, Hamatani et al., 2004). Yet, it is unknown if this second wave requires zygotic transcription for clearance. Factors that trigger decay of maternal mRNA remain elusive. Recently the maternal factor B-cell translocation gene-4 (BTG4) has been suggested to play a key role in maternal clearance (Liu et al., 2016b, Yu et al., 2016): mouse embryos lacking BTG4 arrest at the 1C or 2C stage and display a global delay in maternal mRNA degradation during the MZT. It has been suggested that BTG4 fosters mRNA degradation by promoting RNA de-adenylation (Liu et al., 2016b, Yu et al., 2016). Mechanisms underlying maternal mRNA clearance are still being unraveled.

3.1.2 Zygotic genome activation

When transcription is inhibited in early embryo, cell divisions are maintained until a certain stage that varies across species: zebrafish embryo stops at gastrulation (Kane et al., 1996), *D.melanogaster* embryo can't proceed to cellularization - the process that creates an individual cell membrane for each nucleus in the syncytial *Drosophila* embryo after several nuclear divisions (Edgar et al., 1986) while in mouse development progresses no further than the 2C stage (Golbus et al., 1973). While maternal RNAs and proteins support the first division(s), zygotic transcription is imperative for further embryonic development. The activation of the genome of the embryo otherwise until then silent is referred equally as either zygotic genome activation (ZGA) or embryonic genome activation (EGA).

Techniques used to explore zygotic genome activation are reported in Box 3.

Box 3 - Tools to explore zygotic genome activation

Several tools have been applied for ZGA investigation, from functional approaches to imaging and more recently RNA sequencing. Major difficulty in studying ZGA is to distinguish in between maternally inherited transcripts and newly embryonic transcripts: various strategies have been developed to overcome this question as discussed below.

RNA sequencing

While RT-PCR and microarrays used to give access to expression patterns of limited number of genes, nowadays RNA sequencing (RNA-seq) is a powerful tool that explores gene expression at a genome-wide level. Repeated RNA-seq experiments - at several time points - provide a useful overview of gene expression dynamics throughout development. The recent development of high-throughput single-cell RNA sequencing (Tang et al., 2009) has overcome the problematic sparsity of mammalian embryonic material, providing high-resolution information from a few individual cells and capturing cell-to-cell variability. In this approach, however, both the maternally inherited pool and the zygotic transcripts are detected and they can't be distinguished with certainty at early stages. Furthermore, in order to discriminate parental origin of the transcripts, one can use hybrid embryos from interspecific crosses (Deng et al., 2014, Borensztein et al., 2017): this is mandatory to study monoallelic expression in general or during specific processes such as X chromosome inactivation. To perform an allele-specific analysis of the dataset, fully sequenced strains and sufficient SNP (Single Nucleotide Polymorphism) density are required.

Functional approaches

Metabolic labeling

So as to distinguish in between maternally inherited RNAs and newly transcribed RNAs (Kageyama et al., 2004, Heyn et al., 2014), UTP analogs such as 5-bromouridine, 4-thiouridine or 5-ethynyl uridine may be added to culture medium or directly injected into embryos. Once labeled nucleotides are integrated into nascent RNAs, RNAs are extracted, de novo labeled RNAs are purified and sequenced. One should be cautious when selecting dosage of UTP analogs as they can be toxic at high doses (Burger et al., 2013), and embryo development and viability should be carefully monitored.

Drugs

Chemical inhibitors may be employed to block DNA replication, transcription, and translation in early embryos. For instance, α-amanitin, which inhibits RNA polymerase II, was used to block mRNA synthesis during preimplantation stage in the 1970s already (Warner and Versteegh, 1974). When treated with this inhibitor, mouse embryos would not develop beyond 2-cell stage, suggesting ZGA occurs at that period in mouse. RNA levels from treated and untreated embryos may be compared. Other drugs are widely utilized such as aphidicolin (for DNA replication inhibition), actinomycin D or triptolide (for RNA

transcription inhibition), cycloheximide (for protein translation) (Uh and Lee, 2017). One should select the appropriate dosage and timing of treatment.

RNA FISH and imaging

At the single cell level, RNA FISH can unveil active transcription through nascent transcript visualization thanks to fluorescently labeled probes. RNA FISH thus helps in reporting RNA provenance as it detects only de novo transcription. We precisely described this technique for mouse preimplantation embryo in a recent publication in Methods in Molecular Biology (Ranisavljevic et al., 2017) enclosed in Material & Methods.

Maternal or zygotic transcripts?

Several approaches have been deployed for attributing transcriptome in early embryo to maternal or zygotic origins, by emphasizing or removing zygotic transcripts (see for review (Lee et al., 2014)). Thus to identify de novo zygotic transcripts, two main strategies may be used:

- To deplete zygotic signal relative to the maternal pool:
    - transcription can be globally blocked using chemical treatments to inhibit RNA pol II (discussed above);
    - large chromosomal deletions in *D.melanogaster* or *C.elegans* mutants remove the zygotic contribution for the genes falling in the deleted region (De Renzis et al., 2007, Storfer-Glazer and Wood, 1994).
- To enrich zygotic signal relative to the maternal pool:
    - subtractive hybridization (with biotinylated antisense oligos constructed from oocyte cDNA libraries) selectively depletes complementary maternal transcripts (Zeng and Schultz, 2003). This is accurate for several transcripts but inappropriate for genome-wide analysis.
    - De novo zygotic transcripts can be labeled with modified ribonucleotides or nucleoside analogs (such as 4-thiouridine) associated with subsequent pull down by biotinylation (Heyn et al., 2014).
    - Zygotic transcripts can be identified by properties unique to the zygotic form such as presence of paternal reads (discussed above) or zygotic-specific transcript isoforms (generated by alternative splicing (Aanes et al., 2013), alternative transcription start sites (TSSs) detected with cap analysis of gene expression (CAGE) (Haberle et al., 2014), polyadenylation (Ulitsky et al., 2012). Alternatively, after depleting the total-RNA libraries from ribosomal RNA, zygotic transcripts can be identified as containing introns, that are absent from mature maternal pool (Lee et al., 2013).

These approaches have helped in establishing which genes are the first to be transcribed during zygotic genome activation.

Box 3 - Tools to explore zygotic genome activation

3.1.2.a Two major transient waves of de novo transcription in preimplantation embryo

The zygotic transcription program consists of alternatives waves (Hamatani et al., 2004, Wang and Dey, 2006, Park et al., 2013). The first wave corresponds to ZGA and happens in mouse from late 1C to late 2C - 4C stages, leading to the most marked genetic reprogramming. Then a second wave, termed mid-preimplantation gene activation (MGA), takes place around 4C to 8C stage and precedes the dynamic structural and functional transition from the morula to blastocyst stage. Many genes are expressed at a specific stage while some genes are transcribed throughout pre-implantation development. Major changes occur in transcription profile as embryonic requirements evolve, while differentiation processes, to allow further harmonious development. This creates transcriptional signatures for cells at a specific developmental stage (Zeng et al., 2004, Hamatani et al., 2004, Xue et al., 2013). ZGA wave can be again divided in two phases (Flach et al., 1982): a minor phase of ZGA is initiated at the late 1C stage (see below 5.1.2.b) with weak transcriptional activity and a major phase of ZGA occurs at the late 2C stage with acute and intense transcriptional activation.

In zygotes and 2C stage embryos, genes related to basic biological processes such as ribosome, transcription regulation, ribonucleoprotein complex, RNA binding, cell cycle, protein metabolism, are highly transcribed. These transcripts decrease from the 4C to the 8C stage. In 8C stage embryos, the transcriptional signature involves genes related to transport, biosynthesis, transcription and translation, intercellular junction. This indicates a sequential order of transcriptional changes in pathways of critical biological processes, acting in a step-wise mode throughout development (Xue et al., 2013, Zeng et al., 2004, Hamatani et al., 2004).

3.1.2.b Transcription in minor ZGA in a promiscuous and enhancer-independent fashion

Nuclei transplant experiments in enucleated early or late zygotes have suggested that the embryonic cytoplasm switches from a transcriptionally non-permissive to permissive state during the first cell cycle and prior to initiation of zygotic gene expression (Latham et al., 1992). This permissive state of the zygote is associated with unusual transcriptional regulation: studies using plasmid-borne reporter genes reveal that enhancer is not required for proper reporter gene expression in zygotes, whereas 2C stage embryos necessitate enhancers for efficient expression (Wiekowski et al., 1991). Moreover, this transition in transcriptional regulation involves DNA replication: indeed, 2C stage embryos treated with aphidicolin, a DNA replication inhibitor, recapitulate reporter gene expression in an enhancer-

independent fashion, unlike untreated embryos at the same stage (Wiekowski et al., 1991). Transcription in 1C embryos can also initiate independently of well-characterized core-promoter elements (Abe et al., 2015). Transcriptional regulation in minor ZGA is thus very different, and reflects a cytoplasmic permissive state.

Besides, the first embryonic transcripts are detected in the paternal pronucleus during G2, as suggested by luciferase reporter gene expression in injected zygote (Ram and Schultz, 1993) and as assessed by BrUTP incorporation (Bouniol et al., 1995, Aoki et al., 1997).

More recently, a study based on total RNA sequencing in mouse embryos shows that pervasive transcription occurs in zygotes (Abe et al., 2015), encompassing genic and intergenic regions. Intergenic regions are extensively expressed in the zygote : this stage of development displays the highest frequency of retrotransposon-derived reads among all the stages, involving all classes of repetitive elements. Among them is type L mouse endogenous retrovirus (MuERV-L). As previously described, MuERV-L is transcribed from the beginning of S phase, and is among the first genes to be expressed (Kigami et al., 2003). MuERV-L expression is not inhibited by aphidicolin, suggesting that its expression is controlled by the zygotic clock. MuERV- L might play an important role in the development of mouse embryos at the early preimplantation stage as antisense oligonucleotides block development after the 4C (Kigami et al., 2003).

Furthermore, transcripts from 1C stage are mostly nonfunctional because their 3' end processing and splicing are highly inefficient (Abe et al., 2015).

In brief, minor ZGA starts in paternal pronucleus, display an unusual transcriptional regulation with a very permissive state and a pervasive transcription that includes repetitive elements such as MuERV-L which expression is essential for further development.

3.1.2.c Repetitive elements and maternal factors are key-players of ZGA

A significant fraction of the mammalian genome consists of repetitive transposable elements (see Figure 13), and many are known to be expressed in early mouse embryo (Peaston et al., 2004, Kano et al., 2009). Shortly after fertilization, transcription of repetitive elements is triggered and peaks during the 2C stage with mainly LINE-1; by the time of implantation, most repetitive elements will be repressed (Fadloun et al., 2013). In addition, the long terminal repeat of MuERV-L acts as alternative promoter and first exons for a subset of host genes: it is thought to drive transcription of several EGA genes in embryos (Peaston et al., 2004).

<table>
<tr><th colspan="5">TRANSPOSABLE ELEMENTS</th><th>Recent transposition events</th><th>% of genome</th></tr>
<tr><td rowspan="6">CLASS I
Retrotransposons</td><td>LTRs
i.e. ERV-IAP, ERV-L</td><td colspan="3"></td><td>Yes</td><td>10%</td></tr>
<tr><td rowspan="5">non-LTRs</td><td>SINEs</td><td colspan="2"></td><td>Yes</td><td>8%</td></tr>
<tr><td rowspan="4">LINEs</td><td>V type promoter</td><td></td><td>No</td><td rowspan="4">19%</td></tr>
<tr><td>A type promoter</td><td>Af family
~5300 FL*</td><td>No</td></tr>
<tr><td rowspan="2">F type promoter</td><td>Gf family
~1000 FL*</td><td>Yes</td></tr>
<tr><td>Tf family
~4500 FL*</td><td>Yes</td></tr>
<tr><td>CLASS II
DNA transposons</td><td colspan="4"></td><td>No</td><td>0,9%</td></tr>
</table>
*FL – full length

Figure 13 - Overview of the genomic content of transposable elements in the mouse genome (as in (Jachowicz and Torres-Padilla, 2016))

Major zygotic activation relies also on maternally inherited factors, transmitted either as proteins or transcripts stored in oocytes. Numerous maternal factors have been identified, using knock-out or knock-down models showing arrested progression during cleavage-stage embryogenesis; they are encoded by maternal-effect genes. The first two maternal-effect genes described in mouse are *Hsf1* (Christians et al., 2000) and *Mater* (Tong et al., 2000). Heat shock factor 1 (HSF1) is a master regulator of stress-inducible genes; when maternally depleted, it leads to developmental arrest at the 1C stage (Christians, 2000). *Mater* (for maternal antigen that embryos require; or *Nlrp5*) was originally characterized as an antigen associated with a mouse model of autoimmune oophoritis. It is is essential for embryonic development beyond the 2C stage (Tong et al., 2000). The number of maternal factors identified in the past years is constantly increasing. These maternal factors are also thought to act as transcription factors (i.e. *Oct4/Pou5f1* (Foygel et al., 2008)) and to be involved in maternal clearance (i.e. *Dicer* (Murchison et al., 2007)), genome activation, DNA methylation (i.e. *Dnmt3L* (Bourc'his et al., 2001)), chromatin remodelling (i.e. *Tif1alpha* (Torres-Padilla and Zernicka-Goetz, 2006)). In my result section, I will present a publication from our lab related to one of these maternal factors *Lsd1/Kdm1a*, a histone lysine demethylase involved in chromatin remodelling in the early embryo (Ancelin et al., 2016).

In brief, while numerous maternal factors fill the gap in between oocyte and embryonic gene transcription, repetitive elements drive transcription of several EGA genes in embryos. Both appear essential for correct genome activation as well as for correct reprogramming and subsequent development.

3.1.2.d Mechanisms underlying the temporal regulation of transcription in embryos

Several models of ZGA timing have been suggested, mainly described for *Xenopus* and *Drosophila* models, but none of them can fully explain the temporal regulation for embryonic transcription activation (for review see (Pálfy et al., 2017)). These models are not mutually incompatible and they probably exist simultaneously: among them there are cell cycle length regulation, transcriptional repressors and activators, chromatin competency.

Besides, to gain access to silent genes that are not yet programmed, some binding factors - such as Fox-A and GATA-4 in liver precursor cells in embryos - are able to bind their specific sites, even in compact chromatin, and capable of initiating chromatin opening (Cirillo et al., 2002): they are hence referred as “pioneer factors” (Zaret and Mango, 2016). Such maternally inherited factors have long been known in non-mammalian species for early development; for example, the zinc-factor protein Zelda is a key activator of EGA in *Drosophila melanogaster*. Mutant embryos lacking Zelda fail to activate properly many genes and display an abnormal development (Liang et al., 2008).

The mammalian equivalents of these pioneer factors are not fully characterized. However, recent studies suggest the DUX transcription factors as new regulators of mammalian EGA (Hendrickson et al., 2017, De Iaco et al., 2017, Whiddon et al., 2017). These conserved factors in mouse and human (Hendrickson et al., 2017, Whiddon et al., 2017), seem to activate many genes and retroviral elements (MuERV-L/HERV-L family) and a depletion of Dux achieved by CRISPR-Cas9 injections in mouse zygote leads to impaired early embryonic development and defective ZGA (De Iaco et al., 2017). Furthermore, induced Dux overexpression converts mESC in 2C-like cells. Mouse ESCs cycle into a 2C-like state in which a significant proportion of the transcriptome of 2C-stage embryos is activated (Macfarlan et al., 2012, Ishiuchi et al., 2015). 2C-like cells are identified by reactivation of MuERV-L (Macfarlan et al., 2012). ATAC-seq achieved in 2C-like cells obtained after Dux overexpression displays an open chromatin landscape resembling that of 2-cell mouse embryos (Hendrickson et al., 2017) (for ATAC-seq in early embryo, see (Wu et al., 2016)). Thus a single transcription factor is capable of changing deeply global chromatin organization and remodels the chromatin landscape into one resembling the 2C stage embryo, suggesting a role for DUX in chromatin opening, in line with its role as a pioneer factor. However, the mechanisms leading to Dux expression *in vivo* is unknown and an upstream pioneer activator may be involved. The trigger of ZGA first events remains mysterious.

3.2 Nuclear architecture dynamics in preimplantation embryo

ZGA, this “transcriptional reorganization”, is associated with a huge structural reorganization that remodels the whole nucleus during preimplantation development. For instance, drastic changes are observed in pericentric heterochromatin organization - with a transition from nucleolar-like bodies to chromocenters, in chromosome positioning or at the nuclear envelope.

3.2.1 An atypical nuclear architecture: the nucleolar-like bodies (NLB)

A characteristic feature of mouse somatic cell nuclei is the chromocenters, which are consistent with clusters of pericentric heterochromatin from several chromosomes. Chromocenters, visualized as bright spots of DNA-specific dyes, are surrounded by centromeres (Cerda et al., 1999). These chromocenters are not observed in early embryo. Instead, the interphase nuclei of 1C and 2C stage embryos (Martin et al., 2006), just as in fully grown oocytes (Bonnet-Garnier et al., 2012), display a specific nuclear architecture : the nucleolar-like bodies (NLBs) (Figure 14). NLBs are spherical membrane-free structures that harbor centromeric and pericentromeric heterochromatin.

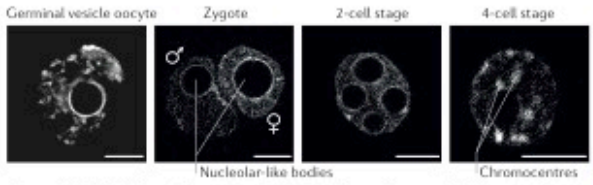

Figure 14 - From NLBs to chromocenters (as in (Burton and Torres-Padilla, 2014)
Confocal sections of DAPI (4',6 - diamidino - 2 - phenylindole) - stained nuclei of a germinal vesicle oocyte, zygote, early 2C stage and 4C stage mouse embryos. Scale bar represents 10µm.

Right after fertilization, nuclear organization of the two parental inherited genomes is different. While pericentromeric regions quickly organize around the NLBs in the female pronucleus (PN), they remain clustered together, forming central masses in the paternal PN (Aguirre-Lavin et al., 2012). It is only by the late zygote stage that this parental asymmetry disappears when both PN centromeric regions display similar “shell” or ring-like organization (Probst et al., 2007). During the 2C stage, the size of NLBs increases while their number decreases, suggesting a fusion process. Subsequently, one of the most visible reorganization of the centromeric and pericentromeric heterochromatin takes place: by the late 2C stage this heterochromatin starts to condense, and by the 4C stage, it is fully

dissociated from NLBs and chromocenters are distributed over the nucleoplasm (Aguirre-Lavin et al., 2012). Timing of chromocenter formation coincide with ZGA in mouse as well as in bovine embryos suggesting that chromocenters might be linked to genome activation (Martin et al., 2006).

Enucleolation of the oocyte or the early zygote impairs subsequent embryonic development with a 2C-stage arrest TFTZ (Ogushi et al., 2008, Fulka and Langerova, 2014), suggesting that NLBs are essential for early embryonic development in mammals. However, when NLBs are removed from late-stage zygotes, the enucleolated embryos develop normally, as *de novo* formation of nucleoli occurs after several divisions (Kyogoku et al., 2014), suggesting that NLBs are not necessary for nucleolus formation and ribogenesis.

In contrast, NLBs might play a role in heterochromatin formation after fertilization as suggested by abnormal remodeling of the centric and pericentric regions in zygotes after enucleolation (OGUSHI and SAITOU, 2010). Besides, another study shows that the H3.3 histone chaperone DAXX fails to stably bind to DNA in nucleolus-less zygotes (Fulka and Langerova, 2014). H3.3 is indeed thought to be specifically necessary for the remodelling of centromere heterochromatin (Santenard et al., 2010). The actual mechanisms underlying regulation of heterochromatin formation by NLBs remain unclear.

To conclude, NLBs appear to be major organizers of embryonic nuclear architecture, with a possible role in regulating or establishing heterochromatin after fertilization.

3.2.2 Chromosome positioning

At the chromosomal scale, positioning in the nucleus also appears to be dynamic and changing. 3D DNA FISH achieved in bovine embryos with chromosome painting probes assesses that gene-rich chromosome 19 and gene-poor chromosome 20 have similar radial distribution up to the 8C stage. However, at the 10C to 16C stage, concomitantly with bovine ZGA, a significant difference sets up as chromosome 19 localizes more internally and chromosome 20 more at the periphery, as what is usually observed in somatic cells (Koehler et al., 2009). This finding corroborates a temporal correlation between transcriptional activation and a major rearrangement of chromosome positioning in blastomere nuclei in bovine embryos.

3.2.3 Modifications at the nuclear envelope

Another example of structural changes mirroring transcriptional modifications is related to the nuclear membrane re-organization. As illustrated by 3D DNA FISH and superresolution microscopy experiments in bovine embryos (Popken et al., 2015), nuclear pore complexes are not uniformly distributed before ZGA: they are restricted to parts of the nuclear envelope in contact with DNA. After ZGA, DNA contacts the whole lamina uniformly and therefore nuclear pore complexes distribution becomes uniform.

Thus zygotic genome activation coincides in time with nuclear reorganization from an "embryonic specific state" to a "somatic-like state" as shown for chromocenters, radial distribution of chromosomes and contact to lamina.

3.3 Dynamic changes in preimplantation embryo chromatin

As the newly formed embryo starts its journey through reprogramming, genome activation, and further differentiation, its nucleus is progressively restructured. Dynamic changes with respect to chromatin also mark preimplantation development process at two levels: locally by regulating the expression of specific genes but also globally by generating a permissive or a repressive chromatin environment.

3.3.1 Dynamics of chromatin accessibility through early development

Electron spectroscopic imaging is a powerful tool to visualize directly the ultrastructural changes in chromatin during the transition from a totipotent zygote to a pluripotent blastocyst (Ahmed et al., 2010, Bošković et al., 2014). While in the zygote chromatin is extensively dispersed, major changes occur from 1C to 2C stage embryos: chromatin forms discrete compact blocks and the nuclear envelope along with the surface of NLBs behave as compartments where chromatin concentrates. After transiting through an intermediate state at 4C stage, chromatin becomes highly dispersed by the 8C, similar to the pattern observed in ESCs. Distribution of chromatin fibers is then more uniform. Moreover, at the 8C stage, the level of ribonucleoproteins is greatly increased, nearly filling the space between the dispersed chromatin, demonstrating high degree of transcription (Ahmed et al., 2010). This highly dispersed chromatin is a common feature of pluripotent cell nuclei as it is also described in epiblast but not in lineage-committed cells such as trophectoderm and primitive endoderm where it gets more compact. Dispersed state in epiblast cells is

subordinate to pluripotency as *in vivo* deletion of the key pluripotency factor Oct4 induces broad chromatin compaction in epiblast cells (Ahmed et al., 2010).

Similarly, histone mobility remarkably evolves through transition toward pluripotency. This was described thanks to fluorescence recovery after photobleaching (FRAP) experiments achieved in the developing mouse embryo (Bošković et al., 2014). While mobility of the core histones H2A, H3.1, and H3.2 is unusually high in 2C stage embryos, it decreases as development proceeds. Again upon lineage allocation, pluripotent cells retain higher mobility than the differentiated trophectoderm (Bošković et al., 2014). Thus, these FRAP data demonstrate that totipotent chromatin is more “open” and it gradually closes as the cells convert from totipotency to pluripotency.

These two examples outline how plastic the chromatin is during early development and how dynamic the changes of chromatin structure are, linked to cellular potency and fate.

Recently, global chromatin landscape and its dynamics during preimplantation development were explored by an improved assay for transposase-accessible chromatin with high throughput sequencing (ATAC-seq) approach, adjusted for low-input of material (Wu et al., 2016). ATAC-seq enables identification of open versus closed chromatin genome wide using hyperactive Tn5 transposase, which inserts sequencing adapters into accessible regions of chromatin. Sequenced reads are subsequently used to infer regions of increased accessibility (Buenrostro et al., 2015). Early 2C embryos display a unique status with non-canonical broad open domains over loci containing repetitive DNA, which are transcriptionally active at this stage, such as SINEs and ERV-Ls. From the 2C stage onward, these broad accessible domains are lost and repressive chromatin state is established along with sharp open chromatin peaks over promoters and cis regulatory elements. A strong correlation is observed in between gene activation kinetics through development and ATAC-seq signal dynamics at promoters of these genes (Wu et al., 2016). Hence, chromatin accessibility in early embryos is extensively dynamic, first occurring at transposable elements with an unusual permissive chromatin state, thereby facilitating ZGA and the remodelling of gametes into totipotent embryos. This is consistent with a pervasive transcription, enhancer-independent, at the time of minor ZGA. These changes could be involved in establishing further chromatin landscape (Abe et al., 2015).

Besides, another assay investigated chromatin accessibility, through low-input DNase I sequencing (DNase-seq) that allows mapping of DNase I-hypersensitive sites (DHSs) in mouse preimplantation embryos (Lu et al., 2016). DNase-seq combines sensitivity to the nonspecific endonuclease DNase I with high-throughput sequencing to identify regions of

regulatory DNA on a genome-wide scale (John et al., 2013). DHSs are progressively established during development and largely maintained once established with a drastic increase at the 8C stage. Indeed, DHSs can mark promoters either actively transcribing or primed for subsequent activation. Moreover, a former study comparing DHS maps in various cell lines indicates that the number of DHSs is positively correlated to pluripotency (Stergachis et al., 2013). Nonetheless, it is surprising and counter-intuitive to find fewer DHSs in early stages when chromatin is described as dispersed and less densely packaged. One can speculate that relaxed chromatin imaged in 1C embryos may outline reduced higher-order chromatin structure rather than reduced density of nucleosome occupancy. This DNase I sequencing puts in perspective the dynamics of regulatory landscape establishment during early development (Lu et al., 2016).

A recent study with a targeted epigenomic approach demonstrates that premature silencing of LINE-elements decreases chromatin accessibility, whereas prolonged activation inhibits chromatin compaction that normally occurs progressively during development (Jachowicz et al., 2017). Timely activation and then repression of LINE-1 elements is required for efficient preimplantation development. LINE-1 elements might therefore be a regulator of global chromatin accessibility in preimplantation embryo (Jachowicz et al., 2017).

Taken together, these findings suggest that initial transcription of retrotransposons (such as LINE, SINE, MuERV-L) is essential for regulating chromatin accessibility in early embryo and its subsequent ZGA.

3.3.2 Choreography of chromatin remodeling

Chromatin accessibility is hence a dynamic feature of the preimplantation genome that is escorted by several types of chromatin remodeling such as DNA methylation or histone tail modifications. Their precise effects on transcription and on ZGA remain unclear. However, several examples of manipulating of histone modification enzymes in early development outline how impaired chromatin reprogramming can lead to misregulated expression and failure in further development.

Two main types of histone modifications have been studied and are thought to be engaged in shaping gene expression during early development: lysine acetylation and lysine methylation. Several IF studies (for review (Burton and Torres-Padilla, 2010, Burton and Torres-Padilla, 2014)) and more recently some ChIP-seq studies (Dahl et al., 2016, Zhang et al., 2016, Liu et al., 2016a, Zheng et al., 2016) have described the genome-wide

reprogramming of histone modifications in mouse gametes and early embryos. They highlight atypical patterns of chromatin marks with parental asymmetry, along with highly dynamic remodeling after fertilization and during early development.

Histone H3 lysine 4 trimethylation (H3K4me3) is an active mark normally found in sharp peaks at transcription start sites (TSS); however non-canonical broad domains of H3K4me3 (Dahl et al., 2016, Zhang et al., 2016, Liu et al., 2016a) are encountered in fully grown oocytes and cover more than 20% of the genome (Dahl et al., 2016). They anti-correlate with DNA methylation (Dahl et al., 2016, Zhang et al., 2016) and have been suggested to play a role in genome silencing during oogenesis (Andreu-Vieyra et al., 2010).

H3K4me3 in MII oocytes and zygotes may mark permissive promoters that are either recently transcribed or poised for future activation. H3K4me3 is also enriched in non-promoter regions such as in repeats (particularly SINE and ERV) that are highly expressed in early embryos (Zhang et al., 2016).

While an extensive reprogramming occurs upon fertilization in the paternal genome that is depleted of H3K4me3 marks in the zygote, non-canonical broad domains of H3K4me3 are inherited and persist in zygotic and early-2C maternal genome (Zhang et al., 2016). Such parental differences of H3K4me3 in zygotes corroborates previous immunofluorescence experiments showing asymmetric H3K4me3 signals (Lepikhov and Walter, 2004). As a matter of fact, whereas maternal chromatin maintains all types of histone H3 methylation throughout the zygotic development, paternal chromosomes acquire new and unmodified histones shortly after fertilization when protamines are removed and replaced by maternally inherited hypomethylated and hypoacetylated histones.

From late-2C stage embryo, concurrent with ZGA, H3K4me3 becomes confined to TSS (Zhang et al., 2016, Dahl et al., 2016): its enrichment strongly correlates with transcription level (Zhang et al., 2016, Liu et al., 2016a). Switch from non-canonical to canonical H3K4me3 distribution is transcription dependent - as alpha-amanitin treatment (RNA polymerase II inhibitor) prevents it - and appears to be an active process and not a simple passive dilution in cell division - as aphidicolin (DNA replication inhibitor) does not impede this switch of distribution (Zhang et al., 2016). H3K4 demethylases - and more specifically KDM5B - are crucial for active removal of non-canonical H3K4me3 broad domains, as demonstrated by depletion experiments (Dahl et al., 2016, Liu et al., 2016a). Depleted embryos conserve the non-canonical H3K4me3 broad domains, display aberrant transcription for ZGA genes and fail to develop to the blastocyst stage. KDM5B are thus required for proper ZGA and further development. In the paternal genome, H3K4me3 also

reappears from the late-2C stage but not as strongly as in the maternal genome: this parental asymmetry persists until the blastocyst stage (Zhang et al., 2016).

Histone H3 lysine 27 trimethylation (H3K27me3) in oocyte is also highly pervasive, in regions depleted of transcription and DNA methylation. At fertilization, there is a global erasure of sperm H3K27me3 but inheritance of distal H3K27me3 from oocytes (Liu et al., 2016a, Zheng et al., 2016). H3K27me3 tends to accumulate after H3K4me3 (Liu et al., 2016a): H3K27me3 is re-established at promoters in post implantation embryos. Some bivalent sites harbouring both H3K4me3 and H3K27me3 are found in ICM but are infrequent, unstable and transient, unlike in ESC (Liu et al., 2016a, Zheng et al., 2016).

Unlike H3K4me3, histone H3 lysine 27 acetylation (H3K27ac) increases strongly from oocytes to 2C-stage embryos (Dahl et al., 2016). In the mouse zygote, permissive H4 acetylation has been found to distinguish transcriptionally active paternal PN from silent maternal PN: shortly after fertilization, the paternal genome is hyperacetylated, during the time window when it exchanges protamines with maternally inherited histones that are hyperacetylated (Adenot et al., 1997).

Parental genome asymmetry is also reported for DNA methylation of cysteine residues, which is generally associated with transcriptional repression (Meissner et al., 2008). In the mouse embryo, immunofluorescence staining experiments revealed that the paternal genome is demethylated within 6–8 hours of fertilization, before the onset of DNA replication, whereas maternal genome is gradually demethylated during the second and third cleavage stages (Mayer et al., 2000). This parental asymmetry remains in place up to the 4C-stage and its loss involves a passive mechanism, at each DNA replication (Rougier et al., 1998). More recently, several studies characterize genome-wide profiles of DNA methylation and assess that active DNA demethylation is not restricted to the paternal genome as previously suggested (Mayer et al., 2000), and that active demethylation - depending among others on 5mC oxidation by Tet dioxygenases and excision of oxidized bases by thymine DNA glycosylase - occurs already in the zygote (Wang et al., 2014, Guo et al., 2014, Shen et al., 2014, Peat et al., 2014). However, the exact function of this massive wave of DNA demethylation regarding ZGA remains mysterious. Indeed, despite extensive parental asymmetry in DNA methylomes, chromatin accessibility assessed by ATAC-seq or DNase-seq is globally comparable in between paternal and maternal genomes, except for some imprinting gene promoters (Wu et al., 2016, Lu et al., 2016). The precise effects of methylation status on transcription of individual genes in early embryo are unclear.

3.4 Three-dimensional chromatin structure reprogramming in preimplantation embryo

After fertilization, the two unipotent gametes undergo an extensive reprogramming to form a totipotent embryo. As shortly described, this reprogramming implies some drastic nuclear reorganization and large-scale chromatin modifications. As previously discussed (see 2.2), higher-order chromatin organization - and more specifically TADs and other sub-megabase scale domains - may have fundamental roles in regulating gene expression. How three-dimensional chromatin structure is transmitted from the gametes, and how it is remodelled through fertilization and early development, in particular in the context of transcriptional activation at ZGA, are fundamental questions in development.

Hug and colleagues recently explored the onset of genome architecture during *Drosophila melanogaster* embryogenesis (Hug et al., 2017). Before ZGA, the genome is mostly unstructured. Chromatin conformation is established at the onset of ZGA and maintained during subsequent development: TAD boundaries are associated with active transcription and open chromatin, they are enriched in chromatin active marks and binding sites for architectural proteins and Zelda. TAD establishment is independent of transcription, however inhibition of transcription alters chromatin conformation. Transcription factor Zelda is required for locus-specific TAD boundary insulation.

As I was preparing my thesis manuscript, several studies were also published (notably in July 2017) relative to this topic. I will introduce them briefly here and review their results thoroughly in my discussion.

Flyamer and colleagues developed a single nucleus HiC protocol to investigate genome conformation in mouse oocytes and zygotes (Flyamer et al., 2017). Notably, they found that TADs and loops, but not compartments, are present in the zygotic maternal genome.

Du and colleagues (Du et al., 2017) together with Ke and colleagues (Ke et al., 2017) studied genome organization during mouse early development using a low input in situ HiC protocol.

	DU ET AL., NATURE 2017	KE ET AL., CELL 2017
TECHNIQUE	In situ HiC low in put	In situ HiC low in put
HYBRID EMBRYOS	C57BL/6N x PWK/PhJ	C57Bl6/J x DBA/2J
STAGES	Oocytes MII, sperm, PN5 1C, early 2C, late 2C, 8C, ICM	Sperm, MII, PN4 1C, 2C, 4C, 8C, E3.5 and E7.5
OOCYTE MII	No TAD	No TAD
1C AND 2C	weak TADs, sparse distal interactions. More maternal TADs.	mainly very short range interaction, poor organization (weak TAD boundaries)
LATER STAGES	gradually more evident as development proceeds, with increasing insulation; in ICM 80% overlap with TADs observed in ESC	TAD reorganization from 4C to E7.5+++
COMPARTMENT ANALYSIS	Present as early as in zygotes for the paternal genome, followed by further segregation of compartments A and B on both alleles in preimplantation development	Weak compartments at 1C and 2C, and even weaker in maternal PN (1C). Some differences for A/B allocation in early embryos. Example of imprinted gene DLK1 with allelic difference.
ALIGNED TO DATASET	Aligned with RNAseq and ATACseq	With RNAseq: compartment switching, with DNA methylation: unmethylated CpG enriched in A compartment in promoter and gene, with DHS map: DHS enriched in A compartment, with ChIPseq: no association in between H3K4me3 broad domains and compartments.
DRUG TREATMENT	Alpha amanitin treatment: TADs continue to consolidate. TRANSCRIPTION INDEPENDENT.	Aphidicolin treatment (blocking DNA replication) at 2C for 2 days: no TAD strengthening. Alpha amanitin treatment (RNAseq+BrdU validation): TAD strengthening. TRANSCRIPTION INDEPENDENT.
NOTES	Parental genome segregation until 8C in the nucleus, differential chromatin organization at early stages: PN3/PN5 fewer paternal distal interaction (“more relaxed chromatin”?)	

Table 2 - Main findings from two recent publications on structure organization in early mouse embryos

These recent results highlight the dynamic and asymmetric genome organization of preimplantation development. However, a number of important questions still remain unanswered, notably in the context of the process of XCI.

To conclude, the advent of C-techniques has revolutionised our understanding of genome organization, highlighting fundamental layers of chromatin structure and their essential roles in gene expression regulation. Development of low-input or single-cell C-techniques provided interesting tools to inquire about genome organization at the onset of development, when the sparsity of material is a major limitation. The embryonic genome after fertilization is uniquely plastic and dynamic. It is an interesting and important setting in which to study the interplay between transcription and chromatin structure, for example as the zygotic genome become activated, or as genes become silenced during imprinted X chromosome inactivation.

RESULTS

As an MD specialized in gynaecology and obstetrics - and more specifically in reproductive medicine, I became deeply interested in mammalian preimplantation development. During this unique period in life, two parental genomes, inherited from highly differentiated cells, undergo a tremendous reprogramming towards totipotency and pluripotency. The cascade of events involved in genome remodelling and concomitant zygotic genome activation is essential for proper subsequent development.

When I started my PhD, I was therefore pleased to join Katia Ancelin to work on a LSD1/KDM1A project, in which I took my first steps in learning to handle mice and to manipulate mouse embryos. LSD1/KDM1A is a histone lysine demethylase involved in H3K4me1 and 2 demethylation, along with H3K9me2 demethylation. We were curious to know how this maternal factor was involved in early development and notably if such a chromatin remodeler is crucial for reprogramming, right after fertilization. Our embryonic model, deficient for maternally deposited LSD1/KDM1A, enabled us to observe the impact of the absence of this chromatin modifier on very early embryonic chromatin landscape. How does deficient epigenetic reprogramming lead to defeated ZGA and thus susbequent developmental arrest? We observed abnormal H3K4 and H3K9 methylation patterns, as well as failure in development and transcriptional misregulation. This encompassed both zygotic genome activation impairment and failure in proper LINE-1 retrotransposon silencing. The results of this work are published and presented in **Article 1 - Maternal LSD1/KDM1A is an essential regulator of chromatin and transcription landscapes during zygotic genome activation.** To explore transcriptional activation in early development, we employed RNA FISH technique in mouse embryos. This approach can assay the expression of specific genes or genetic elements during preimplantation development, in particular during the maternal-to-zygotic transition. It is thus a powerful tool to describe gene expression at the single cell level with such limited amounts of material available. We have published an article describing this method: it is enclosed in my Material and Methods section and is entitled **RNA FISH to Study Zygotic Genome Activation in Early Mouse Embryos**.

After working on genome remodelling at the chromatin level, I decided to move into the more structural aspects of genome re-organization occurring during preimplantation development. This was an exciting time, as the Heard lab had just recently discovered TADs in their work on the Xic) (Nora et al., 2012), and so I became interested in exploring the timing and importance of TADs in pre-implantation development. At the time I began my PhD project, it was aimed at deciphering genome architecture, and more specifically X-

chromosome spatial structure, during early mouse embryo development, particularly in the context of zygotic genome activation and imprinted X chromosome inactivation. For this purpose, I have combined two complementary approaches.

First, we inquired if we could detect TADs in mouse preimplantation embryo using DNA FISH with super-resolution microscopy. We explored the region in the Xic that Elphège Nora had previously investigated in mESCs (Nora et al., 2012) using a DNA FISH protocol specially designed for preimplantation embryos (adapted from (Koehler et al., 2010) - see Material & method section). We could observe at 8C stage a structure similar to the one in ESCs but not before, suggesting formation of domains at 8C for this locus. I then selected two more regions, on the X-chromosome and on an autosome, and my results were suggestive of difference in timing of domain formation, depending of the genomic region (see supplementary results in Appendices). This hinted to us that genome organization might be very dynamic, and also maybe to some extent with a locus specific kinetics. This told us how essential a genome-wide analysis was but the sparsity of available embryonic material was refraining using C-technique approach. Until single-cell HiC was first published by Peter Fraser lab (Nagano et al., 2013), and we had an opportunity to team up with them.

That's how, second, we adapted single-cell HiC to early embryonic cells (with the help of Takashi Nagano, from Peter Fraser lab) to decipher genome architecture during mouse preimplantation development. I prepared all the samples for each stage up to ligation step and sent them to Takashi Nagano who prepared libraries for subsequent sequencing at Babraham. Csilla Varnai performed computational. We are working in a tight collaboration in order to analyze in depth our HiC data ranging from oocytes to blastocyst stage, both at the genome wide level and more specifically concerning the paternal chromosome which is progressively silenced during this time period.

The results of this work are described in **Article 2 - The dynamics of parental genome conformations in early mouse embryogeneis and during imprinted X-chromosome inactivation** (manuscript in preparation).

ARTICLE 1 - MATERNAL LSD1/KDM1A IS AN ESSENTIAL REGULATOR OF CHROMATIN AND TRANSCRIPTION LANDSCAPES DURING ZYGOTIC GENOME ACTIVATION.

eLIFE elifesciences.org

RESEARCH ARTICLE

Maternal LSD1/KDM1A is an essential regulator of chromatin and transcription landscapes during zygotic genome activation

Katia Ancelin[1,2]*, Laurène Syx[1,3,4], Maud Borensztein[1,2], Noémie Ranisavljevic[1,2], Ivaylo Vassilev[1,3,4], Luis Briseño-Roa[5], Tao Liu[6], Eric Metzger[7], Nicolas Servant[1,3,4], Emmanuel Barillot[1,3,4], Chong-Jian Chen[6], Roland Schüle[7], Edith Heard[1,2]*

[1]Institut Curie, Paris, France; [2]Genetics and Developmental Biology Unit, INSERM, Paris, France; [3]Bioinformatics and Computational Systems Biology of Cancer, INSERM, Paris, France; [4]Mines ParisTech, Fontainebleau, France; [5]High Fidelity Biology, Paris, France; [6]Annoroad Gene Technology Co., Ltd, Beijing, China; [7]Urologische Klinik und Zentrale Klinische Forschung, Freiburg, Germany

Abstract Upon fertilization, the highly specialised sperm and oocyte genomes are remodelled to confer totipotency. The mechanisms of the dramatic reprogramming events that occur have remained unknown, and presumed roles of histone modifying enzymes are just starting to be elucidated. Here, we explore the function of the oocyte-inherited pool of a histone H3K4 and K9 demethylase, LSD1/KDM1A during early mouse development. KDM1A deficiency results in developmental arrest by the two-cell stage, accompanied by dramatic and stepwise alterations in H3K9 and H3K4 methylation patterns. At the transcriptional level, the switch of the maternal-to-zygotic transition fails to be induced properly and LINE-1 retrotransposons are not properly silenced. We propose that KDM1A plays critical roles in establishing the correct epigenetic landscape of the zygote upon fertilization, in preserving genome integrity and in initiating new patterns of genome expression that drive early mouse development.
DOI: 10.7554/eLife.08851.001

***For correspondence:** Katia.Ancelin@curie.fr (KA); Edith.Heard@curie.fr (EH)

Competing interests: The authors declare that no competing interests exist.

Funding: See page 20

Received: 21 May 2015
Accepted: 25 January 2016
Published: 02 February 2016

Reviewing editor: Anne C Ferguson-Smith, University of Cambridge, United Kingdom

Introduction

Gametes are highly differentiated cell types and fertilization of the oocyte by sperm requires major epigenetic remodelling to reconcile the two parental genomes and the formation of a totipotent zygote. In particular, the paternal genome arrives densely packed with protamines rather than histones, and the maternal epigenome is highly specialised. Maternal factors must unravel these specialised chromatin states to enable zygotic gene activation and development to proceed. Histone tail post-translational modifications (PTMs), and more specifically lysine methylation, appear to be dynamically regulated during this first step of development (***Burton and Torres-Padilla, 2010***). Histone lysine methylation appears to have different biological read-outs, depending on the modified residue as well as the state of methylation (mono-, di- or tri-). For example, methylation of histone H3 lysine 4 (referred to as H3K4 methylation hereafter) is mainly associated with transcriptionally active chromatin while methylation of histone H3 lysine 9 (referred to as H3K9 methylation hereafter) is usually linked to repressive chromatin. The incorrect setting of some of these histone marks in cloned animals have been correlated with their poor development potential, pointing to their importance during early stages of development (***Matoba et al., 2014***; ***Santos et al., 2003***). However, the

eLife digest During fertilization, an egg cell and a sperm cell combine to make a cell called a zygote that then divides many times to form an embryo. Many of the characteristics of the embryo are determined by the genes it inherits from its parents. However, not all of these genes should be "expressed" to produce their products all of the time. One way of controlling gene expression is to add a chemical group called a methyl tag to the DNA near the gene, or to one of the histone proteins that DNA wraps around.

Soon after fertilization, a process called reprogramming occurs that begins with the rearrangement of most of the methyl tags a zygote inherited from the egg and sperm cells. This dynamic process is thought to help to activate a new pattern of gene expression. Reprogramming is assisted by "maternal factors" that are inherited from the egg cell.

KDM1A is a histone demethylase enzyme that can remove specific methyl tags from certain histone proteins, but how this affects the zygote is not well understood. Now, Ancelin et al. (and independently Wasson et al.) have investigated the role that KDM1A plays in mouse development.

Ancelin et al. genetically engineered mouse eggs to lack KDM1A and used them to create zygotes, which die before or shortly after they have divided for the first time. The zygotes display severe reprogramming faults (because methyl tags accumulate at particular histones) and improper gene expression patterns, preventing a correct maternal-to-zygotic transition. Further experiments then showed that KDM1A also regulates the expression level of specific mobile elements, which indicates its importance in maintaining the integrity of the genome.

These findings provide important insights on the crucial role of KDM1A in establishing the proper expression patterns in zygotes that are required for early mouse development. These findings might help us to understand how KDM1A enzymes, and histone demethylases more generally, perform similar roles in human development and diseases such as cancer.

DOI: 10.7554/eLife.08851.002

actors underlying these dynamic changes in histone modifications after fertilization and their impact on the appropriate regulation of zygotic genome function remain open questions.

Lysine methylation is tightly regulated by distinct families of conserved enzymes, histone lysine methyltransferases (KMTs), which add methyl groups and histone lysine demethylases (KDMs) which remove them (**Black et al., 2012**). Importantly, KMTs and KDMs show different specificities for their target lysine substrates, as well as for the number of methyl group they can add or remove (from unmethylated -me0-, to dimethylated –me2, and trimethylated -me3; and vice versa).

Several KMTs and KDMs have been disrupted genetically in model organisms, including mouse, and their loss often leads to lethality or to severe defects in embryogenesis, or else in tissue-specific phenotypes in adults. This has been linked to their important roles in cell fate maintenance and differentiation, as well as in genome stability (**Black et al., 2012**; **Greer and Shi, 2012**). However, investigating their potential roles during the first steps of development, after fertilization is frequently hampered by their maternal mRNA and/or protein pool, which can persist during early embryogenesis and mask the potential impact that the absence of such factors might have (**Li et al., 2010**). In mice, conditional knock-outs in the female germline that suppress the maternal store of mRNA and protein at the time of fertilization, can be used to examine protein function during the earliest steps of development (**de Vries et al., 2000**; **Lewandoski et al., 1997**). In this way, the roles of KMTs and KDMs during early embryogenesis are just starting to be explored. For example, it has been shown that depletion of maternal EZH2 affects the levels of H3K27 methylation in zygotes, although this did not lead to any growth defects during embryonic development (**Erhardt et al., 2003**; **Puschendorf et al., 2008**). Another study investigated maternal loss of *Mll2* (Mixed lineage leukemia 2), encoding one of the main KMTs targeting H3K4 and revealed its essential role during oocyte maturation and for the embryos to develop beyond the two-cell stage, through gene expression regulation, (**Andreu-Vieyra et al., 2010**). Importantly, in the presence of maternal EZH2 or MLL2 protein (when wt/- breeders are used), both *Ezh2* and *Mll2* null embryos die much later *in utero* (**O'Carroll et al., 2001**; **Glaser et al., 2006**). The roles of these regulators of lysine methylation

can thus be highly stage-specific, with very different effects at the zygote, early cleavage or later developmental stages.

The LSD1/KDM1A protein (encoded by the gene previously known as *Lsd1* but subsequently renamed *Kdm1a,* which will be the used in this manuscript hereafter) was the first histone KDM to be characterized to catalyse H3K4me1 and 2 demethylation and transcriptional repression (**Shi et al., 2004**). KDM1A was later shown to demethylate H3K9me2 and to activate transcription (**Laurent et al., 2015**; **Metzger et al., 2005**). Genetic deletion of murine *Kdm1a* during embryogenesis obtained by mating of heterozygous animals showed early lethality prior to gastrulation (**Foster et al., 2010**; **Macfarlan et al., 2011**, **Wang et al., 2007**; **2009**). In light of the above considerations, we set out to study the impact of eliminating or inhibiting the maternal pool of KDM1A during preimplantation development. We report for the first time the crucial role of *Kdm1a* following fertilization. The absence of KDM1A protein in zygotes derived from *Kdm1a* null oocytes led to a developmental arrest at the two-cell stage, with a severe and stepwise accumulation of H3K9me3 from the zygote stage, and of H3K4me1/2/3 at the two-cell stage. These chromatin alterations coincide with increased perturbations in the gene expression repertoire, based on single embryo transcriptomes, leading to an incomplete switch from the maternal to zygotic developmental programs. Furthermore, absence of KDM1A resulted in deficient suppression of LINE-1 retrotransposon expression, and increased genome damage, possibly as a result of increased LINE-1 activity. Altogether, our results point to an essential role for maternally-inherited KDM1A in maintaining appropriate temporal and spatial patterns of histone methylation while preserving genome expression and integrity to ensure embryonic development beyond the two-cell stage.

Results

Depletion of maternal KDM1A protein results in developmental arrest at two-cell stage

To investigate whether *Kdm1a* might have a role during early mouse development we first assessed whether the protein was present in pre-implantation embryos using immunofluorescence (IF) and western blotting (**Figure 1A and B**). A uniform nuclear localization of KDM1A within both parental pronuclei was observed by IF in the zygote, and at the two-cell stage. The protein was also readily detected by western blot analysis of total extracts of two-cell-stage embryos when compared to nuclear extracts of ESCs. Altogether, these data reveal the presence of a maternal pool of KDM1A.

To assess the function of KDM1A in early mouse embryo development, we deleted the *Kdm1a* gene in the female germline during oocyte growth. To this end $Kdm1a^{tm1Schüle}$ $Zp3^{cre}$ females, carrying a new conditional allele for *Kdm1a* deletion engineered in the Schüle group (**Zhu et al., 2014**), and a *Zp3* promoter driven *cre* transgene exclusively expressed in oocytes (**Lewandoski et al., 1997**) were produced (see also materials and methods). These animals are referred as $Kdm1a^{f/f}$::$Zp3^{cre}$ in this study). $Kdm1a^{f/f}$::$Zp3^{cre}$ females were then mated with wild-type males (**Figure 1C**). We isolated one- and two-cell stage embryos derived from such crosses to obtain maternally depleted *Kdm1a* mutant embryos (hereafter named △m/wt) in parallel to control embryos (hereafter named f/wt) and we confirmed that the KDM1A maternal pool is absent by performing IF (**Figure 1A**, bottom panels). In parallel, RT-qPCR analysis revealed the absence of *Kdm1a* mRNA in mutant oocytes (**Figure 1—figure supplement 1A**).

Numerous $Kdm1a^{f/f}$::$Zp3^{cre}$ females were housed with wild-type males for several months, however no progeny was ever obtained, in contrast to $Kdm1a^{f/f}$ or $^{f/wt}$ females that produced the expected range of pup number (4 to 7; data not shown). This indicated that $Kdm1a^{f/f}$::$Zp3^{cre}$ females are sterile. To determine the possible causes of sterility, control $Kdm1a^{f/f}$ and mutant $Kdm1a^{f/f}$::$Zp3^{cre}$ females were mated with wild-type males and embryos were recovered on embryonic day 2 (E2) (**Figure 1D and E**). The total number of oocytes or embryos scored per female was on average 17 for the mutant background (206 oocytes or embryos obtained for 12 females studied) and 25 for the control (226 oocytes or embryos obtained for 9 females studied) (see **Figure 1D**). We found that the proportion of △m/wt two-cell stage embryos recovered (19%, n = 39/206) was far lower than that obtained with f/wt embryos (75% n = 170/226) (**Figure 1D**). Using $Kdm1a^{f/f}$::$Zp3^{cre}$ females, we also noted a high percentage of fertilized and unfertilized oocytes blocked at meiosis II (MII) (n = 95; 46%) compared to those recovered from control females (n = 34; 15%). Inspection of control

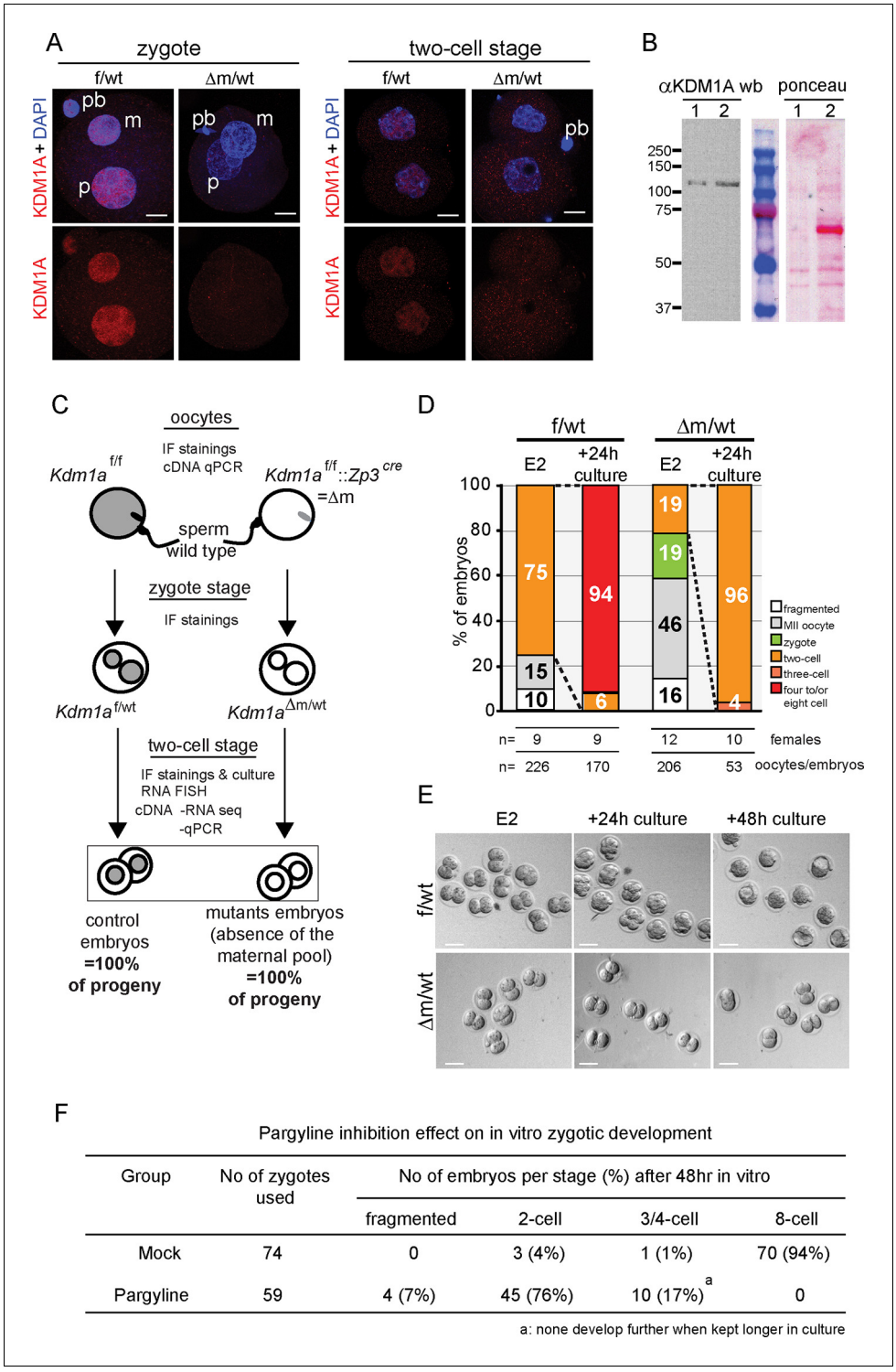

Figure 1. *Kdm1a* maternally deleted embryos arrest at two-cell stage. (**A**) Immunofluorescence using anti-KDM1A antibody (red) at the zygote and two-cell stage shows nuclear accumulation of KDM1A in control embryos (top). Cre-mediated deletion of *Kdm1a* in maternal germline (bottom) leads to depletion of the protein after fertilization. Paternal pronucleus (p), maternal pronucleus (m) and polar body (pb) are indicated. DNA is counterstained by DAPI (blue). (**B**) western blot analysis (left panel) for ESC (lane1) and two-cell stage embryo extracts (lane 2) using anti-KDM1A antibody. Ponceau staining (right panel) is shown as loading control. Molecular weights (kDa) are indicated on the left. (**C**) Mating scheme and experimental outcomes for the different developmental stages used in this study: f/wt control embryos are obtained from superovulated *Kdm1a*$^{f/f}$ females mated with wild-type males,

Figure 1 continued on next page

Figure 1 continued

while △m/wt mutant embryos are obtained from superovulated *Kdm1a*$^{f/f}$::Zp3^{cre} females crossed with wild-type males. (**D**) Distribution of developmental stages found in f/wt and △m/wt embryos collected at embryonic day 2 (E2) (expected two-cell stage) and after 24 hr of *in vitro* culture. Numbers of females used and numbers of oocytes/embryos analysedare shown under the graph. See also ***Figure 1—figure supplement 1*** for oocyte analysisand ***Figure 1—figure supplement 2*** for developmental stage distribution using natural matings without superovulation for females. (**E**) Bright field images representative for two consecutive days of in vitro culture for f/wt and △m/wt embryos collected at E2. (**F**) Phenotypes and distribution of developmental stages obtained after 48 hr treatment *in vitro* culture with a catalytic inhibitor (pargyline) of KDM1A in wild-type zygotes recovered at 17 hr post hCG injection. Scale bars represent, 10 μm and 50 μm, in A and D, respectively.

DOI: 10.7554/eLife.08851.003

The following figure supplements are available for figure 1:

Figure supplement 1. *Kdm1a* loss of function in female germline.

DOI: 10.7554/eLife.08851.004

Figure supplement 2. Embryo recovery at day 2 post fertilization using natural matings.

DOI: 10.7554/eLife.08851.005

(n = 75) and mutant (n = 55) MII oocytes revealed a high proportion of misaligned chromosomes on the metaphase spindle (***Figure 1—figure supplement 1B and C***) in mutants (41%) compared to controls (17%), suggesting that a lack of maternal KDM1A can lead to chromosome segregation defects. Furthermore, upon fertilization, transmission of inherited chromosomal abnormalities was clearly evident, with the frequent presence of micronuclei in KDM1A maternally depleted two-cell embryos (n = 40; 63%) (***Figure 1—figure supplement 1D***). Lastly, 19% (n = 39) of mutant embryos were still at the zygote stage compared to 0% in controls (***Figure 1D***). These results indicate that many MII oocytes lacking germline KDM1A are not competent at ovulation and that when fertilized their first cell cycle is delayed. Similar results were obtained when using females not subjected to superovulation for mating (***Fig1—figure supplement 2***).

We next assessed the progress of surviving △m/wt two-cell embryos by culturing them in vitro. After 24 hr in culture, 96% of the △m/wt embryos were found to be arrested at the two-cell stage, unlike f/wt embryos where only 6% showed an arrest (***Figure 1D and E***). The mutant embryos blocked at the two-cell stage did not progress further in development upon prolonged in vitro culture, and eventually fragmented, while the control embryos progressed towards the blastocyst stage (***Figure 1E***).

Taken together, these results suggest that the sterility of *Kdm1a* germline mutant females is in part caused by a severely compromised spindle organization in some oocytes in the second round of meiosis,as well as for the second round of cleavage after fertilization. This immediate loss of viability of the first generation embryos contrasts with the progressive effect seen across generations when spr-5, the *Kdm1a* homologue in *C.elegans* is mutated in germline precursors for both gametes (***Katz et al., 2009***). Also, targeted disruption of Lsd2/*Kdm1b,* the closest homologue of *Kdm1a*, in the mouse female germline, was reported to have no effect on oogenesis and early mouse development, but only later at mid-gestation, due to misregulation at some imprinted genes (***Ciccone et al., 2009***). Our results show that KDM1B in the female germline is not sufficient to rescue the phenotype of KDM1A maternal depletion after fertilization.

Inhibition of the enzymatic activity of KDM1A from early zygote stage mimics the maternal deletion phenotype

The developmental arrest observed at the two-cell stage of △m/wt embryos could be due to defects carried over by the mutant oocytes, particularly given the chromosome defects observed in a significant proportion of arrested oocytes, and/or to a requirement for KDM1A function after fertilization. To assess a requirement for KDM1A enzymatic activity in early embryos, we tested the impact of KDM1A catalytic inhibition specifically after fertilization. To this end, we treated wild-type zygotes with pargyline, a well-characterized potent chemical inhibitor of KDM1A enzymatic activity (***Fierz and Muir, 2012***; ***Metzger et al., 2005***) and followed their development *in vitro* over 48 hr. As shown in ***Figure 1F***, 76% embryos cultured with pargyline were found to be significantly blocked at the two-cell stage and 17% never progressed beyond the 3/4-cell stage. On the contrary, the

majority (94%) of mock treated embryos developed to the eight-cell stage within 48 hr, as expected. These data parallel the phenotype of genetic ablation of the KDM1A maternal pool, where 96% of △m/wt embryos are developmentally arrested at the two-cell stage and 4% at the 3/4-cell stage. Taken together, the genetic depletion and pargyline inhibition data strongly support a requirement for KDM1A enzymatic activity during the zygote and two-cell stage, for embryos to proceed beyond the two-cell stage.

Abnormal increase of H3K9me3 levels in KDM1A maternally deficient zygotes

The above observations suggested that the histone demethylase KDM1A plays an important role in early development. At the zygote stage, H3K4 and H3K9 methylation levels appear to be tightly regulated and show highly parental specific patterns (***Arney et al., 2002***; ***Lepikhov and Walter, 2004***; ***Santos et al., 2005***; ***Puschendorf et al., 2008***; ***Santenard et al., 2010***; ***Burton and Torres-Padilla, 2010***). Given that KDM1A has been implicated in the regulation of H3K4 and H3K9 mono and di methylation in previous studies (***Shi et al., 2004***; ***Metzger et al., 2005***; ***Di Stefano et al., 2008***; ***Katz et al., 2009***), we investigated whether the methylation levels of these two histone H3 lysines were affected by KDM1A depletion in one-cell stage embryos.

To this end, we collected f/wt and △m/wt embryos at embryonic day 1 and analysed them for both H3K4 and H3K9 methylation using specific antibodies against mono (me1), di (me2) and tri (me3) methylation (***Figure 2***). We used antibodies that show similar patterns in control zygotes to those previously published by others (***Arney et al., 2002***; ***Lepikhov and Walter, 2004***; ***Puschendorf et al., 2008***; ***Santenard et al., 2010***; ***Santos et al., 2005***) (see Material and Methods). We prioritised single-embryo analysis given the limited amount of material that can be recovered at these early developmental time points, particularly in the context of the depletion of KDM1A (***Figure 1D***). We first analysed H3K4 methylation patterns (***Figure 2A and B***). It was previously reported that the paternal pronucleus only gradually shows enrichment in H3K4me2 and me3 during the one-cell stage, while the female pronucleus is enriched with these marks from its oocyte origin (***Burton and Torres-Padilla, 2010***; ***Lepikhov and Walter, 2004***). We compared maternal and paternal pronuclear patterns in control and mutant embryos and categorised them according to previously described nomenclature (***Adenot et al., 1997***). In mid-stage zygotes, the absence of maternal KDM1A does not seem to affect overall H3K4me1, me2 or me3 levels in either the maternal or paternal pronuclei (***Figure 2A and B***).

We also assessed whether H3K9 methylation levels were affected in zygotes lacking a maternal pool of KDM1A (***Figure 2C and D***). H3K9me1 was reported to be equally enriched in both parental pronuclei, while H3K9me2 and me3 are exclusively present in the maternal pronucleus (***Arney et al., 2002***; ***Santos et al., 2005***; ***Lepikhov and Walter, 2004***; ***Puschendorf et al., 2008***; ***Santenard et al., 2010***; ***Burton and Torres-Padilla, 2010***). We found that △m/wt embryos do not seem to differ from f/wt embryos in H3K9me1 levels (***Figure 2C and D***). In the case of H3K9me2, a complete absence of H3K9me2 staining in the paternal pronucleus was recorded for both control and mutant zygotes. However, we did note a small change in the proportion of embryos displaying H3K9me2 staining in the maternal pronucleus. This suggests that absence of KDM1A may slightly impact on oocyte-inherited H3K9me2 profiles.

Although KDM1A was shown to specifically induce demethylation of H3K9me1/2 at target genes (***Laurent et al., 2015***; ***Metzger et al., 2005***), we nevertheless assayed H3K9me3 patterns by IF, in case it could also accumulate in absence of KDM1A, due to the presence of specific H3K9 KMT (***Cho et al., 2012***; ***Puschendorf et al., 2008***). H3K9me3 enrichment is a feature of constitutive heterochromatin, and has been shown to be zygotically enriched at the periphery of nucleolar like bodies (NLBs) within the maternal but not the paternal pronucleus (***Burton and Torres-Padilla, 2010***; ***Puschendorf et al., 2008***; ***Santenard et al., 2010***) (***Figure 2C***). In △m/wt zygotes, strikingly elevated levels H3K9me3 were found in the whole maternal pronucleus when compared to controls (grey arrowhead, ***Figure 2C and D***). Even more surprisingly, in △m/wt zygotes, H3K9me3 could be detected at the periphery of paternal NLBs (yellow arrowhead), when compared to controls. Taken together, these observations show that the absence of maternal KDM1A protein results in specifically elevated levels of H3K9me3 in both parental genomes at the zygote stage, and suggest that KDM1A might be engaged with other chromatin modifiers to regulate H3K9me3 immediately after fertilization.

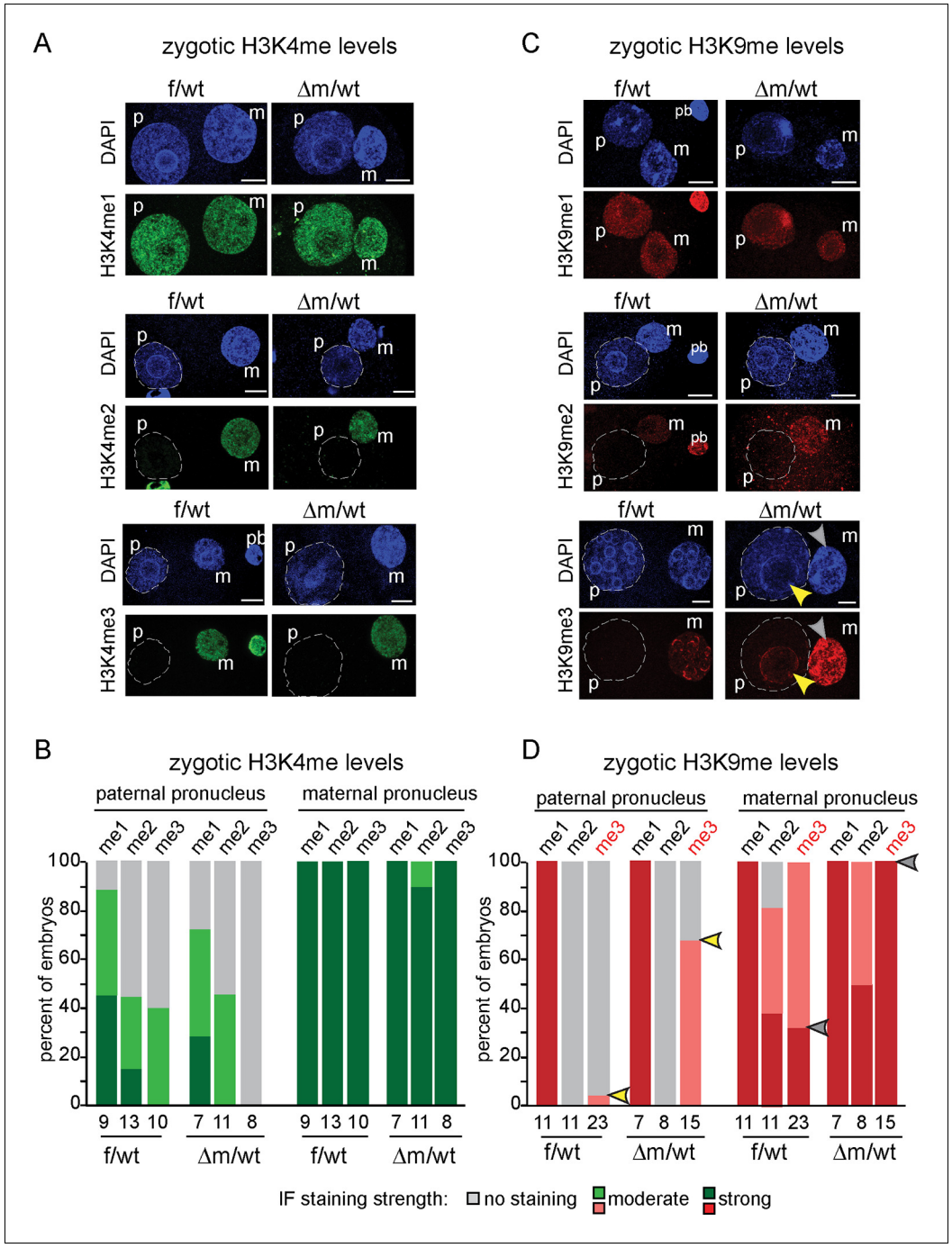

Figure 2. H3K9me3 heterochromatin levels are defined by maternally inherited KDM1A at the zygote stage. (**A** and **C**) IF using antibodies against me1, me2 and me3 of (**A**) H3K4 (in green) and (**C**) H3K9 (in red) during zygotic development. Mid to late f/wt and △m/wt zygote are shown. Paternal pronucleus (p), maternal pronucleus (m) and the polar body (pb) are indicated when present. DNA is counterstained with DAPI (blue). In C, note that in △m/wt zygotes, H3K9me3 is increased in the maternal pronucleus (grey arrowhead) and is localized *de novo* in the paternal pronucleus (yellow arrowhead). (**B** and **D**) Classification of embryos based on staining intensity scores for H3K4/K9me1/2/3) in the paternal versus maternal pronuclei in zygotes. Note that concerning H3K9me2, 50% of △m/wt embryos have a strong staining versus 35% in controls (which are also up to 20% with no IF signal). The most striking and only significant differences in proportions are seen for H3K9me3 both in maternal (grey arrowheads) and paternal (yellow arrowheads) pronuclei, with $p<0.05$ using a Chi square test. The scoring is as follows: light grey for no signal; medium green/red for moderate signal and dark green/red for strong signal. Number of embryos and their genotypes are indicated at the bottom of the graph. Scale bar in A and C represent 10 μm.

DOI: 10.7554/eLife.08851.006

Abnormal H3K4 and H3K9 methylation patterns after the first cleavage division in KDM1A maternally depleted embryos

In order to investigate whether KDM1A activity was important for the regulation of H3K4 and K9 methylation after the first cell cleavage, we examined two-cell stage f/wt and △m/wt embryos by IF to measure the relative fluorescence intensities (***Figure 3***). We found that the overall H3K4 methylation levels for mono, di and tri-methylation were significantly elevated in △m/wt two-cell embryos (***Figure 3A***), with the most striking effect being seen for H3K4me3 where a six-fold increase was found in mutants compared to controls. Thus, a lack of KDM1A protein has a significant impact on H3K4 methylation levels at the two-cell stage. When H3K9me1, me2 and me3 levels were also examined by IF, we found that all three marks were elevated, with the most significant effect being seen for H3K9me3, which showed a 2.2 fold increase in fluorescence intensity particularly at DAPI dense regions of constitutive heterochromatin (***Figure 3B***).

To address the specificity of these effects of KDM1A on H3K4 and H3K9 methylation, we tested other histone marks, reported not to be targeted by KDM1A activity. Two such marks, H3K27me3 and H4K20me3, both associated with heterochromatin, were analysed by IF in f/wt and △m/wt two-cell stage embryos. No significant changes in either of these marks could be detected in mutant compared to control embryos (***Figure 3—figure supplement 1A and B***), underlining the specificity of the defects found in KDM1A maternally depleted embryos. As an additional control, we performed IF analysis of two-cell stage embryos generated from wild-type zygotes grown for 24 hr with pargyline. H3K4me3 and H3K9me3 patterns revealed changes in pargyline-treated when compared to mock-treated embryos (***Figure 3—figure supplement 1C and D***). In both, a global increase in staining was detected when compared to controls, although to a slightly lesser extent than in *Kdm1a* mutant embryos.

Absence of KDM1A abrogates the normal changes in transcriptome by the two-cell stage

After fertilization, development initially proceeds by relying on the maternally inherited pool of RNA and protein, followed by massive induction of transcription of the zygotic genome in different waves as shown in ***Figure 4A***. Newly produced transcripts corresponding to zygotic genome activation (ZGA) appear in two phases, first at the zygote stage (corresponding to minor ZGA) and subsequently at the two-cell stage (major ZGA). Transition from the maternal pool to zygotic products is essential for successful developmental progression (***Flach et al., 1982***). Previous work has shown that KDM1A affects transcription regulation during *in vitro* embryonic stem cell (ESC) differentiation or during peri- or post-implantation mouse development (***Foster et al., 2010***; ***Macfarlan et al., 2011***; ***Wang et al., 2007***; ***Zhu et al., 2014***). However, its role has never been evaluated during the very first steps of embryogenesis, when appropriate transcriptional activity is crucial.

In the light of our results on chromatin changes described above, and to assess whether transcription might be affected by the lack of the KDM1A maternal pool, we performed IF analysis against PolII and its elongating form (PolIISer2P), which did not reveal any obvious difference between f/wt and △m/wt two-cell stage embryos (***Figure 4—figure supplement 1A***). For a direct comprehensive analysis of the transcriptome upon lack of KDM1A, we used RNA sequencing (RNA-seq) for single oocytes and single embryos at the two-cell stage on a cohort of control and mutant samples (***Figure 4***; ***Figure 4—figure supplement 2***; ***Supplementary file 1***). The method used is based on that of (***Tang et al., 2010***) which captures poly(A) tail mRNA and allows examination up to 3kb from the 3' end. The quality of our single oocyte or embryo cDNAs was first checked by qPCR for three housekeeping genes (*Hprt, Gapdh, Ppia*) known to be stably expressed from oocytes to blastocysts (***Mamo et al., 2007***; ***Vandesompele et al., 2002***). Control and mutant samples displayed similar relative expression for these three genes attesting to the quality of our samples (***Figure 4—figure supplement 1C***). We next prepared cDNA libraries from single control and mutant oocytes (n = 5 each), as well as individual f/wt and △m/wt embryos (n = 8 each) and performed Illumina-based deep RNA sequencing on these samples (see experimental procedures and analysis for more details; ***Supplementary file 1***). We used DEseq as a normalization method across our samples to assess the relative gene expression between controls and mutants.

At the two-cell stage, our analysis revealed two sets of genes that become either upregulated (21%; n = 2449; FDR = 5%) or downregulated (24%; n = 2749) in the mutant when compared to

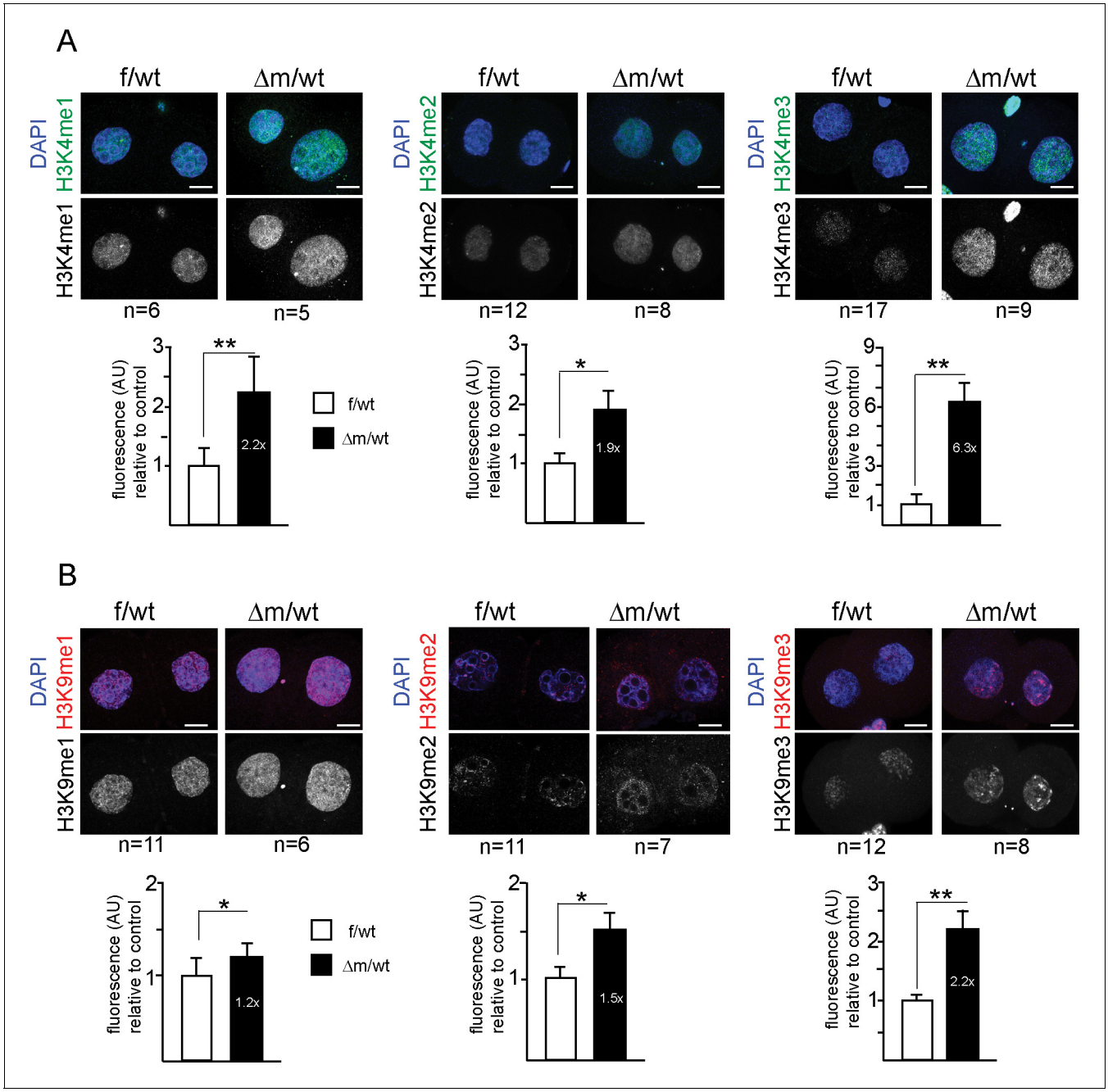

Figure 3. Two-cell stage H3K4 and H3K9 methylation levels are altered upon absence of maternal KDM1A. Immunofluorescence stainings of two-cell stage embryos using antibodies against me1, me2 and me3 of H3K4 (A; in green) and H3K9 (B; in red) were performed on f/wt (left panels) and △m/wt embryos (right panels). Control and mutant samples were processed in parallel and acquired using similar settings at the confocal microscope. DNA is counterstained with DAPI (blue). Projections of z-stacks are shown of representative embryos for each staining. Scale bars, 10 μm. Error bars represent S.E.M. By t-test; $p<0.05$ corresponds to * and $p<0.001$ to ** as performed on the number of embryos indicated below each picture. Below each image are shown the relative quantifications for IF intensity levels of me1, me2 and me3 of △m/wt (in black) relative to f/wt (in white) in two-cell stage embryos. Note that no alteration for H3K27me3 or H4K20me3 could be detected for mutant two-cell stage embryos (Figure 3—figure supplement 1A and B). Also, IF for pargyline-treated two-cell stage embryos revealed changes in both H3K4me3 and H3K9me3 patterns (Figure 3—figure supplement 1C and D).

DOI: 10.7554/eLife.08851.007

The following figure supplement is available for figure 3:

Figure supplement 1. Immunofluorescence analysis of histone tail modifications upon maternal depletion or upon chemical inhibition of KDM1A for two-cell stage embryos.

DOI: 10.7554/eLife.08851.008

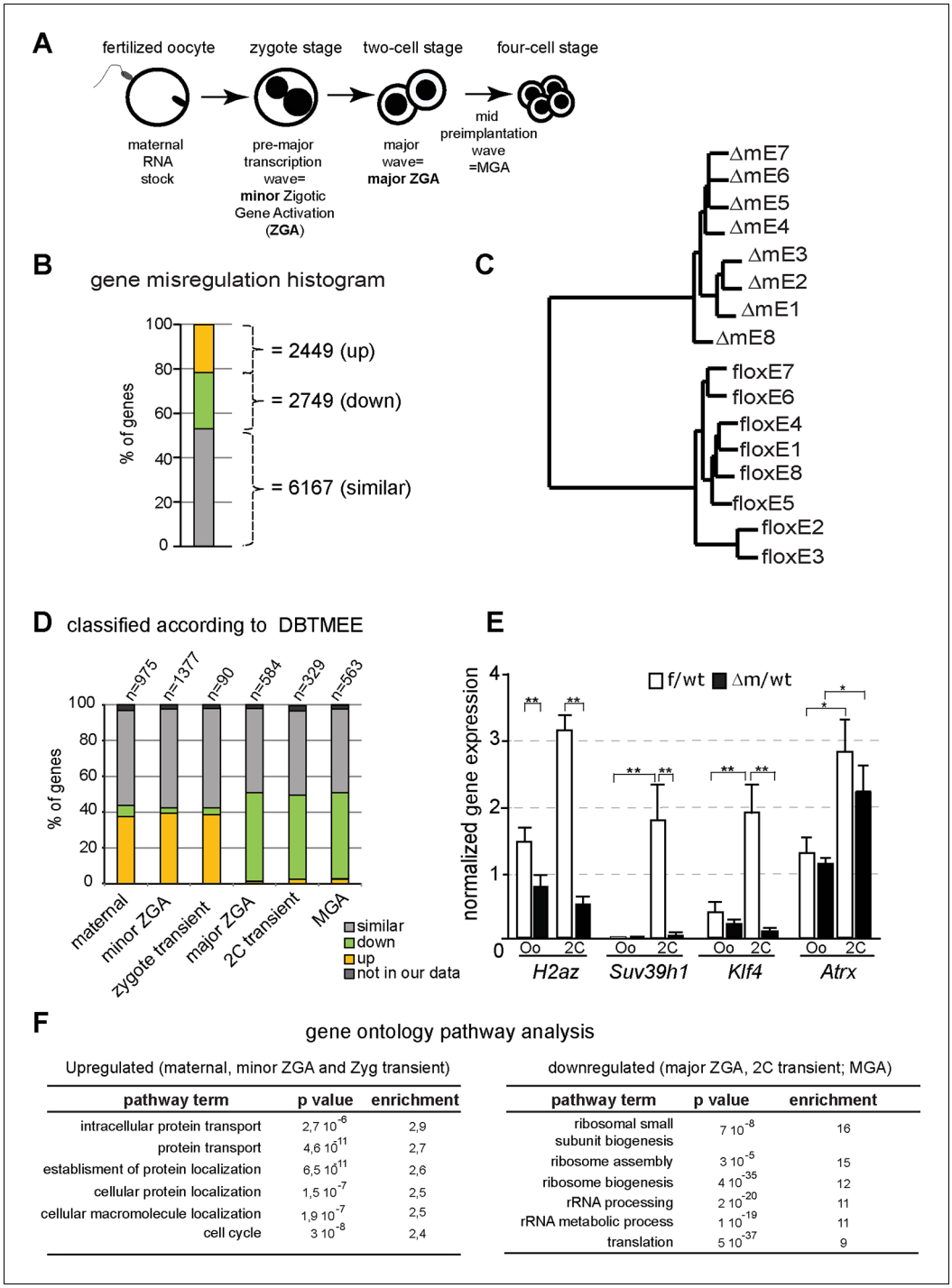

Upregulated (maternal, minor ZGA and Zyg transient)

pathway term	p value	enrichment
intracellular protein transport	$2{,}7\ 10^{-6}$	2,9
protein transport	$4{,}6\ 10^{-11}$	2,7
establisment of protein localization	$6{,}5\ 10^{-11}$	2,6
cellular protein localization	$1{,}5\ 10^{-7}$	2,5
cellular macromolecule localization	$1{,}9\ 10^{-7}$	2,5
cell cycle	$3\ 10^{-8}$	2,4

downregulated (major ZGA, 2C transient; MGA)

pathway term	p value	enrichment
ribosomal small subunit biogenesis	$7\ 10^{-8}$	16
ribosome assembly	$3\ 10^{-5}$	15
ribosome biogenesis	$4\ 10^{-35}$	12
rRNA processing	$2\ 10^{-20}$	11
rRNA metabolic process	$1\ 10^{-19}$	11
translation	$5\ 10^{-37}$	9

Figure 4. Abnormal ZGA upon absence of KDM1A revealed by transcriptome analysis. (**A**) Schematic illustration of the sequential sources of RNA pool over embryonic development. (**B**) Histogram shows the percent of differentially expressed genes in the △m/wt versus f/wt embryos. Fold difference (in log2) is annotated as upregulated (with log2≥ 1; yellow), downregulated (as log2≤-1; green) and similar (as 1<log2>-1; grey). Number of genes is indicated on the right of the graph. Details concerning the RNA seq analysis are described in Materials and Methods section and ***Supplementary file 1*** (**C**) Hierarchical clustering analysis for gene expression pattern of 16 libraries shows dramatic expression changes between f/wt (floxE1 to E8) and △m/wt (△mE1 to E8) two-cell stage embryos. See also ***Figure 4—figure supplement 2*** for analysis between two-cell stage and oocyte transcriptomes (**D**) RNA-seq data comparison with the different categories of the gene catalogue available at the Database of Transcriptome in Mouse Early Embryos (DBTMEE) generated an the ultralarge-scale transcriptome

Figure 4 continued on next page

Figure 4 continued

analysis (***Park et al., 2013***). The total number of genes belongings to each class and found in our RNA seq is indicated on top of the graph (see also ***Table 1***). (**E**) Graphical representation of the normalized mean expression levels ± sem for chromatin-encoding genes in f/wt (in white) or △m/wt (in black) MII oocytes (Oo, n = 7) and two-cell stage embryos (2C, n = 10). *corresponds to $p<0.05$ and ** to $p<0.001$. (**F**) Top 6 representative GO terms (biological functions) enriched in △m/wt mutant embryos. Fold overrepresentation indicates the percentage of misregulated genes in a particular category over the percentage expected on the basis of all GO-annotated genes present within the sequencing. p-value indicates the significance of the enrichment.

DOI: 10.7554/eLife.08851.009

The following figure supplements are available for figure 4:

Figure supplement 1. Immunostainings and RTqPCR analysis for assessing transcription of *Kdm1a* mutant two-cell stage embryos.

DOI: 10.7554/eLife.08851.010

Figure supplement 2. Transcriptome analysis of *Kdm1a* mutant versus control in oocytes or two-cell stage embryos.

DOI: 10.7554/eLife.08851.011

control embryos (***Figure 4B***; ***Figure 4—figure supplement 2A***). Hierarchal clustering based on the transcription profiles showed that all *Kdm1a* mutant embryos clustered distinctly from the controls (***Figure 4C***). Furthermore, the analysis of oocyte transcriptomes also revealed that there were fewer genes misregulated in *Kdm1a* mutant oocytes, than in *Kdm1a* mutant embryos (***Figure 4—figure supplement 2A***). Moreover, Principal Component Analysis demonstrated that the gene expression patterns showed greater differences between controls and mutants at the two-cell stage, than in oocytes, and that the two different stages cluster away from each other (***Figure 4—figure supplement 2B***). The stage comparison also showed that only a subset of genes were misregulated in common, in both oocytes and two-cell stage embryos, upon loss of maternal KDM1A (***Figure 4—figure supplement 2C***). GO analysis of up or down regulated genes at the two-cell stage (***Figure 4F***) or oocytes (***Figure 4—figure supplement 2D***) revealed very little overlap in the specific biological functions affected by loss of function of KDM1A before and after fertilization, with the notable exception of cell cycle associated genes. This connects well with the observed phenotype for poor oocyte competence at fertilization and the total developmental arrest at the two-cell stage. These results reveal that absence of maternal KDM1A most likely leads to transcriptome changes during oocyte maturation, but to even more serious defects after zygotic gene activation, at the two-cell stage. The latter may be due in part to an aberrant maternal supply of transcripts/proteins, or else to aberrant transcriptional regulation of the zygotic genome in absence of maternal KDM1A.

We assessed our two-cell stage RNA-seq data according to the recent Database of Transcriptome in Mouse Early Embryos (DBTMEE) (***Park et al., 2013***). DBTMEE was built from an ultra-large-scale whole transcriptome profile analysis of preimplantation embryos, in which genes are classified depending on which transcription waves (as in ***Figure 4A***) they are expressed. As shown in ***Figure 4D*** (see also Table 1), we assessed the percentage of genes of each of our classes (up; down and not significantly changed) that overlapped with the different DBTMEE categories of transcription switches, from oocyte to two-cell stage. Strikingly, the upregulated genes in △m/wt embryos fall essentially into the earliest stages and belong to genes annotated as maternal (37% of this category), as minor ZGA genes (39%) and as zygotic-transient (38%). We checked whether the misregulation of these three categories of genes might originate from the oocyte stage changes. We found that only 56 out of 360 of maternal genes, 94 out of 540 of minor ZGA genes and 6 out of 34 of 1C transient (Table 1 and data not shown) were already upregulated in mutant oocytes. These results reinforce the conclusion that the maternal and zygotic pools of transcripts become more compromised as development proceeds toward the two-cell stage in mutant embryos, rather than being aberrant right from the *Kdm1a* mutant germline. In clear contrast, the majority of downregulated genes in the △m/wt were found to belong to the three categories of genes that are normally activated at the two-cell stage, with 50% in the major ZGA class, 37% in the two-cell transient and 50% in the MGA (Mid zygotic gene activation). This suggests that absence of KDM1A compromises the activation of gene expression by the two-cell stage.

In order to validate our RNA seq data and the analysis done, we selected four genes with characteristic expression profiles, *Atrx* (maternal), *H2Az* (major ZGA), *Suv39h1* (2C-transient), *Klf4* (MGA),

which all encode chromatin associated factors crucial for early mouse development. Validation was performed by RT-qPCR in control and mutant oocytes and two-cell embryos. As predicted from our RNA seq results (***Supplementary file 2***), *H2AZ, Suv39h1 and Klf4* failed to be expressed at two-cell stage in *Kdm1a* mutant embryos (***Figure 4E***). In contrast *Atrx* which is a known maternal factor, but which is zygotically expressed by the two cell stage, was correctly activated. No difference in expression of *Suv39h1, Klf4* and *Atrx* could be seen between controls and mutants at the oocyte stage, implying that the maternal pool of these mRNAs was not affected by the maternal KDM1A depletion.

This single embryo transcriptome profiling data reveals an aberrant gene expression profile in *Kdm1a* mutant embryos, which is likely due to an absence or delay in the transcription switch from maternal-zygote to the two-cell stage pattern for a substantial set of genes (47%; 1818 out of 3811 considered; ***Figure 4—figure supplement 2***). Together with the changes in chromatin profiles that we observed at the two-cell stage, we conclude that part of the deficiency in developmental progression could be due to the inappropriate setting of a successful zygotic gene expression program upon KDM1A loss.

A gene ontology (GO) analysis of the up-regulated genes classified as maternal to zygote-transient in ***Figure 4D***, revealed a clear over-representation of genes involved in protein transport and localisation as well as contribution to cell cycle (***Figure 4F***). GO analysis of the downregulated genes from major-to-mid-zygotic activation are implicated in ribosome biogenesis and translation processes (***Figure 4F***). Collectively, these results suggest that KDM1A is necessary for the transcriptional regulation of specific genetic pathways implicated in fundamental biological functions such as protein production and localisation, and cell cycle regulation. These combined defects could be consistent with the inability of the mutant embryos to develop further than the two-cell stage

Impact of KDM1A absence on repeat elements, genome integrity and DNA replication

Many transposable elements are known to be expressed in early mouse embryos, as early as zygotic stage, and some of these repeat elements might even be competent for new events of retrotransposition between fertilization and implantation (***Fadloun et al., 2013***; ***Kano et al., 2009***; ***Peaston et al., 2004***). The repression of some of these transposable elements during preimplantation has been correlated with loss of active chromatin marks such as H3K4me3, rather than acquisition of heterochromatic marks such as H3K9me3 (***Fadloun et al., 2013***). Interestingly, a previous study using *Kdm1a* mutant mESCs and late preimplantation embryos found a significant impact on MERVL:LTR repeat expression (for Murine endogenous retrovirus-like LTR), as well as a good correlation for the presence of remnant ERVs within 2kb of the transcription start site of KDM1A-repressed genes (***Macfarlan et al., 2011***). The increased levels of H3K4me3 and H3K9me3 that we found in △m/wt two-cell stage embryos and the reported role of KDM1A in late preimplantation embryos prompted us to analyze the effects of maternal KDM1A depletion on repetitive element expression after fertilization. To this end, we investigated our RNA-seq data from control and *Kdm1a* mutant

Table 1. Comparing the two-cell stage transcriptome of the *Kdm1a* mutant embryos to DBTMEE
Numbers of genes found for the comparison of our two-cell stage RNA-seq data with the different categories for the gene catalogue found in DBTMEE. Total genes considered = 3811 and total genes changed = 1818 (48%). Our dataset cover the genes categorized on the public resource with a minimum of 96% of genes.

	Up	Down	Similar	Not in our data	Total in DBTMEE
maternal	360	63	521	31	975
minor ZGA	540	47	750	40	1377
1C transient	34	4	51	1	90
major ZGA	10	297	297	10	584
2C transient	8	156	156	12	329
MGA	13	286	286	13	563

DOI: 10.7554/eLife.08851.012

two-cell embryos for the relative expression of repetitive elements. As our single embryo RNA seq approach was based on oligo-dT priming this restricted our analysis to reads at the 3' ends of transcripts, which somewhat limited our capacity to detect repeat variation. In particular we could not determine which specific LINE-1 families were expressed in the mutants, nor whether the LINE-1 reads we detected corresponded to full-length,and/or intact elements. Nevertheless, our results shows that by far the most abundant categories of expressed repeats at this stage of development were LTRs (long terminal repeat) and non-LTR retrotransposons in f/wt and △m/wt (95% and 92%, respectively) (***Figure 5A***). However, no significant impact on expression could be detected in the mutants, with the exception within the non-LTR elements, of quite a significant overrepresentation of LINEs, but not SINEs (for Long/Short Interspersed Nuclear Elements element) (***Figure 5A and B***). We validated this result by RT-qPCR using individually prepared cDNAs of two-cell stage embryos for three transposable element classes. LINE-1, SINE B1 and MuERV-L transcripts are all abundantly expressed in control and mutant embryos, but LINE-1 levels show a two-fold increase in the △m/wt embryos (***Figure 5C***). No significant up-regulation was seen in ERV-promoter driven genes, that had previously reported to be affected by loss of KDM1A in ESCs (***Macfarlan et al., 2011***).

To further assess the impact that KDM1A depletion has on active LINE-1 transcription, we used a single-cell method, RNA fluorescent in situ hybridization (RNA FISH), which enables the detection of nascent transcripts. We first assessed the quality of our assay by checking the *Atrx* gene, known to be transcribed at the two-cell stage (***Patrat et al., 2009***) and expressed at similar levels in mutant and control (***Figure 5—figure supplement 1***). A comparable proportion of f/wt embryos and △m/wt two-cell embryos displayed detectable ongoing transcription, as registered by a pinpoint at this locus. Using a probe spanning the full-length LINE-1 element (***Chow et al., 2010***), we detected LINE-1 RNA in control two-cell stage embryos as displayed by the punctate pattern in nuclei (***Fadloun et al., 2013***), while RNase-A treated embryos showed no signal (***Figure 5D***). In the maternally depleted embryos, the arrangement of fluorescent foci appeared extensively modified (***Figure 5D***). This was confirmed upon analysis of the fluorescence intensity distributions (***Figure 5E*** left) as well as the image composition for the foci (***Figure 5E*** right), which in both cases significantly separated the two types of samples. Our analysis revealed that the active LINE-1 transcription profiles were extensively modified upon the loss of maternal KDM1A.

To investigate whether the increase in nascent LINE-1 transcription observed might correspond to full length LINE-1 elements, we assessed by IF for the presence of ORF1, one of the two LINE-1 encoded proteins. At the two-cell stage, we found an approximately four-fold increase in the proportion of △m/wt embryos displaying a stronger IF signal, notably in the nucleus (***Figure 5F***). These results suggest that the LINE-1 deregulation observed at the RNA level might indeed lead to the production and nuclear import of increased levels of LINE-1 ORF1 proteins. We next investigated whether expression of such proteins from transposable elements would have any consequences. We thus performed γH2AX IF staining to assess whether increased DNA damage signalling could be seen in △m/wt compared to f/wt embryos (***Figure 5G***; ***Figure 5—figure supplement 2***). Half of the mutant embryos displayed a stronger staining for γH2AX, with a significant increase compared to controls (***Figure 5G***). We also assessed whether this accumulation of γH2AX signals could also be related to replication delays, as reported previously in the case of maternal loss of two components of the polycomb complex PRC1 (***Posfai et al., 2012***). We performed EdU pulse treatment (a nucleoside analog of thymidine incorporated into DNA) in two-cell embryos, at a stage when they have normally completed S phase (40–41 hr post hCG injection). This revealed that S phase is delayed in the △m/wt embryos given the incorporation of EdU in the mutants, while none of the control embryos used in parallel were stained (***Figure 5—figure supplement 2***). All the mutant embryos delayed in their replication displayed concomitantly intense γH2AX signals. However, 38% of the mutant embryos did not show any EdU incorporation, indicating that they exit S phase, yet, they still show high levels of γH2AX signals. Finally, although, no significant enrichment was directly found for DNA damage pathways when running our GO analysis (***Figure 4E***), many genes related to DNA damage repair were upregulated (***Supplementary file 2***). Taken all together, these results suggest that the elevated DNA damage signalling observed could be independent from replication defaults in KDM1A maternally depleted embryos, but might be related either to changes in transcript levels for DNA damage genes or else to the observed increase in LINE-1 activity in *Kdm1a* mutant embryos at this stage.

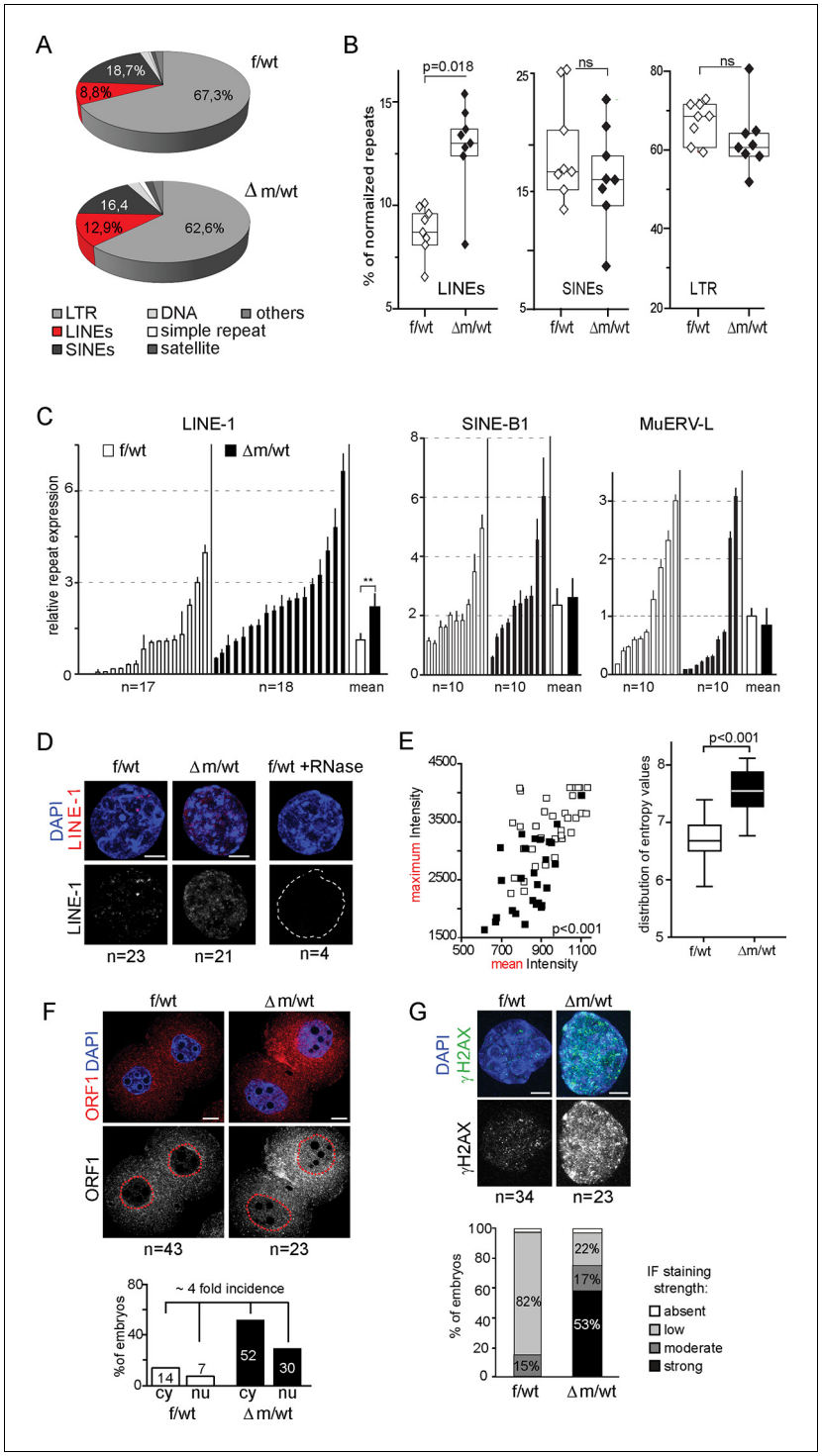

Figure 5. Increased LINE-1 protein levels and γH2AX foci in two-cell embryos depleted for KDM1A. (**A**) Pie chart representing the percent of each category of repeats analyzed in our 16 RNA-seq data of individual embryos. (**B**) Box-plot for percent of LINEs, SINEs and LTR element expression for f/wt (white) or △m/wt (black) embryos over the total of reads mapping repeats for each of our 16 samples of RNA-seq. Details of the analysis are in experimental analysis. (**C**) qPCR analysis for LINE-1, SinesB1 and MuERV-L expression levels from individual two-cell stage cDNAs of f/wt (white) or △m/wt (black). Each embryo is represented as a single bar. Data are expressed as normalized expression to three house-keeping genes. On the right of each graph is represented the mean ± sem. Two asterisks indicate p<0.01 as calculated using a Student's t-test. (**D**) Nascent *LINE-1* transcripts are detected by RNA FISH (signal in red) using a TCN7 probe on f/wt or △m/wt two-cell stage embryos. RNAse A

Figure 5 continued on next page

Figure 5 continued

treated control embryos processed in parallel display no signal for RNA transcription. Also see ***Figure 5—figure supplement 1*** for *Atrx* expression control. (**E**) Quantification of LINE-1 RNA FISH. On the left, the graph represents the fluorescent quantification with the mean intensity of fluorescence plotted on the x axis against the respective maximum intensity on the y axis) for each nucleus of the two–cell embryos for the two populations (white squares = f/wt controls and black square = △m/wt mutants). On the right, box-plot representation of the entropy levels analysis of the RNA FISH images for the control versus mutant embryos as defined by Haralick parameters measuring the pattern of the image with each dot corresponding to a f/wt (white) or △m/wt (black) nucleus.P value is calculated with a student T-test and indicated that the two populations are significantly different. (**F**) IF of two-cell stage embryos using anti-ORF1 antibodies (in red). A dotted line indicates the nucleus. Below is the graphical representation of the percentage of embryos displaying enriched fluorescent signal in either the cytoplasm (cy) or the nucleus (nu) for f/wt or △m/wt embryos. (**G**) IF of two-cell stage embryos using antibodies directed against phosphorylated histone H2A variant X (γH2AX, in green) for f/wt and △m/wt. Below is the corresponding quantification of embryo percentage according to the strength of γH2AX staining. DNA is counterstained by DAPI (blue). Number of processed embryos is indicated. Scale bar, 2 μm (**D**, **G**)) 10 μm (**F**).

DOI: 10.7554/eLife.08851.013

The following figure supplements are available for figure 5:

Figure supplement 1. RNA FISH controls for LINE-1 ongoing transcription.

DOI: 10.7554/eLife.08851.014

Figure supplement 2. EdU labeling and γH2AX immunofluorescence of *Kdm1a* mutant versus control two-cell stage embryos.

DOI: 10.7554/eLife.08851.015

Discussion

The oocyte stores maternal factors that besides ensuring the first steps of development prior to zygotic genome activation, also enable the epigenetic reprogramming of the parental genomes (***Burton and Torres-Padilla, 2010***; ***Li et al., 2010***; ***Messerschmidt et al., 2012***; ***Lorthongpanich et al., 2013***; ***Seisenberger et al., 2013***). Although the dynamics of histone modifications have been assessed, the biological relevance of such changes and the identification of the histone modifying enzymes involved in this process are only starting to be identified. In this study, we have focused on the critical function of KDM1A, a histone demethylase for H3K4me1/2 and H3K9me1/me2, that we find acts as a maternal chromatin factor at the time egg fertilization. We show that maternal KO results in abnormal oocytes at the time of ovulation (at meiosis II stage) and prevents development of fertilized eggs beyond the two-cell stage. Similar oocyte defects and developmental block were also observed in the accompanying paper by Wasson et al, where two other independent conditional alleles were used to induce deletion of KDM1A in oocytes, using Zp3-Cre or Gdf9 Cre. In a recent study maternal depletion of KDM1A was found to affect the first division of meiosis and leads to early apoptosis during oocyte growth (***Kim et al., 2015***). Taken together, these studies show that KDM1A is required during the formation of the female gametes for the two steps of meiosis (***Kim et al., 2015***; this study; Wasson et al.). Our study also reveals that KDM1A is required as a key factor during early post-zygotic embryo development, as the enzymatic inhibition of KDM1A in wild-type embryos resulted in developmental arrest at the two-cell stage, comparable to maternal deletion. We further show that KDM1A is a major regulator of histone H3K4 and H3K9 methylation patterns at the one-two cell stages and that it controls early switches in transcription patterns during development. KDM1A may also have a potential role in the appropriate repression of some LINE-1 retroviral elements.

KDM1A and the modulation of histone methylation after fertilization

H3K4me1/2/3 levels have been shown to increase from the zygote to the two-cell stage, before decreasing again by the four-cell stage (***Shao et al., 2014***). To date, only one H3K4 KMT, MLL2, has been shown to be necessary at the two-cell stage (***Andreu-Vieyra et al., 2010***). Here, we report that the maternal pool of the KDM, KDM1A, is also necessary at this stage, with its loss leading to global elevation of H3K4me1/2/3. Noticeably, no changes in transcription levels of genes encoding the main H3K4me2/3 KMTs were recorded (***Supplementary file 2***). This suggests that KDM1A is a key regulator of H3K4 methylation post-fertilization.

Moreover, in absence of KDM1A, the transcripts encoding for two main KMTs (SUV39H2/KMT1B and SETDB1/KMT1E) targeting H3K9me1/2 during preimplantation (**Cho et al., 2012**; **Puschendorf et al., 2008**) are well detected in two-cell stage mutant embryos (**Supplementary file 2**). These KMTs could be able to generate H3K9me3 from the excess of H3K9me1/2, produced because of the absence of KDM1A.

In conclusion, KDM1A most likely acts in combination with other chromatin regulators in order to keep a tight balance of the global H3K4/K9 methylation levels during early embryonic development.

KDM1A is involved in the transcriptional switch at the two-cell stage

One of the most striking consequences of lack of maternal KDM1A that we observed was the disruption of the wave-like gene expression patterns previously described at the onset of mouse development (**Hamatani et al., 2004**; **Xue et al., 2013**). At the two-cell stage, we saw a significant increase in mRNA levels of genes normally expressed maternally or at the zygote stage, and this increase relates more to post-fertilization disruption rather than inherited defects from *Kdm1a* mutant germline. The accompanying manuscript by Wasson et al reports similar findings concerning transcriptional regulation by maternal KDM1A in early stage post fertilization. Maternal and zygotic mRNA excess could reflect a reduced rate of mRNA degradation, maybe related to the developmental arrest, or else the severe impairment of the mutant embryos in the ribosome biogenesis pathways could preclude the translation machinery of their usage and clearance or else a change in the cytoplasmic polyadenylation of the maternal pool of mRNA could also be disturbing their utilization. Lastly, their abundance could also be due, maybe partly, to an increased transcription rate for these genes (and more specifically the one corresponding to the minor ZGA). Given the accumulation of H3K4 methylation that we show in our study for the mutants at this stage and the proven link of this mark with enhanced transcription (**Black et al., 2012**), we hypothesise that KDM1A might normally be involved in the transcriptional down-regulation of these genes via H3K4 demethylation. Chromatin-based repression is thought to be superimposed on zygotic genome activation and is necessary for the transition from the two-cell to the four-cell stage (**Ma, 2001**; **Ma and Schultz, 2008**; **Nothias et al., 1995**; **Wiekowski et al., 1997**). We propose that KDM1A might be part of such a mechanism, and required for a transition towards two-cell stage specific gene expression patterns (ie in the major ZGA and MGA waves), and therefore for proper development beyond the two-cell stage. The significant absence of the major ZGA and MGA waves in the transcriptome of *Kdm1a* mutants supports this hypothesis. Whether misplaced or increased H3K9 methylation (**Figure 3B**) could be involved in failure of transcription activation is not known, but one can speculate that such repressive chromatin and/or absence of KDM1A itself might impair correct recruitment of transcription regulators. So far, a small subset of such factors (TFs and co-regulators) acting at ZGA-gene promoters has recently been suggested to orchestrate the appropriate gene expression patterns following fertilization (**Park et al., 2013**; **Xue et al., 2013**). Although, KDM1A was not reported in this study, our results suggest that maternal KDM1A is nonetheless crucial for shaping the transcriptome in early life. Its role in oocyte and embryogenesis may have long lasting effects, as reported in the accompanying paper by Wasson et al where a hypomorphic maternal KDM1A, associated with perinatal lethality, showed alterations in imprinted gene expression much later in life. The importance of the maternal pool of KDM1A opens up exciting prospects for the roles of this remarkable histone demethylase in early development.

KDM1A is instrumental in preserving the genome integrity

The control of repeat elements by epigenetic mechanisms, including histone KMTs and KDMs, may be critical in early development. Previous work has suggested that KDM1A may contribute to MERVL element repression in late pre-implantation embryos (**Macfarlan et al., 2011**). We did not detect any impact on these elements in the *Kdm1a* mutants immediately post fertilization. However, we did see a small but significant increase in LINE-1 expression and LINE-1 ORF1 protein levels in the *Kdm1a* mutant embryos. This observation, together with the striking elevation in H3K4me3 levels, is of particular interest in the context of a recent study which proposed that loss of H3K4m3 at LINE-1 elements (rather than a gain in H3K9 methylation) might be critical for their repression during early pre-implantation development (**Fadloun et al., 2013**). Whether this increase in LINE-1 expression actually leads to an increase in LINE-1 element retrotransposition (ie new insertions) remains to

be seen, but the increase in LINE-1 proteins observed in *Kdm1a* mutant embryos is potentially consistent with such a possibility. In this context, we speculate that misregulation of LINE-1 elements in the absence of KDM1A might participate in the early developmental arrest that is observed, via an increased potential of genome instability and activation of some specific DNA damage checkpoints. The increase in γH2AX foci we detected in *Kdm1a* mutants, independently from replication stalling problems, could also be consistent with this hypothesis. Our results thus support the hypothesis that histone-based defence mechanisms act to safeguard the genome from LINE-1 retrotransposition during preimplantation development, when global DNA hypomethylation might compromises their usual silencing route (**Leung & Lorincz, 2012**).

Finally, chromatin status and regulated expression of another family of repeats, located within pericentric heterochromatin, has been proposed to be involved in developmental progression after fertilization, ensuring correct chromosome segregation and heterochromatin propagation (**Probst et al., 2010**; **Santenard et al., 2010**). In the absence of KDM1A, we detected aberrant accumulation of H3K9me3 at presumptive pericentric heterochromatin (NLBs) post-fertilization, as well as lagging chromosomes in oocytes, and micronuclei accumulation following fertilisation. Collectively, this data points to maternal KDM1A protein having a potential role at pericentromere/centromere regions that merits future exploration.

In conclusion, our findings demonstrate the instrumental role of KDM1A as a maternally provided protein at the beginning of life in shaping the histone methylation landscape and the transcriptional repertoire of the early embryo.

Materials and methods

Experimental methods

Collection of mouse embryos and in vitro culture

All mice used were handled with care and according to the guidelines from French legislation and institutional policies. Mice (*Kdm1a*^{tm1Schüle}) carrying the targeted mutation allowing the conditional deletion of the first exon of *Kdm1a* by insertion of two flanking LoxP sites has been engineered and described by R.Schüle group (**Zhu et al., 2014**). We received mice carrying two copies of this new conditional allele *Kdm1a*^{tm1Schüle}, and after transfer in our animal facitilities, they were bred over the well know Zp3^{cre} deleter strain which allow CRE mediated recombination specifically in the female germline (**Lewandoski et al., 1997**). The genetic background of the mice *Kdm1a*$^{f/f}$::*Zp3*^{cre} is a mixture of C57BL/6J and a 129 substrains, and are referred in this manuscript as *Kdm1a*$^{f/f}$::*Zp3*^{cre} mice (as carrying two *Kdm1a* conditional alleles and a *Zp3.cre* transgene). To evaluate KDM1A functions during early development, embryos were obtained from superovulated *Kdm1a*$^{f/f}$::*Zp3*^{cre} or *Kdm1a*$^{f/f}$ females (aged 4–8 weeks) mated with B6D2F1 males (see **Figure 1C**), and collected in M2 medium (Sigma, Saint-Louis, MO) at 21–28 hr (zygote) and 40–42 hr (two-cell) after hCG (human chorionic gonadotropin) injection. For pargyline treatment (Sigma;1 mM final during 24 hr) zygotes were in vitro cultured in M16 (Sigma) droplets under mineral oil in a 5% CO2 atmosphere at 37°C. For replication assays, two-cell-stage embryos were collected at 39–40 hphCG, and embryos were cultured in M16 medium 1 hr, then transferred to M16 containing 50 µM EdU (Click it Life Technologies, Santa Clara, CA) for 45 min. Following fixation in 4% PFA for 15 min, permeabilization in PBS 0.5% Triton X-100 for 15 min, blocking in PBS 3% BSA. Click-it reaction was performed for 1 hr. Washes and new blocking were followed by immunostaining with antibodies against γH2AX (see next section).

Immunofluorescence staining

Immunofluorescence was carried out as described previously (**Torres-Padilla et al., 2006**), with some modifications. After removal of the zona pellucida with acid Tyrode's solution (Sigma), embryos were fixed in 4% paraformaldehyde, 0,2% sucrose, 0.04% Triton-X100 and 0.3% Tween20 in PBS for 15 min at 37˚C. After permeabilisation with 0.5% Triton-X100 in PBS for 20 min at room temperature, embryos were washed in PBStp (0.05% Triton-X100; 1 mg/ml polyvinyl pyrrolidone (PVP;Sigma)) then blocked and incubated with the primary antibodies in 1% BSA, 0.05% Triton-X100 for ~16 hr at 4˚C. Embryos were washed in PBStp twice and blocked 30 min in 1% BSA in PBStp and incubated for 2 hr with the corresponding secondary antibodies at room temperature. After

washing, embryos were mounted in Vectashield (Vector Laboratories, Burlingame, CA) containing DAPI (4',6'-diamidino-2-phénylindole) for visualizing the DNA. Full projections of images taken every 0.5 µm along the z axis are shown for all stainings, except for the ORF1 for which the middle section is shown only. Antibody staining for H3K4 methylation is in green, and in red for H3K9 methylation, DNA is counterstained with DAPI (blue). For each antibody, embryos were processed identically and analyzed using the same settings for confocal acquisition Stainings were repeated independently at least twice. The following antibodies were used (Antibody/Vendor/Catalog #/Concentration): anti-rabbit KDM1A/Abcam (UK)/ab17721/ 1:750, anti mouse H3K4me1/Cosmobio (Japan)/MCA-MBAI0002/ 1:700, anti mouse H3K4me2/Cosmobio /MCA-MBAI0003/ 1:700, anti mouse H3K4me3/ Cosmobio/MCA-MBAI0004/ 1:700, anti-rabbit H3K9me1 kind gift from T.Jenuwein, anti mouse H3K9me2/Cosmobio /MCA-MBAI0007/ 1:500, anti rabbit H3K9me2/ActiveMotif (Carlsbad, CA) / 39239/ 1:800, anti rabbit H3K9me3/ Millipore (Billerica, MA/07–442/ 1:200, anti-mouse H3K27me3/ Abcam/ab6002/ 1:400, anti-rabbit H4K20me3/ Abcam/ab 9053/ 1:200, anti-mouse γH2AX/ Millipore/05–623/ 1/200, anti-mouse β-TUBULIN/ Invitrogen (Carlsbad, CA)/32–2600/ 1:1000, anti-mouse POLII CTD4/ Millipore/05–623/1:200, anti-rabbit POLII CTD4 S2P/Abcam/ab5095/1:200, anti-rabbit ORF1, kind gift from A.Bortvin/ 1:500, Alexa488 goat anti-mouse IgG/ Invitrogen/A11029/ 1:500, Alexa568 goat anti-rabbit IgG/ Invitrogen A11036/ 1:500.

Western-blot procedure

50 two-cell stage embryos were resuspended in 2-mercaptoethanol containing loading buffer and heated at 85°C for 15 m. SDS-PAGE, Ponceau staining, and immunoblots were performed following standard procedures using a Mini-PROTEAN Tetra Cell System (Bio-Rad, Hercules, CA). Primary anti-KDM1A (dilution 1:500) and secondary HRP-conjugated goat anti-rabbit (DAKO, Santa Clara, CA, Cat.#K4002) were used. 2 µg of ESC nuclear extracts were used as control.

RNA FISH procedure

RNA FISH was performed as described (***Patrat et al., 2009***). Nick translation (Vysis Abbott, Chicago, IL) using Spectrum green or Spectrum red (Vysis) was used to label double stranded probes. The LINE-1 probe used consisted of a full- length Tf element cloned into a Bluescript plasmid as previously described (***Chow et al., 2010***). The *Atrx* probe consisted of a BAC (CHORI, Oakland, CA; reference RP23-260I15). Briefly, embryos were taken at 42 hr post hCG and the *zona pellucida* was removed. Embryos were transferred onto coverslips previously coated in Denhardt's solution, dried down for 30 min at room temperature, after all excess liquid was removed. Samples were fixed in 3% paraformaldehyde (pH 7.2) for 10 min at RT and permeabilized in ice-cold PBS 0.5% triton for 1 min on ice and then directly stored in ETOH 70°C ethanol at -20°C until processed for RNA FISH. Hybridizations, without *Cot1* competition for LINE-1, were performed overnight at 37°C in a humid chamber. Excess of probes was eliminated through three washes in 2xSSC at 42°C for 5 min each. Slides were mounted in Vectashield containing DAPI.

Single embryo RNA RT-qPCR and deep sequencing

After *zona pellucida* removal and 3 consecutive washes in PBS-0.1% BSA, individual oocytes or whole two-cell stage embryos were transferred into a 0.2 ml eppendorf tube (care was taken to add a minimum liquid volume of PBS BSA) and directly frozen in -80°C until use. RNA was extracted and amplified as described previously (***Tang et al. 2010***). For quality control and gene expression analysis, quantitative real-time PCR was performed for gene expression on 1/10 dilution of cDNA preparation in 10 µl final volume with Power SYBR green PCR master mix (Applied Biosystems, Foster City, CA) on a ViiA7 apparatus (Life Technologies). The level of gene expression was normalized to the geometric mean of the expression level ofFoster City Hprt, Gapdh and Ppia housekeeping genes as according to (***Vandesompele et al., 2002***). For $p<0.05$ corresponds to * and $p<0.001$ to ** by t-test. The following primers used in this study are listed as name/ forward primer 5' to 3' / reverse primer 5' to 3' *Hprt*/ ctgtggccatctgcctagt / gggacgcagcaactgacatt, *Gapdh*/ ccccaacactgagcatctcc / attatgggggtctgggatgg, *Ppia*/ ttacccatcaaaccattccttctg / aacccaaagaacttcagtgagagc (as in ***Duffie et al., 2014***Atrx/ tgcctgctaaattctccaca / aggcaagtcttcacagctgt, *H2AZ*/ acacatccacaaatcgctga / aagcctccaacttgctcaaa, *Klf4*/ agccattattgtgtcggagga/ agtatgcagcagttggagaac, *Suv39h1*/ ctgggtccacttgtctcagt/ ctgggaagtatgggcaggaa, SineB1/ gtggcgcacgcctttaatc /

gacagggtttctctgtgtag (**Martens et al., 2005**), MuERVL/ atctcctggcacctggtatg / agaagaaggcatttgccaga (**Macfarlan et al., 2011**), *Kdm1a*/ tggagaacacacaatccgga / tgccgttggatctctctgtt, LINE-1 3'UTR/ atggaccatgtagagactgcca / caatggtgtcagcgtttgga

For RNA deep sequencing, library construction was performed following Illumina (San Diego, CA) manufacturer suggestions. The 26 samples (5 f/f or wt/wt and 5 Δm/Δm oocytes; 8 f/wt and 8 Δm/wttwo-cell embryos) were sequenced in single-end 49 bp reads on an Illumina HiSeq 2500 instrument. The depth of sequencing was ranged from 12,500,000 to 35,000,000 with an average around 18,000,000 reads per sample (**Supplementary file 1**).

Data procession and analysis

Confocal acquisition and image analysis

Imaging of embryos following IF and FISH was performed on an inverted confocal microscope Zeiss (Germany) LSM700 with a Plan apo DICII (numerical aperture 1.4) 63x oil objective. Z sections were taken every 0.4 µm (**Figure 1–3**) or 1 µm (**Figure 4** and **5**). For fluorescence intensity measurement on immunofluorescence Z stacks acquisitions, the nuclear area of the stack image was selected, and then the integrated Intensity (intensity divided by the number of voxels represented within the nuclear area) was obtained using the 3D object counter plugin in Image J (**Bolte and Cordelieres, 2006**). For LINE-1 RNA FISH analysis, home-made script for ImageJ were developed that used descriptors defined as (**Haralick, 1979**) to quantitatively study the texture and structure of images (see related manuscript file containing the code in Java text). Distribution of fluorescence intensities or of Haralick parameters (eg entropy) were compared using t-tests, after all data had been tested as belonging to normally distributed populations (Origin8Pro software, Northampton, MA). For $p<0.05$ corresponds to * and $p<0.001$ to **.

RNA sequencing

For the gene-based differential analysis, quality control was applied on raw data. Sequencing reads characterized by at least one of the following criteria were discarded from the analysis: (more than 50% of low quality bases (Phred score <5); more than 5% of N bases; more than 80% of AT rate At least 30% (15 bases) of continuous A and/or T). Reads passing these filters were then aligned to the mouse mm10 genome using the TopHat software v2.0.6 (**Trapnell et al., 2009**). Only unique best alignments with less than 2 mismatches were reported for downstream analyses. Count tables of gene expression were generated using the RefSeq annotation and the HTSeq v0.6.1 software (**Anders et al., 2015**). The DESeq R package v1.16.0 (**Anders and Huber, 2010**) was then used to normalize and identify the differentially expressed genes between control and mutant embryos. Genes with 0 counts in all samples were filtered out and only the 60% of the top expressed genes were used for the analysis, as described in the DESeq reference manual. Genes with an adjusted p-value lower than $\alpha = 0.05$ were consider as differentially expressed. Hierarchical clustering analysis for gene expression pattern of 16 libraries was based on Spearman correlation distance and the Ward method, and performed using the hclust function implemented in the gplots v2.16.0 R package.

In order to study the transposons expression, we performed the mapping of reads passing the quality control using the Bowtie v1.0.0 software (**Langmead et al., 2009**). This mapping was performed in 2 steps: (i) reads aligned on ribosomal RNA (unique best alignments with less than 3 mismatches in the seed) (GenBank identifiers:18S, NR_003278.3; 28S, NR_003279.1; 5S, D14832.1; and 5.8S, KO1367.1) were discarded (ii) remaining reads were aligned to the mouse mm10 genome, reporting a maximum of 10,000 genomic locations (best alignments without mismatches). Aligned reads were then annotated and intersected with repeats annotation from the repeatMasker database. The transposon counts table was generated using the reads that fully overlap with an annotated repeat and for which all possible alignments are concordant, i.e associated with the same repeat family in more than 95% of cases. The resulting count table was normalized by the total number of reads aligned on repeats. Statistical analysis to identify repeat families with significant changes in expression between control and mutant embryos was performed using the limma R package v3.20.4 (**Ritchie et al., 2015**). Repeats family with an adjusted p-value lower than $\alpha = 0.05$ were consider as significant.

The tool AmiGO 2 (**Carbon et al., 2009**) was used to perform the enrichment Gene Ontology items with the misregulated genes from the *Kdm1a* mutant two-cell stage embryos.

Data access

The Gene Expression Omnibus (GEO) accession number for the data sets reported in this paper is GSE68139

Acknowledgements

We thank A Bortvin and T Jenuwein for kind gift of antibodies. We thank Simao Teixeira Da Rocha, Rafael Galupa and Petra Hajkova for critical reading of the manuscript, and members of the EH laboratory for feedback. We acknowledge the pathogen-free barrier animal facility of the Institut Curie, in particular Colin Jouhanneau, and the UMR3215/U934 Imaging Platform (PICT-IBiSA), in particular Olivier Leroy and Nicolas Signolle. MB was supported by the DIM-Stem Pôle, Ile de France, Funding for EH: Equipe labellisée ''La Ligue Contre Le Cancer''; EU FP7 MODHEP EU grant no. 259743; Labex DEEP (ANR-11-LBX-0044) part of the IDEX PSL (ANR-10-IDEX-0001-02 PSL).

Additional information

Funding

Funder	Grant reference number	Author
EU FP7 MODHEP EU	259743	Edith Heard
Labex DEEP	ANR-11-LBX-0044	Edith Heard
IDEX idx PSL	ANR-10-IDEX-001-02 PSL	Edith Heard

The funders had no role in study design, data collection and interpretation, or the decision to submit the work for publication.

Author contributions

KA, Conception and design, Acquisition of data, Analysis and interpretation of data, Drafting or revising the article; LS, IV, TL, NS, EB, Analysis and interpretation of data, Drafting or revising the article; MB, NR, LB-R, Acquisition of data, Drafting or revising the article; EM, RS, Drafting or revising the article, Contributed unpublished essential data or reagents; C-JC, Acquisition of data, Analysis and interpretation of data, Drafting or revising the article; EH, Conception and design, Analysis and interpretation of data, Drafting or revising the article

Author ORCIDs

Edith Heard, http://orcid.org/0000-0001-8052-7117

Ethics

Animal experimentation: All mice used were handled with care and according to approved institutional animal care and use committee of the Institut Curie (CEEA-IC) protocols(C 75-05-18). The work has also been conducted under the approval from the French Ministry of Higher Education and Research for the use of Genetically Modified Organisms (agreement number 5549CA-I).

Additional files

Supplementary files

• Supplementary file 1. Summary of RNA seq data for control and maternally depleted oocytes or two-cell stage embryos. Statistical analysis of all the single oocyte or individual two-cell stage embryo RNA-seq used in this study. Datasets are available from GEO under access number GSE75054 and GSE68139.

DOI: 10.7554/eLife.08851.016

• Supplementary file 2. Differential gene expression at the two-cell stage and oocyte stage upon loss of maternal KDM1A. The DESeq R package was used to normalize and identify the differentially expressed genes between control and mutant embryos. Genes with 0 counts in all samples were filtered out and only the 60% of the top expressed genes were used for the analysis Differentially expressed genes were identified using a minimum Log2>1 (upregulation) or <-1 (downregulation) fold change (FC) and with an adjusted p-value lower than $\alpha = 0.05$.
DOI: 10.7554/eLife.08851.017

Major datasets

The following datasets were generated:

Author(s)	Year	Dataset title	Dataset URL	Database, license, and accessibility information
Ancelin K, Six L, Chen C, Heard E	2015	LSD1 is an essential regulator of the chromatin and transcriptional landscapes during the maternal-to-zygotic	http://www.ncbi.nlm.nih.gov/geo/query/acc.cgi?acc=GSE68139	Publicly available at the NCBI Gene Expression Omnibus (Accession no: GSE68139).
Ancelin K, Vassilev, Chen C, Heard E	2015	LSD1 is an essential regulator of the chromatin and transcriptional landscapes during the maternal-to-zygotic	http://www.ncbi.nlm.nih.gov/geo/query/acc.cgi?acc=GSE75054	Publicly available at the NCBI Gene Expression Omnibus (Accession no: GSE75054).

The following previously published dataset was used:

Author(s)	Year	Dataset title	Dataset URL	Database, license, and accessibility information
Park S-J, Komata M, Inoue F, Yamada K, Nakai K, Ohsugi M, Shirahige K	2013	Inferring the choreography of parental genomes during fertilization from ultralarge-scale whole-transcriptome analysis	http://trace.ddbj.nig.ac.jp/DRASearch/submission?acc=DRA001066	Publicly available at the DDBJ Sequence Read Archive (accession no: DRA001066).

References

Adenot PG, Mercier Y, Renard JP, Thompson EM. 1997. Differential H4 acetylation of paternal and maternal chromatin precedes DNA replication and differential transcriptional activity in pronuclei of 1-cell mouse embryos. *Development* **124**:4615–4625.

Anders S, Huber W. 2010. Differential expression analysis for sequence count data. *Genome Biology* **11**:R106. doi: 10.1186/gb-2010-11-10-r106

Anders S, Pyl PT, Huber W. 2015. HTSeq–a python framework to work with high-throughput sequencing data. *Bioinformatics* **31**:166–169. doi: 10.1093/bioinformatics/btu638

Andreu-Vieyra CV, Chen R, Agno JE, Glaser S, Anastassiadis K, Stewart AF, Matzuk MM. 2010. MLL2 is required in oocytes for bulk histone 3 lysine 4 trimethylation and transcriptional silencing. *PLoS Biology* **8**:e1000453. doi: 10.1371/journal.pbio.1000453

Arney KL, Bao S, Bannister AJ, Kouzarides T, Surani MA. 2002. Histone methylation defines epigenetic asymmetry in the mouse zygote. *The International Journal of Developmental Biology* **46**:317–320.

Black JC, Van Rechem C, Whetstine JR. 2012. Histone lysine methylation dynamics: establishment, regulation, and biological impact. *Molecular Cell* **48**:491–507. doi: 10.1016/j.molcel.2012.11.006

Bolte S, Cordelieres FP. 2006. A guided tour into subcellular colocalization analysis in light microscopy. *Journal of Microscopy* **224**:213–232. doi: 10.1111/j.1365-2818.2006.01706.x

Burton A, Torres-Padilla M-E. 2010. Epigenetic reprogramming and development: a unique heterochromatin organization in the preimplantation mouse embryo. *Briefings in Functional Genomics* **9**:444–454. doi: 10.1093/bfgp/elq027

Carbon S, Ireland A, Mungall CJ, Shu S, Marshall B, Lewis S.AmiGO HubWeb Presence Working Group. 2009. AmiGO: online access to ontology and annotation data. *Bioinformatics* **25**:288–289. doi: 10.1093/bioinformatics/btn615

Cho S, Park JS, Kwon S, Kang Y-K. 2012. Dynamics of Setdb1 expression in early mouse development. *Gene Expression Patterns* **12**:213–218. doi: 10.1016/j.gep.2012.03.005

Chow JC, Ciaudo C, Fazzari MJ, Mise N, Servant N, Glass JL, Attreed M, Avner P, Wutz A, Barillot E, et al. 2010. LINE-1 activity in facultative heterochromatin formation during x chromosome inactivation. *Cell* **141**:956–969. doi: 10.1016/j.cell.2010.04.042

Ciccone DN, Su H, Hevi S, Gay F, Lei H, Bajko J, Xu G, Li E, Chen T. 2009. KDM1B is a histone H3K4 demethylase required to establish maternal genomic imprints. *Nature* **461**:415–418. doi: 10.1038/nature08315

de Vries WN, Binns LT, Fancher KS, Dean J, Moore R, Kemler R, Knowles BB. 2000. Expression of cre recombinase in mouse oocytes: a means to study maternal effect genes. *Genesis* **26**:110–112. doi: 10.1002/(SICI)1526-968X(200002)26:2<110::AID-GENE2>3.0.CO;2-8

Di Stefano L, Ji J-Y, Moon N-S, Herr A, Dyson N. 2007. Mutation of *Drosophila* Lsd1 Disrupts H3-K4 Methylation, Resulting in Tissue-Specific Defects during Development. *Current Biology* **17**:808–812. doi: 10.1016/j.cub.2007.03.068

Duffie R, Ajjan S, Greenberg MV, Zamudio N, Escamilla del Arenal M, Iranzo J, Okamoto I, Barbaux S, Fauque P, Bourc'his D. 2014. The Gpr1/Zdbf2 locus provides new paradigms for transient and dynamic genomic imprinting in mammals. *Genes & Development* **28**:463–478. doi: 10.1101/gad.232058.113

Erhardt S, Su IH, Schneider R, Barton S, Bannister AJ, Perez-Burgos L, Jenuwein T, Kouzarides T, Tarakhovsky A, Surani MA. 2003. Consequences of the depletion of zygotic and embryonic enhancer of zeste 2 during preimplantation mouse development. *Development* **130**:4235–4248. doi: 10.1242/dev.00625

Fadloun A, Le Gras S, Jost B, Ziegler-Birling C, Takahashi H, Gorab E, Carninci P, Torres-Padilla M-E. 2013. Chromatin signatures and retrotransposon profiling in mouse embryos reveal regulation of LINE-1 by RNA. *Nature Structural & Molecular Biology* **20**:332–338. doi: 10.1038/nsmb.2495

Fierz B, Muir TW. 2012. Chromatin as an expansive canvas for chemical biology. *Nature Chemical Biology* **8**:417–427. doi: 10.1038/nchembio.938

Flach G, Johnson MH, Braude PR, Taylor RA, Bolton VN. 1982. The transition from maternal to embryonic control in the 2-cell mouse embryo. *The EMBO Journal* **1**:681–686.

Foster CT, Dovey OM, Lezina L, Luo JL, Gant TW, Barlev N, Bradley A, Cowley SM. 2010. Lysine-specific demethylase 1 regulates the embryonic transcriptome and CoREST stability. *Molecular and Cellular Biology* **30**:4851–4863. doi: 10.1128/MCB.00521-10

Glaser S, Schaft J, Lubitz S, Vintersten K, van der Hoeven F, Tufteland KR, Aasland R, Anastassiadis K, Ang SL, Stewart AF. 2006. Multiple epigenetic maintenance factors implicated by the loss of Mll2 in mouse development. *Development* **133**:1423–1432. doi: 10.1242/dev.02302

Greer EL, Shi Y. 2012. Histone methylation: a dynamic mark in health, disease and inheritance. *Nature Reviews Genetics* **13**:343–357. doi: 10.1038/nrg3173

Hamatani T, Carter MG, Sharov AA, Ko MSH. 2004. Dynamics of global gene expression changes during mouse preimplantation development. *Developmental Cell* **6**:117–131. doi: 10.1016/S1534-5807(03)00373-3

Haralick RM. 1979. Statistical and structural approaches to texture. *Proceedings of the IEEE* **67**:786–804. doi: 10.1109/PROC.1979.11328

Kano H, Godoy I, Courtney C, Vetter MR, Gerton GL, Ostertag EM, Kazazian HH. 2009. L1 retrotransposition occurs mainly in embryogenesis and creates somatic mosaicism. *Genes & Development* **23**:1303–1312. doi: 10.1101/gad.1803909

Katz DJ, Edwards TM, Reinke V, Kelly WG. 2009. A c. elegans LSD1 demethylase contributes to germline immortality by reprogramming epigenetic memory. *Cell* **137**:308–320. doi: 10.1016/j.cell.2009.02.015

Kim J, Singh AK, Takata Y, Lin K, Shen J, Lu Y, Kerenyi MA, Orkin SH, Chen T. 2015. LSD1 is essential for oocyte meiotic progression by regulating CDC25B expression in mice. *Nature Communications* **6**:10116. doi: 10.1038/ncomms10116

Langmead B, Trapnell C, Pop M, Salzberg SL. 2009. Ultrafast and memory-efficient alignment of short DNA sequences to the human genome. *Genome Biology* **10**:R25. doi: 10.1186/gb-2009-10-3-r25

Laurent B, Ruitu L, Murn J, Hempel K, Ferrao R, Xiang Y, Liu S, Garcia BA, Wu H, Wu F, et al. 2015. A specific LSD1/KDM1A isoform regulates neuronal differentiation through H3K9 demethylation. *Molecular Cell* **57**:957–970. doi: 10.1016/j.molcel.2015.01.010

Lepikhov K, Walter J. 2004. Differential dynamics of histone H3 methylation at positions K4 and K9 in the mouse zygote. *BMC Developmental Biology* **4**:12. doi: 10.1186/1471-213X-4-12

Leung DC, Lorincz MC. 2012. Silencing of endogenous retroviruses: when and why do histone marks predominate? *Trends in Biochemical Sciences* **37**:127–133. doi: 10.1016/j.tibs.2011.11.006

Lewandoski M, Wassarman KM, Martin GR. 1997. Zp3–cre, a transgenic mouse line for the activation or inactivation of loxP-flanked target genes specifically in the female germ line. *Current Biology* **7**:148–151. doi: 10.1016/S0960-9822(06)00059-5

Li L, Zheng P, Dean J. 2010. Maternal control of early mouse development. *Development* **137**:859–870. doi: 10.1242/dev.039487

Lorthongpanich C, Cheow LF, Balu S, Quake SR, Knowles BB, Burkholder WF, Solter D, Messerschmidt DM. 2013. Single-cell DNA-methylation analysis reveals epigenetic chimerism in preimplantation embryos. *Science* **341**:1110–1112. doi: 10.1126/science.1240617

Ma J. 2001. Regulation of zygotic gene activation in the preimplantation mouse embryo: global activation and repression of gene expression. *Biology of Reproduction* **64**:1713–1721. doi: 10.1095/biolreprod64.6.1713

Ma P, Schultz RM. 2008. Histone deacetylase 1 (hDAC1) regulates histone acetylation, development, and gene expression in preimplantation mouse embryos. *Developmental Biology* **319**:110–120. doi: 10.1016/j.ydbio.2008.04.011

Macfarlan TS, Gifford WD, Agarwal S, Driscoll S, Lettieri K, Wang J, Andrews SE, Franco L, Rosenfeld MG, Ren B, et al. 2011. Endogenous retroviruses and neighboring genes are coordinately repressed by LSD1/KDM1A. *Genes & Development* **25**:594–607. doi: 10.1101/gad.2008511

Mamo S, Gal A, Bodo S, Dinnyes A. 2007. Quantitative evaluation and selection of reference genes in mouse oocytes and embryos cultured in vivo and in vitro. *BMC Developmental Biology* **7**:14. doi: 10.1186/1471-213X-7-14

Martens JHA, O'Sullivan RJ, Braunschweig U, Opravil S, Radolf M, Steinlein P, Jenuwein T. 2005. The profile of repeat-associated histone lysine methylation states in the mouse epigenome. *The EMBO Journal* **24**:800–812. doi: 10.1038/sj.emboj.7600545

Matoba S, Liu Y, Lu F, Iwabuchi KA, Shen L, Inoue A, Zhang Y. 2014. Embryonic development following somatic cell nuclear transfer impeded by persisting histone methylation. *Cell* **159**:884–895. doi: 10.1016/j.cell.2014.09.055

Messerschmidt DM, de Vries W, Ito M, Solter D, Ferguson-Smith A, Knowles BB. 2012. Trim28 is required for epigenetic stability during mouse oocyte to embryo transition. *Science* **335**335; :1499–1502. doi: 10.1126/science.1216154

Metzger E, Wissmann M, Yin N, Müller JM, Schneider R, Peters AHFM, Günther T, Buettner R, Schüle R. 2005. LSD1 demethylates repressive histone marks to promote androgen-receptor-dependent transcription. *Nature* **437**:436–439. doi: 10.1038/nature04020

Nothias J-Y, Majumder S, Kaneko KJ, DePamphilis ML. 1995. Regulation of gene expression at the beginning of mammalian development. *Journal of Biological Chemistry* **270**:22077–22080. doi: 10.1074/jbc.270.38.22077

O'Carroll D, Erhardt S, Pagani M, Barton SC, Surani MA, Jenuwein T. 2001. The polycomb-group gene Ezh2 is required for early mouse development. *Molecular and Cellular Biology* **21**:4330–4336. doi: 10.1128/MCB.21.13.4330-4336.2001

Park S-J, Komata M, Inoue F, Yamada K, Nakai K, Ohsugi M, Shirahige K. 2013. Inferring the choreography of parental genomes during fertilization from ultralarge-scale whole-transcriptome analysis. *Genes & Development* **27**:2736–2748. doi: 10.1101/gad.227926.113

Patrat C, Okamoto I, Diabangouaya P, Vialon V, Le Baccon P, Chow J, Heard E. 2009. Dynamic changes in paternal x-chromosome activity during imprinted x-chromosome inactivation in mice. *Proceedings of the National Academy of Sciences* **106**:5198–5203. doi: 10.1073/pnas.0810683106

Peaston AE, Evsikov AV, Graber JH, de Vries WN, Holbrook AE, Solter D, Knowles BB. 2004. Retrotransposons regulate host genes in mouse oocytes and preimplantation embryos. *Developmental Cell* **7**:597–606. doi: 10.1016/j.devcel.2004.09.004

Posfai E, Kunzmann R, Brochard V, Salvaing J, Cabuy E, Roloff TC, Liu Z, Tardat M, van Lohuizen M, Vidal M, et al. 2012. Polycomb function during oogenesis is required for mouse embryonic development. *Genes & Development* **26**:920–932. doi: 10.1101/gad.188094.112

Probst AV, Okamoto I, Casanova M, El Marjou F, Le Baccon P, Almouzni G. 2010. A strand-specific burst in transcription of pericentric satellites is required for chromocenter formation and early mouse development. *Developmental Cell* **19**:625–638. doi: 10.1016/j.devcel.2010.09.002

Puschendorf M, Terranova R, Boutsma E, Mao X, Isono Kyo-ichi, Brykczynska U, Kolb C, Otte AP, Koseki H, Orkin SH, et al. 2008. PRC1 and Suv39h specify parental asymmetry at constitutive heterochromatin in early mouse embryos. *Nature Genetics* **40**:411–420. doi: 10.1038/ng.99

Ritchie ME, Phipson B, Wu D, Hu Y, Law CW, Shi W, Smyth GK. 2015. Limma powers differential expression analyses for RNA-sequencing and microarray studies. *Nucleic Acids Research* **43**:e47. doi: 10.1093/nar/gkv007

Santenard A, Ziegler-Birling C, Koch M, Tora L, Bannister AJ, Torres-Padilla M-E. 2010. Heterochromatin formation in the mouse embryo requires critical residues of the histone variant H3.3. *Nature Cell Biology* **12**:853–862. doi: 10.1038/ncb2089

Santos F, Peters AH, Otte AP, Reik W, Dean W. 2005. Dynamic chromatin modifications characterise the first cell cycle in mouse embryos. *Developmental Biology* **280**:225–236. doi: 10.1016/j.ydbio.2005.01.025

Santos F, Zakhartchenko V, Stojkovic M, Peters A, Jenuwein T, Wolf E, Reik W, Dean W. 2003. Epigenetic marking correlates with developmental potential in cloned bovine preimplantation embryos. *Current Biology* **13**:1116–1121. doi: 10.1016/S0960-9822(03)00419-6

Seisenberger S, Peat JR, Hore TA, Santos F, Dean W, Reik W. 2013. Reprogramming DNA methylation in the mammalian life cycle: building and breaking epigenetic barriers. *Philosophical Transactions of the Royal Society of London. Series B, Biological Sciences* **368**. doi: 10.1098/rstb.2011.0330

Shao G-B, Chen J-C, Zhang L-P, Huang P, Lu H-Y, Jin J, Gong A-H, Sang J-R. 2014. Dynamic patterns of histone H3 lysine 4 methyltransferases and demethylases during mouse preimplantation development. *In Vitro Cellular & Developmental Biology - Animal* **50**:603–613. doi: 10.1007/s11626-014-9741-6

Shi Y, Lan F, Matson C, Mulligan P, Whetstine JR, Cole PA, Casero RA, Shi Y. 2004. Histone demethylation mediated by the nuclear amine oxidase homolog LSD1. *Cell* **119**:941–953. doi: 10.1016/j.cell.2004.12.012

Tang F, Barbacioru C, Nordman E, Li B, Xu N, Bashkirov VI, Lao K, Surani MA. 2010. RNA-seq analysis to capture the transcriptome landscape of a single cell. *Nature Protocols* **5**:516–535. doi: 10.1038/nprot.2009.236

Torres-Padilla M-E, Bannister AJ, Hurd PJ, Kouzarides T, Zernicka-Goetz M. 2006. Dynamic distribution of the replacement histone variant H3.3 in the mouse oocyte and preimplantation embryos. *The International Journal of Developmental Biology* **50**:455–461. doi: 10.1387/ijdb.052073mt

Trapnell C, Pachter L, Salzberg SL. 2009. TopHat: discovering splice junctions with RNA-seq. *Bioinformatics* **25**:1105–1111. doi: 10.1093/bioinformatics/btp120

Vandesompele J, De Preter K, Pattyn F, Poppe B, Van Roy N, De Paepe A, Speleman F. 2002. Accurate normalization of real-time quantitative RT-PCR data by geometric averaging of multiple internal control genes. *Genome Biology* **3**:research0034. doi: 10.1186/gb-2002-3-7-research0034

Wang J, Hevi S, Kurash JK, Lei H, Gay F, Bajko J, Su H, Sun W, Chang H, Xu G, et al. 2009. The lysine demethylase LSD1 (kDM1) is required for maintenance of global DNA methylation. *Nature Genetics* **41**:125–129. doi: 10.1038/ng.268

Wang J, Scully K, Zhu X, Cai L, Zhang J, Prefontaine GG, Krones A, Ohgi KA, Zhu P, Garcia-Bassets I, et al. 2007. Opposing LSD1 complexes function in developmental gene activation and repression programmes. *Nature* **446**:882–887. doi: 10.1038/nature05671

Wiekowski M, Miranda M, Nothias JY, DePamphilis ML. 1997. Changes in histone synthesis and modification at the beginning of mouse development correlate with the establishment of chromatin mediated repression of transcription. *Journal of Cell Science* **110 (Pt 10**:1147–1158.

Xue Z, Huang K, Cai C, Cai L, Jiang Chun-yan, Feng Y, Liu Z, Zeng Q, Cheng L, Sun YE, et al. 2013. Genetic programs in human and mouse early embryos revealed by single-cell RNA sequencing. *Nature* **500**:593–597. doi: 10.1038/nature12364

Zhu D, Hölz S, Metzger E, Pavlovic M, Jandausch A, Jilg C, Galgoczy P, Herz C, Moser M, Metzger D, et al. 2014. Lysine-specific demethylase 1 regulates differentiation onset and migration of trophoblast stem cells. *Nature Communications* **5**. doi: 10.1038/ncomms4174

ARTICLE 2 - THE DYNAMICS OF PARENTAL GENOME CONFORMATIONS IN EARLY MOUSE EMBRYOGENESIS AND DURING IMPRINTED X-CHROMOSOME INACTIVATION (MANUSCRIPT IN PREPARATION).

Title: The dynamics of parental genome conformation in early mouse embryogenesis and imprinted X-chromosome inactivation

Authors: Noémie Ranisavljevic*, Takashi Nagano*, Csilla Varnai*, Katia Ancelin, Wing Leung, Tristan Piolot, Laurène Syx, Edith Heard† & Peter Fraser†
* Equal contributions; † Co-corresponding authors

Abstract: Upon fertilization, the highly differentiated genomes of the two gametes are reprogrammed to become totipotent and undergo an exquisite and orchestrated choreography of epigenetic changes. What exactly this genome reorganisation entails is still unknown. Furthermore, in female embryos, the paternal X chromosome undergoes X-chromosome inactivation (XCI). This first wave of imprinted XCI ensure dosage compensation between sexes, but how the X chromosome is reorganised as genes become silenced during these early steps of development is unknown. In order to explore parental genome structure and more specifically the conformation of the X chromosome during preimplantation development, we applied an allele-specific single-cell HiC approach in F1 hybrid mouse embryos. This single-cell approach enabled us to phase the blastomeres along the cell cycle in an allele-specific fashion and revealed dramatic differences in maternal and paternal genome organisation and dynamics during early development in particular during imprinted XCI First, we observed that the parental genomes are initially asynchronous in their progression through the cell cycle with the maternal genome being more advanced than the paternal genome during the first embryonic cleavages. The parental genomes are also spatially separated in the zygote and gradually intermingle during subsequent development. Furthermore, chromosome folding in early embryos displays unique features and the characteristic organisation of somatic cells is only progressively established.[IC1] In particular, the paternal X chromosome changes structure as early as the 8-cell stage during imprinted X-chromosome inactivation, although organisation into megadomains is a late event.

INTRODUCTION

At fertilization, two highly differentiated gametes meet to form a totipotent embryo. Notably, the paternal genome inherited from sperm is tightly packed with protamines instead of histones. Massive genome remodelling is required to coordinate the two epigenetically distinct parental genomes for further development, and to ensure zygotic genome activation (ZGA). Reprogramming occurs not only at the chromatin level (for review see Burton and Torres-Padilla, 2014) but also at the 3D organization level as described recently by low-input genome-wide chromosome conformation capture (3C) studies (Du et al., 2017, Ke et al., 2017).

Indeed, “C” technologies in somatic cells and stem cells have revealed that the eukaryotic genome is partitioned into several layers of organization, including large multi-megabase compartments, with “A” compartments tending to be active while “B” compartments are more inactive (Lieberman-Aiden et al., 2009); and topologically associating domains (TADs), which appear to be a functionally privileged, sub-megabase scale of chromosome folding (Zhan et al., 2017). TADs are domains of preferential interaction, that are conserved between mammals and appear to be well preserved through differentiation (Dixon et al., 2015, Nora et al., 2012). Within TADs, smaller contact domains can be detected, containing chromatin loops, involved in cell type-specific interactions. Recent studies have revealed that TADs are rather dynamic structures in certain contexts. They appear to be reshaped during the mitotic cell cycle (Naumova et al., 2013, Nagano et al., 2017). During early mammalian development, they appear after fertilization and are strengthened gradually as development proceeds (Du et al., 2017, Ke et al., 2017). Recent studies have also revealed that TADs are lost during X-chromosome inactivation (XCI) in female cells. XCI is an essential process that achieves dosage compensation between the sexes. It takes place in two waves during mouse embryogenesis: a first wave of imprinted XCI occurs shortly after fertilization, where the paternal X-chromosome (Xp) is progressively silenced (Okamoto et al., 2004, Borensztein et al., 2017); the Xp remains silent in the trophectoderm (Takagi and Sasaki, 1975, Okamoto et al., 2004, Mak et al., 2004) but it is reactivated a few cell divisions later, in the inner cell mass. A second wave of random inactivation occurs in the peri-implantation period (Mak, 2004). XCI is a progressive and potentially reversible process and represents a paradigm for epigenetics and chromosome folding. A second wave of random inactivation occurs in the peri-implantation period (Mak et al., 2004). XCI is thus a progressive and potentially reversible process and represents a paradigm for epigenetics and chromosome folding.

Strikingly different conformations of the active (Xa) and inactive (Xi) X-chromosomes were originally reported thanks to cytological observations (BARR and BERTRAM, 1949), FISH

studies (Clemson et al., 2006, Chaumeil et al., 2006) and more recently using chromosome conformation capture techniques (C-techniques), which revealed a unique conformation of the Xi (Rao et al., 2014, Minajigi et al., 2015, Deng et al., 2015, Giorgetti et al., 2016, Darrow et al., 2016, Splinter et al., 2011). While the Xa harbours TAD structure as autosomes, its inactive counterpart displays a more random organisation of inactive genes within its territory, with a general loss of TAD structure, while escapee genes tend to preferentially colocalize through very long-range distance interactions (Splinter et al., 2011, Giorgetti et al., 2016). Indeed RNA/DNA FISH previously showed that escapee genes tend to reside outside the Xist RNA coated domain of the inactive X. HiC analysis more recently revealed that the Xi is partitioned in two large mega-domains separated by a hinge region including the DXZ4 macrosatellite (Rao et al., 2014, Minajigi et al., 2015, Deng et al., 2015, Giorgetti et al., 2016, Darrow et al., 2016). How the inactive X becomes reorganised during XCI has never been examined in the context of development. In particular the structure of Xi during imprinted inactivation represents a unique opportunity to understand the extent to which progressive gene silencing might be linked with chromosomal organisation.

In this study, we set out to explore how the maternal and paternal genomes change organisation during early embryogenesis, from the zygote to the blastocyst stage, particularly at the level of the X chromosomes, and how this relates to gene expression, cell cycle and developmental stage. To this end we applied an allele-specific single-cell HiC approach to male and female F1 hybrid mouse embryos. This has revealed a number of remarkable features of early chromosome folding in early embryo. We also show that after fertilization, the parental genomes are asynchronous in terms of their cell cycle progression and that this is progressively lost as development proceeded. Furthermore we find that parental genomes are spatially segregated in the zygote and gradually intermingle through to the blastocyst stage. Furthermore, TAD structure establishment appeared to be dynamic. Interestingly the paternal X-chromosome displayed structural changes as early as 8-cell stage during imprinted X-chromosome inactivation. In this study, we describe differences in maternal and paternal genome conformation and their dynamic changes during early development, at a genome-wide level and more specifically for the X-chromosome undergoing imprinted XCI.

RESULTS & DISCUSSION

Adapted single-cell HiC for preimplantation mouse embryos

To investigate the extent of changes in chromatin structure after fertilization and during the first steps of mouse development, we adapted the single-cell HiC (scHiC) protocol previously published to single blastomeres (Nagano et al., 2013, Nagano et al., 2017). These were

derived from embryos ranging from fertilization to preimplantation development (metaphase II oocytes, pronuclear stage 3 to 4 zygotes (hereafter referred as 1-cell stage embryos or 1C), late 2-cell (2C), 4-cell (4C), 8-cell embryos (8C) and blastocysts (approximately 60-64 cell stage embryos or 64C)). This period of development covers several important stages including ZGA, as well as the initiation of imprinted XCI (**Figure 1a**). In order to distinguish between parental alleles, F1 embryos were derived from highly polymorphic strains with *Mus musculus domesticus* (C57Bl6/J) female mice and *Mus musculus castaneus* (Cast/EiJ) male mice. As shown in **Figure 1b**, embryos were dissociated into single cells and processed together up to the ligation step in order to conduct optimized scHiC for each stage (**Figure 1b**). A total of 906 cells were sequenced, with 209,606 unique valid read pairs per cell on average. Analysis of various quality control metrics (**Figure 1c; Extended Data Figure 1a-d**) confirmed the quality of the datasets, and identified cells with abnormal karyotype within the single-cell sample (27, 3.6% of cells with at least 25,000 unique valid read pairs and below 15% inter-chromosomal contacts) (**Extended Data Figure 1a** - chromosome coverage). Overall, 719 cells (64.0%) passed stringent quality control filters for further analysis. This provided median coverage of 252,645 distinct valid contacting pairs per cell (ranging from 40,900 to 1,090,116; **Extended Data Figure 1d**). We found the incidence of trans-chromosomal contacts in the single-cell maps was low (median 2.3% ranging from 0.2% to 11.4 %, **Figures 1d and e and Extended Table 1**), indicative of high library quality (Nagano et al., 2015). These Hi-C data are highly reproducible among male and female samples (**Extended Data Figure 1f**). Single-cell maps displayed mostly preferential intra-chromosomal contacts along the diagonal, reflecting of known chromosomal organisation (**Figure 1e** as a representative example) (Nagano et al., 2013). We merged our single cell datasets (number of pooled cells indicated for each stage) to obtain high-resolution reference ensemble maps (**Figure 1f**). As shown for chromosome 13 at various scales, we observed a progressive and step-wise establishment of genomic structure. In summary, we confirmed the validity of our approach which provided us with the opportunity to explore dynamics in chromosomal conformation through mouse preimplantation development in an allele-specific fashion.

Cell-cycle and contact profile distribution in mouse metaphase II oocytes and early embryos

We applied *in silico* cell-cycle phasing methods as previously described (Nagano et al., 2017) to our single-cell datasets (**Figure 2a**): based on short-range (<2Mb) and mitotic-range contacts (2 to 12Mb), we could infer the cell-cycle position of each blastomere across all stages (**Figure 2b and 2c**). Metaphase II oocytes displayed mainly mitotic-range contacts as expected, given their arrested meiotic status. The frequency of short-range (<100kb)

contacts was higher with fewer mitotic-range contacts in a subpopulation of oocytes, which might reflect poor oocyte quality. Except for the 1C stage, few blastomeres were retrieved at the G1 stage. This is consistent with a short (1 to 2 hour) G1 phase after the first division in mouse embryos (Artus and Cohen-Tannoudji, 2008). From the 4C stage onwards, retrieved cells were well-distributed across the cycle, consistent with shorter cell cycle (Artus and Cohen-Tannoudji, 2008) and asynchronous divisions (Kelly et al., 1978, Johnson et al., 1986). We noted that for all embryonic stages examined, from 1C to 64C, the frequency of ultra-short range contacts (around 10kb) was surprisingly high, in contrast to mouse embryonic stem cells (mESCs) (data from (Nagano et al., 2017)). These ultra-short range contacts appeared enriched mainly during the G1 phase compared to short range contacts (around 100kb) that pertain to TAD-scale contacts.

In addition, while long range contacts were almost absent at 1C stage, they became more abundant from the 2C stage, and the length of these long range contacts increased gradually up to the 64C stage where they reached the range found in mESCs. We wondered if nuclear size, which decreases substantially (by a factor of 10 from 2C to 64C (Aguirre-Lavin et al., 2012)) during early pre-implantation embryogenesis could impact frequency distribution. This decrease in nuclear size might imply closer chromosome proximity and more long range contacts.

Taken together, our data show that the distribution of contact frequencies in early embryos displays several unique features compared to somatic cells and stem cells, including unusual, ultra-short range contacts around 10kb, and increasingly ultra-long range contacts. This suggests that early after fertilization, chromosome folding presents unique characteristics which could have important implications for the transition from totipotency to pluripotency that occurs during this developmental time window.

Parental genomes seem asynchronized at least until the 8C stage

Following fertilization, the paternal and the maternal genomes are strikingly different with regard to their chromatin composition and remodelling, as described for histone marks (for review see Burton and Torres-Padilla, 2014 ; Zhang et al., 2016, Zheng et al., 2016) and DNA methylation (Mayer et al., 2000a). As our HiC data were generated from F1 hybrid embryos this allowed us to ask whether the two parental genomes show differential reprogramming of their chromatin structure. scHi-C sequenced reads were assigned to their parental origins based on single nucleotide polymorphisms (SNPs) (see methods). We computed the autosome contact frequency distributions separately for each genome (**Figure 3a and 3b**), and plotted the maternal-paternal differential map to highlight the differences between the two parental genomes (**Figure 3c**). At the 1C stage, the contact distributions

were remarkably divergent. While short range contacts were more abundant in the paternal genome, the maternal genome was more enriched for long range contacts. The parental difference in distribution of contacts weakened gradually over development until differences diminish at the 64C stage, apart from few outlier cells (one 2C-blastomere and four 64C-blastomeres). These data are in agreement with recent Hi-C studies of preimplantation mouse embryos, which used lower amounts of material (200-500 cells per Hi-C library, (Du et al., 2017, Ke et al., 2017)). Altogether, our data highlights the asymmetry between maternal and paternal genomes after fertilization and raises the possibility that this might mirror the difference in kinetics of chromosome decondensation at the exit of meiosis between sperm and oocyte.

One intriguing question concerns the behaviour of the two parental genomes through the cell cycle during preimplantation, given that it was shown that the paternal pronucleus displays earlier signs of replication than the maternal one (Bouniol et al., 1995). Using our blueprint of cell cycle phasing based on the contact frequency distribution (**Figures 2b and 2c**) separately for the parental genomes, we asked if parental genomes were synchronized through their cell cycle during preimplantation development. Despite our relative homogeneity in embryo collection timing and thus unequal distribution of blastomeres along the cell cycle, this representation offers a nice overview of cell distribution along the inferred cell cycle and allows visualization of possible discrepancies in between parental genomes (**Figure 3d**). In these graphs, the paternal genome is plotted in blue while the maternal genome is plotted in red for each cell and at each developmental stage with ESC and NPCs (from similar F1 hybrid parents) as controls. Parental genomes from the same cell are joined by an arrow: the arrow is black when maternal genome is found ahead in cell-cycle, whereas it is grey when paternal genome is found ahead in cell-cycle. As specified above, the paternal genome globally displayed a lower ratio of mitotic contacts compared to its maternal counterpart in zygotes (1C). In some 1C stage cells, the maternal genome was found to be delayed with regard to cell cycle (grey arrows). This might reflect a persistent condensed state of post-meiotic maternal chromosomes and the faster decondensation of paternal pronuclei chromatin. As we could not assess replication status using the repli-score as published in mESC (Nagano et al., 2017) for lack of early-late replicating domains in embryos unlike in ESC (Stamatoyannopoulos et al., 2012), we speculated that these cells may have already started DNA replication in the paternal pronuclei as previously published (Bouniol et al., 1995).

However in most 1C stage cells as well as in 2C- 4C- and 8C-blastomeres, the maternal genome was systematically found to be more advanced with regard to cell cycle (black arrows). The highest parental shift was observed in G2 phase of 2C stage embryos (median

of 24°). This maternal advance was noted at all cell cycle phases of 4C- embryos (median of 4°, P<0.01 one-sided Mann Whitney test for phases with n>10) and 8C- embryos (median of 1°, P< 0.01 in G1, early-S and G2 phases), and its intensity decreased along development. At 64C no biologically significant difference was detected between parental genomes (median of 0.6°, although this difference was still statistically significant in G1 phase cells, P<0.01 one-sided MW test, n=44), similarly to what we found in ESCs (median of -0.1°, P>0.1) and differentiated cells such as neuronal progenitor cells (NPCs, median of 0.3°, P>0.1 two-sided MW test, n>300, unpublished dataset) in which small and random variations in parental cell cycle distribution were observed. Thus even though they share the same nucleus, maternal and paternal genomes appeared to have different kinetics with regard to cell cycle during early cleavage stages. Except in some zygotes in which the paternal genome starts replicating earlier, our cell cycle phasing suggests that the maternal genome is most likely ahead of the paternal genome in the cell cycle up to the 8C stage and that this timing difference is resolved by the blastocyst stage. This asymmetry in cell cycle progression could be linked to a spatial asymmetry at early stages (as described in next section).

Parental genomes are initially segregated and progressively intermingled as early development proceeds

Observations based on visualisation of chromatin according to parental origin - with two techniques (5-bromodeoxyuridine-labeled sperm followed by detection of BrdU in early diploid embryos, and differential heterochromatin staining in mouse interspecific hybrid embryos) - reported a persistent separation of maternal and paternal genomes up to the 4C stage before gradual disappearance (Mayer et al., 2000b). To explore this the spatial separation of parental genomes at the molecular level and to follow its dynamics of appearance and disappearance we were able to use our genome-wide allele-specific data at each developmental stage up to blastocyst stage, along with scHiC ESCs and NPCs as controls (**Figures 3a to 3g**). No trans-parental contact could be seen at the 1C stage while intra-parental contacts were enriched (**Figure 3a**), which is consistent with physical separation of the parental genomes into two distinct pronuclei in PN3-PN4 zygotes. From the 2C stage onwards, we observed initial separation but progressive homogenization in between intra- and trans-parental HiC contact maps (**Figure 3a to 3g, middle panels**). This was quantified **(Figure 3h)** and the trans-parental contacts distribution confirmed a gradual increase, at least up to blastocyst stage (**Figure 3h**). Progressive mixing of parental genomes is also illustrated by allele-specific whole-genome 3D models from single cell Hi-C data (see Methods) for each developmental stage (**Figure 3a to g bottom panels**), of cells coming from the same cell cycle phase (S phase) (**Figure 3i, circled cells**). Our results thus

reveal for the first time the initial segregation and progressive intermingling of the paternal and maternal genomes at the first stages of embryonic development. We validate that this initiates as early as the 2C stage (Mayer et al., 2000b). At the 64C stage, despite a near similar pattern to ESCs and NPCs, the trans-contact ratios are still statistically different ($P<0.05$, one-sided MW test) suggesting that parental genomes are not fully mixed, even by the blastocyst stage. These findings have interesting implications for the potential perpetuation of information specific to parental genomes through early embryonic development.

TAD establishment: a dynamic and region-specific process

Unlike established cell lines, in which compartments and loop domains can vary between cell lines, but TAD partitioning appears to be relatively unchanged (Dixon et al., 2012, Nora et al., 2012), during early mouse development, higher-order chromatin architecture including chromatin loops, TADs and A/B compartments have been recently described to be much more dynamic and to be established progressively (Flyamer et al., 2017, Du et al., 2017, Ke et al., 2017). While Flyamer and colleagues described TAD structure as early as the zygote stage (Flyamer et al., 2017), Du and colleagues (Du et al., 2017) and Ke and colleagues (Ke et al., 2017) suggested that during the first two stages after fertilization TADs are “in priming state” or “obscure”. We set out to explore the kinetics of TAD formation in our single cell HiC datasets, using directionality index for subsequent TAD calling (Dixon et al., 2012). Strong TAD boundaries (TADBs) from ESC single-cell HiC datasets (as published in Nagano et al., 2017 and showing good correlation with population HiC TADB (Dixon et al., 2012)) were selected as a reference map and we analyzed the strengths of these TAD boundaries across preimplantation development. The results are presented in the heat map in **Figure 5a**. Almost no TADBs were observed in meiotic metaphase II oocytes, in agreement with the absence of TAD reported in mitotic cells containing condensed chromosomes (Du et al., 2017, Ke et al., 2017, Flyamer et al., 2017, Naumova et al., 2013). Strikingly, some TADBs were observed as early as the 1C-stage (977 TADBs in 1C among the 4523 TADBs called in ESCs, 21,6%). Some persisted until the 64C stage and were also present in the ESCs (top of the column), while others appeared to be transient, since they disappeared by the 2C stage (bottom of the column). Similar observations were made for the 2C and 4C stages, with both stable and transient TADBs. Nonetheless, the number and intensity of TADBs gradually increased (**Figure 5a**) as quantified in the Venn diagrams (**Figure 5b**). These results are consistent with the fact that TADBs are dynamically set up, as early as the zygote stage. More work will be needed in order to characterize and quantify the first and/or transient TADBs that seemed to arise at the early stages (1C, 2C and 4C).

In order to better describe the clear TADBs that are in common with the ESCs at least by the 64C stage (**Figure 5a** - orange on the heatmap, top of the column), we chose to explore in detail one specific region on chromosome 13 as shown in contact maps (**Figure 5c**). The directionality index plotted for each stage indicated a TADB profile similar to ESCs at 64C stage and also as early as 8C, while no such boundary could be seen in 1C, 2C and 4C (**Figure 5c and 5d**). For this specific locus, these results are consistent with the step-wise appearance, from 8C onwards, of domain structure during development. To validate this HiC based information, we examined the spatial organisation of this region using an alternative method based on DNA FISH (Fluorescent *in situ* Hybridization) and structured illumination microscopy (OMX). Using an assay first described in (Nora et al., 2012), we designed two pools of tiled bacterial artificial chromosome (BAC) probes spanning up to 1 Mb around the TAD border of interest (**Figure 5c**, ESC panel for DNA FISH probe position). We confirmed in ESCs that the pool of probes covering DNA segments from the same TAD (referred as pool I) colocalized to a greater extent than the pool of probes covering DNA segments located in adjacent domains (referred as pool II) (**Figure 5e and 5f**). These results are in agreement with the expected structure from the pooled single-cell HiC map (**Figure 5c**). We performed similar experiments on 2C, 4C and 8C stage embryos. No significant differences were observed in colocalization coefficients at the 2C and 4C stages between pool I and pool II DNA FISH data. In contrast, 8C stage embryos displayed a similar distribution to that reported in ESCs, suggesting that TAD partitioning has indeed occurred by this stage (**Figure 5e and 5f**). We conclude that the spatial arrangement for this region is established only after the 4C stage, based on HiC and FISH data.

Taken together, our data indicate that sub-megabase folding of the genome into TADs is a progressive process, starting as early as the 1C stage with different kinetics for different genomic regions.

X-chromosome structure is progressively modified during imprinted XCI

In mammalian somatic cells, such as neural progenitor cells and fibroblasts, the active (Xa) and the inactive X (Xi) chromosome fold very differently as previously shown using allele-specific 4C (Splinter et al., 2011) and HiC (Rao et al., 2014, Minajigi et al., 2015, Deng et al., 2015, Giorgetti et al., 2016, Darrow et al., 2016) approaches. The inactivation of the paternal X chromosome initiates at the 4-cell stage with paternal Xist RNA accumulation and culminates in general silencing of the paternal X by the blastocyst stage. At the zygote the Xp is fully active, like the maternal X (Deng et al., 2014, Borensztein et al., 2017). Imprinted XCI follows a series of well defined transcriptional changes, based on both RNA FISH and scRNA seq studies, unlike the process of random XCI in differentiating ESCs which is far more heterogeneous. Our allelic scHiC data from the zygote to the blastocyst stage thus

provided us with a unique opportunity to explore the changes in X-chromosome folding during the process of XCI and the links between transcriptional status and long range interactions. We thus investigated whether any intra chromosomal structural differences were detectable between the paternal and maternal X chromosomes in female embryos at different stages of development. We first computed contact distributions in all samples for the maternal (Xm) and paternal (Xp) X chromosomes. As a control, we first applied this to F1 hybrid NPC allele-specific scHiC dataset obtained from clonal cells (unpublished data). This revealed loss of short-range contacts and enrichment of long-range contacts on the inactive X compared to the active X (**Figure 6a**).

At the 1C stage, the X chromosome specifically displayed paternally enriched short-range contacts and maternally enriched long-range contacts, as found for autosomes (**Figure 3c**). However, from the 8C and more noticeably at the 64C stage, the paternal X was enriched for long-range contacts while the maternal X was enriched for short-range contacts. This is very different to the situation found for autosomes where both paternal and maternal copies generally show similar contact maps (**Figure 3c**). However the contact distributions on the Xp in 64C embryos were similar to those found for the Xi in NPCs (**Figure 6b**). This loss of short-range contacts on the Xp during pre-implantation development might reflect loss of TAD structures, as has been found for the Xi in NPCs (Giorgetti et al., 2016) and fibroblasts (Minajigi et al., 2015). Indeed, at the 64C stage, the Xp harboured 30 TADs while 80 TADs were detected on the Xm (**Figure 6c**) using directionality index (see Methods). In NPCs, 9 TADs were detected on the Xi versus 78 on the Xa. Thus the Xp has indeed lost some of its organisation into TADs during the XCI in vivo, similarly to NPCs though to a lesser extent.

We also examined allele-specific contact maps for the whole X chromosome in our scHiC data. As a control we checked that pooled single-cell maps of the Xi in NPCs showed mega-domain organisation of the Xi (**Figure 6d**), as previously reported using population based HiC (Giorgetti et al., 2016). This bipartite structure is not present on the paternal or maternal X chromosomes at any stage during pre-implantation development, even at the 64C when the Xp is almost fully inactivated in all cells (Borensztein et al., 2017). The boundary between the megadomains on the Xi appears to be created by an unusual macrosatellite DXZ4 (Rao et al., 2014, Deng et al., 2015, Giorgetti et al., 2016, Darrow et al., 2016). To assess the degree to which a boundary might appear at these early stages, we plotted the insulation score around the DXZ4 region for the Xm (active) and Xp (inactive) chromosomes at each developmental stage as well as in ESCs (both Xs active) and NPCs (active and inactive X) (**Figure 6e**). The insulation score profile around DXZ4 was similar for all cell types and stages on the active X. In early embryos, no insulation was observed at DXZ4 region on the Xp, similarly to ESCs. This corroborated the HiC contact maps that did not

reveal megadomain formation, even at the 64C stage when Xp silencing is complete. To explore Xp structure with a different approach, we also performed 3D DNA FISH using 18-Mb oligo probe sets, located within one mega-domain (probes a–b, as in Giorgetti, 2016 and shown in **Figure 6d** NPC panel), with concomitant RNA FISH to detect Xist RNA (in order to identify the Xp chromosome) (**Figure 6f**). Although there was cell-to-cell variation, regions within the same mega-domain tended to show a greater overlap on the Xi than on the Xa chromosome at the 64C stage, but not at earlier stages (16-cell stage). The difference in colocalization on the Xi versus the Xa was similarly to that observed in NPCs albeit milder (Giorgetti et al., 2016). Thus, although the Xp does not appear to be organised into distinct megadomains even at the 64C stage, there are significantly increased intra-domain contacts by this stage suggesting that the inactive Xp is indeed adopting a different structure.

Taken together, our data report that X-chromosome structure is progressively modified during imprinted XCI in mouse early development, with a loss of TADs from the 8C stage (which also corresponds to the early steps of X-linked gene silencing) and an increase in long-range contacts. Although the Xp at the 64C stage does not show as dramatic a loss of TAD-like structures as the Xi in differentiated somatic cells, nor the formation of megadomains, it nevertheless has a globally reorganised structure compared to the Xm.

CONCLUSION

The dramatic changes in epigenomes and gene expression that occur during the first steps of life have fascinated scientists for decades. In this report we explore the changes in parental genome organisation during the early stages of development, revealing several unique and highly dynamic features of genome structure - and the paternal X chromosome in particular - during preimplantation mouse development.

First, we describe progressive parental genome intermingling as development proceeds. Whether this process occurs stochastically or involves specific regions of the genome remains to be found. Our results reveal that the parental genomes are not fully intermingled even by the blastocyst stage. We speculate that genome reprogramming is a long-lasting process that spans the whole preimplantation development period. Parental genome intermingling and establishment of genome architecture may in fact be coordinated.

Our study also reveals that early embryo genomic conformation displays some unexpected very short-range contacts, throughout development. These very short-range contacts were previously described using another technique - low-input HiC (Du et al., 2017) - and are thus unlikely to be due to technical artefacts. However their biological significance remains unclear. We speculate that the early genome is packaged in a rather naive form following fertilization - that either requires ultra-short contacts to drive progressive strengthening of

genome architecture or that it harbors interaction domains with a different scale, much smaller than the canonical TADs. Increasingly long-range contacts during development might reflect either a progressive compaction of embryonic chromatin or the decrease in nuclear size observed at each cleavage and subsequent genome rearrangement in a smaller space, thereby allowing contacts between genomic regions far apart. Another explanation could relate to the gradual establishment of transcriptional compartments on the longer length-scale.

In addition to this unusual range of interactions and progressive changes in chromosome folding during pre-implantation development, our data also point to remarkable parental asymmetries with strikingly different contact distributions in the zygote and in cell-cycle allocation. To our knowledge, this is the first time that parental genome asymmetries in cell cycle have been reported in preimplantation development.

Finally, our study has revealed that the onset of imprinted X-inactivation is associated with paternal X-chromosome structural modifications as early as the 8C stage. We show that megadomain formation is a late event in XCI, not apparent even at the 64C stage when the Xi is globally silent. The loss of sub-megabase scale folding and TADs appears to coincide with global transcriptional silencing of the Xp. Future work will clarify the specific links between kinetics of gene silencing and kinetics of structural changes (such as TAD loss and compartment changes) on the Xp during imprinted XCI.

In summary, our study provides several key insights into parental genome conformation dynamics during early mammalian development and more specifically on the behaviour of the paternal X chromosome as it transitions from a fully active to a fully inactive state. This paves the way to a deeper understanding of how function and structure interplay at the onset of genome transcription and X-chromosome silencing.

MATERIAL & METHODS

Mouse crosses and collection of embryos.

All experimental design and procedures were in agreement with the guidelines from French legislation and institutional policies. Embryos were derived from natural mating or after superovulation between C57BL/6J (B6) females crossed with CAST/EiJ (Cast) males or between C57BL/6J (B6) females crossed with C57BL/6J (B6) males for scHiC and for DNA FISH respectively. Embryos were harvested at 1-cell (PN3 or PN4), late 2-cell, 4-cell, 8-cell, 16-cell and blastocyst stages (approximately 60 to 64 cells). B6 pure oocytes were collected at E0.5 after superovulating females. Hours of collection and mode of mating (natural or superovulation) are indicated in the table:

Stage	DNA FISH	ScHiC
Metaphase II oocyte	[redacted]	Superovulated
1C		Both
2C	Superovulated	Both
4C	Superovulated	Superovulated
8C	Superovulated	Natural mating
16C	Superovulated	[redacted]
64C	Natural mating	Natural mating
E4.5	Natural mating	[redacted]

Stage	Timing in natural mating (hours post fertilization)	Timing in superovulated (hours post hcg injection)
Metaphase II oocyte	[redacted]	15
1C	14	21
2C	37	44
4C	48	55
8C	55	62
16C	61	[redacted]
64C	80	

The collected embryos were included in the analyses only if they showed a normal morphology and the correct number of blastomeres for their developmental stage. No statistical method was used to predetermine sample size.

Single-cell dissociation from preimplantation mouse embryos.

Oocytes and embryos were collected by flushing oviducts (until 16C) or uteri (64C) with M2 medium (Sigma). The zona pellucida was removed with acid Tyrode's solution (Sigma), and embryos were washed twice with M2 medium (Sigma). To remove second polar body in zygotes and to isolate individual cells, we then incubated embryos in Ca2+- and Mg2+-free M2 medium for 5 to 30 min, depending on the embryonic stage. First polar body was lost during zona pellucida removal. For 2C stage and onward, second polar body was dissociated during single cell dissociation. For the blastocyst stage, incubation with Ca2+- and Mg2+-free M2 medium was replaced with a 5-min incubation in TrypLE (Invitrogen). After incubation, each blastomere was mechanically dissociated by mouth pipetting with a

thin glass capillary. Single cells were then washed three times in PBS/acetylated BSA (Sigma) before being processed for scHiC without delay.

Hi-C processing

Cells (oocytes or dissociated blastomeres) were fixed for 10 min by adding formaldehyde at a final concentration of 2% at room temperature before quenching with 127 mM glycine for 5 min on ice. The cells were then washed three times in PBS/acetylated BSA (Sigma) and permeabilized in 10 mM Tris-HCl (pH 8), 10 mM NaCl, 0.2% IGEPAL CA-630 with cOmplete EDTA-free protease inhibitor cocktail (Roche) for 30 min on ice.

Cells were then washed with 1.24 x NEBuffer 3 (New England Biolabs; 62 mM Tris-HCl [pH 7.9], 124 mM NaCl, 12.4 mM MgCl2, 1.24 mM DTT) and transferred to a protein lobinding tube (Sigma) in 200 µl of 1.24 x NEBuffer 3 containing three µl of 20% SDS and incubated at 37˚C for 60 min with constant agitation, then 20 µl of 20% Triton X-100 was added and incubated at 37˚C for 60 min with constant agitation. Next, 25 µl of 25 U/µl Mbo I (New England Biolabs) was added and incubated at 37˚C overnight with constant agitation. To label the digested DNA ends, 1.56 µl of 5 mM dCTP, 1.56 µl of 5 mM dGTP, 1.56 µl of 5 mM dTTP, 19.5 µl of 0.4 mM biotin-14-dATP (Thermo Fisher) and 5.2 µl of 5 U/µl DNA polymerase I, large (Klenow) fragment (New England Biolabs) were added and incubated at 37˚C for 60 min with constant agitation. The sample was then spun and supernatant partially removed leaving 50 µl with cells, followed by addition of 100 µl of 10x T4 DNA ligase reaction buffer (New England Biolabs), 10 µl of 100x BSA (New England Biolabs), water and 10 µl of 1 U/µl T4 DNA ligase (Thermo Fisher) were added to make the total volume 1 ml, and incubated at 16˚C for at least 4 hours. The sample was then spun and supernatant partially removed leaving 50 µl with cells. Cells were resuspended with PBS 1x and BSA 1 mg/mL. Single nuclei were sorted into individual empty tubes in PCR strips under the binocular using a mouth pipette. The PCR strips were sealed and stored at -80˚C until further processing.

Library preparation and sequencing

To prepare single-cell Hi-C libraries from single nuclei in PCR strips, 5 µl of PBS was added to each well and crosslinks reversed by incubating at 65˚C overnight. Hi-C concatemer DNA was fragmented and linked with sequencing adapters using the Nextera XT DNA Library Preparation Kit (Illumina), by adding 10 µl of Tagment DNA Buffer and 5 µl of Amplicon Tagment Mix, incubating at 55˚C for 20 min, then cooling down to 10˚C, followed by addition 5 µl of Neutralize Tagment Buffer and incubation for 5 min at room temperature. Hi-C ligation junctions were then captured by Dynabeads M-280 streptavidin beads (Thermo Fisher; 20 µl of original suspension per single-cell sample). Beads were prepared by washing with 1 x BW

buffer (5 mM Tris-Cl pH 7.5, 0.5 mM EDTA, 1 M NaCl), resuspended in 4 x BW buffer (20 mM Tris-Cl pH 7.5, 2 mM EDTA, 4 M NaCl; 8 µl per sample), and then mixed with the 25 µl sample and incubated at room temperature overnight with gentle agitation. The beads were then washed four times with 200 µl of 1 x BW buffer, twice with 200 µl of 10 mM Tris-Cl pH 7.5 at room temperature, and resuspended in 25 µl of 10 mM Tris-Cl pH 7.5. Single-cell Hi-C libraries were amplified from the beads by adding 15 µl of Nextera PCR Master Mix, 5 µl of i7 Index primer of choice and 5 µl of i5 Index primer of choice. Samples were then incubated at 72˚C for 3 min, 95˚C for 30 sec followed by the thermal cycling at 95˚C for 10 sec, 55˚C for 30 sec and 72˚C for 30 sec for 18 cycles, then incubated at 72˚C for 5 min. The supernatant was separated from the beads and purified one by one with AMPure XP beads (Beckman Coulter; 0.6 times volume of the supernatant) according to manufacturer's instructions and eluted with 30 µl each of 10 mM Tris-Cl pH 8.5. The eluate was purified once more with AMPure XP beads (equal volume to the previous eluate) and eluted with 11 µl of 10 mM Tris-Cl pH 8.5.

Before sequencing, the libraries were quantified by qPCR (Kapa Biosystems) and the size distribution was assessed with Agilent 2100 Bioanalyzer (Agilent Technologies). They were sequenced by 2 x 150 bp paired-end run by either HiSeq 1500, HiSeq 2500 or NextSeq 500 (Illumina).

Computational analysis.

Mapping, filtering and gender assignment.

The sequenced data was mapped against the corresponding N-masked genome (based on the MM10 assembly), using HiCUP v0.5.8 (Wingett et al., 2015) with Bowtie2 (Langmead and Salzberg, 2012) as the aligner. This resulted in a median of 209,676 unique read pairs across all oocyte and embryo datasets. The uniquely mapped reads were then assigned to the maternal and paternal alleles using SNPSplit (Krueger and Andrews, 2016), exploiting the allelic differences. As the read length (150 bp) was shorter than the average SNP frequency in the genome (around one SNP every 200 bp on autosomes and every 500 bp on the X chromosome), on median 44.4% of reads were unambiguously mapped onto the maternal or paternal alleles. After allele assignment, a median of 20.4% of read pairs had both reads, and 47.6% had exactly one read mapping unambiguously to either the maternal or the paternal alleles. For further statistical analysis, apart from the read pairs with both reads mapping unambiguously, we also retained the read pairs where one read mapped unambiguously (e.g. chr7 of G1), the other allele fell onto the same or homologous chromosome (chr7 but unidentifiable allele), and the genomic distance of reads was no more than 1Mb away. In this case, the SNP-less read was assigned the same chromosome as the unambiguously mapping read (chr7 of G1). This is a reasonable approximation, because the

probability of a read pair falling onto the same chromosome (vs onto the homologous chromosomes) is over > 97% (based on the identified read pairs in oocytes and embryos, **Extended Data Figure 1b**). The mismapping rate between the maternal and paternal genomes can also be measured as 0.2% for oocytes, for which the paternal genome is missing.

We filtered out cells with fewer than 25,000 contacts, cells with more than 15% trans-chromosomal contacts (**Extended Data Table 1**), and cells with missing autosome chromosomes (with a coverage of <0.1% total coverage) to avoid cells with karyotype aberration. The median number of contacts in the filtered libraries was 160,295. For these cells, we identified the gender of the embryos, as well as if a cell come from a fertilised or unfertilised egg in the case of the putative 1-cell-stage embryos (1CSE and unk datasets). We defined unfertilised eggs as cells with < 5% paternal genome coverage (**Extended Data Figure 1c**). For the fertilised eggs and embryos, an embryo was identified as male if the paternal/maternal X chromosome coverage ratio was < 0.1, and female otherwise (**Extended Data Figure 1d**).

The quality control results for each cell is shown in **Extended Data Table 1** and **Extended Data Figure 1a**. From all cells that belonged to the same developmental stage, we created merged datasets. For the unfertilised eggs, we used all read pairs before allele splitting. For the female embryos we used the filtered reads as described above. For the male embryos we used the filtered reads as described above for the autosome chromosomes, and the read pairs before allele splitting for the X and Y chromosomes. The numbers of cells and the coverage of the merge datasets are summarised in **Extended Data Figure 1f**.

Contact frequency distributions and cell cycle phasing.

We used the contact frequency distribution of all contacts to infer the cell cycle phase of unfertilised eggs and embryos, similarly to (Nagano et al., 2017). Since there was no available replication data for embryos, instead, we defined a cell cycle phase angle, based on the positions of cells on the percentage of short-range (25kb-2Mb) vs mitotic-range (2-12Mb) contact plot (**Figure 2b**) around the centre-of-mass of all oocyte and embryo cells studied. We assigned cells into five cell-cycle phases, using the following criteria (**Figure 2c**):

M: phase_angle >= -1/4 π and phase_angle < 0

pre-M: phase_angle >= 0 and phase_angle < 1/2 π

late-S/G2: phase_angle >= 1/2 π and phase_angle < 3/4 π

early-S: phase_angle >= 3/4 π and phase_angle < 9/8 π

G1: phase_angle >= 9/8 π and phase_angle < 7/4 π

Within each stage, cells were ordered according to decreasing order of the phase angle (e.g. **Figure 2a**).

To compare the contact frequency distributions of the different parental genomes, we computed the maternal and paternal contact frequency distributions and their difference, for each cell, ordered according to embryonic developmental stage and cell cycle phase (**Figure 3a-c**). When plotting the contact frequencies in the 25kb-2Mb and 2-12Mb contact ranges separately for the maternal and paternal chromosomes, a cell cycle phase angle lag between the parental genomes can be visualised by a vector pointing from the maternal to the paternal genome's position on the plot. A rotational vector field can indicate a systematic in the cell cycle positions of the parental genomes. We computed the median maternal - paternal phase angle difference as the magnitude of this bias, and used a Mann-Whitney U test to test if the phase angle difference of cells were coming from a distribution with mean zero (no bias).

3D modelling of oocytes and early embryos.

For all oocytes and female embryos, we computed allele-specific whole-genome 3D models, as described for haploid data in (Nagano et al., 2017). We only used contacts where both ends mapped unambiguously to the maternal or paternal genomes, and were also supported by other contacts. We binned the contacts at a 1 Mb resolution, and computed five whole-genome 3D models for each cell. As control, we also computed 3D models for F1 hybrid ESCs (Nagano 2017 single-cell Hi-C data) and F1 hybrid NPCs (unpublished data).

Spatial mixing of parental genomes.

To test the spatial separation of the parental genomes in early embryonic development, we computed the percentage of trans-chromosomal contacts that fell between maternal and paternal chromosomes. For this test, we only used read pairs with both reads mapping unambiguously, and omitted homologous chromosome contacts. For the merged female embryo datasets and the ESCs and NPCs, we plotted chromosome level contact maps, scaled by the total number of trans-chromosomal contacts. We also selected 3D models for embryo cells that were at similar phases of the cell cycle, and had a percentage of parental genome crossing contacts close to the median value at the specific developmental stages.

Topological domain analysis.

At each developmental stage, we identified TADs in the merged non-allele-specific Hi-C datasets, using HOMER v4.7 (Heinz et al., 2010), based on a directionality index based method as described in (Freire-Pritchett et al., 2017). We collected all TAD boundaries

identified at the 2- or 8-cell stages of embryonic development, and ordered them by the strength of these boundaries in the ESCs (**Figure 5a**). We defined TAD boundary strength as the difference in directionality index values between the positive and negative peak positions of a TAD boundary. We counted the number of overlapping TADs between the developmental stages and ESCs (**Figure 5b**). We selected a TAD boundary appearing between the 2- and 8-cell stages, characterised by one of the largest changes in TAD boundary strength (at 90.90Mb on chromosome 13). We plotted the Hi-C matrices in a +/- 1Mb region around this boundary (**Figure 5c**), and the directionality index profile around this boundary (**Figure 5d**), at the different developmental stages.

X-chromosome analysis.

To see X-chromosome-specific changes in chromatin organisation, we compared the contact frequency distributions of the maternal and paternal X chromosomes, showing the parental distributions and their difference, for each cell, ordered according to embryonic developmental stage and cell cycle phase (**Figure 6a**). We also showed the contact frequency distributions for the inactive and active X chromosomes of NPCs, with the inactive X aligned with the inactivating paternal X chromosome of the early embryos. For each chromosome of each cell, we measured the enrichment of long-range (>10 Mb) contacts on the paternal (for NPC, the genome with the inactive X) and maternal (for NPC, the genome with the active X), defined as log2(f_long,paternal / f_long,maternal) with f_long denoting the frequency of long-range contacts of all >1kb contacts on the chromosome (**Figure 6b**). At each developmental stage, to test if the long-range contact enrichment on the inactivating X chromosome was the same as on the autosome chromosomes, we used a one-sided Mann-Whitney U-test with the alternative hypothesis that the enrichment was higher on the X chromosomes.

To assess changes in the local structure on the X chromosomes, we also called TADs genome-wide using the merged allele-specific Hi-C datasets for female cells. For each developmental stage, we compared the paternal-to-maternal ratio of the number of called TADs on the X chromosome to the ratio of autosome chromosomes (**Figure 6c**).

We also tested if an appearance of the megadomains typical of the inactive X chromosome coincides with the increase in long-range contact enrichment and the reduction of TAD numbers on the inactivating X chromosome. We plotted whole-chromosome coverage-corrected Hi-C matrices of the X chromosomes, and the maternal-paternal difference Hi-C count matrices (**Figure 6d**). We measured the magnitude of the insulation score around the DXZ4 gene, using a 2Mb sliding window every 40kb, where the insulation score at a given genomic position was defined as -log2 (a / (a + $b1$ + $b2$)) where a is the number of contacts

between and *b1* and *b2* the number of contacts within the upstream and downstream 1Mb regions around the position (**Figure 6e**).

DNA FISH using BAC probes

DNA FISH probes.

BACs were obtained from the CHORI. Each probe was tested separately to ensure it effectively mapped to the chromosome 13 and gave robust DNA FISH signal. Coordinates refer to the mm10 assembly.

GREEN BACs pool-I			
RP24-278M23	chr13	89761320	89900154
RP23-325G4	chr13	89903372	90125927
RP23-2B17	chr13	90107822	90308777
RED BACs (common)			
RP23-222A16	chr13	90310893	90506036
RP24-389D15	chr13	90513189	90658357
RP23-302B3	chr13	90620826	90839364
GREEN BACs pool-II			
RP23-359G6	chr13	90842898	91053560
RP23-326J5	chr13	91063985	91263254
RP23-307F19	chr13	91255421	91390052

DNA FISH oligo-probes. In experiments to detect the mega-domain boundary, fluorescent oligonucleotides (average length 45 bp, 5'-modified with Atto 448 or Atto 550, average density: one oligonucleotide every 3 kb) were obtained from MYcroarray Inc. Oligonucleotides were designed to tile the following consecutive 18-Mb regions: chrX:35,000,000–53,000,000 (termed "probes a") and chrX:53,000,000– 72,000,000 (termed "probes b") (Giorgetti et al., 2016).

DNA FISH procedure on ESCs.

FISH on cells from tissue culture was performed as described previously (Chaumeil et al., 2008, Nora et al., 2012). Feeder-free mESCs were cultured on gelatin-coated coverslips #1.5 (1mm) and fixed in 3% paraformaldehyde for 10 min at room temperature. Permeabilization was then performed on ice for 5 min in 1X PBS containing 0.5%Triton X-100 and 2mM Vanadyl-ribonucleoside complex (New England Biolabs). Coverslips were preserved in 70% EtOH at -20°C. Prior to FISH, samples were dehydrated through an

ethanol series (80%, 95%,100% twice) and air-dried quickly. DNA FISH was preceded by sample denaturation in 50% formamide in 2X SSC at pH=7.2 at 80°C for 40min. After overnight hybridization at 42°C, washes were carried out at 45°C, three times 5min in 50% formamide in 2X SSC at pH=7.2 and three times 5min in 2X SSC. 0.2mg/mL DAPI was used for counterstaining and mounting medium consisted in 90% glycerol, 0.1X PBS, 0.1% p-phenylenediamine at pH9 (Sigma).

3D DNA FISH procedure on embryos and Xist RNA/DNA FISH using oligonucleotide probes

DNA FISH protocole was designed for pre implantation embryos.

Collected embryos were pre-fixed for 1 min at room temperature (RT) in paraformaldehyde (PFA) 1%. Embryos were pre-permeabilized for 1 min at RT in PFA 0,5% and TritonX100 0,4%. Embryos were fixed for 10 min at RT in PFA 4%. Embryos were washed briefly in PBS 1x with PVP 1mg/mL and TritonX100 0,05%. Embryos were permeabilized for 1 hour at 37°C in PBS 1x with TritonX100 0,5% and with RNAse A 5uL/mL. Embryos were washed briefly in PBS 1x with PVP 1mg/mL and TritonX100 0,05%.

Nick translation (Vysis Abbott, Chicago, IL) using Spectrum green (Vysis) or Atto550 (Jena Bioscience) was used to label double stranded probes. Embryos were washed in DNA hybridization buffer drops and then transferred into an hybridization buffer solution containing some Cot1 for subsequent competition. After an overnight buffering at 37°C, embryos and probes were denatured for 10min at 83°C for embryos in Cot1. Competition was performed for at least 3h at 37°C and then hybridization overnight at 37°C.

Excess of probes was eliminated through three washes at 45°C in SSC 2x solution and SSC 0,2x solution for 10 min each. Embryos were then briefly washed in PBS 1x and mounted in a Vectashield drop containing DAPI under oil on a glass bottom plate, coated with Polylysine.

Microscopy and image analysis

RNA DNA FISH imaging was performed on an inverted confocal microscope Zeiss (Germany) LSM700 with a Plan apo DICII (numerical aperture 1.4) 63x oil objective. Z sections were taken every 0.4 mm

Structured illumination was performed using an OMX system (Applied Precision). Signal from all channels were realigned using fluorescent beads prior to each session of image acquisition.

Colocalization analysis.

For colocalization analysis, distribution of pearson correlation coefficient in the respective intensities of red and green channels were retrieved semi-automatically using the JACOP ImageJ plugin, and compared using Wilcoxon rank-sum statistics with R (http://www.r-project.org). Analysis was restricted to a region of interest of identical volume around the FISH signal in between pool I and pool II embryos.

FIGURE LEGENDS

Figure 1 - Single-cell HiC in mouse preimplantation embryos

a. Preimplantation development timeline from oocyte to blastocyst highlighting main events and timing for embryo collection (hours post fertilization).

b. Schematic of single-cell HiC (scHiC) in hybrid mouse embryos (C57Bl6/J x Cast) for probing genome architecture dynamics along preimplantation development.

c. Number of informative contacts retrieved per cell that passed the quality control filter, for each developmental stage.

d. Percentage of trans-chromosomal contacts per cell that passed the quality control filter, for each developmental stage.

e. Example single-cell Hi-C heatmap of a 4-cell stage embryo cell, at 20 Mb bin resolution.

f. Chromosomal contact maps of pooled female cells per developmental stage (chromosome 13, 1Mb resolution) in mouse metaphase II oocytes, embryos and embryonic stem cells. Zoom in views (250kb resolution and 25kb resolution). Number of samples per stage is indicated.

Figure 2 - Cell cycle phasing in mouse preimplantation embryos

a. Single-cell contact frequency distributions ordered by *in silico* inferred cell-cycle phasing and per developmental stage (in metaphase II oocytes, embryos and embryonic stem cells (ESC, published data from Nagano, 2017)). Each column represents a single cell. Developmental stage is indicated in bottom line (dark and light colours distinguish female and male cells respectively). Inferred approximative cell-cycle phase is specified in upper line.

b. Percentage of short-range (<2 Mb) versus mitotic band (2–12 Mb) contacts per cell in all cells coloured according to their developmental stage.

c. Percentage of short-range (<2 Mb) versus mitotic band (2–12 Mb) contacts per cell in all cells coloured according to their cell-cycle stage.

Figure 3 - Cell cycle shift in between parental genomes

a - c. Allele specific single-cell frequency distributions ordered by *in silico* inferred cell-cycle phasing and per developmental stage (in embryos and ESC) for autosomes in female cells only. Each column represents a single cell. Developmental stage is indicated in bottom line. Cell-cycle phase is specified in upper line. **a** for maternal reads, **b** for paternal reads, **c** (maternal-paternal) differential map (maternally enriched contacts are represented in red whereas paternally enriched contacts are in blue).

d. Percentage of short range (<2 Mb) versus mitotic band (2–12 Mb) contacts per cell for the oocytes, 1C, 2C, 4C, 8C, 64C, ESC and NPCs. For each cell, paternal genome is represented by a blue dot while maternal genome is represented by a red dot. Arrows connect parental genomes from the same cell: arrows are dark when maternal genome is ahead in the cell cycle while they are grey when paternal genome is ahead. Cell cycle positions are reminded in the NPC scheme and when relevant in embryo schemes, with coloured dots (G1, eS, lS, preM#G2, M).

Figure 4 - Parental genome behavior in early embryos

a to g. Genome-wide allele-specific contact maps for merged data at each stage (oocyte, 1C, 2C, 4C, 8C, 64C, ESC and NPC) showing cis-, trans- and cross-genome contacts. Homologue chromosome contacts appear strong partly due to mismapping of the alleles (dark off-diagonal pixels along a diagonal). 3D models of whole-genome conformation with paternal genome represented in blue and maternal genome represented in red. Models were computed from single cell datasets at 1Mb resolution.

h. Fraction of trans genome contacts over all non-homologuous trans contacts for each stage from 1C to 64C stages with ESCs and NPCs as control.

i. Cell cycle phasing of the 5 embryonic cells used for 3D models in Figures 4a-e, with a black dot marked with corresponding color for each stage (1C, 2C, 4C, 8C, 64C).

Figure 5 - TAD dynamics in preimplantation embryos

a. Heatmap representing TAD boundary (TADB) kinetics during early development. All TADBs present in ESC are ordered by strength in columns. Color code indicates the strength of TADB at each developmental stage.

b. Venn diagrams showing number of TADB in 2C/8C/ESC and in 8C/64C/ESC.

c. Contact maps of pooled cells of region around chromosome 13:91,04Mb for each cell type (25kb resolution). Positions of DNA FISH probes.

d. Directionality index around 13:91,04Mb for each developmental stage and ESC.

e. Boxplots for 2C, 4C, 8C and ESC showing the distribution of Pearson's correlation coefficient between red and green channels, with whiskers and boxes encompassing all and 50% of values, respectively; central bars denote the median correlation coefficient. Statistical significance was assessed using Wilcoxon's rank sum test.

f. Examples of images in 2C, 4C, 8C and ESC with structured illumination microscopy (OMX).

Figure 6 - X chromosome in preimplantation embryos

a. Allele specific single-cell frequency distributions ordered by in silico inferred cell-cycle phasing and per developmental stage (in embryos and NPCs) for X-chromosome in female cells only. Each column represents a single cell. Developmental stage is indicated in bottom line. Cell-cycle phase is specified in upper line. For maternal reads on top, for paternal reads in the middle, (maternal-paternal) differential map at bottom (maternally enriched contacts are in red whereas paternally enriched contacts are in blue).

b. Long range contact enrichment on paternal genome for autosomes and X-chromosome at each developmental stage and in ESCs and NPCs. One-sided Mann-Whitney U-test.

c. Boxplot showing ratio of number of TADs on maternal versus paternal autosomes or X-chromosome at each developmental stage and in ESCs and NPCs.

d. Allele-specific and parental differential chromosomal contact maps of pooled female cells per developmental stage (chromosome X, 1Mb resolution) in embryos, ESCs and NPCs. Position of DNA FISH probes (oligonucleotides a and oligonucleotides b).

E. Insulation score around DXZ4 region in maternal and paternal X-chromosomes in each cell type.

f. 3D RNA DNA FISH analysis. Right, in 16-cell stage embryos (16C), probes a–b (within the same mega-domain) are identically distributed on the Xp and on the Xm chromosomes.

Left, in blastocyst (64C) probes a–b are more overlapping on the Xp than on the Xm chromosome (Wilcoxon's test). NS, not significant. n denotes number of cells and N number of female embryos analysed in DNA FISH. Centre lines: medians, all experiments were performed in biological duplicates.

Extended Data Figure 1 - Quality controls

a. Quality control metrics of single cells by batch (each cell is represented as a dot coloured according to its developmental stage; vertical lines mark experimental batches). Shown from top to bottom: total number of contacts and filtered contacts; percentage of unsupported contacts; percentage of contacts that are inter-chromosomal contacts (%trans); inter-chromosomal and homologous contacts (%trans homologous); number of constraints used for 3D modelling at 1Mb bin resolution; chromosome coverage fractions used for; maternal-to-paternal X chromosome coverage ratio used for gender identification .

b. The percentage of cis-chromosomal contacts of all contacts with both reads mapping unambiguously to the same or homologous chromosomes, as a function of genomic distance, for the oocytes and 1C-stage embryos.

c. Paternal/maternal coverage ratio in fertilized (XX/XY) and unfertilized (oocytes) eggs.

d. Paternal X-chromosome/maternal X-chromosome coverage ratio in embryos.

e. For each cell stage, the number of cells collected, sequenced and passing quality control, as well as the allele specific and non-allele specific coverages in the gender-separated merged cells passing quality control.
f. For XX and XY samples, at each stage, from merged samples: left panel, average contact density as a function of genomic distance; middle panel, number of contacts per cell; right panel, number of trans-chromosomal contacts per cell.

Extended Table 1: Number of contacts and frequency of trans-contacts per stage

References

Aguirre-Lavin, T., Adenot, P., Bonnet-Garnier, A., Lehmann, G., Fleurot, R., Boulesteix, C., Debey, P. and Beaujean, N. (2012) '3D-FISH analysis of embryonic nuclei in mouse highlights several abrupt changes of nuclear organization during preimplantation development', *BMC Dev Biol,* 12, pp. 30.

Artus, J. and Cohen-Tannoudji, M. (2008) 'Cell cycle regulation during early mouse embryogenesis', *Mol Cell Endocrinol,* 282(1-2), pp. 78-86.

BARR, M. L. and BERTRAM, E. G. (1949) 'A morphological distinction between neurones of the male and female, and the behaviour of the nucleolar satellite during accelerated nucleoprotein synthesis', *Nature,* 163(4148), pp. 676.

Borensztein, M., Syx, L., Ancelin, K., Diabangouaya, P., Picard, C., Liu, T., Liang, J. B., Vassilev, I., Galupa, R., Servant, N., Barillot, E., Surani, A., Chen, C. J. and Heard, E. (2017) 'Xist-dependent imprinted X inactivation and the early developmental consequences of its failure', *Nat Struct Mol Biol,* 24(3), pp. 226-233.

Bouniol, C., Nguyen, E. and Debey, P. (1995) 'Endogenous transcription occurs at the 1-cell stage in the mouse embryo', *Exp Cell Res,* 218(1), pp. 57-62.

Burton, A. and Torres-Padilla, M. E. (2014) 'Chromatin dynamics in the regulation of cell fate allocation during early embryogenesis', *Nat Rev Mol Cell Biol,* 15(11), pp. 723-34.

Chaumeil, J., Augui, S., Chow, J. C. and Heard, E. (2008) 'Combined immunofluorescence, RNA fluorescent in situ hybridization, and DNA fluorescent in situ hybridization to study chromatin changes, transcriptional activity, nuclear organization, and X-chromosome inactivation', *Methods Mol Biol,* 463, pp. 297-308.

Chaumeil, J., Le Baccon, P., Wutz, A. and Heard, E. (2006) 'A novel role for Xist RNA in the formation of a repressive nuclear compartment into which genes are recruited when silenced', *Genes Dev,* 20(16), pp. 2223-37.

Clemson, C. M., Hall, L. L., Byron, M., McNeil, J. and Lawrence, J. B. (2006) 'The X chromosome is organized into a gene-rich outer rim and an internal core containing silenced nongenic sequences', *Proc Natl Acad Sci U S A,* 103(20), pp. 7688-93.

Darrow, E. M., Huntley, M. H., Dudchenko, O., Stamenova, E. K., Durand, N. C., Sun, Z., Huang, S. C., Sanborn, A. L., Machol, I., Shamim, M., Seberg, A. P., Lander, E. S., Chadwick, B. P. and Aiden, E. L. (2016) 'Deletion of DXZ4 on the human inactive X chromosome alters higher-order genome architecture', *Proc Natl Acad Sci U S A,* 113(31), pp. E4504-12.

Deng, Q., Ramsköld, D., Reinius, B. and Sandberg, R. (2014) 'Single-cell RNA-seq reveals dynamic, random monoallelic gene expression in mammalian cells', *Science,* 343(6167), pp. 193-6.

Deng, X., Ma, W., Ramani, V., Hill, A., Yang, F., Ay, F., Berletch, J. B., Blau, C. A., Shendure, J., Duan, Z., Noble, W. S. and Disteche, C. M. (2015) 'Bipartite structure of the inactive mouse X chromosome', *Genome Biol,* 16, pp. 152.

Dixon, J. R., Jung, I., Selvaraj, S., Shen, Y., Antosiewicz-Bourget, J. E., Lee, A. Y., Ye, Z., Kim, A., Rajagopal, N., Xie, W., Diao, Y., Liang, J., Zhao, H., Lobanenkov, V. V., Ecker, J. R., Thomson, J. A. and Ren, B. (2015) 'Chromatin architecture reorganization during stem cell differentiation', *Nature,* 518(7539), pp. 331-6.

Dixon, J. R., Selvaraj, S., Yue, F., Kim, A., Li, Y., Shen, Y., Hu, M., Liu, J. S. and Ren, B. (2012) 'Topological domains in mammalian genomes identified by analysis of chromatin interactions', *Nature,* 485(7398), pp. 376-80.

Du, Z., Zheng, H., Huang, B., Ma, R., Wu, J., Zhang, X., He, J., Xiang, Y., Wang, Q., Li, Y., Ma, J., Zhang, K., Wang, Y., Zhang, M. Q., Gao, J., Dixon, J. R., Wang, X., Zeng, J. and Xie, W. (2017) 'Allelic reprogramming of 3D chromatin architecture during early mammalian development', *Nature,* 547(7662), pp. 232-235.

Flyamer, I. M., Gassler, J., Imakaev, M., Brandão, H. B., Ulianov, S. V., Abdennur, N., Razin, S. V., Mirny, L. A. and Tachibana-Konwalski, K. (2017) 'Single-nucleus Hi-C reveals

unique chromatin reorganization at oocyte-to-zygote transition', *Nature,* 544(7648), pp. 110-114.
Freire-Pritchett, P., Schoenfelder, S., Várnai, C., Wingett, S. W., Cairns, J., Collier, A. J., García-Vílchez, R., Furlan-Magaril, M., Osborne, C. S., Fraser, P., Rugg-Gunn, P. J. and Spivakov, M. (2017) 'Global reorganisation of cis-regulatory units upon lineage commitment of human embryonic stem cells', *Elife,* 6.
Giorgetti, L., Lajoie, B. R., Carter, A. C., Attia, M., Zhan, Y., Xu, J., Chen, C. J., Kaplan, N., Chang, H. Y., Heard, E. and Dekker, J. (2016) 'Structural organization of the inactive X chromosome in the mouse', *Nature,* 535(7613), pp. 575-9.
Heinz, S., Benner, C., Spann, N., Bertolino, E., Lin, Y. C., Laslo, P., Cheng, J. X., Murre, C., Singh, H. and Glass, C. K. (2010) 'Simple combinations of lineage-determining transcription factors prime cis-regulatory elements required for macrophage and B cell identities', *Mol Cell,* 38(4), pp. 576-89.
Johnson, M. H., Maro, B. and Takeichi, M. (1986) 'The role of cell adhesion in the synchronization and orientation of polarization in 8-cell mouse blastomeres', *J Embryol Exp Morphol,* 93, pp. 239-55.
Ke, Y., Xu, Y., Chen, X., Feng, S., Liu, Z., Sun, Y., Yao, X., Li, F., Zhu, W., Gao, L., Chen, H., Du, Z., Xie, W., Xu, X., Huang, X. and Liu, J. (2017) '3D Chromatin Structures of Mature Gametes and Structural Reprogramming during Mammalian Embryogenesis', *Cell,* 170(2), pp. 367-381.e20.
Kelly, S. J., Mulnard, J. G. and Graham, C. F. (1978) 'Cell division and cell allocation in early mouse development', *J Embryol Exp Morphol,* 48, pp. 37-51.
Krueger, F. and Andrews, S. R. (2016) 'SNPsplit: Allele-specific splitting of alignments between genomes with known SNP genotypes', *F1000Res,* 5, pp. 1479.
Langmead, B. and Salzberg, S. L. (2012) 'Fast gapped-read alignment with Bowtie 2', *Nat Methods,* 9(4), pp. 357-9.
Lieberman-Aiden, E., van Berkum, N. L., Williams, L., Imakaev, M., Ragoczy, T., Telling, A., Amit, I., Lajoie, B. R., Sabo, P. J., Dorschner, M. O., Sandstrom, R., Bernstein, B., Bender, M. A., Groudine, M., Gnirke, A., Stamatoyannopoulos, J., Mirny, L. A., Lander, E. S. and Dekker, J. (2009) 'Comprehensive mapping of long-range interactions reveals folding principles of the human genome', *Science,* 326(5950), pp. 289-93.
Mak, W., Nesterova, T. B., de Napoles, M., Appanah, R., Yamanaka, S., Otte, A. P. and Brockdorff, N. (2004) 'Reactivation of the paternal X chromosome in early mouse embryos', *Science,* 303(5658), pp. 666-9.
Mayer, W., Niveleau, A., Walter, J., Fundele, R. and Haaf, T. (2000a) 'Demethylation of the zygotic paternal genome', *Nature,* 403(6769), pp. 501-2.
Mayer, W., Smith, A., Fundele, R. and Haaf, T. (2000b) 'Spatial separation of parental genomes in preimplantation mouse embryos', *J Cell Biol,* 148(4), pp. 629-34.
Minajigi, A., Froberg, J., Wei, C., Sunwoo, H., Kesner, B., Colognori, D., Lessing, D., Payer, B., Boukhali, M., Haas, W. and Lee, J. T. (2015) 'Chromosomes. A comprehensive Xist interactome reveals cohesin repulsion and an RNA-directed chromosome conformation', *Science,* 349(6245).
Nagano, T., Lubling, Y., Stevens, T. J., Schoenfelder, S., Yaffe, E., Dean, W., Laue, E. D., Tanay, A. and Fraser, P. (2013) 'Single-cell Hi-C reveals cell-to-cell variability in chromosome structure', *Nature,* 502(7469), pp. 59-64.
Nagano, T., Lubling, Y., Várnai, C., Dudley, C., Leung, W., Baran, Y., Mendelson Cohen, N., Wingett, S., Fraser, P. and Tanay, A. (2017) 'Cell-cycle dynamics of chromosomal organization at single-cell resolution', *Nature,* 547(7661), pp. 61-67.
Nagano, T., Várnai, C., Schoenfelder, S., Javierre, B. M., Wingett, S. W. and Fraser, P. (2015) 'Comparison of Hi-C results using in-solution versus in-nucleus ligation', *Genome Biol,* 16, pp. 175.
Naumova, N., Imakaev, M., Fudenberg, G., Zhan, Y., Lajoie, B. R., Mirny, L. A. and Dekker, J. (2013) 'Organization of the mitotic chromosome', *Science,* 342(6161), pp. 948-53.

Nora, E. P., Lajoie, B. R., Schulz, E. G., Giorgetti, L., Okamoto, I., Servant, N., Piolot, T., van Berkum, N. L., Meisig, J., Sedat, J., Gribnau, J., Barillot, E., Blüthgen, N., Dekker, J. and Heard, E. (2012) 'Spatial partitioning of the regulatory landscape of the X-inactivation centre', *Nature,* 485(7398), pp. 381-5.

Okamoto, I., Otte, A. P., Allis, C. D., Reinberg, D. and Heard, E. (2004) 'Epigenetic dynamics of imprinted X inactivation during early mouse development', *Science,* 303(5658), pp. 644-9.

Rao, S. S., Huntley, M. H., Durand, N. C., Stamenova, E. K., Bochkov, I. D., Robinson, J. T., Sanborn, A. L., Machol, I., Omer, A. D., Lander, E. S. and Aiden, E. L. (2014) 'A 3D map of the human genome at kilobase resolution reveals principles of chromatin looping', *Cell,* 159(7), pp. 1665-80.

Splinter, E., de Wit, E., Nora, E. P., Klous, P., van de Werken, H. J., Zhu, Y., Kaaij, L. J., van Ijcken, W., Gribnau, J., Heard, E. and de Laat, W. (2011) 'The inactive X chromosome adopts a unique three-dimensional conformation that is dependent on Xist RNA', *Genes Dev,* 25(13), pp. 1371-83.

Stamatoyannopoulos, J. A., Snyder, M., Hardison, R., Ren, B., Gingeras, T., Gilbert, D. M., Groudine, M., Bender, M., Kaul, R., Canfield, T., Giste, E., Johnson, A., Zhang, M., Balasundaram, G., Byron, R., Roach, V., Sabo, P. J., Sandstrom, R., Stehling, A. S., Thurman, R. E., Weissman, S. M., Cayting, P., Hariharan, M., Lian, J., Cheng, Y., Landt, S. G., Ma, Z., Wold, B. J., Dekker, J., Crawford, G. E., Keller, C. A., Wu, W., Morrissey, C., Kumar, S. A., Mishra, T., Jain, D., Byrska-Bishop, M., Blankenberg, D., Lajoie, B. R., Jain, G., Sanyal, A., Chen, K. B., Denas, O., Taylor, J., Blobel, G. A., Weiss, M. J., Pimkin, M., Deng, W., Marinov, G. K., Williams, B. A., Fisher-Aylor, K. I., Desalvo, G., Kiralusha, A., Trout, D., Amrhein, H., Mortazavi, A., Edsall, L., McCleary, D., Kuan, S., Shen, Y., Yue, F., Ye, Z., Davis, C. A., Zaleski, C., Jha, S., Xue, C., Dobin, A., Lin, W., Fastuca, M., Wang, H., Guigo, R., Djebali, S., Lagarde, J., Ryba, T., Sasaki, T., Malladi, V. S., Cline, M. S., Kirkup, V. M., Learned, K., Rosenbloom, K. R., Kent, W. J., Feingold, E. A., Good, P. J., Pazin, M., Lowdon, R. F., Adams, L. B. and Consortium, M. E. (2012) 'An encyclopedia of mouse DNA elements (Mouse ENCODE)', *Genome Biol,* 13(8), pp. 418.

Takagi, N. and Sasaki, M. (1975) 'Preferential inactivation of the paternally derived X chromosome in the extraembryonic membranes of the mouse', *Nature,* 256(5519), pp. 640-2.

Wingett, S., Ewels, P., Furlan-Magaril, M., Nagano, T., Schoenfelder, S., Fraser, P. and Andrews, S. (2015) 'HiCUP: pipeline for mapping and processing Hi-C data', *F1000Res,* 4, pp. 1310.

Zhan, Y., Mariani, L., Barozzi, I., Schulz, E. G., Blüthgen, N., Stadler, M., Tiana, G. and Giorgetti, L. (2017) 'Reciprocal insulation analysis of Hi-C data shows that TADs represent a functionally but not structurally privileged scale in the hierarchical folding of chromosomes', *Genome Res,* 27(3), pp. 479-490.

Zhang, B., Zheng, H., Huang, B., Li, W., Xiang, Y., Peng, X., Ming, J., Wu, X., Zhang, Y., Xu, Q., Liu, W., Kou, X., Zhao, Y., He, W., Li, C., Chen, B., Li, Y., Wang, Q., Ma, J., Yin, Q., Kee, K., Meng, A., Gao, S., Xu, F., Na, J. and Xie, W. (2016) 'Allelic reprogramming of the histone modification H3K4me3 in early mammalian development', *Nature,* 537(7621), pp. 553-557.

Zheng, H., Huang, B., Zhang, B., Xiang, Y., Du, Z., Xu, Q., Li, Y., Wang, Q., Ma, J., Peng, X., Xu, F. and Xie, W. (2016) 'Resetting Epigenetic Memory by Reprogramming of Histone Modifications in Mammals', *Mol Cell,* 63(6), pp. 1066-79.

Figure 1 - Ranisavljevic et al

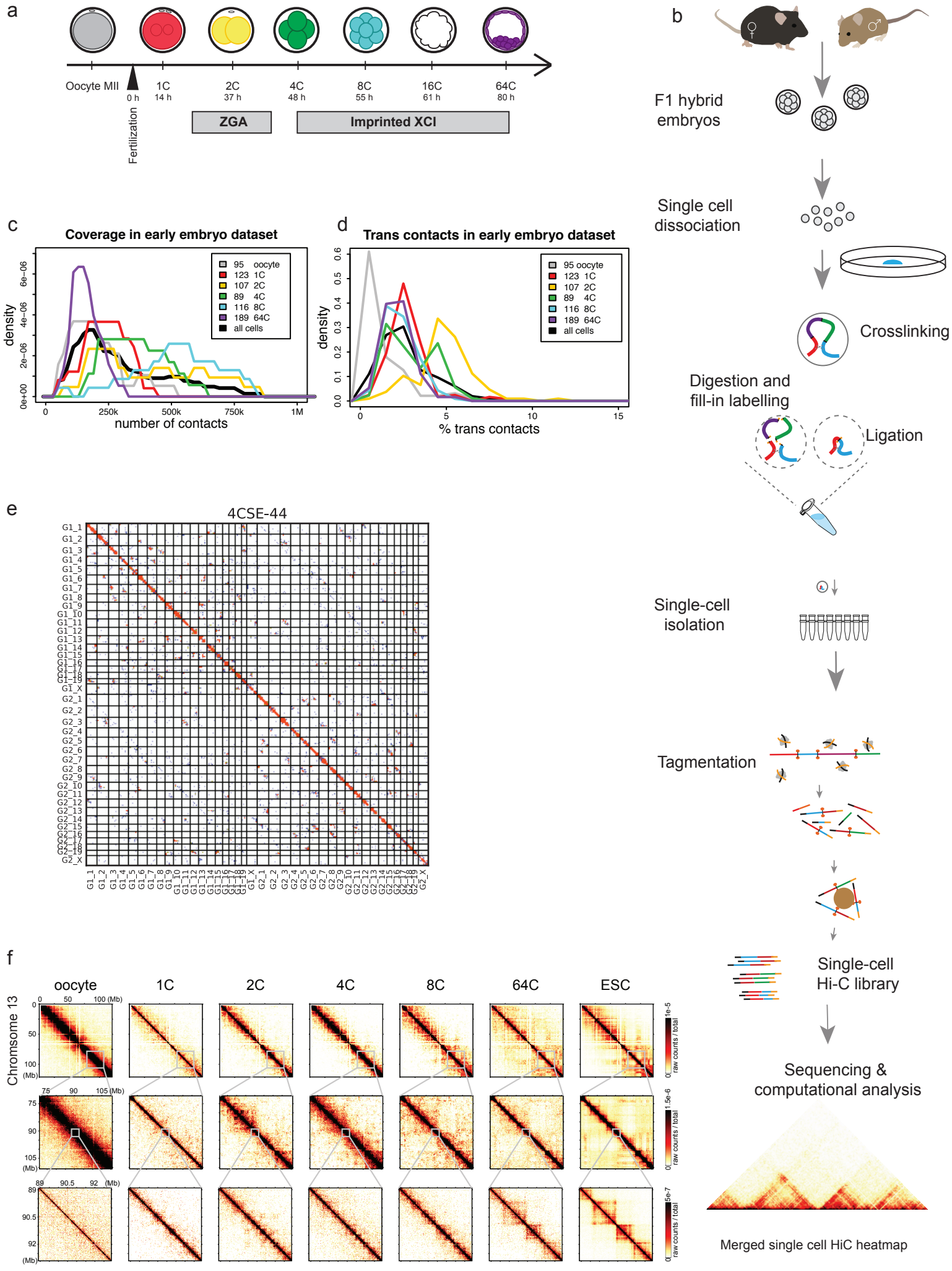

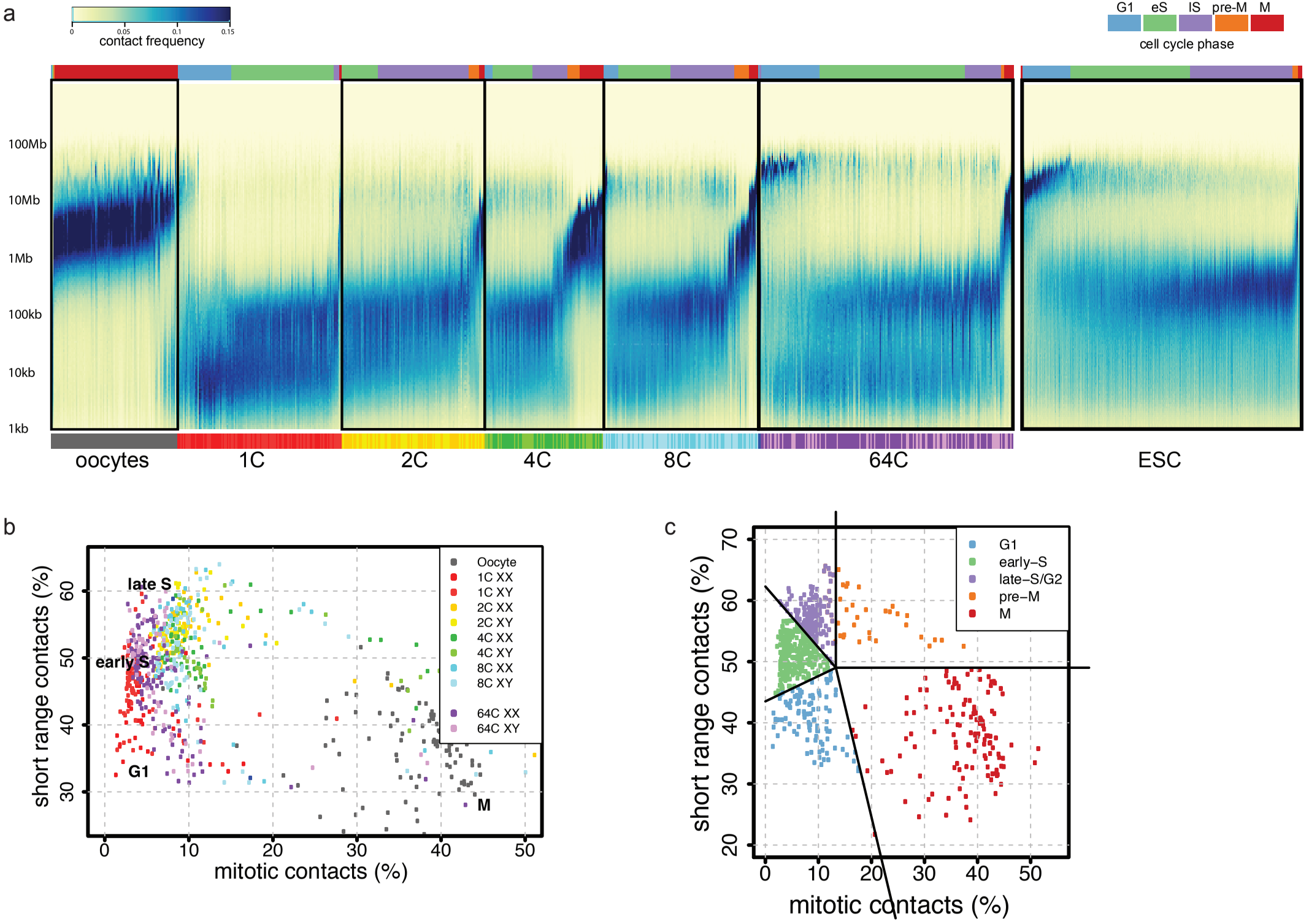

Figure 2 - Ranisavljevic et al

Figure 3 - Ranisavljevic et al

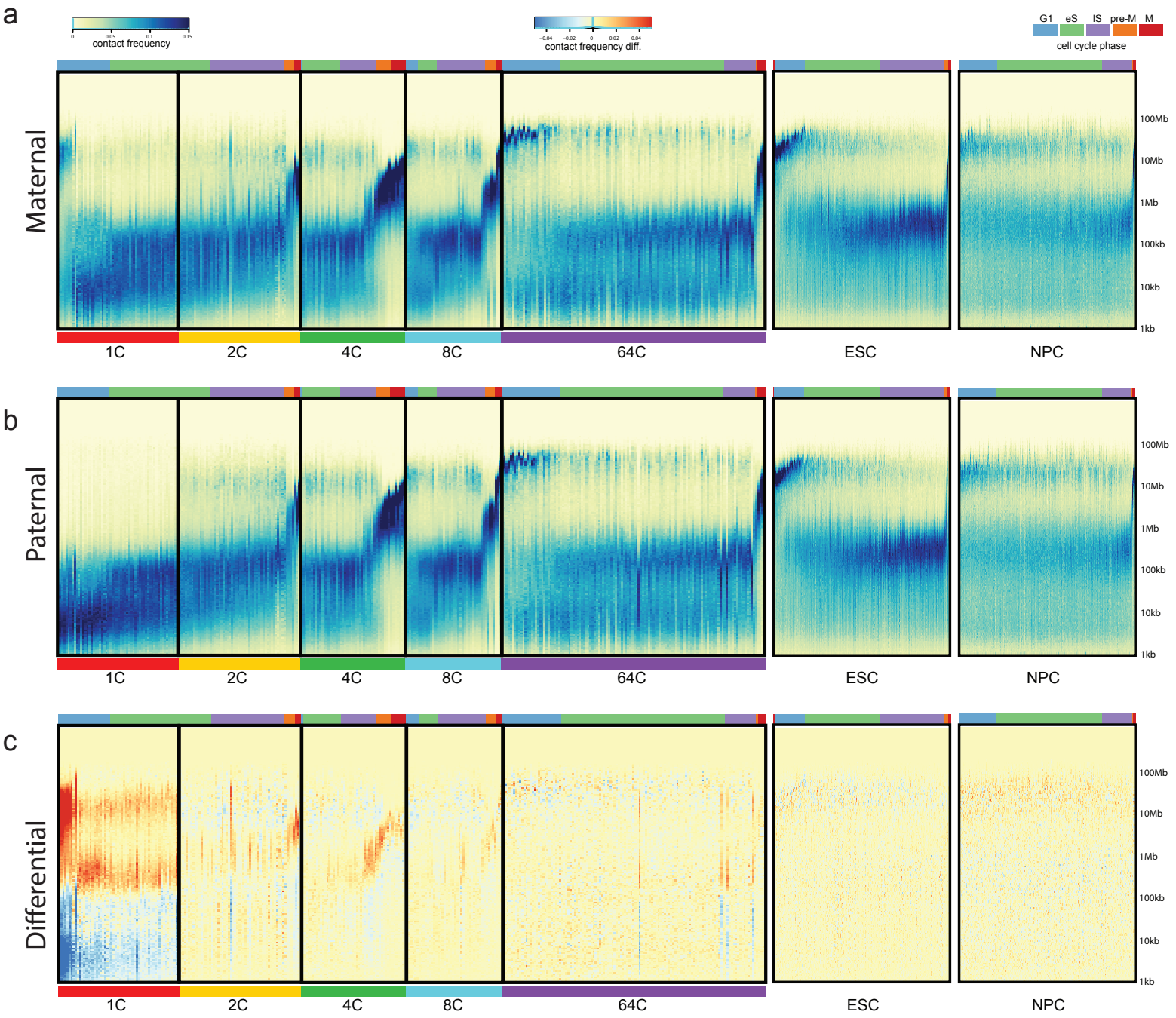

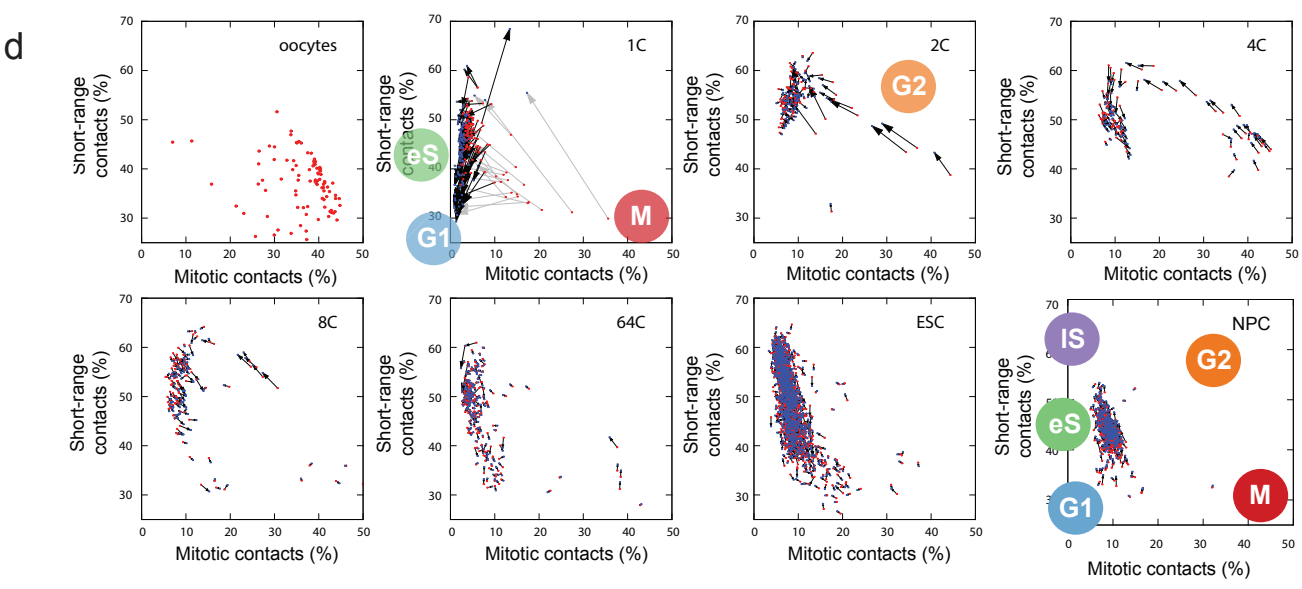

Figure 4 - Ranisavljevic et al

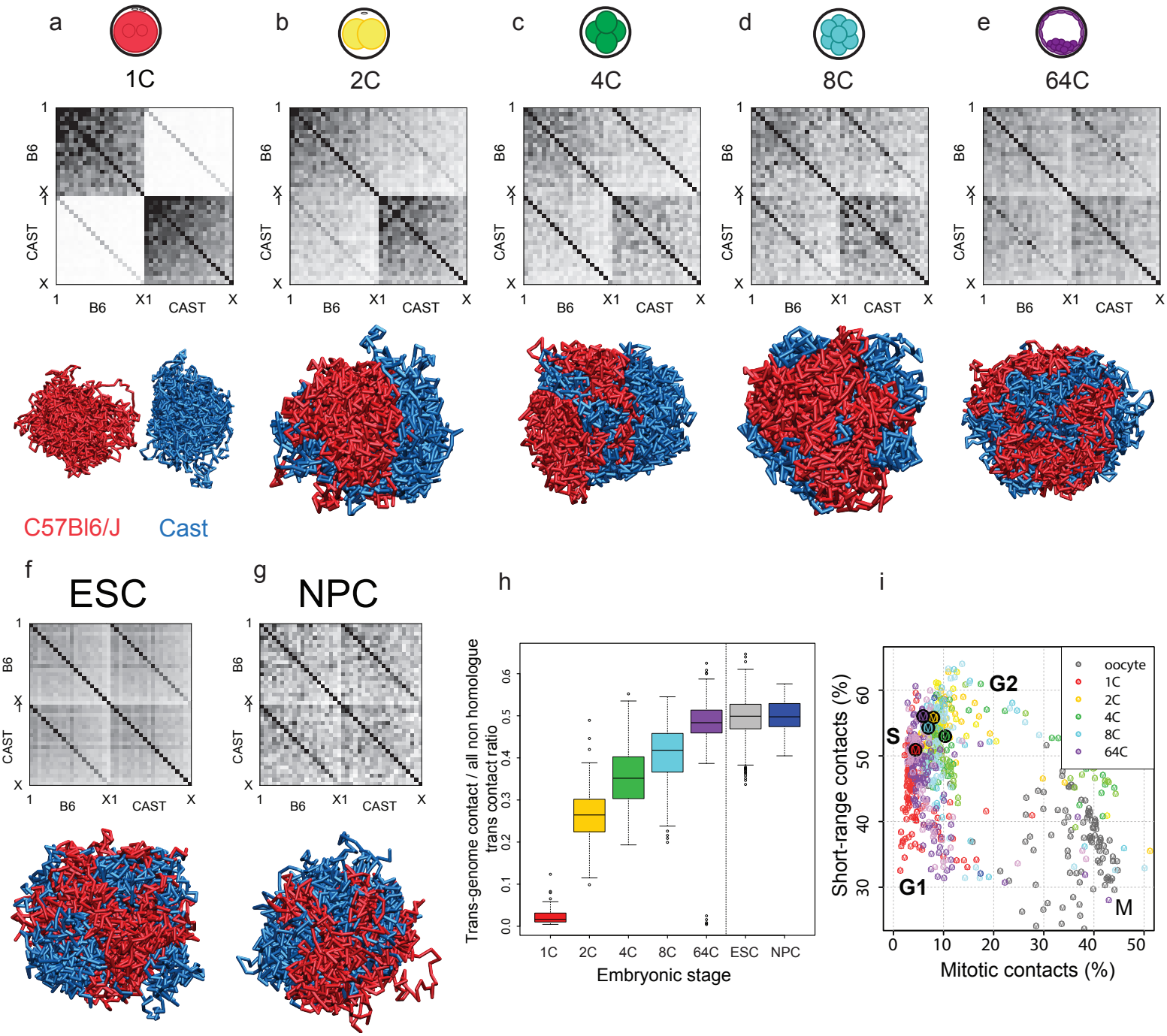

Figure 5 - Ranisavljevic et al

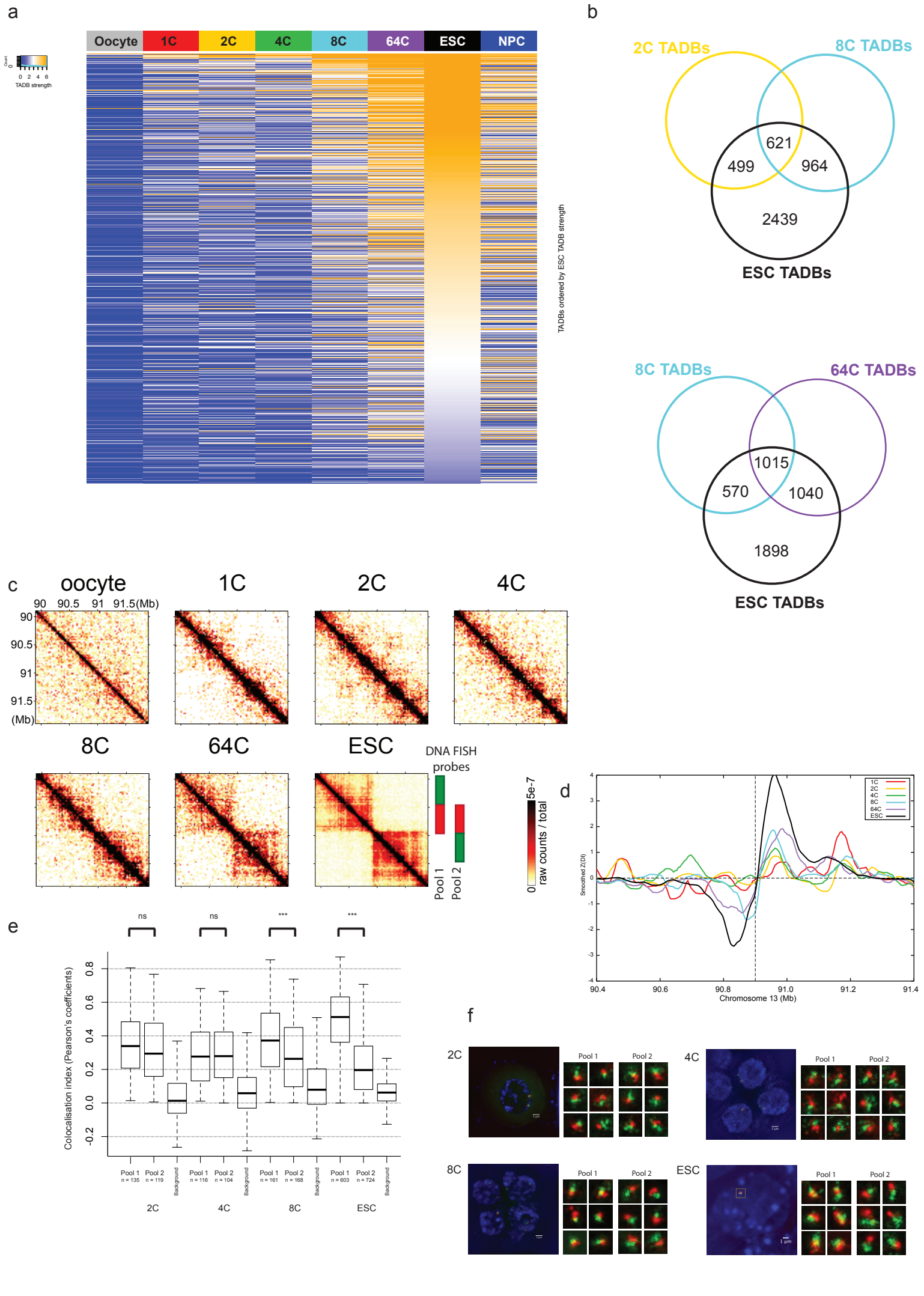

Figure 6 - Ranisavljevic et al

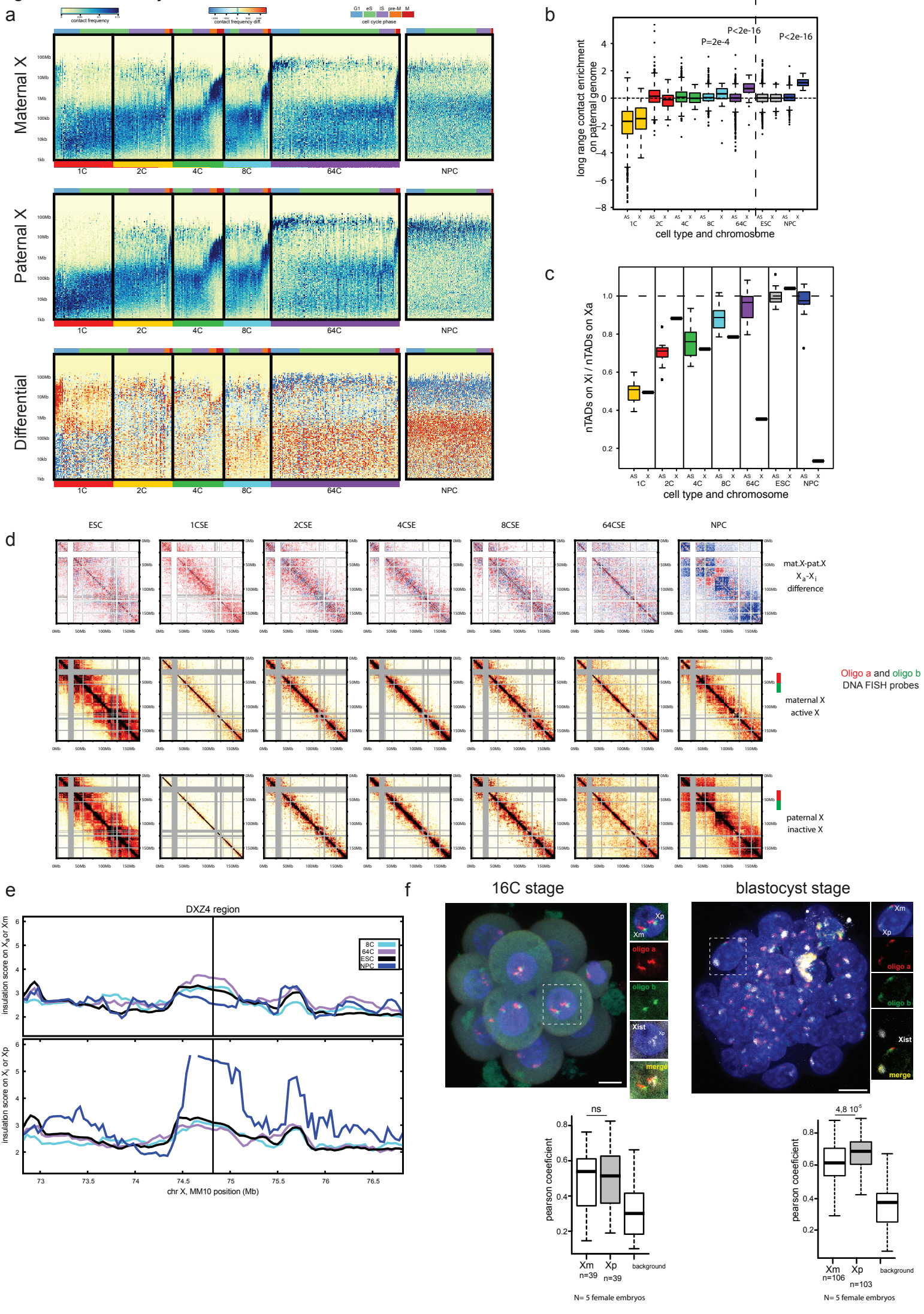

Extended Data Figure 1 - Ranisavljevic et al

a

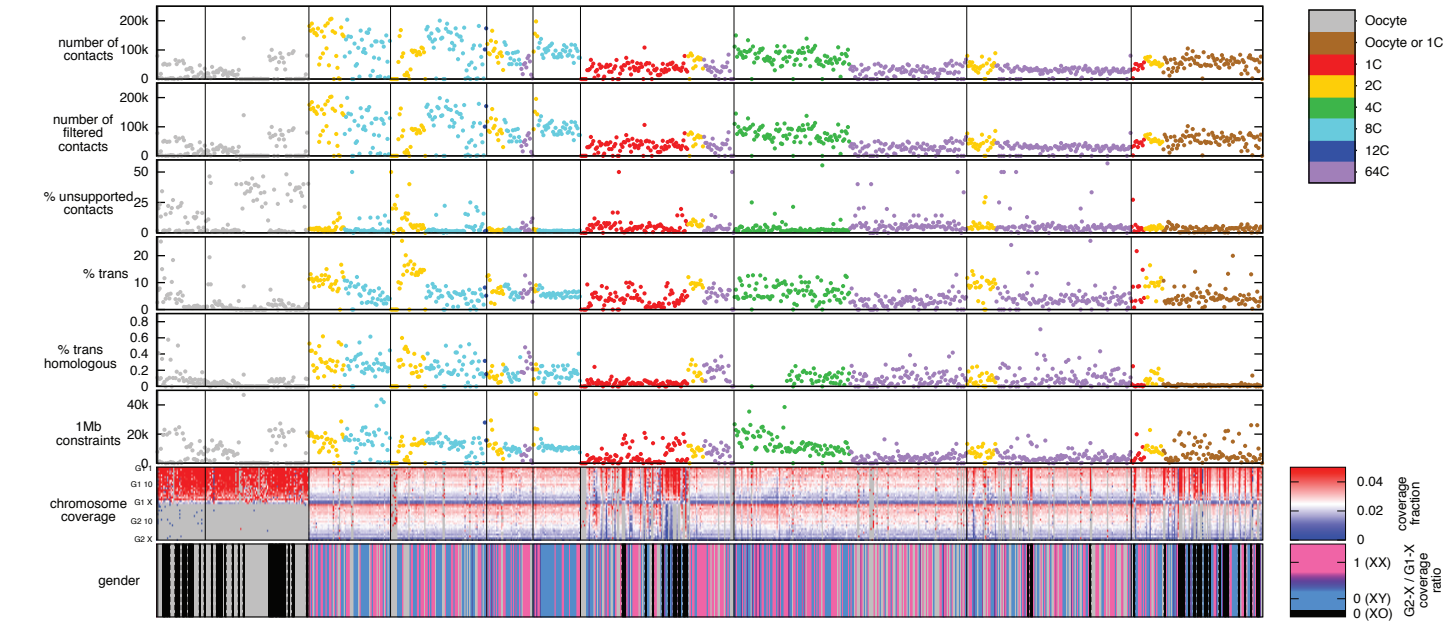

b

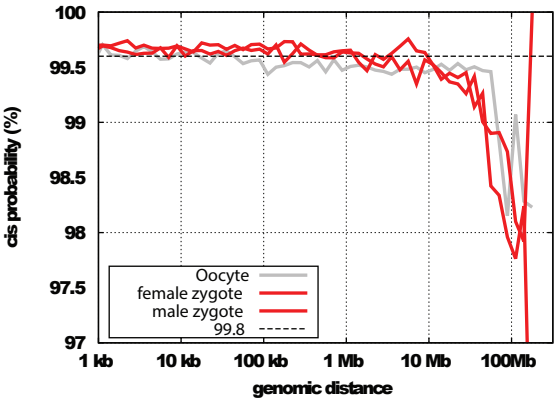

c

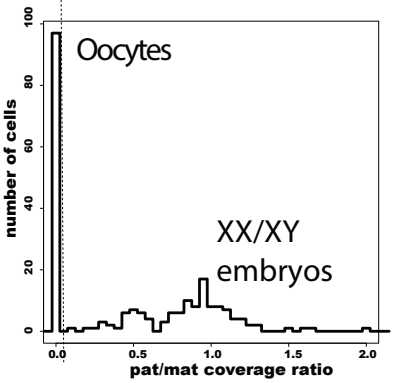

d

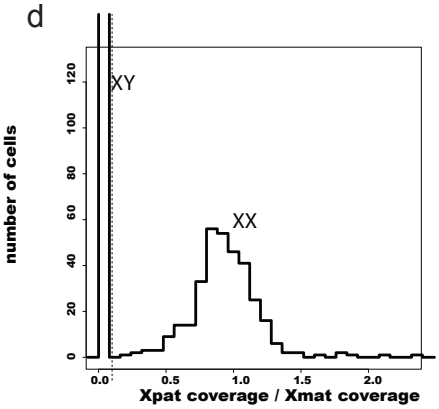

e

	sample	collected[a]	sequenced[b]	total passed QC[c]	XO[d]	coverage	XX	AS coverage	NS coverage	XY	AS coverage	NS coverage
oocyte	EHP	272	125	59								
oocyte/zygote unkown[e]	unk	105	82	77								
1C stage (zygote)	1CSE	105	99	82	95	20 491 062	58	8 519 283	13 733 399	65	10 299 088	15 700 950
2C stage	2CSE	153	128	107			58	15 692 035	25 396 944	49	12 010 058	18 655 274
4C stage	4CSE	95	95	89			50	11 939 281	18 547 528	39	9 641 006	14 413 622
8C stage	8CSE	142	135	116			46	16 461 495	25 881 556	70	22 992 704	35 544 281
64C stage (blastocyst)	64CSE	251	242	189			126	13 807 767	21 725 300	63	6 728 134	10 216 189
ESC				1 100			1 100	133 665 406	197 490 274			
NPC				41			41	2 733 114	4 007 761			
NPC-4[f]				393			393	25 023 664	36 982 467			

a: the maximum cell ID for each condition
b: the number of cells that had non-0 reads
c: QC criteria: >25,000 allele-specific reads, <15% trans-ratio and no missing chromosomes
d: all XO cells are treated as unfertilised eggs
e: all XO cells are treated as unfertilised eggs, and all XX and XY cells are treated as fertilised eggs
f: including cells with chr4 aberration
AS: allele-specific; NS: non-allele-specific

f

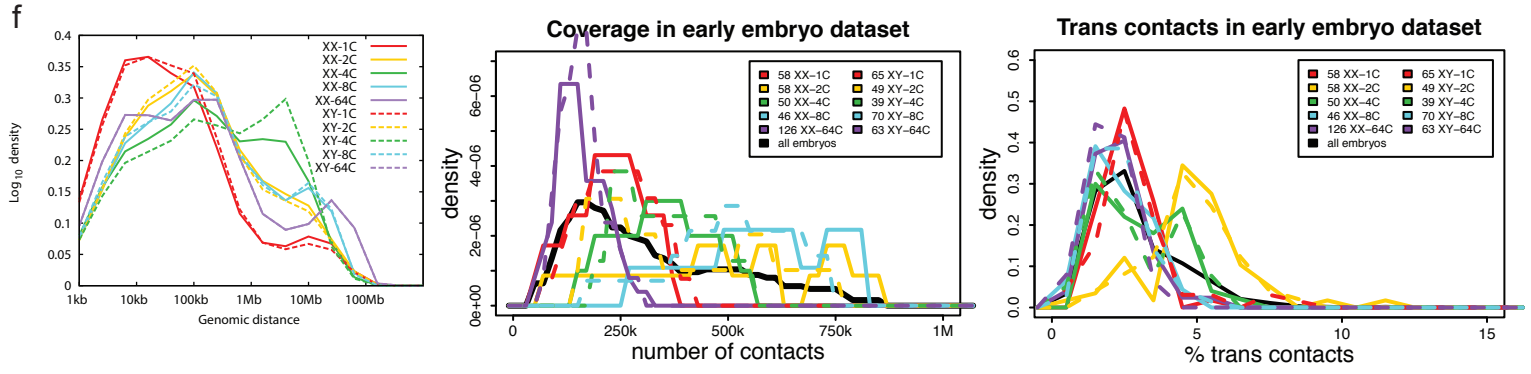

Extended Table 1 - Ranisavljevic et al

Number of contacts

Stage	min	median	max
all	40 899	252 645	1 090 116
Oocyte	51 287	192 887	692 472
1C	43 703	243 045	624 704
2C	63 248	360 199	1 089 263
4C	128 244	360 441	823 488
8C	40 899	534 525	1 090 116
64C	44 132	158 401	468 311

Trans contacts (%)

Stage	min	median	max
all	0,202	2,298	11,428
Oocyte	0,202	0,808	6,004
1C	0,756	2,441	8,677
2C	0,828	4,849	11,428
4C	0,861	2,699	6,590
8C	0,615	2,121	5,798
64C	0,602	2,088	5,855

MATERIAL & METHODS

Single cell HiC on preimplantation mouse embryo

Mouse crosses, collection of embryos and single cell dissociation

All experimental design and procedures were in agreement with the guidelines from French legislation and institutional policies (French ethical committee of animal experimentation: APAFIS#8812-2017020611033784v2).

Embryos and oocytes were derived from either natural mating or after female superovulation. To induce ovulation, females were administered 5 IU of hCG intraperitoneally, 46–48 h after injection of 5 IU of PMSG.

Stage	DNA FISH	ScHiC
Metaphase II oocyte		Superovulated
1C		Both
2C	Superovulated	Both
4C	Superovulated	Superovulated
8C	Superovulated	Natural mating
16C	Superovulated	
64C	Natural mating	Natural mating
E4.5	Natural mating	

Stage	Timing in natural mating (hours post fertilization)	Timing in superovulated (hours post hcg injection)
Metaphase II oocyte		15
1C	14	21
2C	37	44
4C	48	55
8C	55	62
16C	61	
64C	80	
E4.5	Natural mating	

For DNA FISH, C57BL/6J (B6) females were crossed with C57BL/6J (B6) males ; for single cell HiC, C57BL/6J (B6) females were crossed with CAST/EiJ (Cast) males.

The collected embryos were included in the analyses only if they showed a normal morphology and the correct number of blastomeres for their developmental stage.

No statistical method was used to predetermine sample size.

Oocytes and embryos were collected by flushing oviducts (until 16C) or uteri (64C) with M2 medium (Sigma). The zona pellucida was removed with acid Tyrode's solution (Sigma), and embryos were washed twice with M2 medium (Sigma). To remove second polar body in zygotes and to isolate individual cells, we then incubated embryos in Ca2+- and Mg2+-free M2 medium for 5 to 30 min, depending on the embryonic stage. First polar body was lost during zona pellucida removal. For 2C stage and onward, second polar body was dissociated during single cell dissociation.

Embryonic stage	Incubation time in Ca2+- and Mg2+-free M2 medium
1C	20 to 30 min
2C	20 min
4C	10 to 15 min
8C	5 to 10 min

For the blastocyst stage, incubation with Ca2+- and Mg2+-free M2 medium was replaced with a 5-min incubation in TrypLE (Invitrogen). After incubation, each blastomere was mechanically dissociated by mouth pipetting with a thin glass capillary. Single cells were then washed three times in PBS/acetylated BSA (Sigma) before being processed for scHiC without delay.

Single cell HiC protocol: from single cells to ligation step

MATERIALS

REAGENTS

• Freshly dissociated blastomeres from fresh mouse embryos.

> **! CAUTION** Approved governmental and institutional regulations for animal work must be adhered to, and experiments should be reported according to the ARRIVE (Animal Research: Reporting *in vivo* Experiments) guidelines.

• M2 medium with HEPES, without penicillin and streptomycin, liquid, sterile-filtered, suitable for mouse embryo (Sigma, cat. no. M7167)

• Formaldehyde (16% solution; Agar Scientific, cat. no. R1026)

> **! CAUTION** Follow the appropriate health and safety regulations to handle formaldehyde solution, as it is toxic.

• PBS, pH 7.4 (10×; Life Technologies, cat. no. 70011-036)

• Water (molecular biology grade; Sigma-Aldrich, cat. no. W4502)

• Glycine (freshly prepared 2 M solution)

• NP-40 (also known as IGEPAL CA-630; Sigma-Aldrich, cat. no. I8896)

• cOmplete, EDTA-free (Roche Diagnostics, cat. no. 11873580001)

• SDS, 20% (wt/vol) solution (Bio-Rad Laboratories, cat. no. 161-0418)

• Triton X-100 (20% (vol/vol); Sigma-Aldrich, cat. no. T8787)

- MboI (5,000 U/ml; New England Biolabs, cat. No. R0147L)
- NEBuffer 3 (10×) (New England Biolabs, cat. no. B7003S)
- dCTP (10 mM; Life Technologies, cat. no. 18253-013)
- dGTP (10 mM; Life Technologies, cat. no. 18254-011)

- dTTP (10 mM; Life Technologies, cat. no. 18255-018)
- dATP (10 mM; Life Technologies, cat. no. 18252-015)
- Biotin-14-dATP (0.4 mM; Life Technologies, cat. no. 19524-016)
- DNA polymerase I, large (Klenow) fragment (5,000 U/ml; New England Biolabs, cat. no. M0210S)
- T4 DNA ligase reaction buffer (10×; New England Biolabs, cat. no. B0202S)
- BSA (100× (10 mg/ml); New England Biolabs, cat. no. B9001)
- Acetylated BSA
- T4 DNA ligase (1 U/l; Life Technologies, cat. no. 15224-025)
- DNA LoBind tube (1.5 ml; Eppendorf, cat. no. 0030 108.051)
- PCR strips
- Polyvinylpyrrolidone PVP

EQUIPMENT

- Centrifuge
- Petri dish
- Pasteur pipettes and/or thin capillary glasses
- Aspirator tube assemblies for calibrated microcapillary pipettes
- Silicone tubing (6.0 mm bore, 2.0-mm-thick wall)
- Phase contrast microscope
- Benchtop centrifuge
- Thermomixer

REAGENT SETUP

PBS 1X acetylated BSA 1mg/mL To prepare 2mL PBS 1X acetylated BSA buffer, add 100uL of acetylated BSA and 200uL PBS10X to 1700uL of water. Mix well, filter the solution, aliquot and store at -20°C (200uL aliquots) for one year.

PVP 100mg/mL To prepare 1mL of PVP 100mg/mL, add 100mg PVP to 1mL of water. Mix well.

cOmplete EDTA free stock solution 25X To prepare 2mL cOmplete EDTA free stock solution, add 1 tablet to 2mL of water and mix well to dissolve the tablet. Store some 50uL aliquots at -20°C. ▲**CRITICAL** Check the tablet expiration date and report it on the solution stored at -20°C.

Glycine 2M To prepare 1mL of Glycine 2M, add 150mg Glycine (ultrapure, 75.07 MW) to water so as to have 1mL solution. Mix well.

NP-40, 20%(vol/vol) To prepare 1mL of 20%(vol/vol) NP-40, add 800uL of water to 200uL of NP-40, and mix it well. ▲**CRITICAL** Freshly prepare the solution on the day of the cell permeabilization. Make sure it is well mixed.

Triton X-100, 20% (vol/vol) To prepare 1 mL of 20% (vol/vol) Triton X-100, add 800uL of water to 200uL of Triton X-100 and mix it well. ▲**CRITICAL** Freshly prepare the solution for each restriction digestion. Make sure it is well mixed.

1M TrisHCl (pH=8) buffer To prepare 500mL of 1M TrisHCl (pH=8) buffer, add 60,75g (121.14 MW) to water and add HCl to adjust pH to 8. Keep at room temperature.

1M NaCl buffer To prepare 500mL of 1M NaCl buffer, add 29,22g (58.44 MW) to water. Keep at room temperature.

Fixation buffer To prepare 2mL of fixation buffer add 250uL of 16% formaldehyde to 200uL PBS 10x and 40uL PVP (100mg/mL); add 1510uL of water. ▲**CRITICAL** Freshly prepare the solution on the day of the cell fixation.

Quenching buffer To prepare 400uL of quenching buffer, add 400uL of fixation buffer and 25uL of Glycine 2M (0.125M final concentration). Chill the tube on ice.

Permeabilization buffer Permeabilization buffer is10mM Tris-HCl, 10mM NaCl and 0.2% (vol/vol) NP-40, cOmplete EDTA-free; to prepare a volume of 1 mL, add 10uL of 1 M

Tris-HCl (pH 8.0), 10uL of 1 M NaCl, 10uL of 20% (vol/vol) NP-40 and 10uL BSA 10X to 920 uL of water. Then, add 40uL of cOmplete EDTA-free buffer, mix it well and chill the buffer on ice. ▲**CRITICAL** Freshly prepare the buffer on the day of the cell permeabilization.

NEBuffer 3, 1.24× To prepare 1 mL of 1.24× NEBuffer 3, add 124uL of NEBuffer 3 (10×), 10uL of BSA 10X, 20 uL of PVP 100mg/mL to 846uL of water and mix it well. ▲ **CRITICAL** Freshly prepare the solution for each restriction digestion.

Ligation mix To prepare 1mL of ligation mix, add 100uL of 10X ligase reaction buffer, 10uL of BSA 10X to 880uL of water. Mix well and then add 10uL of T4 DNA liagase and chill the tube on ice.

PROCEDURE

! CAUTION While using mouth pipette to transfer cells from solution to solution, make sure to fill it with the new solution and to use as few volume as possible to reduce carry over. Transferring the cells through at least two drops of the new solution allows to reduce the carry over too. The same Petri dish may be used through the whole procedure. Make sure the drops don't mix, don't dry and are well identified if prepared in advance.

▲**CRITICAL** When processing smaller cells (such as 64C stage blastomeres), reduce the size of the drops to 5uL and work under oil.

Cell fixation TIMING about 30 min

1| Prepare some fresh single cells from oocyte or embryos and wash them in PBS 1X BSA buffer drops three times.

2| Prepare two 30-40uL drops of fixation buffer on a Petri dish. Transfer the cells quickly from PBS 1X BSA through the two drops.

3| Fix for exactly 10 min at room temperature.

! CAUTION As formaldehyde is toxic, it should be handled in a fume hood and discarded according to relevant institutional and local regulations.

4| Prepare two 30-40uL drops of ice-cold quenching buffer on a Petri dish. Transfer the cells quickly from fixation buffer to quenching buffer drops. Chill the Petri dish on ice for 5

min. ▲**CRITICAL STEP** Using a foil sheet on ice allows a better transmission of the cold. Cells might sometimes end up at the very surface of the quenching buffer drop.

5| Prepare three 30-40uL drops of BPS 1X BSA (washing buffer) on a Petri dish. The third one should be circled with an hydrophobic pen. Transfer the cells from quenching buffer to the washing buffer.

PAUSE POINT The cells can be held in PBS 1X BSA on ice if needed (so as to process a new batch of embryo/single cell dissociation/fixation for example). Use a lid for the Petri dish to reduce evaporating and make sure the drop containing the cells doesn't dry.

Cell permeabilization and the first restriction digestion TIMING 3 h + incubation for 12–16 h (overnight)

9| Prepare two circles with the hydrophobic pen on the Petri dish and fill them with two 30-40uL drops of ice-cold permabilization buffer. Transfer the cells from washing buffer to permeabilization buffer. ▲**CRITICAL STEP** Hydrophobic pen is needed due to the use of NP-40.

10| Incubate the cells for 30 min on ice. ▲**CRITICAL STEP** Use a lid for the Petri dish to reduce evaporating and make sure the drop containing the cells doesn't dry.

11| Prepare two circles with the hydrophobic pen on the Petri dish and fill them with two 30-40uL drops of NEB3 1.24X buffer. Transfer the cells from permeabilization buffer to NEB3 buffer. ▲**CRITICAL STEP** Cells tend to spin up as transferred from permeabilization to NEB3X buffer. Keep them in sight through the whole process.

12| Prepare in a DNA Lo-binding tube 200uL of NEB3 1.24X mix and 3uL SDS20%. Mix well. ▲**CRITICAL STEP** SDS20% is very corrosive: add it to the NEB3 buffer BEFORE adding the cells so as to homogeneize the buffer as much as possible.

13| Transfer the cells from the NEB3 buffer drops to the Lo-binding tube.

14| Shake at 550 r.p.m. for 1 h at 37 °C on a thermomixer.

16| Add 20uL of 20% Triton X-100 (final concentration 1.8%, vol/vol) and shake at 550 r.p.m. for 1 h at 37 °C on a thermomixer. ▲**CRITICAL STEP** When adding the 20%

Triton X-100 to the tube, avoid pipetting up and down. Prefer depositing the Triton along the tube wall.

17| Add 1,250U of MboI (25 uL of 25U/uL solution) and shake at 550 r.p.m. at 37 °C on a thermomixer for 12–16 h. ▲**CRITICAL STEP** When adding the MboI to the tube, avoid pipetting up and down. Prefer depositing the MboI along the tube wall.

Biotin labeling and Hi-C ligation TIMING ~80 min + incubation for 4 h to overnight

18| Add the following components to the sample. ▲**CRITICAL STEP** When adding the new components to the tube, avoid pipetting up and down. Prefer depositing them along the tube wall:

Components	Amount per tube (uL)	Final concentration or units
dCTP, 5mM	1.56	28.4M
dGTP, 5mM	1.56	28.4M
dTTP, 5mM	1.56	28.4M
Biotin-14-dATP, 0.4mM	19.5	28.4M
DNA polymerase I, large (Klenow) fragment	5.2	50U

19| Shake at 550 r.p.m. for 1 h at 37 °C on a thermomixer.

20| Centrifuge the tube at 500*g* for 5 min at 4 °C. ▲**CRITICAL STEP** As cell number is low, prefer a centrifuge with an horizontal axis of rotation. If 1.5mL tubes don't fit in the centrifuge, use a 50mL Falcon filled with some paper to hold the 1.5mL tube inside.

21| Remove the supernatant, leaving ~50 uL.

22| Add the ligation mix.

23| Incubate the sample at 16 °C for 4 h or more (overnight is fine).

Single-cell isolation TIMING ~1 h

24| Centrifuge the tube at 500*g* for 5 min at 4 °C. ▲**CRITICAL STEP** As cell number is low, prefer a centrifuge with an horizontal axis of rotation. If 1.5mL tubes don't fit in the centrifuge, use a 50mL Falcon filled with some paper to hold the 1.5mL tube inside.

25| Remove the supernatant leaving ~50 uL and resuspend the pellet with 100uL of PBS1x BSA using a large Pasteur pipette.

26| With the large Pasteur pipette, make several drops on a Petri dish with the cell suspension. ▲**CRITICAL STEP** As looking for cells might be long sometimes, make sure the drops don't dry: prefer fewer and larger drops. Be aware that if remaining supernatant has been too abundant, the cell resuspension drops will tend to spread too much.

27| Under the microscope, collect all the single cells and wash them in a PBS1X BSA drop.

26| Pick and isolate the single cells in PCR tubes with a minimum amount of liquid. Spin down the drops quickly and freeze at -80°C as soon as possible.

PAUSE POINT The cells can be stored at -80°C for several weeks.

Library preparation and sequencing - *performed by Takashi Nagano*

To prepare single-cell Hi-C libraries from single nuclei in PCR strips, 5 µl of PBS was added to each well and crosslinks reversed by incubating at 65˚C overnight. Hi-C concatemer DNA was fragmented and linked with sequencing adapters using the Nextera XT DNA Library Preparation Kit (Illumina), by adding 10 µl of Tagment DNA Buffer and 5 µl of Amplicon Tagment Mix, incubating at 55˚C for 20 min, then cooling down to 10˚C, followed by addition 5 µl of Neutralize Tagment Buffer and incubation for 5 min at room temperature. Hi-C ligation junctions were then captured by Dynabeads M-280 streptavidin beads (Thermo Fisher; 20 µl of original suspension per single-cell sample). Beads were prepared by washing with 1 x BW buffer (5 mM Tris-Cl pH 7.5, 0.5 mM EDTA, 1 M NaCl), resuspended in 4 x BW buffer (20 mM Tris-Cl pH 7.5, 2 mM EDTA, 4 M NaCl; 8 µl per sample), and then mixed with the 25 µl sample and incubated at room temperature overnight with gentle agitation. The beads were then washed four times with 200 µl of 1 x BW buffer, twice with 200 µl of 10 mM Tris-Cl pH 7.5 at room temperature, and resuspended in 25 µl of 10 mM Tris-Cl pH 7.5. Single-cell Hi-C libraries were amplified from the beads by adding 15 µl of Nextera PCR Master Mix, 5 µl of i7 Index primer of choice and 5 µl of i5 Index primer of choice. Samples were then incubated at 72˚C for 3 min, 95˚C for 30 sec followed by the thermal cycling at 95˚C for 10 sec, 55˚C for 30 sec and 72˚C for 30 sec for 18 cycles, then incubated at 72˚C for 5 min. The supernatant was separated from the beads and purified one by one with AMPure XP beads (Beckman Coulter; 0.6 times volume of the supernatant) according to manufacturer's instructions and eluted with 30 µl each of 10 mM Tris-Cl pH 8.5. The eluate was purified once more with AMPure XP beads (equal volume to the previous eluate) and eluted with 11 µl of 10 mM Tris-Cl pH 8.5.

Before sequencing, the libraries were quantified by qPCR (Kapa Biosystems) and the size distribution was assessed with Agilent 2100 Bioanalyzer (Agilent Technologies). They were sequenced by 2 x 150 bp paired-end run by either HiSeq 1500, HiSeq 2500 or NextSeq 500 (Illumina).

Imaging approach to explore genome structure in preimplantation mouse embryo

DNA FISH on preimplantation mouse embryo

MATERIALS

- 4x 3cm Petri dishes coated with 1% agarose 0.9N NaCl
- 96 well flexible plate U bottom (BD falcon)
- Pasteur pipets and mouth pipet (see Ranisavljevic et al 2017)
- Glass bottom 35 mm petri dishes (MatTek corporation #P35G-1.5-14-C)

REAGENTS

- PFA 4%
- 1X PBS 0.5% Triton X-100 1mg/ml Polyvinylpyrrolidone (PVP) = PBS TP
- First fixative :1% PFA in PBS 1X PVP
- First permeabilization:0.5% PFA; 0.4% TritonX-100 in PBS 1X PVP
- Second fixative :4% PFA; 0.5% TritonX-100 1mg/ml Polyvinylpyrrolidone (PVP)
- Second permeabilization:0.5% TritonX-100 in PBS 1X PVP
- 2X hybridization buffer (hyb 2X):20% dextran sulfate; 4X SSC; 1mM EDTA; 0.1% TritonX-100; 2mg/mlPVP; 1mg/ml BSA (pH is adjusted to 7.0 with NaOH)
- Cot1 DNA 10mg/ml
- Labelled probes (from nick translation reaction)
- Deionised formamide (FA)
- 2X and 0.2X SSC with 0.5% Triton X-100 1mg/ml Polyvinylpyrrolidone (PVP)
- Mineral oil
- Vectashield with DAPI

REAGENT SETUP

▲ CRITICAL POINT: prepare and check labelled probes before starting DNA FISH. Probes have been obtained from BACs. 1–2 µg of DNA is labelled in a 50µl reaction. Briefly, 1 µg of BAC or

plasmid DNA is mixed with water up to a volume of 17.5 µl. Add 2.5 µl of 0.2 mM SR dUTP or SG-dUTP, 10 µl of 0.1 mM each dNTP mix (dGTP, dATP, dCTP), 5 µl of 0.1 mM dTTP, 5 µl of 10× nick translation buffer, and 10 µl of nick translation enzyme. The enzymatic reaction is incubated for 16 h at 15 °C in the dark. For each hybridization reaction, approximatively 100ng of probes are precipitated with 50µg of Cot1 DNA by EtOH precipitation and subsequently resuspended in 1µl of FA. 1µl of hyb2X is added just before use.

DNA FISH probes used are listed in Appendix 1.

PROCEDURE

Embryos are collected and moved using Pasteur pipets device (see Ranisavljevic et al 2017 figure 1)

1| Embryos are collected in M2 medium after flushing the oviduct /uterus depending on the developmental stages. Zona pellucida is removed with rapid passage in Tyrod Acid

The four following steps are performed on agarose coated petri dishes to which the different solutions have been added.

2| Embryos are added in pre fixation 1 for 1min at RT

3| Embryos are added in pre permeabilization 1 for 1min at RT. During incubation, the solution is aspirate around the embryos to extract cytoplasm

4| Embryos are added in fixation 2 for 10 min (up to 20min) at RT

5| Embryos are briefly washed in PBS 1X TP

6| Embryos are added in permeabilization 2 for 1HR at 37°C

7| Embryos are briefly washed in PBS 1X TP

8| 1µl of hybridization mix 1X 50% FA and 1µl of Cot1 mix (10mg/ml in hyb 1X /50% FA) and 1µl probes mix are spotted on a glass bottom dish, and recovered with mineral oil.

9| Embryos are equilibrated in a the drop of hybridization buffer 1X / 50% FA and then moved in the Cot1 mix drop. Dishes is placed at 37°C overnight.

10| embryos and probes are denatured 10 min at 83°C

11| plate is put back at 37°C for at least two hours (competition steps)

12| embryos are moved to the drop containing the probe mix and plate is kept at 37°C overnight.

13| Washes are performed in U bottom 96 well plate: embryos are rinced in 2X SSC TP and washed twice in 0.2X SSC TP for 15 min at 45°C.

14| Embryos are mounted in Vectashield containing DAPI directly on a glass bottom dishes and used for imaging

HR-SIM acquisition - *performed by Tristan Piolot*

Images are acquired on API-GE Heathcare Lifescience V3 OMX. This system enables multicolor fluorescence acquisition and doubles lateral (xy) and axial (z) resolutions compared to widefield microscopy.

Hardware description

All images are acquired using a 100X UPLSAPO objective with a numerical aperture of 1.4. Excitation laser, coupled through a shaked multimode optical fiber, illuminates a grating mounted on a piezo held by a rotary stage. Three laser wavelengths are available (405 nm, 488 nm and 561 nm with respective power of 100 mW, 150 mW and 150 mW).

The beams of light corresponding to order -1, 0 and 1 are kept while others are blocked by a diaphragm. These three beams are injected into the objective, thus generating a 3D illumination pattern used to excite fluorescent molecules from the sample (Gustafsson, 2008).

Emission fluorescence is collected by 3 EMCCD cameras (Evolve, photometrics, https://www.photometrics.com/products/emccdcams/evolve/512.php) each one dedicated to a specific spectral band (500 nm-550nm, 570 nm-610 nm, 420nm-470nm for camera 1, 2 and 3 respectively). An additional 2X lens is added between the emission filter and the cameras. The physical pixel size on the camera is 16µmx16µm: using a 100X magnification, final pixel size on the object is 80nmx80nm.

In order to speed up image acquisition, each camera is driven by a specific PC, for image buffering. Images are collected on an additional PC also used to run the acquisition software and to drive devices required for acquisition (piezo, rotary stage, Z,X,Y motors, neutral density wheel...).

Image acquisition

For each optical slice, 15 images are acquired per channel: from 3 different angular positions (rotation in steps of 60°) and with 5 lateral translations of the excitation pattern (step of 1/5 of the diffracted pattern) for a total of 3x5=15 images per optical slice. In our configuration, in order to increase acquisition speed, the acquisition sequence is the following : for each rotary stage position, the 5 phases of each Z position are first acquired before heading to next Z. Once all Z positions are achieved for the first angle, the second and the third one are successively acquired. EMMCD are set on intensified mode using a 10Mhz converter frequency and gain is set to 300 as previously identified as the best signal

to noise ratio on these cameras. Exposure time ranges from 30 ms to 150 ms depending on sample preparation quality and fluorescence brightness. The Z step is set to 125 nm.

Beads acquisition

To test lateral and axial resolutions and for post-acquisition image alignment (crucial step in image processing owing to multi-camera acquisition), a 100 nm TetraSpeck bead preparation field is acquired before each experiment (TetraSpeck™ Microspheres, 0.1 µm, fluorescent blue/green/orange/dark red, ThermoFisher Scientific ref: T7279). 1µl of bead solution is diluted in 4µl of distilled water and spotted on a 0.16 µm-thick coverslip. After drying for 2 hours, coverslips are mounted in Vectashield (Vector Laboratories, ref: H-1000) and imaged on the OMX. Isolated beads are used for resolution evaluation while high-density bead fields are acquired for post-processing alignment purpose.

Image reconstruction and alignment

Image reconstruction is achieved using Softworx software. Wiener filter parameters are first tested on a few images to select optimal parameters for subsequent batch processing. All images with either a drift larger than subpixel or a bleaching higher than 20% are excluded from the batch and discarded. Resolution is then evaluated on bead images and subsequent realignment is achieved whenever resolution is lower than 130 nm in X,Y and 260 nm in Z.

For multichannel alignment a correction matrix is obtained from the bead images using ImageJ UnwarpJ plugin (Sorzano, 2005). This correction matrix is applied to all multichannel images acquired on the system.

Colocalization analysis

For colocalization analysis, distribution of pearson correlation coefficient in the respective intensities of red and green channels were retrieved semi-automatically using the JACOP ImageJ plugin (https://imagej.nih.gov/ij/plugins/track/jacop.html). Analysis was restricted to a region of interest of constant volume around the FISH signal. The exact size of this region was adapted for each sample.

For the OMX images, we adjusted crop size on developmental stage; same crop size was used in pool 1 and pool 2:

Cell	Size of crop (in xy and in z, pixels)
2C	60, 26
4C	56, 26
8C	50, 20
16C	40, 20
64C	40, 20
E4.5	40, 20
ESC	40, 12

The only criteria for rejecting cells from this analysis were:

- if they were in mitosis,
- If they were aneuploïd,
- if the signal was too close to image borders (in xyz),
- If the signal was over saturated.

We compared distribution of pearson correlation coefficient using Wilcoxon rank-sum statistics with R (http://www.r-project.org). In both pool 1 and pool 2, absolute values were conserved to avoid an artificial strengthening of a difference in between pool 1 and pool 2.

Macro used for analysis is enclosed in Appendix 2.

RNA DNA FISH (oligonucleotide based) on preimplantation mouse embryo

MATERIALS

- 4x 3cm Petri dishes coated with 1% agarose 0.9N NaCl
- 96 well flexible plate U bottom (BD falcon)
- Pasteur pipets and mouth pipet (see Ranisavljevic et al 2017)
- Glass bottom 35 mm petri dishes (MatTek corporation #P35G-1.5-14-C)

REAGENTS

- PFA 4%
- 1X PBS 0.5% Triton X-100 1mg/ml Polyvinylpyrrolidone (PVP) = PBS TP
- Fixative : % PFA; 0.5% TritonX-100 1mg/ml Polyvinylpyrrolidone (PVP)
- Permeabilization: 0.5% TritonX-100 in PBS 1X PVP
- 2X hybridization buffer RNA FISH(RNA hyb 2X):20% dextran sulfate; 4X SSC; 0.1% TritonX-100; 2mg/ml PVP; 1mg/ml BSA. 20mM Vanadyl ribonucleoside complex (pH is adjusted to 7.0 with NaOH)
- 2X hybridization buffer DNA FISH(DNA hyb 2X):20% dextran sulfate; 4X SSC; 1mM EDTA; 0.1% TritonX-100; 2mg/mlPVP; 1mg/ml BSA (pH is adjusted to 7.0 with NaOH)
- Cot1 DNA 10mg/ml
- Labelled probes (from nick translation reaction)
- Deionised formamide (FA)
- 2X SSC with 0.5% Triton X-100 1mg/ml Polyvinylpyrrolidone (PVP)
- Mineral oil
- Vectashield with DAPI

REAGENT SETUP - For p510 (Xist) probe

▲ CRITICAL POINT: prepare and check labelled probes before starting FISH. Probes have been obtained from fosmid. 1–2 µg of DNA is labelled in a 50µl reaction. Briefly, 1 µg of BAC or plasmid DNA is mixed with water up to a volume of 17.5 µl. Add 2.5 µl of 0.2 mM Cy5 dUTP, 10 µl of 0.1 mM each dNTP mix (dGTP, dATP, dCTP), 5 µl of 0.1 mM dTTP, 5 µl of 10× nick translation buffer, and 10 µl of nick translation enzyme. The enzymatic reaction is incubated for 16 h at 15 °C

in the dark. For each hybridization reaction, approximatively 100ng of probes are precipitated with 50µg of Cot1 DNA by EtOH precipitation and subsequently resuspended in 1µl of FA. 1µl of hyb2X is added just before use.

DNA FISH oligo-probes. In experiments to detect the mega-domain boundary, fluorescent oligonucleotides (average length 45 bp, 5'-modified with Atto 448 or Atto 550, average density: one oligonucleotide every 3 kb) were obtained from MYcroarray Inc. Oligonucleotides were designed to tile the following consecutive 18-Mb regions: chrX:35,000,000–53,000,000 (termed "probes a") and chrX:53,000,000– 72,000,000 (termed "probes b").

PROCEDURE

Embryos are collected and moved using Pasteur pipets device (see Ranisavljevic et al 2017 figure 1)

1| Embryos are collected in M2 medium after flushing the oviduct /uterus depending on the developmental stages. Zona pellucida is removed with rapid passage in Tyrod Acid

The four following steps are performed on agarose coated petri dishes to which the different solutions have been added.

2| Embryos are added in fixation for 30min at RT

3| Embryos are added in permeabilization for 15 min at RT.

4| Embryos are briefly washed in PBS 1X TP

5| 1µl of RNA hybridization mix 1X 50% FA and 1µl probes mix for RNA FISH (this has been denature for 7 min at 75°C and kept on ice shortly before) are spotted on a glass bottom dish, and recovered with mineral oil.

7| Embryos are equilibrated in a drop of hybridization buffer 1X/50% FA and then moved in the RNA probe mix drop. The dish is placed at 37°C overnight.

8| Washes are performed in U bottom 96 well plate: embryos are rinsed in 2X SSC TP and washed 3 times in 2X SSC TP for 5 min at 42°C.

9| Embryos are post fixed in 4% PFA for 10 min at RT

10| Embryos are briefly washed in PBS 1X TP

11| 1µl of DNA hybridization mix 1X 10% FA and 1µl oligo probes mix (10% FA final) are spotted on a glass bottom dish, and recovered with mineral oil.

12| Embryos are equilibrated in a drop of hybridization buffer 1X / 10% FA and then moved in the oligo probe mix drop.

13| embryos and probes are denatured 10 min at 83°C and placed back at 37°C for overnight incubation.

14| Washes are performed in U bottom 96 well plate: embryos are rinsed in 2X SSC TP and washed twice in 2X SSC TP for 10 min at 45°C.

9| Embryos are mounted in Vectashield containing DAPI directly on a glass bottom dishes and used for imaging

Imaging approach to explore zygotic genome activation in preimplantation mouse embryo

METHOD ARTICLE - RNA FISH TO STUDY ZYGOTIC GENOME ACTIVATION IN EARLY MOUSE EMBRYOS

Chapter 9

RNA FISH to Study Zygotic Genome Activation in Early Mouse Embryos

Noémie Ranisavljevic, Ikuhiro Okamoto, Edith Heard, and Katia Ancelin

Abstract

Characterizing the maternal-to-zygotic transition (MZT) is a central question in embryogenesis, and is critical for our understanding of early post-fertilization events in mammals. High-throughput RNA sequencing (RNA Seq) of mouse oocytes and early embryos has recently revealed that elaborate transcription patterns of genes and repeats are established post-fertilization. This occurs in the context of the gradually depleted maternal pool of RNA provided by the oocyte, which can confound the accurate analysis of the zygotic genome activation when the mRNA population is sequenced. In this context, and given the limited amounts of material available from embryos, particularly when studying mutants, as well as the cost of sequencing, an alternative, complementary single cell approach is RNA FISH. This approach can assay the expression of specific genes or genetic elements during preimplantation development, in particular during the MZT. Here, we describe how RNA FISH can be applied to visualize nascent transcription at specific genomic loci in embryos at different stages of preimplantation development and also discuss possible analytical methods of RNA FISH data.

Key words RNA FISH, Nascent transcripts, Mouse preimplantation development, Maternal-to-zygotic transition

1 Introduction

Fertilization of an oocyte by a sperm embarks the two highly differentiated parental genomes into a major epigenetic remodeling process and launches the formation of a totipotent zygote. In animals, oocytes are supplied with proteins and RNAs, designated as the maternal pool that ensures the very first stages of development. Zygotic products gradually replace this preloaded maternal material through transcriptional activation, known as zygotic genome activation (ZGA).

The maternal-to-zygotic transition (MZT) is crucial for developmental progression after fertilization [1] and its characterization is a central question in early embryogenesis. In mammals, this massive shift in the transcriptional program is achieved at different times after

Kiho Lee (ed.), *Zygotic Genome Activation: Methods and Protocols*, Methods in Molecular Biology, vol. 1605,
DOI 10.1007/978-1-4939-6988-3_9,

fertilization, from as early as the 2-cell stage (mouse), or later at the 8-cell stage (cow, human). This has been analyzed by microarray or RNA-seq analyses [2–6]. Notably in mouse embryos, a fine choreography of gene expression patterns is established post-fertilization, between the inherited maternal pool of RNA, the first wave of ZGA (also called minor ZGA), at the 1-cell stage, and then the second wave of ZGA (also called major ZGA), at the 2-cell stage [4].

One challenge for our understanding of the mechanisms underlying this complex series of important events has been to try to define the maternal factors that are pivotal during the MZT. In particular, the factors that unravel the specialized chromatin states of the differentiated gametes to a totipotent zygote, and those that underlie zygotic genome activation still remain largely unknown. Indeed, due to the sparse availability of material for biochemical approaches, the involvement at the molecular level of chromatin factors on gene expression dynamic in vivo during early development is under-investigated.

In recent years, genetic approaches have been developed that can specifically assess the role of maternal factors during female germline formation as well as during preimplantation development [7]. These tools are based on the induction of gene deletion (conditional knock-out) during oocyte growth, which can thus eliminate the RNA and protein products of the gene in question in the oocyte and in the early preimplantation embryo after fertilization. Thanks to such approaches, using conditional knock-out mouse models, several studies have at last started to define the key roles that certain chromatin factors play during early development and in particular in the critical steps of MZT and the first cleavage stages [8–10]. We recently used a maternal deletion of KDM1A (LSD1), a master regulator of histone methylation, to reveal its critical role in establishing the correct chromatin landscape upon fertilization and in initiating new patterns of genome expression in early mouse development [10].

In such a study, the use of a combination of RNA sequencing and RNA FISH was very powerful for assessing the impact of loss of this factor on ZGA in particular. RNA seq was used to analyze steady-state levels of mRNA pools (maternal, 1-cell stage; 2-cell stage), while RNA FISH could assess the de novo (active) transcription of genes and specific repeat elements through the visualization of nascent transcripts, at the single cell level. RNA FISH is also useful at the maternal-to-zygotic transition to discriminate between the absence of degradation of maternal RNAs and aberrant active transcription at later stage. When fluorescently labeled probes (DNA or RNA) are hybridized to fixed and permeabilized embryos that have not been denatured, then single-stranded RNA rather than double-stranded DNA can be detected. This technique can be applied to study the expression of specific genes as well as the repetitive fraction of the genome, such as LINEs or pericentromeric satellite sequences [10–14].

In this chapter, we outline RNA FISH methods applied to preimplantation mouse embryos, which might also be a starting point for optimization for oocytes stages. We present in particular (a) how embryos are fixed, permeabilized, and placed on coverslips; (b) the RNA FISH procedure and imaging using these coverslips. It should be noted that embryos analyzed by RNA FISH can subsequently be analyzed by DNA FISH, following denaturation [11]. The RNA FISH procedure can also be combined with immunofluorescence (for a protocol on fixed cells, *see* [15, 16]).

2 Materials

2.1 Preimplantation Embryo Isolation and Manipulation

1. Petri dish 10 mm × 35, sterile.
2. Tweezers for dissection (fine stainless steel Dumont #5).
3. Scissors (fine, stainless steel, dissection).
4. Dissection binocular with 100× magnification.
5. Pasteur pipette: pulled the thin extremity as shown in Fig. 1; will be referred to as transfer pipette.
6. Aspirator tube assemblies (Fig. 1).
7. M2 medium for embryo (Sigma).
8. Tyrod Acid.

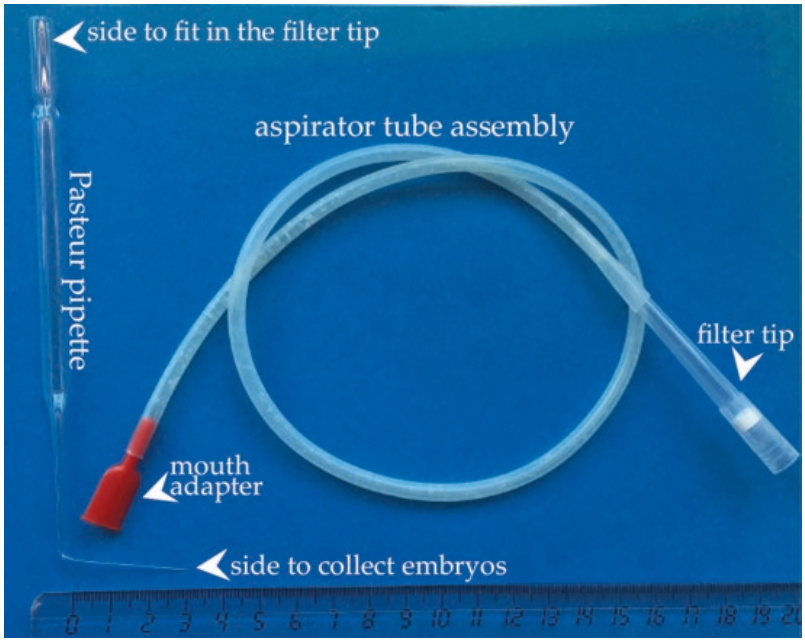

Fig. 1 Equipment setup for the mouth device used for handling by slightly suctions the mouse 2-cell stage embryos. An aspirator tube assembly as shown in the center is connected by the filter tip to a modified Pasteur pipette. The Pasteur pipette (on the *left*) is drawn to a diameter of ~100 μm with an angle to the rest of the pipette. Numbers on the ruler are indicated in centimeter

9. Coverslips (18 mm diameter, 1.5 mm thickness; borosilicate glass; Marienfield).
10. 6-well tissue culture plates.
11. Liquiport Liquid pump.

2.2 RNA FISH

1. Coating solution for coverslip: 3× SSC, 0.2 mg/ml BSA, 0.2 mg/ml Ficoll-400, 0.2 mg/ml Polyvinylpyrrolidone 40 (PVP40).
2. Tri-ethanolamine solution: 0.0025% Glacial acetic acid, 0.013% TE.
3. Methanol/glacial acetic acid (v/v) 3:1.
4. Fixation solution: 3% paraformaldehyde in PBS (freshly prepared, pH adjusted).
5. Permeabilization solution: 0.5% Triton X-100 in 1× PBS supplemented with 2-mM vanadyl ribonucleoside complex (VRC).
6. 70, 80, 95% ethanol in double-processed tissue-culture water; 100% ethanol.
7. Nick translation kit (Abbott) containing nick translation enzyme, dNTP solutions, and 10× nick translation buffer.
8. Green-dUTP or Orange-dUTP (Enzo) or Cyanine 5-dUTP (Roche).
9. Formamide (FA; Sigma). Upon opening, aliquot immediately and keep at −20 °C.
10. Mouse Cot-1 DNA (Life Technologies, ThermoFisher Scientific).
11. DNA, molecular biology grade from fish sperm (Roche).
12. 3 M sodium acetate pH 5.2.
13. 20× SSC buffer concentrate.
14. 2× Hybridization buffer: 20%, dextran sulfate, 2 mg/ml BSA (NEB), 20 mM VRC; 4× SSC.
15. Post-hybridization wash buffer: freshly prepared 50% formamide/2× SSC pH 7.2–7.4.
16. DNA counterstaining solution: 4′,6-diamidino-2-phenylindodihydrochloride (DAPI) in 2× SSC at 1 μg/ml.
17. Mounting solution: 90% v/v glycerol, 0.1% (w/v) *p*-phenylenediamine (Sigma), pH 9 in PBS; or else non-hardening Vectashield (Vector Laboratories) with DAPI.
18. 6-well tissue culture plates.
19. Fine wiper tissues (e.g., Kimwipes).
20. Dark chamber light tight plastic, capable of holding microscope slides (*see* Fig. 2).

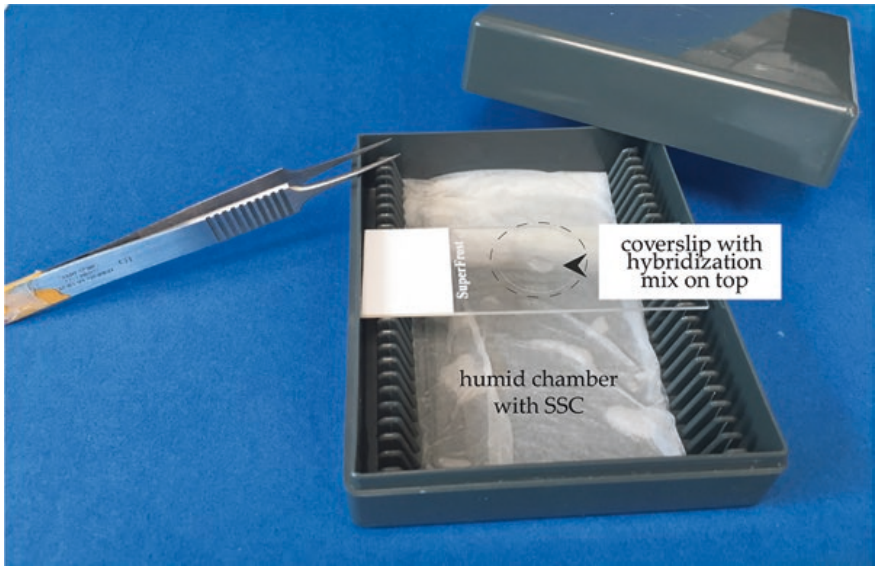

Fig. 2 Equipment setup for the hybridization incubation. A slide holder is used to create a humid chamber where the slides are positioned to hold the coverslips with the attached embryos facing up. Coverslips can be recovered from the slide using fine forceps

21. Microscope slides (always use gloves to handle them out of the package and through the procedure).
22. Nail varnish for sealing.
23. Eppendorf Centrifuge 5417R.
24. Eppendorf Concentrator plus.
25. Eppendorf Thermomixer comfort.
26. Liquiport Liquid pump.
27. Shake'N'Bake Hybridization Oven.

2.3 Microscopy and Image Analysis

1. Inverted confocal microscope (Zeiss LSM700).
2. Plan apo DICII (numerical aperture 1.4) 63× oil immersion objective.
3. ImageJ software.

3 Methods

The following methods described here were adapted from [12, 15]. Our study focused on mouse 2-cell stage embryos [10], but they can be applied to any preimplantation stages from zygote to 3.5 days *post-coïtum* (early blastocyst) embryos, provided some adjustments, such as the time of embryo collection, or the permeabilization conditions (see details below). We recommend that RNA FISH is started on the day of embryo recovery, as soon as possible after fixation of embryos on coverslips, to minimize the risk of RNA degradation (*see* **Notes** 1–**3**). Conditions should be RNAse free throughout.

3.1 Preparation and Fixation of Mouse 2-Cell Stage Embryos on Coverslips

Affixing embryos to coverslip facilitates their subsequent processing through the different steps of our procedure.

3.1.1 Coverslip Coating and Attaching Embryos to Glass Coverslips

1. The coverslips used for preimplantation embryo analyses are treated by three successive incubations in the following solutions to allow the embryo to stay fixed and partially dehydrated: first treat coverlips in coating solution 3 h at 65 °C, second methanol/glacial acetic acid solution for 20 min at room temperature, and finally in tri-ethanolamine solution for 10 min at room temperature. Each coverslip is rinsed twice with distilled water, then twice with 100% ethanol. Coverslips are dried on a Kimwipe at room temperature and stock at room temperature in a closed tube (*see* **Note 4**).
2. Embryos are collected in M2 medium as described [17], using a mouth aspirator device connected to a transfer pipette (*see* Fig. 1). After the removal of the *Zona pellucida* with tyrode acid, embryos are rinsed in the M2 medium.
3. Using a transfer pipette, embryos are quickly moved into a 0.5 µl drop of PBS 1× placed at the center of a coated coverslip (around five embryos per coverslip; see the previous section). Using the transfer pipette, liquid is carefully removed around the embryos. Blastomeres will spread out, but should not be destroyed. Good attachment will occur only if PBS does not contain proteins such as BSA or serum.
4. The coverslips should be dried for 30 min at room temperature, after placing them into a 6-well plate (one per well).

3.1.2 Fixation and Permeabilization

1. In the following steps, we routinely work with the coverslips in the 6-well plate, using 2 ml per well for each solution. Replacement of solutions is done always removing liquid (without touching the coverslip) by rapid aspiration (using Liquiport Liquid pump) and rapidly, but gently replacing the solution (with a 10 ml pipette for example) to prevent the coverslips from drying.
2. Embryos on coverslips are fixed with 3% paraformaldehyde in 1× PBS for 10 min at room temperature.
3. Coverslips are washed twice with 1× PBS.
4. Embryos are permeabilized for 1 min on ice with ice-cold 0.5% Triton X-100, 2 mM vanadyl-ribonucleoside complex in PBS. The length of treatment of the coverslips with the permeabilization solution is critical and is dependent on the developmental stage, e.g., 2 min for zygotes, and 2-cell stage; 8 min for 8-cell stage, 15 min for blastocyst stage (*see* **Note 5**).
5. In order to test the specificity of a probe for nascent transcripts (and not DNA in case of partial recognition with the DNA probes), we recommend incubation of one coverslip with

RNAse A as a control. Incubation can be done in PBS 1× with RNAse A (40 µg/ml final) at 37 °C for 15 min; after the permeabilization and prior to dehydration.

6. The permeabilization solution is replaced by ice-cold 70% ethanol, and the coverslips can then be stored at −20 °C, until the hybridization mix preparation is ready. Ideally, they should be processed within the same day, but can be kept overnight.

3.2 Generating and Labeling Probes for RNA FISH by Nick Translation

The design of the probes needs to cover introns and exons for specific genes to detect the nascent transcripts (as a punctuate signal at the genomic locus). The use of cDNA probes is not recommended as this will largely detect mRNA and not nascent transcripts. Several strategies are currently available to generate FISH probes that enable efficient visualization of nascent transcripts that are based on genomic probes that are several kilobase pairs long, or plasmid probes or else labeled oligos [16, 18–20]. The procedure we describe here relies on generating fluorescently labeled DNA probes by nick translation on BAC or plasmid DNA, using fluorescent dUTPs (Spectrum Green SG, Spectrum Red SR) to label genomic probes (plasmids, fosmids, or BACs). 1–2 µg of DNA is labeled in a 50 µl reaction.

1. 1 µg of BAC or plasmid DNA is mixed with water up to a volume of 17.5 µl. Add 2.5 µl of 0.2 mM SR dUTP or SG-dUTP, 10 µl of 0.1 mM each dNTP mix (dGTP, dATP, dCTP), 5 µl of 0.1 mM dTTP, 5 µl of 10× nick translation buffer, and 10 µl of nick translation enzyme.
2. The enzymatic reaction is incubated for 16 h at 15 °C in the dark (*see* **Notes 6** and **7**).
3. The reaction is inactivated by freezing at −20 °C. Probes can be stored for up to 6 months at −20 °C.

3.3 RNA FISH Procedure on 2-Cell Stage Embryos

3.3.1 Probe Mix Preparation

1. 200 ng (per coverslip) of each probe to be used is precipitated by adding 10 µg salmon sperm DNA (as carrier), 1/10 volume 3 M sodium acetate pH 5.2, and 3 volumes of 100% ethanol; and spun at 4 °C, 16,100 × *g* for 30 min. In order to ensure probe specificity, Cot-1 DNA competition is required for most probes based on fosmid or BACs as they can contain repeat sequences that will cross hybridize and increase background unless competed away prior to hybridization. It is often not the case for probes based on plasmid (if they do not contain repetitive elements) and it is also often not the case if the aim is to assess specifically the expression level of repetitive fraction of the genome (e.g., LINEs, SINEs, Satellite sequences). Cot-1 DNA should be added at this stage in the precipitation mix (*see* [16, 21], **Note 8**).
2. The pellet is washed in 70% ethanol and spun down at 16,100 × *g* and 4 °C for 5 min.

3. The pellet is dried for 1 min in a concentrator/speed vacuum.
4. The pellet is resuspended in an appropriate volume of formamide (half the volume required for hybridization if final % is 50% FA). For example, for 5 µl hybridization mix the pellet needs to be dissolved in a 2.5 µl of FA.
5. The tube is placed in a heat block preferably with shaking for at least 15 min at 37 °C to dissolve the pellet in FA.
6. The probe is denatured for 10 min at 75 °C by placing the tube in a thermomixer.
7. After denaturation, the tube is rapidly transferred to ice, or if competition is to be performed with Cot-1 DNA, put directly at 37 °C for at least 1 h in a thermomixer.
8. An equal volume of 2× hybridization buffer (ideally freshly prepared or else a fresh aliquot from −20 °C) is added to the probe mix, according to the amount of FA used in the previous step (*see* **Note 9**).

3.3.2 Hybridization

1. Coverslips with embryos (in a 6-well plate) are dehydrated by sequential incubation in 80, 95, and 100% ethanol (this last step is repeated twice) for 5 min each at room temperature.
2. Coverslips are then air dried by being placed on fine tissues (Kimwipes). Remember the embryo side should always be facing up.
3. During the air-drying step for coverslips, the hybridization chamber is prepared with tissue soaked in FA/2× SSC (*see* Fig. 2). A drop of water is spotted on a clean slide, in order to receive the coverslip (with the *embryo side still facing up*) (*see* **Note 10**).
4. Hybridization: 5 µl probe hybridization mix containing the probe (*see* **step 8** in subheading 3.3.1) is spotted, just on the side of the dried embryos, carefully monitoring this step under the binocular to place it as close as possible of the embryos, avoiding bubbles.
5. The humid chamber containing the slides and coverslips is covered and placed at 37 °C overnight (*see* **Note 11**).

3.3.3 Post-hybridization Washes

1. The following day, 1 ml of pre-warmed, freshly prepared 50%FA/2× SSC is added onto the coverslip on the slide to loosen it, and to allow removing it carefully from the slide. It is then placed (with embryos facing upward), into a 6-well plate containing pre-warmed 50%FA/2× SSC (2 ml/well) at 42 °C for 7 min.
2. Washes in 2× SSC are repeated twice at 42 °C for 5 min (*see* **Note 12**).
3. Nuclei are counterstained by washing in 2× SSC with DAPI (1 µg/ml) for 5 min at 42 °C.

4. Coverslips are then rinsed three times with 2× SSC at room temperature.
5. 10 µl mounting medium is spotted onto a glass slide and the coverslip is placed on the top of the drop with embryos facing down, avoiding bubbles. Excess mounting medium can be carefully removed with a fine tissue, without moving the coverslip. The coverslip is sealed on the slide with a minimal amount of nail polish.
6. Slides should ideally be imaged immediately, as signal can sometimes fade quickly but can also be stored at −20 °C until imaging, or at −80 °C for longer storage.

3.4 Image Acquisition and Analysis

3.4.1 Microscopy

In the examples we show in Fig. 3, we imaged the embryos following RNA FISH with an inverted confocal microscope Zeiss (Germany) LSM700 with a Plan apo DICII (numerical aperture 1.4) 63× oil objective, and Z sections were taken every 0.4 µm. It is critical to have used the correct coverslip thickness and the correct oil adapted to the lens to obtain correct images.

3.4.2 Analysis

Depending on the target for the hybridization (i.e., a specific gene or else specific repetitive elements), the pattern of hybridization will be different, as displayed in Fig. 3b. For a unique gene (Fig. 3a), one can expect two pinpoints for each allele of an autosomal gene in a diploid cell (if the two alleles are both expressed). For X chromosome one or two alleles can be detected depending on sex or also the expression status of the X chromosome [12]. When testing a new probe it is important to compare it to a previously tested probe, and if possible to test it on cultured cells [16, 21] in which the gene is known to be expressed to ensure the good detection of the nascent transcript. Finally, a critical point in RNA FISH is that, in case of suboptimal RNA FISH conditions or probes, fewer cells with a signal may be detected, leading to an underestimation of the degree to which a gene is expressed. In the case of mono versus biallelic expression, this can be critical as one can conclude monoallelic expression when in fact it is biallelic.

After fertilization, embryos from a same female might not be at the same stage of the cell cycle. Depending on whether they have passed S phase or not, and the degree to which the sister chromatids are separated, the signal corresponding to the nascent transcript can be seen as a singlet or a doublet (*see* Fig. 3a lower signal) corresponding to transcription of well-separated sister chromatids.

In Fig. 3b an example of hybridization following hybridization to repetitive elements such as LINE-1 (a retrotransposon family) is shown. In this case, the pattern is more complex as it is associated with many different pinpoints of different intensities reflecting the many sites of ongoing transcription. A treatment with the RNAse A,

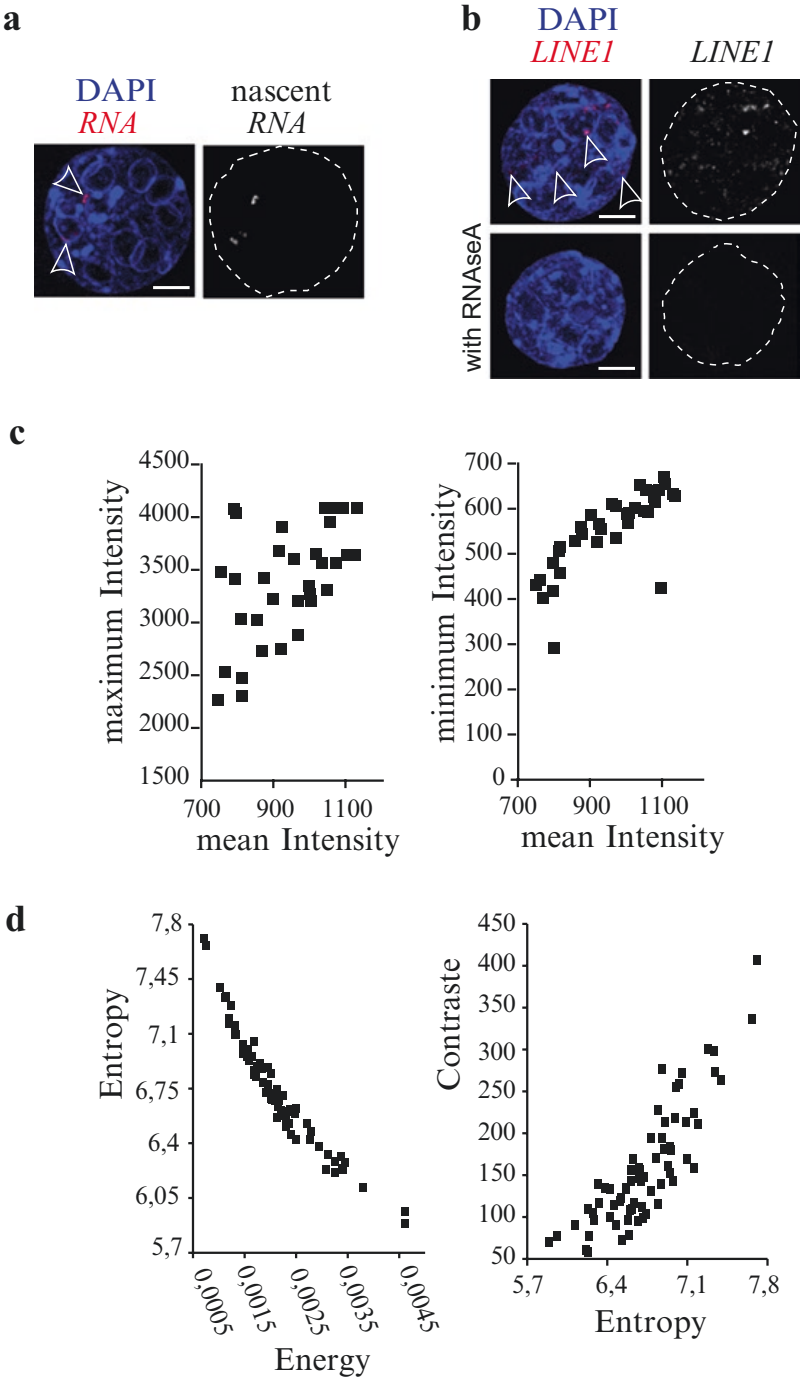

Fig. 3 Examples of RNA FISH and analysis performed on mouse 2-cell stage embryos (reproduced by permission of eLife Sciences Publications). (**a**) A nucleus showing the DNA probe hybridized (in *red*) to a single loci on the X chromosome (from a female embryo). The nascent transcripts arising from these two spots can be seen. (**b**) A nucleus showing plasmid probes hybridizing to repetitive elements *LINE1* transcripts (*top*) and a nucleus after RNAse A treatment using the same probe (*bottom*). The DNA is counterstained with DAPI. Scale is 10 μm. (**c**) Scatter plots showing the distribution according to the fluorescence intensity measurement of nuclei as the one shown in (**b**). Criteria such as maximum or minimum intensity values can be used to discriminate the hybridization results from one nucleus to another (or from one embryo to another). (**d**) Scatter plots showing analysis of hybridization results according to the pattern/texture of the obtained image such as in (**b**). Examples in (**c**) and (**d**) indicate means to analyze complex patterns of RNA FISH results such as in (**b**), rather than in (**a**)

prior to the hybridization, attests for the probe specificity and the RNA nature of the signal. When such complex patterns are to be analyzed, one alternative is to study fluorescent intensities within each nucleus of every embryo as displayed in Fig. 3c or else the fluorescence arrangement as shown in Fig. 3d.

1. Images are opened in Image J software.
2. For fluorescence intensity measurements, the 3D object counter plugin can be used [22].
3. For fluorescence arrangement analysis, we used a custom-made ImageJ macro [10] based on descriptors defined as [23] that quantitatively study the texture and structure of images.

4 Notes

1. Wear gloves throughout the whole procedure, from drying the embryos onto coverslips up to the hybridization step of the RNA FISH procedure. This is critical to minimize risk of RNases contamination.
2. Use clean sterile forceps for handling coverslips, and process them either in Petri dishes or in 6-well plates.
3. All solutions are prepared with double-processed (i.e., distilled and sterile) tissue culture water in RNase-free conditions (although no specific treatment to eliminate RNAses needs to be used).
4. Prepare the coating solution for coverslips receiving embryos the night before the preparation of the coverslips or autoclave it and store at 4 °C for 6 months. Always transfer coverslips one by one from one solution to another. Use 50 ml Falcon tubes for each solution. Coverslips can be stored at room temperature up to 4 months.
5. Permeabilization solution must be prepared fresh every time and kept on ice before collecting the preimplantation embryos.
6. Following nick translation reaction, the size range of the labeled DNA is always checked by electrophoresis on an agarose gel (1.8%). The optimal range size of a FISH probe is between 50 and 300 base pairs, short enough to enter the nucleus and long enough to be specific. Larger size fragments will not be able to enter the nucleus efficiently. Note that the efficiency of incorporation is specific for each nucleotide conjugated to a fluorophore and needs to be tested.
7. Test run should be performed on culture cells that are known to express the gene targeted for RNA FISH to test the quality of new probes. Ideally, one should always test new sets of probes along with probes for which the hybridization pattern is known.

8. Cot1 DNA: competition is required for most probes as they can contain repeat sequences that will cross hybridize and increase background, unless competed away prior to hybridization. We routinely use between 2 and 5 μg of Cot1 DNA per 5 μl of nick translation mix/per probe type.
9. We recommend preparation of small aliquots of hybridization buffer (about 50 μl and kept at −20 °C), and using each of them two to three times only. A final volume of 5 μl hybridization mix/coverslip is ideal for overnight incubation.
10. The chamber, once closed, should protect the hybridization from light (*see* material in Fig. 2 or else use foil to cover the box).
11. Hybridization temperature: 37 °C is a routinely used temperature in our conditions. But higher temperature (up to 45 °C) can also give good results, depending on the probe.
12. If stringency of detection needs to be increased, additional washes with lower concentration in SSC can be performed (down to 0.2× SSC).

Acknowledgments

Research in the Heard lab is supported by "La Ligue Contre Le Cancer"; by an ERC Advanced Investigator award (ERC-2014-AdG no. 671027); Labex DEEP ANR-11-LBX-0044.

References

1. Flach G, Hjohnson M, Braude PR, Taylor RAS, Bolton VN (1982) The transition from maternal to embryonic control in the 2-cell mouse embryo. EMBO J 1:681–686
2. Hamatani T, Carter MG, Sharov AA, Ko MSH (2004) Dynamics of global gene expression changes during mouse preimplantation development. Dev Cell 6:117–131. doi:10.1016/S1534-5807(03)00373-3
3. Wang QT, Piotrowska K, Ciemerych MA, Milenkovic L, Scott MP, Davis RW, Zernicka-Goetz M (2004) A genome-wide study of gene activity reveals developmental signaling pathways in the preimplantation mouse embryo. Dev Cell 1:133–144
4. Park S-J, Komata M, Inoue F, Yamada K, Nakai K, Ohsugi M, Shirahige K (2013) Inferring the choreography of parental genomes during fertilization from ultralarge-scale whole-transcriptome analysis. Genes Dev 27:2736–2748. doi:10.1101/gad.227926.113
5. Dufort I, Robert C, Sirard MA (2015) Studying bovine early embryo transcriptome by microarray. Methods Mol Biol 1222:197–208. doi:10.1007/978-1-4939-1594-1_15
6. Petropoulos S, Edsgärd D, Reinius B, Deng Q, Panula SP, Codeluppi S, Plaza Reyes A, Linnarsson S, Sandberg R, Lanner F (2016) Single-cell RNA-seq reveals lineage and X chromosome dynamics in human preimplantation embryos. Cell 165:1012–1026. doi:10.1016/j.cell.2016.03.023
7. De Vries WN, Binns LT, Fancher KS, Dean J, Moore R, Kemler R, Knowles BB (2000) Expression of Cre recombinase in mouse oocytes: a means to study maternal effect genes. Genesis 26:110–112
8. Bultman SJ, Gebuhr TC, Pan H, Svoboda P, Schultz RM, Magnuson T (2006) Maternal BRG1 regulates zygotic genome activation in the mouse. Genes Dev 20:1744–1754. doi:10.1101/gad.1435106

9. Andreu-Vieyra CV, Chen R, Agno JE, Glaser S, Anastassiadis K, Stewart AF, Matzuk MM (2010) MLL2 is required in oocytes for bulk histone 3 lysine 4 trimethylation and transcriptional silencing. PLoS Biol 8:e1000453. doi:10.1371/journal.pbio.1000453
10. Ancelin K, Syx L, Borensztein M, Ranisavljevic N, Vassilev I, Briseño-Roa L, Liu T, Metzger E, Servant N, Barillot E, Chen C-J, Schüle R, Heard E (2016) Maternal LSD1/KDM1A is an essential regulator of chromatin and transcription landscapes during zygotic genome activation. Elife 5. pii: e08851. doi: 10.7554/eLife.08851.
11. Okamoto I, Arnaud D, Le Baccon P, Otte AP, Disteche CM, Avner P, Heard E (2005) Evidence for de novo imprinted X-chromosome inactivation independent of meiotic inactivation in mice. Nature 438:369–373. doi:10.1038/nature04155
12. Patrat C, Okamoto I, Diabangouaya P, Vialon V, Le Baccon P, Chow J, Heard E (2009) Dynamic changes in paternal X-chromosome activity during imprinted X-chromosome inactivation in mice. Proc Natl Acad Sci U S A 106:5198–5203. doi:10.1073/pnas.0810683106
13. Probst AV, Okamoto I, Casanova M, El Marjou F, Le Baccon P, Almouzni G (2010) A strand-specific burst in transcription of pericentric satellites is required for chromocenter formation and early mouse development. Dev Cell 19:625–638. doi:10.1007/s00412-007-0106-8
14. Fadloun A, Le Gras S, Jost B, Ziegler-Birling C, Takahashi H, Gorab E, Carminci P, Torres-Padilla M-E (2013) Chromatin signatures and retrotransposon profiling in mouse embryos reveal regulation of LINE-1 by RNA. Nat Struct and Mol Biol 20:332–338. doi:10.1038/nsmb.2495
15. Okamoto I, Otte AP, Allis CD, Reinberg D, Heard E (2004) Epigenetic dynamics of imprinted X inactivation during early mouse development. Science 303:644–649. doi:10.1126/science.1092727
16. Chaumeil J, Okamoto I, Heard E (2004) X-chromosome inactivation in mouse embryonic stem cells: analysis of histone modifications and transcriptional activity using immunofluorescence and FISH. Methods Enzymol 376:405–419. doi:10.1016/S0076-6879(03)76027-3
17. Hogan BL, Beddington R, Costantini F, Facy E (1994) Manipulating the mouse embryo. Cold Spring Harbor Laboratory Press, New York, NY
18. Giorgetti L, Piolot T, Heard E (2015) High-resolution 3D DNA FISH using plasmid probes and computational correction of optical aberrations to study chromatin structure at the submegabase scale. Methods Mol Biol 1262:37–53. doi:10.1007/978-1-4939-2253-6_3
19. Lai LT, Meng Z, Shao F, Zhang LF (2016) Simultaneous RNA-DNA FISH. Methods Mol Biol 1402:135–145. doi:10.1007/978-1-4939-3378-5_11
20. Orjalo AV Jr, Johansson HE (2016) Stellaris® RNA fluorescence in situ hybridization for the simultaneous detection of immature and mature long noncoding RNAs in adherent cells. Methods Mol Biol 1402:119–134. doi:10.1007/978-1-4939-3378-5_10
21. Pollex T, Piolot T, Heard E (2013) Live-cell imaging combined with immunofluorescence, RNA, or DNA FISH to study the nuclear dynamics and expression of the X-inactivation center. Methods Mol Biol 1042:13–31. doi:10.1007/978-1-62703-526-2_2
22. Bolte S, Cordelières FP (2006) A guided tour into subcellular colocalization analysis in light-microscopy. J Microsc 224(Pt 3):213–232
23. Haralick RM (1979) Statistical and structural approaches to texture. Proc IEEE 67:786–804. doi:10.1109/PROC.1979.11328

DISCUSSION AND PERSPECTIVES

During my PhD, my goal was to try to decipher genome organization in mouse preimplantation embryo, combining two complementary approaches: super resolution imaging and single-cell HiC. In this thesis, I have presented our efforts to describe and understand the highly dynamic process of architectural reprogramming of maternal and paternal genomes during the first stage of life.

We particularly devoted our attention to the asymmetrical aspect of this remodelling in early development. The quality of our allelic datasets throughout this preliminary analysis seems to be promising. It will enable us to explore in more detail genome features through cell cycle phasing or 3D modelling, which are powerful tools requiring single-cell datasets.

We also revealed the important modifications in Xp structure occurring during imprinted XCI in mouse early development.

In this final chapter, I will elaborate more extensively on our findings, and on the numerous questions that we addressed and are still pending further analysis. I will first comment on genome-wide structure, from chromosome territories to TADs and then present some final considerations regarding imprinted Xi structure.

Chromosome territories: 3D models and CT dynamics in early embryo

A recent publication concluded that chromosome territories may be inferred from a single-cell dataset (Stevens et al., 2017). We have also successfully modelled chromosome territories in our embryonic single-cell datasets in an allele-specific fashion (unshown data). We thus have in hand a robust tool to explore the dynamics of chromosome territories (CT) in early embryo. We may speculate that spatial chromosome distribution in a very large nucleus such as in 1C or 2C stage embryos is much less constrained compared to their allocation in a smaller nucleus later during development, at blastocyst stage for instance. It is possible that chromosomes need to condense and to organize more precisely as nucleus size decreases at each cleavage during preimplantation development and also as transcription regulation and genome organization are progressively established.

In our data, we have observed an increased frequency of trans-contacts in 2C stage blastomeres. We might hypothesize that this could be due to a more relaxed or elongated shape of chromosome territories and explore through 3D modelling the dynamics of CT establishment during development. We have also shown, like others (Du et al., 2017) that parental genomes are initially separated in space and progressively intermingle through development. Are homologous chromosomes similarly apart in the nucleus in early embryo? When do they start “clustering” in the same neighborhood as CT? Are there some preferential chromosomes that initiate the parental intermingling?

Chromosomal positioning has been studied in early bovine development (Koehler et al., 2009, Orsztynowicz et al., 2017) but remains unexplored in mouse embryo. When does radial rearrangement take place translocating gene-rich chromosome internally and gene-poor chromosome at the nuclear periphery? Is it concomitant with ZGA? Is it linked to gene expression patterns? Furthermore, X-chromosomes have been reported to lie apart in female mouse embryo as imprinted XCI proceeds with the Xp frequently localized around the nucleolus unlike the Xm (Namekawa et al., 2010). How are X-chromosomes positioned in the nucleus during imprinted XCI? Do they behave differently from other chromosomes in early embryo development? Is the Xp localization correlated with its silencing status?

We hope to address these questions thanks to 3D modelling of our allele-specific single-cell datasets.

A/B compartment formation:

Compartment partitioning during early development has been suggested to appear progressively, with a poor segregation in maternal zygotic genome compared to its paternal counterpart (Flyamer et al., 2017, Du et al., 2017, Ke et al., 2017). Compartmentalization of the genome seems to correlate well with chromatin accessibility, DNA methylation, H3K4me3, HE3K27me3 and gene expression (Du et al., 2017, Ke et al., 2017).

Analysis is ongoing with regards to A/B compartments in our datasets. We wonder if parental genome intermingling is initiated preferentially and specifically in A or B compartment.

TADs: what underlies the kinetics of TAD establishment during early embryo development?

Our data are in agreement with recent publications stressing progressive establishment of TAD structure (Du et al., 2017, Ke et al., 2017). We will obviously compare our data to the recently published data in mouse oocytes and early embryos (Flyamer et al., 2017, Du et al., 2017, Ke et al., 2017) and reanalyze their datasets with our analysis pipelines.

Nonetheless, substantial TAD dynamics still requires more investigation. We question which TADs are the first to appear. Is order of appearance correlated or independent of early transcription events in the zygote? We aim to align our scHiC datasets to RNAseq datasets obtained from identical F1 hybrid embryos in our lab (Borensztein et al., 2017): this will enable us to compare transcriptional and structural kinetics side by side. Besides, recent

ChIPseq published data are available for H3K4me3 and H3K27me3 in an allele-specific fashion: we wish to integrate them in our combinative analysis. On one hand, it has been reported that TAD strengthening at the onset of development is independent of transcription owing to alpha-amanitin experiment results in mouse (Du et al., 2017, Ke et al., 2017) and *Drosophila* (Hug et al., 2017): when transcription is blocked in early embryo, development is impaired but TAD structure still arises. On the other hand, we have specifically explored some genomic regions by DNA FISH (see Article 2 - Figure 5 and supplemental data in Appendix for 3 additional regions on the X-chromosome and on chromosome 13): in these regions TAD boundaries appeared only by the 8C or even later (by the blastocyst stage for region#2) while genes contained in adjacent TADs are strongly expressed from much earlier stages. Thus, TAD structure onset might either precede or on the contrary follow transcriptional onset. Exploring the interplay in between structure and function at a genome-wide scale will hopefully provide us stronger arguments and conclusion.

TAD structure establishment was recently proposed to require DNA replication in aphidicolin experiments achieved in mouse embryo (Ke et al., 2017). When DNA replication is blocked, TAD structure remains weak. This echoes CTCF degron experiments (for CTCF depletion) in non-cycling cells (Nora et al., 2017) which highlighted that passage through the cell cycle might be required for restoring insulation. We may speculate that in early embryo, cell divisions are requisite steps to recruit insulators and architectural elements and to progressively build TAD structure. Unfortunately, CTCF ChIPseq data in preimplantation embryo are not available presently, because of the technical challenge of such experiment.

Approximately half of the mammalian genome consists of repetitive elements, including retrotransposons, some of which are transcribed after fertilization. Repetitive elements such as LINE-1 elements have recently been suggested to play a role in chromatin accessibility remodelling during early development (Jachowicz et al., 2017). We hypothesize that active LINE-1 elements might be involved in TAD formation. We may address this question by looking for an enrichment for LINE-1 mappable active elements around firstly formed TAD boundaries.

From our data (Article 2 - Figure 5), it appears that some TADBs might be transient and specific of one particular stage of development. We plan to explore precisely these transient TADBs for each stage and to investigate if such transient structure is associated with transient expression, with transient or specific chromatin mark patterns. Are transient

TADBs homogeneously distributed in the genome or are they clustered? How do they disappear? In one of the regions that we have studied by DNA FISH (region#1, in the *Xic* region as in (Nora et al., 2012) - in Appendix), we observed that the TADB observed in ESC only appeared in embryo at the 8C stage. However, we could see a significant organization in 2C stage embryos, with a possible different TADB shifted a few hundred kb upstream the expected TADB from ESC. This locus-specific observation corroborates with what was observed by Ke and colleagues (Ke et al., 2017): while most TADs are stable across development, some TADs are either merged, split or rearranged from one stage to the other. Changes in TAD structure and boundary during development have also been described for the *HoxD* cluster (as discussed in introduction) ((Andrey et al., 2013); Rodriguez-Carballo, biorxiv 2017).

Thanks to the allele specificity of our approach, we are able to explore separately the structure of each parental genome in preimplantation embryos. We could, for example, notice that maternal genome harbours more TADs than the paternal genome in early stages. This finding corroborates with what Du and colleagues observed (Du et al., 2017). Are these "supernumerary" TADs maternal specific? Are they inherited from oocytes? Are they transient or do they persist during development with a simple delay in their establishment in paternal genome? We hope to answer all these questions in the near future.

Besides, we have modelled parental genome intermingling from our allele-specific data. A compelling question is the description of intermingling choreography, as already tackled at CT and compartment scale. Do parental genomes intermingle similarly in all blastomeres or is it a stochastic process? Which genomic regions are involved in initial intermingling? Are 1C or 2C-stage specific TADs the first regions to intermingle? We could also speculate that the first regions to intermingle are the one harbouring 2C transiently expressed genes or showing an earlier loss in H3K4me3 broad domains. Many more questions might be inquired with regards to genome structure and TAD dynamics in early development.

One last point concerning the topic of TADs, and TAD calling strategy. As discussed in my introduction, several algorithms have been described to call TADs. The two mostly used are based on directionality index (Dixon et al., 2012) and insulation score (Crane et al., 2015). For one as for the other, two parameters have to be determined before TAD calling: window (or bin) size and contact cutoff. A recent tool - CaTCH - has been developed to identify and stratify nested hierarchical domains in the genome (Zhan et al., 2017). Unlike

previous TAD callers, CaTCH uses a single parameter, the reciprocal insulation between adjacent domains, to generate multiple sets of domains from a given map. This parameter is systematically varied to define and stratify the entire hierarchy of domains, without imposing limitation such as domain length. In early embryo, we might take advantage of this kind of approach to explore genome architecture with no *a priori* in domain size for instance. We might need to explore the embryonic genome and its enriched ultrashort range contacts, scanning for an "infra-TAD" domain structure. Or on the contrary, we might miss higher order structure by limiting our domain caller to a certain domain length. It will be worth considering the CaTCH algorithm to revisit our datasets. However, we will need to anticipate how to compare called domains in different conditions (in other words, at each stage) and we might be challenged by the "low" resolution of our single-cell datasets.

Xi structure: dynamic changes in Xp conformation during imprinted XCI

To our knowledge, it is the first time that the structure of the inactive X-chromosome has been described during imprinted XCI. We have revealed significant changes in the structure of the paternal X-chromosome, although milder than the one observed in differentiated cells.

Single cells obtained from 64C stage embryos were dissociated from an entire blastocyst (unlike what could be achieved in other studies in which only ICM cells are processed, following immunosurgery to remove trophectoderm cells). However, many cells from each blastocyst were lost through the processes of single cell dissociation, multiple mouth-pipetting steps, spinning and resuspending. Single-cell HiC "by hand" with such small cells is indeed quite challenging. Thereby, we do not know how many cells from each layer were sent for sequencing and can't distinguish neither in between cells from the inner cell mass or from the trophectoderm after sequencing. It is very unlikely that the mix in between the two populations could mask a specific inactive X-chromosome structure at such early stages. As a matter of fact, only few cells from the ICM start to re-activate their Xp by the 64C stage. It is hence very likely that the sequenced 64C stage blastomeres that we analyze have a similar status with regard to XCI.

We can speculate that imprinted inactive X-chromosome structure is different from random inactive X-chromosome structure due to its reversibility (Wutz and Jaenisch, 2000) in ICM. However, imprinted inactive X-chromosome might always be different, even when stably established in extra-embryonic tissues. To explore imprinted Xi, we could either choose an *in vivo* or an *in vitro* approach. Limitations of *in vivo* approach are mainly tissue accessibility during peri-implantation development and later aneuploidies in trophoblast giant

cells due to endoreplication. We could achieve single-cell or even population HiC in a trophectoderm cell line to assess if in a stable cell line imprinted inactive X chromosome displays similar conformation as in early blastocyst.

X-linked gene silencing during XCI is a gradual process. Once *Xist* monoallelic upregulation is stable, Xist RNA spreads across the X-chromosome for subsequent gene silencing. During random XCI, Xist RNA has been suggested to exploit the three-dimensional conformation of the X chromosome, spreading through "Xist entry sites" (Engreitz et al., 2013). In mouse preimplantation embryo, it has been shown that early inactivated genes tend to lie inside or close to these Xist RNA entry sites (Borensztein et al., 2017). It would thus be interesting to investigate if *Xist* locus contacts similar entry sites during imprinted XCI, inferring a virtual 4C contact map with *Xist* locus as a viewpoint. This could extend our understanding of Xist RNA spreading and progressive gene silencing in imprinted XCI.

Finally, our allele specific single-cell HiC datasets enable us to compute 3D models of the inactive X-chromosome at several time points during imprinted XCI. 3D models will facilitate our visualization of spatial distribution of X-chromosome and its possible changes during imprinted XCI. This will be an interesting tool, notably for exploring escapee localization. Escapees resist gene-silencing and are localized at the periphery of X-chromosome (Chaumeil et al., 2006) and tend to cluster (Giorgetti et al., 2016) during random XCI. 3D models for X-chromosome during preimplantation development will enlarge our knowledge about escapee spatial organization in link with imprinted XCI. We may also inquire if early-, mid- and late-silenced genes are clustered in 3D space and if earlier silenced genes are relocated more internally.

APPENDICES

Appendix 1 - DNA FISH probes

					Coverage (pb)	Gap (pb)
	REGION#1: chrX:105,0					
GREEN BAC pool-I	RP23-35L3	chrX	104024627	104234448		
	RP23-453P7	chrX	104257814	104451522		
	RP23-280L7	chrX	104461550	104680260	655 633	
RED BAC	RP23-117O12	chrX	104680374	104882097		114
	RP23-79G15	chrX	104879920	105114144	433 770	
GREEN BAC pool-II	RP24-217I10	chrX	105107535	105264193		-6 609
	RP23-469A2	chrX	105270313	105455684		
	RP23-331L13	chrX	105453223	105639084		
	RP24-396M14	chrX	105609015	105781008	673 473	
	REGION#2: chrX:94,2					
GREEN BAC pool-I	RP23-86N6	chrX	93250891	93494786		
	RP23-294H14	chrX	93510687	93715229		
	WI1-380M18	chrX	93713973	93751582	500 691	
RED BAC	WI1-2183N21	chrX	93754238	93791953		2 656
	RP23-36D11	chrX	93782732	93966858		
	RP23-289C13	chrX	93916516	94080897		
	RP24-192J20	chrX	94078102	94209859	455 621	
GREEN BAC pool-II	RP23-475N3	chrX	94212348	94388428		2 489
	RP23-345N13	chrX	94382411	94598100		
	RP23-134J13	chrX	94602891	94822263	609 915	
	REGION#3: chr13:14,6					
GREEN BAC pool-I	RP23-149C22	chr13	13532698	13733652		
	RP23-269A6	chr13	13735452	13917042		
	RP24-347C12	chr13	13902810	14066492		
	WI1-1971N7__G135P603846B9	chr13	14069844	14115556	582 858	
RED BAC	RP24-377A11	chr13	14113756	14288086		-1 800
	RP24-117B12	chr13	14262546	14415733		
	RP24-186M19	chr13	14400568	14567355		
	WI1-1298N15__G135P602914B5	chr13	14544523	14584519	517 465	

	WI1-2769L5__G135P60506C10	chr14	13814526	13852692		
	WI1-1690N16__G135P65400B5	chr15	14755609	14793733		
GREEN BAC pool-II	RP23-149G21	chr13	14617776	14816858		-13 445
	RP23-339I22	chr13	14826248	15025656		
	RP23-205P22	chr13	15026064	15225538	607 762	
	REGION#4: chr13:90,9					
GREEN BAC pool-I	RP24-278M23	chr13	89761320	89900154		
	RP23-325G4	chr13	89903372	90125927		
	RP23-2B17	chr13	90107822	90308777	547 457	
RED BAC	RP23-222A16	chr13	90310893	90506036		2 116
	RP24-389D15	chr13	90513189	90658357		
	RP23-302B3	chr13	90620826	90839364	528 471	
GREEN BAC pool-II	RP23-359G6	chr13	90842898	91053560		3 534
	RP23-326J5	chr13	91063985	91263254		
	RP23-307F19	chr13	91255421	91390052	547 154	

Appendix 2 - ImageJ macro for colocalization analysis

```
// Macro for ImageJ - on 3D DNA FISH images from the OMX to analyze colocalisation index (Pearson coefficient)
// By Nicolas Signolle, Olivier Leroy, Tristan Piolot & Noémie Ranisavljevic
//To define : input parameters
//crop box size (Be aware that dx, dy and dz need to be multiple of 2)
// for the 2C dx/dy = 60 and dz = 26
// for the 4C dx/dy = 56 and dz = 26
// for the 8C dx/dy = 50 and dz = 20
// for the 16C dx/dy = 40 and dz = 20
// for the 64C dx/dy = 40 and dz = 20
// for the E4.5 dx/dy = 40 and dz = 20
// for ESC dx/dy = 40 and dz = 12
dx = 50;
dy = 50;
dz = 20;
//Coste randomisation iteration number
iter = 100;
//Ask to user if it s a Male or Female Embryo
// For autosomal TAD borders, always select "FEMALE" as there will be 2 pinpoints per cell
Dialog.create("Female or Male Embryo ?");
Dialog.addChoice("Female or Male Embryo ?", newArray("Female", "Male"));
Dialog.show();
sex = Dialog.getChoice();
// Result table title
NewResultsTable="[output]";
//Result table creation
run("New... ", "name="+NewResultsTable+" type=Table");
// Result table column title
print(NewResultsTable, "\\Headings:Embryon \t Sexe \t object \t numero ROI manager \t Pearson \t Pearson (randomized) \t Pearson (sigma) \t Iterations \t P-Value \t IntDensityGreen \t IntDensityRed \t Z_slice ");
// Clean ROI manager (if it's not empty)
if(roiManager("count")!=0)
{
	roiManager("Delete");
}
// Reset MinMax before displaying image
// Take notice : nSlices is divided by 6 as there are 2 * 3 channels
// Change it if the image doesn't have 3 channels!
Stack.setSlice(round(nSlices/6));
Stack.setDisplayMode("composite");
Stack.setChannel(1);
resetMinAndMax();
Stack.setChannel(2);
resetMinAndMax();
Stack.setChannel(3);
resetMinAndMax();
// get Image info and reset display and calibration
run("Properties...", "channels=3 slices="+nSlices/3+" frames=1 unit=pixel pixel_width=1 pixel_height=1 voxel_depth=1"); //Attention : nSlices divisé par 3 car 3 channels -> à changer si plus ou omins de channels
```

```
run("Make Composite");
idori = getImageID();
dir = getDirectory("image");
Titre = getTitle() ;
suffixe = ".tif";
sousTitre = substring(Titre, 0, lengthOf(Titre)-lengthOf(suffixe));
Stack.getDimensions(width, height, nbchannels, nbslices, frames);
run("Set Measurements...", "integrated redirect=None decimal=0");
//create a result folder
File.makeDirectory(dir+File.separator+sousTitre+"_Coste");
out_dir=dir+File.separator+sousTitre+"_Coste";
//Initialization
fini=false;       //exit macro flag
nb_crop=0;     //crop counter
firstPinPoint = false; //first pinpoint found flag
secondPinPoint=false; //second pinpoint found flag
// Loop for each cell with the variable "nb_crop" to number each crop
while(!fini)
{
////////////////////////////// First Pinpoint //////////////////////////////
        setTool("Point");
        selectImage(idori);
        if(sex=="Male")
        waitForUser("Please, select pinpoint");
        if(sex=="Female")
        waitForUser("Please, select first pinpoint");

        if (selectionType() == 10)
        {
                //get point coordinates
                getSelectionCoordinates(Xpos, Ypos);
                Stack.getPosition(channel, slice, frame);
        }
        else
        {
                //if we can not get point coordinates : exit
                exit("Problem with the point selection tool : exit");;
        }

        setBatchMode(true);
        Zmin = maxOf(1, slice-(dz/2));
        Zmax = minOf(nbslices, slice+(dz/2));



        if( ((slice-(dz/2))<=0) || ((slice+(dz/2) > nbslices)) || ((Xpos[0]-(dx/2))<0) ||
((Xpos[0]+(dx/2))>width) || ((Ypos[0]-(dy/2))<0)|| ((Ypos[0]+(dy/2))>height)  )
        {
                //pinpoint not found : out of bounds !
                firstPinPoint = false;
                run("Select None");
                if(sex=="Male")
                showMessage("Box out of bounds, try another cell");
                else
                showMessage("First pinpoint box out of bounds, try another pinpoint");
```

```
	}
	else
	{
		//(First) pinpoint found !
		firstPinPoint = true;
		// Make selection
		selectImage(idori);
		makeRectangle((round(Xpos[0])-(dx/2)), (round(Ypos[0])-(dy/2)), dx, dy);

		nb_crop=nb_crop+1;
		roiManager("add");
		roiManager("Show All with labels");
		run("Restore Selection");
		run("Duplicate...", "title=crop_green duplicate channels=1  slices=" + Zmin + "-
" + Zmax);

		Stack.getStatistics(voxelCount, mean, min, max, stdDev)
		if(max==4095)
		{
			showMessage("Warning : Green oversaturated");
		}
		run("Measure");
		IntDensityGreen=getResult("RawIntDen", (nResults-1));

		// Red channel
		selectImage(idori);
		run("Duplicate...", "title=crop_red duplicate channels=2  slices=" + Zmin + "-" +
Zmax);
		Stack.getStatistics(voxelCount, mean, min, max, stdDev)
		if(max==4095)
		{
			showMessage("Warning : Red oversaturated");
		}
		run("Measure");
		IntDensityRed=getResult("RawIntDen", (nResults-1));

		//clear log window
		print("\\Clear");


		// Colocalization measurement
		run("JACoP ", "imga=crop_red imgb=crop_green costesrand=2-1-"+iter+"-
0.0010-0-false-false-false");


		//get values from log window
		ContenuLog = getInfo("Log");
		s_coef = substring (ContenuLog,lastIndexOf(ContenuLog, "r
(original)=")+13,lastIndexOf(ContenuLog, "r (randomized)=")-1);
		s_coef_R_mean = substring (ContenuLog,lastIndexOf(ContenuLog, "r
(randomized)=")+15,lastIndexOf(ContenuLog, "±"));
		s_coef_R_sigma = substring (ContenuLog,lastIndexOf(ContenuLog,
"±")+1,lastIndexOf(ContenuLog, "P-value")-35);
		s_P_value = substring (ContenuLog,lastIndexOf(ContenuLog, "P-
value")+8,lastIndexOf(ContenuLog, "%"));
```

```
		s_nb_random = substring (ContenuLog,lastIndexOf(ContenuLog,
"randomization rounds")+21,lastIndexOf(ContenuLog, ", Resolution (bin"));
		//transform string into float
		coef = parseFloat(s_coef);
		coef_R_mean =  parseFloat(s_coef_R_mean);
		coef_R_sigma = parseFloat(s_coef_R_sigma);
		P_value = parseFloat(s_P_value);
		nb_random = parseFloat(s_nb_random);

		selectWindow("Costes' method (crop_red & crop_green)");
		close();

		// Fill the result table
		if(sex=="Male")
		{
			print (NewResultsTable, sousTitre +"\t"+ sex +"\t"+ "pinpoint" +"\t"+
nb_crop +"\t"+ coef +"\t"+ coef_R_mean+"\t"+ coef_R_sigma+"\t"+ nb_random+"\t"+
P_value+"\t"+ IntDensityGreen +"\t"+ IntDensityRed +"\t"+ slice);
		}
		else
		{
			print (NewResultsTable, sousTitre +"\t"+ sex +"\t"+ "pinpoint 1" +"\t"+
nb_crop +"\t"+ coef +"\t"+ coef_R_mean+"\t"+ coef_R_sigma+"\t"+ nb_random+"\t"+
P_value+"\t"+ IntDensityGreen +"\t"+ IntDensityRed +"\t"+ slice);
		}


		// Saving crop and close crop image
		selectImage(idori);
		run("Select None");
		resetMinAndMax();
		run("Merge Channels...", "c1=crop_green c2=crop_red create");

		if(sex=="Male")
			saveAs("Tiff",
out_dir+File.separator+sousTitre+"_crop["+nb_crop+"]_Pearson_"+coef+"_[Random_Pearso
n_"+coef_R_mean+"±"+coef_R_sigma+"_"+nb_random+"it_P-value_"+P_value+"].tif");
		else
			saveAs("Tiff",
out_dir+File.separator+sousTitre+"_crop["+nb_crop+"]_Pin1_Pearson_"+coef+"_[Random_P
earson_"+coef_R_mean+"±"+coef_R_sigma+"_"+nb_random+"it_P-value_"+P_value+"].tif");


		close();
	}//End of First pinpoint

//////////////////////////////// Second Pinpoint ////////////////////////////
	//We look for a second pinpoint only if we found a first pinpoint and we are on a
female embryo case
	if(firstPinPoint && sex=="Female")
	{
		setTool("Point");
		selectImage(idori);
		waitForUser("Please, select second pinpoint");
```

```
		if (selectionType() == 10)
		{
			//get point coordinates
			getSelectionCoordinates(Xpos, Ypos);
			Stack.getPosition(channel, slice, frame);
		}
		else
		{
			//if we can not get point coordinates : exit
			showMessage("Problem with the point selection tool : exit");
			exit;
		}

		setBatchMode(true);

		Zmin = maxOf(1, slice-(dz/2));
		Zmax = minOf(nbslices, slice+(dz/2));



		if( ((slice-(dz/2))<=0) || ((slice+(dz/2) > nbslices)) || ((Xpos[0]-(dx/2))<0) ||
((Xpos[0]+(dx/2))>width) || ((Ypos[0]-(dy/2))<0)|| ((Ypos[0]+(dy/2))>height)  )
		{
			//Second pinpoint not found
			showMessage("Second pinpoint out of bounds");
			//table line is empty
			print (NewResultsTable, sousTitre +"\t"+ sex +"\t"+ "pinpoint 2" +"\t"+ "-
" +"\t"+ "-" +"\t"+ "-"+"\t"+ "-"+"\t"+ "-"+"\t"+ "-"+"\t"+ "-" +"\t"+ "-" +"\t"+ slice);
			secondPinPoint = false;
			run("Select None");
		}
		else
		{
			secondPinPoint = true;
			// Make Selection
			selectImage(idori);
			makeRectangle((round(Xpos[0])-(dx/2)), (round(Ypos[0])-(dy/2)), dx,
dy);

			nb_crop=nb_crop+1;
			roiManager("add");
			roiManager("Show All with labels");
			run("Restore Selection");
			run("Duplicate...", "title=crop_green duplicate channels=1  slices=" +
Zmin + "-" + Zmax);

			Stack.getStatistics(voxelCount, mean, min, max, stdDev)
			if(max==4095)
			{
				showMessage("Warning : Green oversaturated");
			}
			run("Measure");
			IntDensityGreen=getResult("RawIntDen", (nResults-1));

			// Red channel
```

```
                        selectImage(idori);
                        run("Duplicate...", "title=crop_red duplicate channels=2  slices=" + Zmin
+ "-" + Zmax);
                        Stack.getStatistics(voxelCount, mean, min, max, stdDev)
                        if(max==4095)
                        {
                                showMessage("Warning : Red oversaturated");
                        }
                        run("Measure");
                        IntDensityRed=getResult("RawIntDen", (nResults-1));

                        //clear log window
                        print("\\Clear");

                        // Colocalization measurement
                        run("JACoP ", "imga=crop_red imgb=crop_green costesrand=2-1-
"+iter+"-0.0010-0-false-false-false");

                        //get values from log window
                        ContenuLog = getInfo("Log");
                        s_coef = substring (ContenuLog,lastIndexOf(ContenuLog, "r
(original)=")+13,lastIndexOf(ContenuLog, "r (randomized)=")-1);
                        s_coef_R_mean = substring (ContenuLog,lastIndexOf(ContenuLog, "r
(randomized)=")+15,lastIndexOf(ContenuLog, "±"));
                        s_coef_R_sigma = substring (ContenuLog,lastIndexOf(ContenuLog,
"±")+1,lastIndexOf(ContenuLog, "P-value")-35);
                        s_P_value = substring (ContenuLog,lastIndexOf(ContenuLog, "P-
value")+8,lastIndexOf(ContenuLog, "%"));
                        s_nb_random = substring (ContenuLog,lastIndexOf(ContenuLog,
"randomization rounds")+21,lastIndexOf(ContenuLog, ", Resolution (bin"));
                        //transform string into float
                        coef = parseFloat(s_coef);
                        coef_R_mean =  parseFloat(s_coef_R_mean);
                        coef_R_sigma = parseFloat(s_coef_R_sigma);
                        P_value = parseFloat(s_P_value);
                        nb_random = parseFloat(s_nb_random);

                        selectWindow("Costes' method (crop_red & crop_green)");
                        close();

                        // Fill the result table
                        print (NewResultsTable, sousTitre +"\t"+ sex +"\t"+ "pinpoint 2" +"\t"+
nb_crop +"\t"+ coef +"\t"+ coef_R_mean+"\t"+ coef_R_sigma+"\t"+ nb_random+"\t"+
P_value+"\t"+ IntDensityGreen +"\t"+ IntDensityRed +"\t"+ slice);

                        // Saving crop and close crop image
                        selectImage(idori);
                        run("Select None");
                        resetMinAndMax();
                        run("Merge Channels...", "c1=crop_green c2=crop_red create");
                        saveAs("Tiff",
out_dir+File.separator+sousTitre+"_crop["+nb_crop+"]_Pin2_Pearson_"+coef+"_[Random_P
earson_"+coef_R_mean+"±"+coef_R_sigma+"_"+nb_random+"it_P-value_"+P_value+"].tif");
                        close();
                }
```

```
	}
	//End of Second pinpoint
//////////////////////////////// Background ////////////////////////////////

	//we look for background only if we found at least one pintpoint
	if(firstPinPoint || secondPinPoint)
	{

		backgroundFound= false; // background found flag

		while(!backgroundFound)
		{
			setTool("Point");
			selectImage(idori);
			waitForUser("Please, select background");

			if (selectionType() == 10)
			{
				//get point coordinates
				getSelectionCoordinates(Xpos, Ypos);
				Stack.getPosition(channel, slice, frame);
			}
			else
			{
				//if we can not get point coordinates : exit
				showMessage("Problem with the point selection tool : exit");
				exit;
			}

			setBatchMode(true);


			z = slice;
			y = Ypos[0];
			x = Xpos[0];


			if( ((slice-(dz/2))<=0) || ((slice+(dz/2) > nbslices)) || ((Xpos[0]-(dx/2))<0)
|| ((Xpos[0]+(dx/2))>width) || ((Ypos[0]-(dy/2))<0)|| ((Ypos[0]+(dy/2))>height)  )
			{
				//Background out of bounds : try again !
				backgroundFound = false;

				showMessage("Background box out of bounds : try again in
another area");
				run("Select None");

			}
			else
			{
				//Background found !
				backgroundFound = true;
				//make selection
				makeRectangle((x-(dx/2)), (y-(dy/2)), dx, dy);
```

```
                                nb_crop=nb_crop+1;
                                roiManager("add");
                                roiManager("Show All with labels");
                                run("Restore Selection");
                                run("Duplicate...", "title=crop_green duplicate
channels=1  slices=" + Zmin + "-" + Zmax);

                                Stack.getStatistics(voxelCount, mean, min, max, stdDev)
                                if(max==4095)
                                {
                                        showMessage("Warning : Green oversaturated");
                                }
                                run("Measure");
                                IntDensityGreen=getResult("RawIntDen", (nResults-1));

                                // Red channel
                                selectImage(idori);
                                run("Duplicate...", "title=crop_red duplicate channels=2  slices="
+ Zmin + "-" + Zmax);
                                Stack.getStatistics(voxelCount, mean, min, max, stdDev)
                                if(max==4095)
                                {
                                        showMessage("Warning : Red oversaturated");
                                }
                                run("Measure");
                                IntDensityRed=getResult("RawIntDen", (nResults-1));

                                //clear log window
                                print("\\Clear");

                                // Colocalization measurement
                                run("JACoP ", "imga=crop_red imgb=crop_green costesrand=2-
1-"+iter+"-0.0010-0-false-false-false");

                                //get values from log window
                                ContenuLog = getInfo("Log");
                                s_coef = substring (ContenuLog,lastIndexOf(ContenuLog, "r
(original)=")+13,lastIndexOf(ContenuLog, "r (randomized)=")-1);
                                s_coef_R_mean = substring
(ContenuLog,lastIndexOf(ContenuLog, "r (randomized)=")+15,lastIndexOf(ContenuLog, "±"));
                                s_coef_R_sigma = substring
(ContenuLog,lastIndexOf(ContenuLog, "±")+1,lastIndexOf(ContenuLog, "P-value")-35);
                                s_P_value = substring (ContenuLog,lastIndexOf(ContenuLog,
"P-value")+8,lastIndexOf(ContenuLog, "%"));
                                s_nb_random = substring
(ContenuLog,lastIndexOf(ContenuLog, "randomization
rounds")+21,lastIndexOf(ContenuLog, ", Resolution (bin"));
                                //transform string into float
                                coef = parseFloat(s_coef);
                                coef_R_mean =  parseFloat(s_coef_R_mean);
                                coef_R_sigma = parseFloat(s_coef_R_sigma);
                                P_value = parseFloat(s_P_value);
                                nb_random = parseFloat(s_nb_random);

                                selectWindow("Costes' method (crop_red & crop_green)");
```

```
                                    close();

                                    // Fill the result table
                                    print (NewResultsTable, sousTitre +"\t"+ sex +"\t"+
"background" +"\t"+ nb_crop +"\t"+ coef +"\t"+ coef_R_mean+"\t"+ coef_R_sigma+"\t"+
nb_random+"\t"+ P_value+"\t"+ IntDensityGreen +"\t"+ IntDensityRed +"\t"+
slice);

                                    // Saving crop and close crop image
                                    selectImage(idori);
                                    run("Select None");
                                    resetMinAndMax();
                                    run("Merge Channels...", "c1=crop_green c2=crop_red create");
                                    saveAs("Tiff",
out_dir+File.separator+sousTitre+"_crop["+nb_crop+"]_Background_Pearson_"+coef+"_[Ran
dom_Pearson_"+coef_R_mean+"±"+coef_R_sigma+"_"+nb_random+"it_P-
value_"+P_value+"].tif");
                                    close();
                                }
                            }

        }//End of Background


        // Ask to the user if he wants to analyze another cell
        setBatchMode(false);
        Dialog.create("More cells ?");
        Dialog.addCheckbox("No more cells ? ", false);
        Dialog.show();
        fini = Dialog.getCheckbox();
        //reset pinpointFlag
        firstPinPoint = false;
        secondPinPoint=false;

}
//save the result table
selectWindow("output");
saveAs("Text", out_dir+File.separator+sousTitre+".xls");
selectWindow("output");
run("Close");
run("From ROI Manager");
saveAs ("Tiff", out_dir+File.separator+sousTitre+"_ROI.tif");
```

Appendix 3 - Supplementary results for other regions studied by DNA FISH

Region#1 - chrX:105 (mm10), Xic region, as in Nora et al.,2012

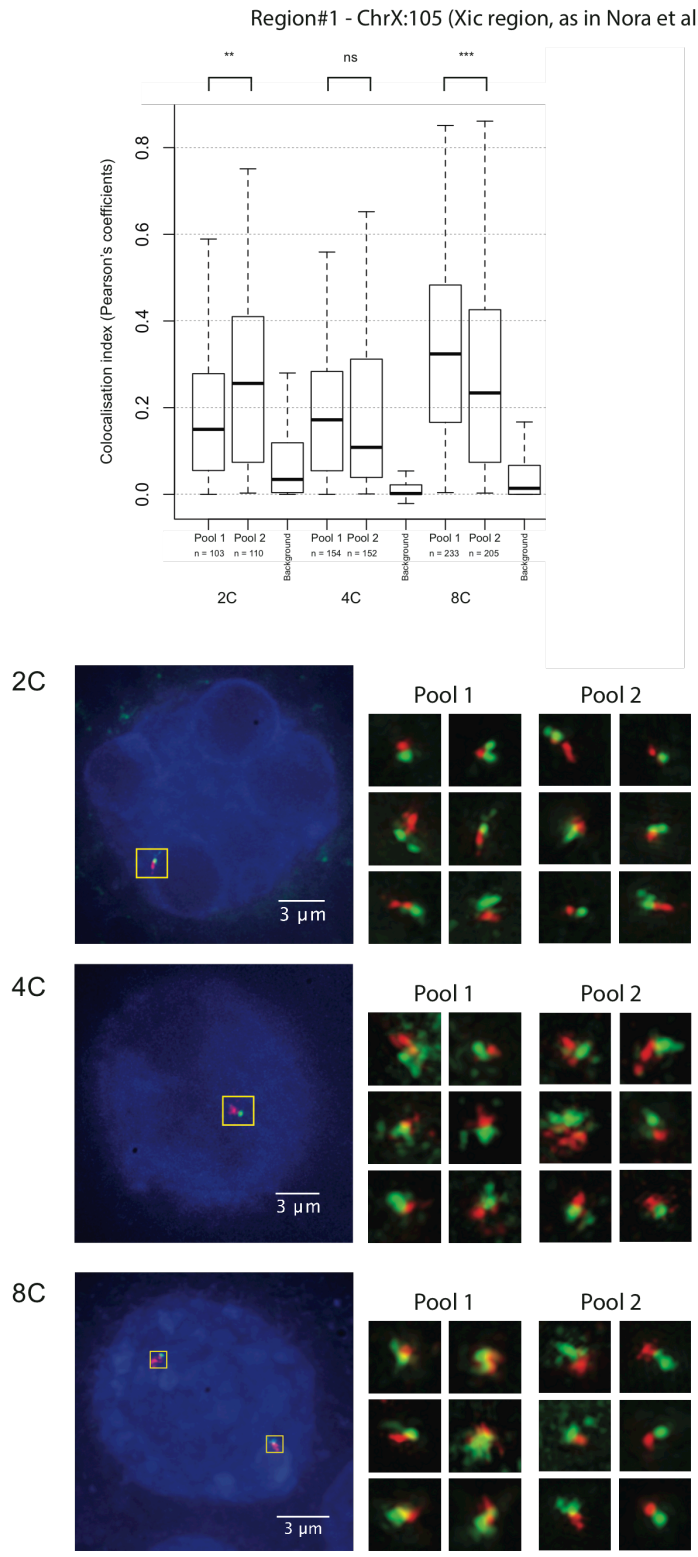

Directionality index around chr X: 105

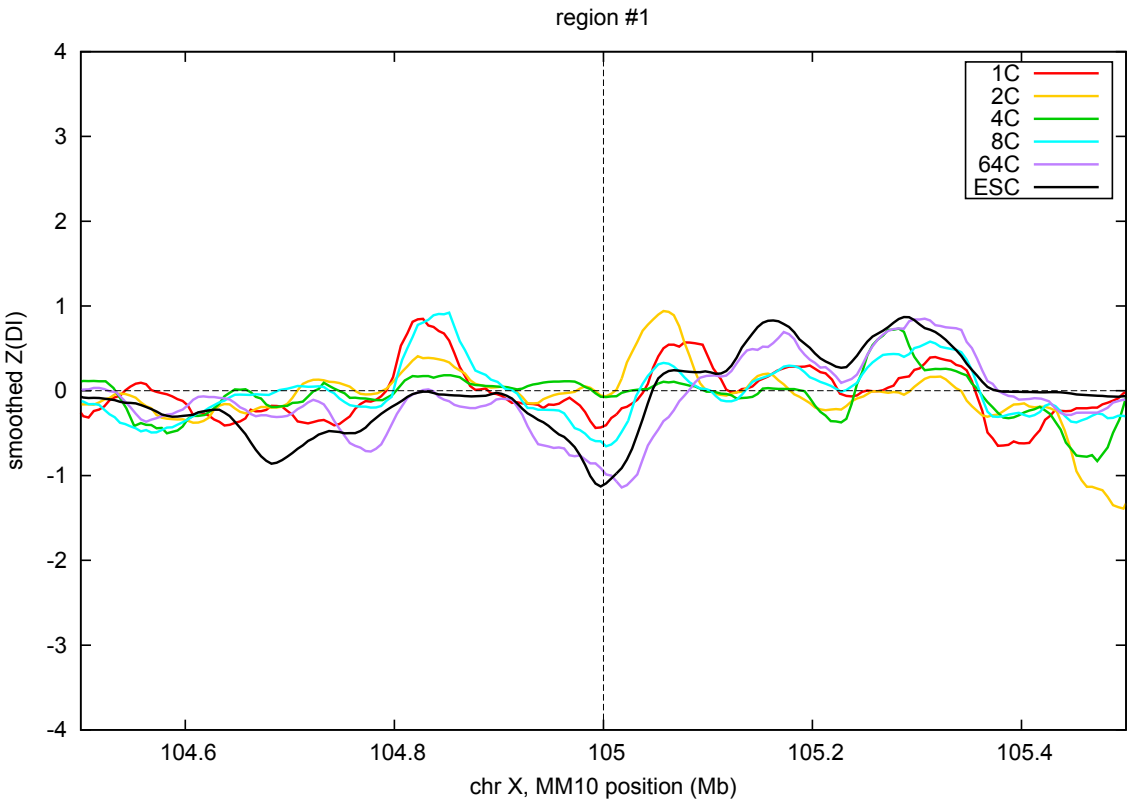

Region#2 - chrX:94,2 (mm10)

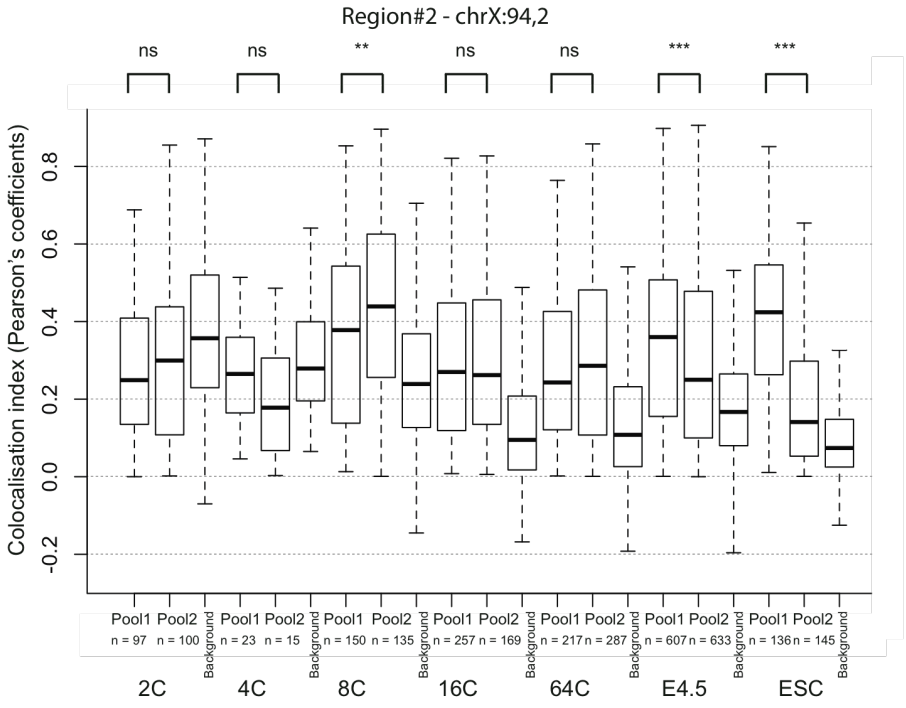

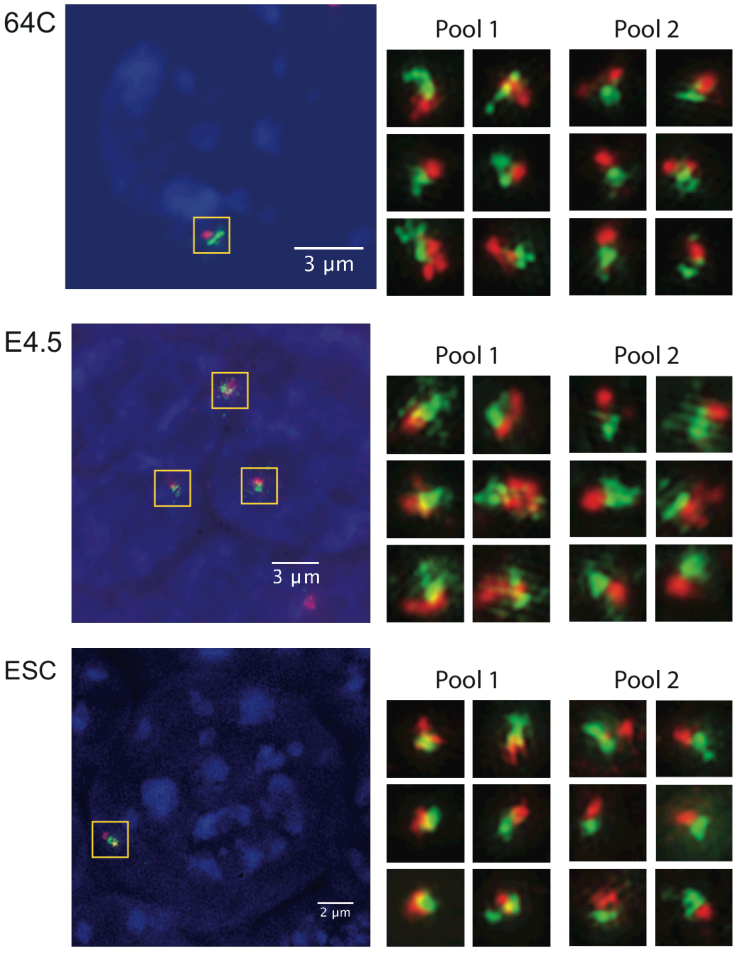

Directionality index around chr X : 94,2

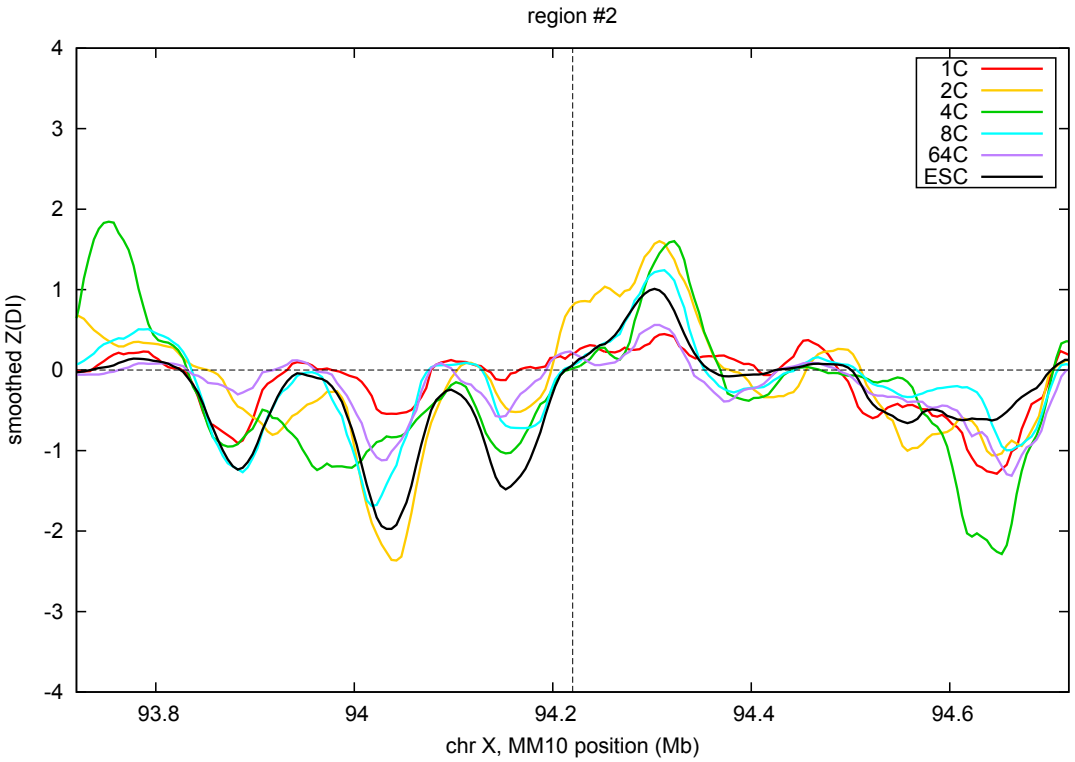

Region#3 - chr13:14,6

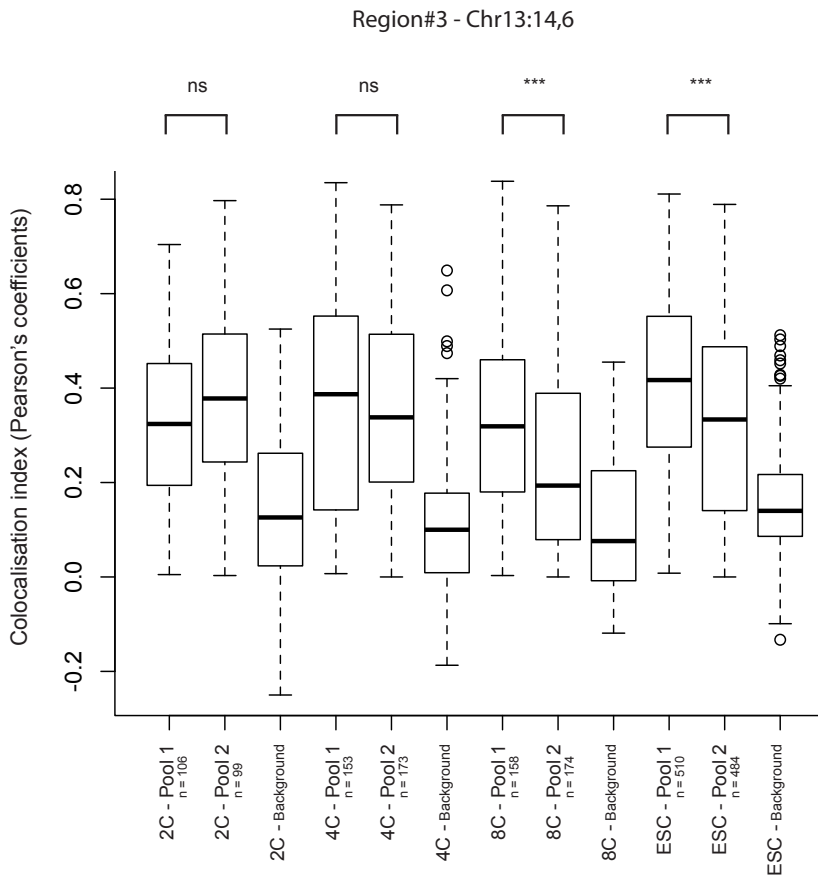

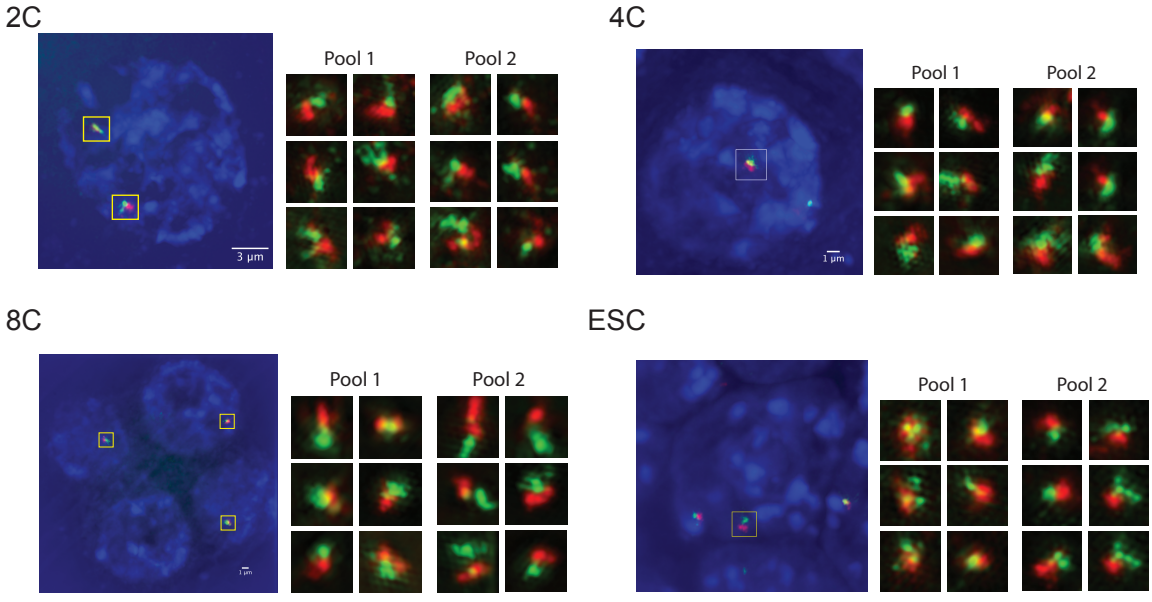

Directionality index around chr13 : 14,6

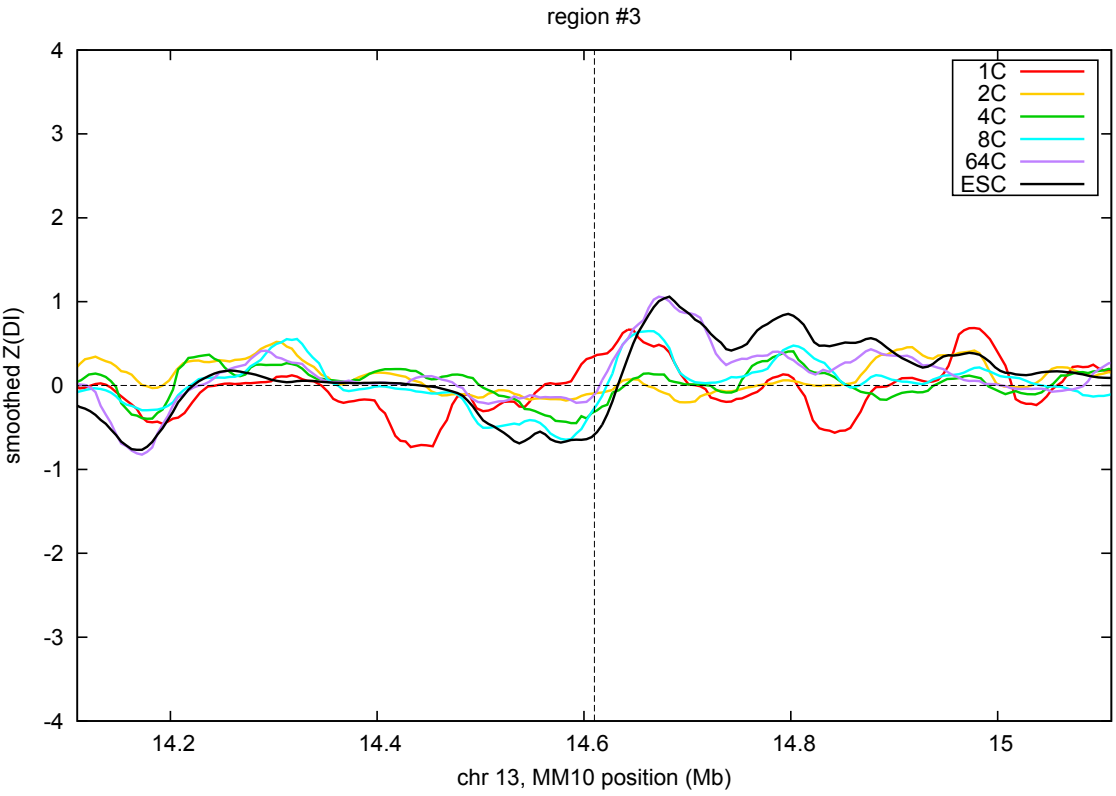

REFERENCES

Aanes, H., Østrup, O., Andersen, I. S., Moen, L. F., Mathavan, S., Collas, P. and Alestrom, P. (2013) 'Differential transcript isoform usage pre- and post-zygotic genome activation in zebrafish', *BMC Genomics,* 14, pp. 331.

Abe, K., Yamamoto, R., Franke, V., Cao, M., Suzuki, Y., Suzuki, M. G., Vlahovicek, K., Svoboda, P., Schultz, R. M. and Aoki, F. (2015) 'The first murine zygotic transcription is promiscuous and uncoupled from splicing and 3' processing', *EMBO J,* 34(11), pp. 1523-37.

Adenot, P. G., Mercier, Y., Renard, J. P. and Thompson, E. M. (1997) 'Differential H4 acetylation of paternal and maternal chromatin precedes DNA replication and differential transcriptional activity in pronuclei of 1-cell mouse embryos', *Development,* 124(22), pp. 4615-25.

Aguirre-Lavin, T., Adenot, P., Bonnet-Garnier, A., Lehmann, G., Fleurot, R., Boulesteix, C., Debey, P. and Beaujean, N. (2012) '3D-FISH analysis of embryonic nuclei in mouse highlights several abrupt changes of nuclear organization during preimplantation development', *BMC Dev Biol,* 12, pp. 30.

Ahmed, K., Dehghani, H., Rugg-Gunn, P., Fussner, E., Rossant, J. and Bazett-Jones, D. P. (2010) 'Global chromatin architecture reflects pluripotency and lineage commitment in the early mouse embryo', *PLoS One,* 5(5), pp. e10531.

Alekseyenko, A. A., Peng, S., Larschan, E., Gorchakov, A. A., Lee, O. K., Kharchenko, P., McGrath, S. D., Wang, C. I., Mardis, E. R., Park, P. J. and Kuroda, M. I. (2008) 'A sequence motif within chromatin entry sites directs MSL establishment on the Drosophila X chromosome', *Cell,* 134(4), pp. 599-609.

Almeida, M., Pintacuda, G., Masui, O., Koseki, Y., Gdula, M., Cerase, A., Brown, D., Mould, A., Innocent, C., Nakayama, M., Schermelleh, L., Nesterova, T. B., Koseki, H. and Brockdorff, N. (2017) 'PCGF3/5-PRC1 initiates Polycomb recruitment in X chromosome inactivation', *Science,* 356(6342), pp. 1081-1084.

Ancelin, K., Syx, L., Borensztein, M., Ranisavljevic, N., Vassilev, I., Briseño-Roa, L., Liu, T., Metzger, E., Servant, N., Barillot, E., Chen, C. J., Schüle, R. and Heard, E. (2016) 'Maternal LSD1/KDM1A is an essential regulator of chromatin and transcription landscapes during zygotic genome activation', *Elife,* 5.

Andergassen, D., Dotter, C. P., Wenzel, D., Sigl, V., Bammer, P. C., Muckenhuber, M., Mayer, D., Kulinski, T. M., Theussl, H. C., Penninger, J. M., Bock, C., Barlow, D. P., Pauler, F. M. and Hudson, Q. J. (2017) 'Mapping the mouse Allelome reveals tissue-specific regulation of allelic expression', *Elife,* 6.

Andreu-Vieyra, C. V., Chen, R., Agno, J. E., Glaser, S., Anastassiadis, K., Stewart, A. F. and Matzuk, M. M. (2010) 'MLL2 is required in oocytes for bulk histone 3 lysine 4 trimethylation and transcriptional silencing', *PLoS Biol,* 8(8).

Andrey, G., Montavon, T., Mascrez, B., Gonzalez, F., Noordermeer, D., Leleu, M., Trono, D., Spitz, F. and Duboule, D. (2013) 'A switch between topological domains underlies HoxD genes collinearity in mouse limbs', *Science,* 340(6137), pp. 1234167.

Aoki, F., Worrad, D. M. and Schultz, R. M. (1997) 'Regulation of transcriptional activity during the first and second cell cycles in the preimplantation mouse embryo', *Dev Biol,* 181(2), pp. 296-307.

Aranda, S., Mas, G. and Di Croce, L. (2015) 'Regulation of gene transcription by Polycomb proteins', *Sci Adv,* 1(11), pp. e1500737.

Arney, K. L. and Fisher, A. G. (2004) 'Epigenetic aspects of differentiation', *J Cell Sci,* 117(Pt 19), pp. 4355-63.

Augui, S., Nora, E. P. and Heard, E. (2011) 'Regulation of X-chromosome inactivation by the X-inactivation centre', *Nat Rev Genet,* 12(6), pp. 429-42.

BARR, M. L. and BERTRAM, E. G. (1949) 'A morphological distinction between neurones of the male and female, and the behaviour of the nucleolar satellite during accelerated nucleoprotein synthesis', *Nature,* 163(4148), pp. 676.

Bashirullah, A., Halsell, S. R., Cooperstock, R. L., Kloc, M., Karaiskakis, A., Fisher, W. W., Fu, W., Hamilton, J. K., Etkin, L. D. and Lipshitz, H. D. (1999) 'Joint action of two RNA degradation pathways controls the timing of maternal transcript elimination at the midblastula transition in Drosophila melanogaster', *EMBO J,* 18(9), pp. 2610-20.

Battulin, N., Fishman, V. S., Mazur, A. M., Pomaznoy, M., Khabarova, A. A., Afonnikov, D. A., Prokhortchouk, E. B. and Serov, O. L. (2015) 'Comparison of the three-dimensional organization of sperm and fibroblast genomes using the Hi-C approach', *Genome Biol,* 16, pp. 77.

Bell, A. C. and Felsenfeld, G. (2000) 'Methylation of a CTCF-dependent boundary controls imprinted expression of the Igf2 gene', *Nature,* 405(6785), pp. 482-5.

Bell, A. C., West, A. G. and Felsenfeld, G. (1999) 'The protein CTCF is required for the enhancer blocking activity of vertebrate insulators', *Cell,* 98(3), pp. 387-96.

Belmont, A. S., Bignone, F. and Ts'o, P. O. (1986) 'The relative intranuclear positions of Barr bodies in XXX non-transformed human fibroblasts', *Exp Cell Res,* 165(1), pp. 165-79.

Bischoff, A., Albers, J., Kharboush, I., Stelzer, E., Cremer, T. and Cremer, C. (1993) 'Differences of size and shape of active and inactive X-chromosome domains in human amniotic fluid cell nuclei', *Microsc Res Tech,* 25(1), pp. 68-77.

Bonnet-Garnier, A., Feuerstein, P., Chebrout, M., Fleurot, R., Jan, H. U., Debey, P. and Beaujean, N. (2012) 'Genome organization and epigenetic marks in mouse germinal vesicle oocytes', *Int J Dev Biol,* 56(10-12), pp. 877-87.

Borden, J. and Manuelidis, L. (1988) 'Movement of the X chromosome in epilepsy', *Science,* 242(4886), pp. 1687-91.

Borensztein, M., Syx, L., Ancelin, K., Diabangouaya, P., Picard, C., Liu, T., Liang, J. B., Vassilev, I., Galupa, R., Servant, N., Barillot, E., Surani, A., Chen, C. J. and Heard, E. (2017) 'Xist-dependent imprinted X inactivation and the early developmental consequences of its failure', *Nat Struct Mol Biol,* 24(3), pp. 226-233.

Borsani, G., Tonlorenzi, R., Simmler, M. C., Dandolo, L., Arnaud, D., Capra, V., Grompe, M., Pizzuti, A., Muzny, D., Lawrence, C., Willard, H. F., Avner, P. and Ballabio, A. (1991) 'Characterization of a murine gene expressed from the inactive X chromosome', *Nature,* 351(6324), pp. 325-9.

Bouniol, C., Nguyen, E. and Debey, P. (1995) 'Endogenous transcription occurs at the 1-cell stage in the mouse embryo', *Exp Cell Res,* 218(1), pp. 57-62.

Bourc'his, D., Xu, G. L., Lin, C. S., Bollman, B. and Bestor, T. H. (2001) 'Dnmt3L and the establishment of maternal genomic imprints', *Science,* 294(5551), pp. 2536-9.

Bourgeois, C. A., Laquerriere, F., Hemon, D., Hubert, J. and Bouteille, M. (1985) 'New data on the in-situ position of the inactive X chromosome in the interphase nucleus of human fibroblasts', *Hum Genet,* 69(2), pp. 122-9.

, Die Blastomerenkerne von Ascaris megalocephala und die Theorie der Chromosomen individualita¨t.

Boyle, A. L., Ballard, S. G. and Ward, D. C. (1990) 'Differential distribution of long and short interspersed element sequences in the mouse genome: chromosome karyotyping by fluorescence in situ hybridization', *Proc Natl Acad Sci U S A,* 87(19), pp. 7757-61.

Bošković, A., Eid, A., Pontabry, J., Ishiuchi, T., Spiegelhalter, C., Raghu Ram, E. V., Meshorer, E. and Torres-Padilla, M. E. (2014) 'Higher chromatin mobility supports totipotency and precedes pluripotency in vivo', *Genes Dev,* 28(10), pp. 1042-7.

Braun, R. E. (2001) 'Packaging paternal chromosomes with protamine', *Nat Genet,* 28(1), pp. 10-2.

Brockdorff, N. (2017) 'Polycomb complexes in X chromosome inactivation', *Philos Trans R Soc Lond B Biol Sci,* 372(1733).

Brockdorff, N., Ashworth, A., Kay, G. F., Cooper, P., Smith, S., McCabe, V. M., Norris, D. P., Penny, G. D., Patel, D. and Rastan, S. (1991) 'Conservation of position and exclusive expression of mouse Xist from the inactive X chromosome', *Nature,* 351(6324), pp. 329-31.

Brown, C. J., Ballabio, A., Rupert, J. L., Lafreniere, R. G., Grompe, M., Tonlorenzi, R. and Willard, H. F. (1991a) 'A gene from the region of the human X inactivation centre is expressed exclusively from the inactive X chromosome', *Nature,* 349(6304), pp. 38-44.

Brown, C. J., Lafreniere, R. G., Powers, V. E., Sebastio, G., Ballabio, A., Pettigrew, A. L., Ledbetter, D. H., Levy, E., Craig, I. W. and Willard, H. F. (1991b) 'Localization of the X inactivation centre on the human X chromosome in Xq13', *Nature,* 349(6304), pp. 82-4.

Brown, C. J. and Willard, H. F. (1994) 'The human X-inactivation centre is not required for maintenance of X-chromosome inactivation', *Nature,* 368(6467), pp. 154-6.

Buenrostro, J. D., Wu, B., Chang, H. Y. and Greenleaf, W. J. (2015) 'ATAC-seq: A Method for Assaying Chromatin Accessibility Genome-Wide', *Curr Protoc Mol Biol,* 109, pp. 21.29.1-9.

Burger, K., Mühl, B., Kellner, M., Rohrmoser, M., Gruber-Eber, A., Windhager, L., Friedel, C. C., Dölken, L. and Eick, D. (2013) '4-thiouridine inhibits rRNA synthesis and causes a nucleolar stress response', *RNA Biol,* 10(10), pp. 1623-30.

Burton, A. and Torres-Padilla, M. E. (2010) 'Epigenetic reprogramming and development: a unique heterochromatin organization in the preimplantation mouse embryo', *Brief Funct Genomics,* 9(5-6), pp. 444-54.

Burton, A. and Torres-Padilla, M. E. (2014) 'Chromatin dynamics in the regulation of cell fate allocation during early embryogenesis', *Nat Rev Mol Cell Biol,* 15(11), pp. 723-34.

Busslinger, G. A., Stocsits, R. R., van der Lelij, P., Axelsson, E., Tedeschi, A., Galjart, N. and Peters, J. M. (2017) 'Cohesin is positioned in mammalian genomes by transcription, CTCF and Wapl', *Nature,* 544(7651), pp. 503-507.

Carrel, L. and Brown, C. J. (2017) 'When the Lyon(ized chromosome) roars: ongoing expression from an inactive X chromosome', *Philos Trans R Soc Lond B Biol Sci,* 372(1733).

Carrel, L. and Willard, H. F. (2005) 'X-inactivation profile reveals extensive variability in X-linked gene expression in females', *Nature,* 434(7031), pp. 400-4.

Cerda, M. C., Berríos, S., Fernández-Donoso, R., Garagna, S. and Redi, C. (1999) 'Organisation of complex nuclear domains in somatic mouse cells', *Biol Cell,* 91(1), pp. 55-65.

Chadwick, B. P. (2008) 'DXZ4 chromatin adopts an opposing conformation to that of the surrounding chromosome and acquires a novel inactive X-specific role involving CTCF and antisense transcripts', *Genome Res,* 18(8), pp. 1259-69.

Chaumeil, J., Le Baccon, P., Wutz, A. and Heard, E. (2006) 'A novel role for Xist RNA in the formation of a repressive nuclear compartment into which genes are recruited when silenced', *Genes Dev,* 20(16), pp. 2223-37.

Chaumeil, J., Okamoto, I., Guggiari, M. and Heard, E. (2002) 'Integrated kinetics of X chromosome inactivation in differentiating embryonic stem cells', *Cytogenet Genome Res,* 99(1-4), pp. 75-84.

Chen, C. K., Blanco, M., Jackson, C., Aznauryan, E., Ollikainen, N., Surka, C., Chow, A., Cerase, A., McDonel, P. and Guttman, M. (2016a) 'Xist recruits the X chromosome to the nuclear lamina to enable chromosome-wide silencing', *Science,* 354(6311), pp. 468-472.

Chen, Y., Wang, Y., Xuan, Z., Chen, M. and Zhang, M. Q. (2016b) 'De novo deciphering three-dimensional chromatin interaction and topological domains by wavelet transformation of epigenetic profiles', *Nucleic Acids Res,* 44(11), pp. e106.

Chen, Z., Hagen, D. E., Wang, J., Elsik, C. G., Ji, T., Siqueira, L. G., Hansen, P. J. and Rivera, R. M. (2016c) 'Global assessment of imprinted gene expression in the bovine conceptus by next generation sequencing', *Epigenetics,* 11(7), pp. 501-16.

Chiba, H., Hirasawa, R., Kaneda, M., Amakawa, Y., Li, E., Sado, T. and Sasaki, H. (2008) 'De novo DNA methylation independent establishment of maternal imprint on X chromosome in mouse oocytes', *Genesis,* 46(12), pp. 768-74.

Chow, J. and Heard, E. (2009) 'X inactivation and the complexities of silencing a sex chromosome', *Curr Opin Cell Biol,* 21(3), pp. 359-66.

Chow, J. C., Ciaudo, C., Fazzari, M. J., Mise, N., Servant, N., Glass, J. L., Attreed, M., Avner, P., Wutz, A., Barillot, E., Greally, J. M., Voinnet, O. and Heard, E. (2010) 'LINE-1 activity in facultative heterochromatin formation during X chromosome inactivation', *Cell,* 141(6), pp. 956-69.

Christians, E., Davis, A. A., Thomas, S. D. and Benjamin, I. J. (2000) 'Maternal effect of Hsf1 on reproductive success', *Nature,* 407(6805), pp. 693-4.

Chu, C., Zhang, Q. C., da Rocha, S. T., Flynn, R. A., Bharadwaj, M., Calabrese, J. M., Magnuson, T., Heard, E. and Chang, H. Y. (2015) 'Systematic discovery of Xist RNA binding proteins', *Cell,* 161(2), pp. 404-16.

Cirillo, L. A., Lin, F. R., Cuesta, I., Friedman, D., Jarnik, M. and Zaret, K. S. (2002) 'Opening of compacted chromatin by early developmental transcription factors HNF3 (FoxA) and GATA-4', *Mol Cell,* 9(2), pp. 279-89.

Clemson, C. M., Hall, L. L., Byron, M., McNeil, J. and Lawrence, J. B. (2006) 'The X chromosome is organized into a gene-rich outer rim and an internal core containing silenced nongenic sequences', *Proc Natl Acad Sci U S A,* 103(20), pp. 7688-93.

Clemson, C. M., McNeil, J. A., Willard, H. F. and Lawrence, J. B. (1996) 'XIST RNA paints the inactive X chromosome at interphase: evidence for a novel RNA involved in nuclear/chromosome structure', *J Cell Biol,* 132(3), pp. 259-75.

Cohen, H. R., Royce-Tolland, M. E., Worringer, K. A. and Panning, B. (2005) 'Chromatin modifications on the inactive X chromosome', *Prog Mol Subcell Biol,* 38, pp. 91-122.

Cooper, S., Grijzenhout, A., Underwood, E., Ancelin, K., Zhang, T., Nesterova, T. B., Anil-Kirmizitas, B., Bassett, A., Kooistra, S. M., Agger, K., Helin, K., Heard, E. and Brockdorff, N. (2016) 'Jarid2 binds mono-ubiquitylated H2A lysine 119 to mediate crosstalk between Polycomb complexes PRC1 and PRC2', *Nat Commun,* 7, pp. 13661.

Costanzi, C., Stein, P., Worrad, D. M., Schultz, R. M. and Pehrson, J. R. (2000) 'Histone macroH2A1 is concentrated in the inactive X chromosome of female preimplantation mouse embryos', *Development,* 127(11), pp. 2283-9.

Crane, E., Bian, Q., McCord, R. P., Lajoie, B. R., Wheeler, B. S., Ralston, E. J., Uzawa, S., Dekker, J. and Meyer, B. J. (2015) 'Condensin-driven remodelling of X chromosome topology during dosage compensation', *Nature,* 523(7559), pp. 240-4.

Cremer, M., von Hase, J., Volm, T., Brero, A., Kreth, G., Walter, J., Fischer, C., Solovei, I., Cremer, C. and Cremer, T. (2001) 'Non-random radial higher-order chromatin arrangements in nuclei of diploid human cells', *Chromosome Res,* 9(7), pp. 541-67.

Cremer, T. and Cremer, C. (2006) 'Rise, fall and resurrection of chromosome territories: a historical perspective. Part I. The rise of chromosome territories', *Eur J Histochem,* 50(3), pp. 161-76.

Criscione, S. W., De Cecco, M., Siranosian, B., Zhang, Y., Kreiling, J. A., Sedivy, J. M. and Neretti, N. (2016) 'Reorganization of chromosome architecture in replicative cellular senescence', *Sci Adv,* 2(2), pp. e1500882.

Croft, J. A., Bridger, J. M., Boyle, S., Perry, P., Teague, P. and Bickmore, W. A. (1999) 'Differences in the localization and morphology of chromosomes in the human nucleus', *J Cell Biol,* 145(6), pp. 1119-31.

Csankovszki, G., McDonel, P. and Meyer, B. J. (2004) 'Recruitment and spreading of the C. elegans dosage compensation complex along X chromosomes', *Science,* 303(5661), pp. 1182-5.

Csankovszki, G., Nagy, A. and Jaenisch, R. (2001) 'Synergism of Xist RNA, DNA methylation, and histone hypoacetylation in maintaining X chromosome inactivation', *J Cell Biol,* 153(4), pp. 773-84.

Csankovszki, G., Panning, B., Bates, B., Pehrson, J. R. and Jaenisch, R. (1999) 'Conditional deletion of Xist disrupts histone macroH2A localization but not maintenance of X inactivation', *Nat Genet,* 22(4), pp. 323-4.

da Rocha, S. T., Boeva, V., Escamilla-Del-Arenal, M., Ancelin, K., Granier, C., Matias, N. R., Sanulli, S., Chow, J., Schulz, E., Picard, C., Kaneko, S., Helin, K., Reinberg, D., Stewart, A. F., Wutz, A., Margueron, R. and Heard, E. (2014) 'Jarid2 Is Implicated in the Initial Xist-Induced Targeting of PRC2 to the Inactive X Chromosome', *Mol Cell,* 53(2), pp. 301-16.

Dahl, J. A., Jung, I., Aanes, H., Greggains, G. D., Manaf, A., Lerdrup, M., Li, G., Kuan, S., Li, B., Lee, A. Y., Preissl, S., Jermstad, I., Haugen, M. H., Suganthan, R., Bjørås, M., Hansen, K., Dalen, K. T., Fedorcsak, P., Ren, B. and Klungland, A. (2016) 'Broad histone H3K4me3 domains in mouse oocytes modulate maternal-to-zygotic transition', *Nature,* 537(7621), pp. 548-552.

Darrow, E. M., Huntley, M. H., Dudchenko, O., Stamenova, E. K., Durand, N. C., Sun, Z., Huang, S. C., Sanborn, A. L., Machol, I., Shamim, M., Seberg, A. P., Lander, E. S., Chadwick, B. P. and Aiden, E. L. (2016) 'Deletion of DXZ4 on the human inactive X chromosome alters higher-order genome architecture', *Proc Natl Acad Sci U S A,* 113(31), pp. E4504-12.

DAVIDSON, R. G., NITOWSKY, H. M. and CHILDS, B. (1963) 'DEMONSTRATION OF TWO POPULATIONS OF CELLS IN THE HUMAN FEMALE HETEROZYGOUS FOR GLUCOSE-6-PHOSPHATE DEHYDROGENASE VARIANTS', *Proc Natl Acad Sci U S A,* 50, pp. 481-5.

De Iaco, A., Planet, E., Coluccio, A., Verp, S., Duc, J. and Trono, D. (2017) 'DUX-family transcription factors regulate zygotic genome activation in placental mammals', *Nat Genet,* 49(6), pp. 941-945.

De La Fuente, R., Hahnel, A., Basrur, P. K. and King, W. A. (1999) 'X inactive-specific transcript (Xist) expression and X chromosome inactivation in the preattachment bovine embryo', *Biol Reprod,* 60(3), pp. 769-75.

De Renzis, S., Elemento, O., Tavazoie, S. and Wieschaus, E. F. (2007) 'Unmasking activation of the zygotic genome using chromosomal deletions in the Drosophila embryo', *PLoS Biol,* 5(5), pp. e117.

Deakin, J. E., Chaumeil, J., Hore, T. A. and Marshall Graves, J. A. (2009) 'Unravelling the evolutionary origins of X chromosome inactivation in mammals: insights from marsupials and monotremes', *Chromosome Res,* 17(5), pp. 671-85.

Deng, Q., Ramsköld, D., Reinius, B. and Sandberg, R. (2014) 'Single-cell RNA-seq reveals dynamic, random monoallelic gene expression in mammalian cells', *Science,* 343(6167), pp. 193-6.

Deng, X., Ma, W., Ramani, V., Hill, A., Yang, F., Ay, F., Berletch, J. B., Blau, C. A., Shendure, J., Duan, Z., Noble, W. S. and Disteche, C. M. (2015) 'Bipartite structure of the inactive mouse X chromosome', *Genome Biol,* 16, pp. 152.

Denker, A. and de Laat, W. (2016) 'The second decade of 3C technologies: detailed insights into nuclear organization', *Genes Dev,* 30(12), pp. 1357-82.

Disteche, C. M. and Berletch, J. B. (2015) 'X-chromosome inactivation and escape', *J Genet,* 94(4), pp. 591-9.

Dixon, J. R., Gorkin, D. U. and Ren, B. (2016) 'Chromatin Domains: The Unit of Chromosome Organization', *Mol Cell,* 62(5), pp. 668-80.

Dixon, J. R., Jung, I., Selvaraj, S., Shen, Y., Antosiewicz-Bourget, J. E., Lee, A. Y., Ye, Z., Kim, A., Rajagopal, N., Xie, W., Diao, Y., Liang, J., Zhao, H., Lobanenkov, V. V., Ecker, J. R., Thomson, J. A. and Ren, B. (2015) 'Chromatin architecture reorganization during stem cell differentiation', *Nature,* 518(7539), pp. 331-6.

Dixon, J. R., Selvaraj, S., Yue, F., Kim, A., Li, Y., Shen, Y., Hu, M., Liu, J. S. and Ren, B. (2012) 'Topological domains in mammalian genomes identified by analysis of chromatin interactions', *Nature,* 485(7398), pp. 376-80.

Du, Z., Zheng, H., Huang, B., Ma, R., Wu, J., Zhang, X., He, J., Xiang, Y., Wang, Q., Li, Y., Ma, J., Zhang, K., Wang, Y., Zhang, M. Q., Gao, J., Dixon, J. R., Wang, X., Zeng, J. and Xie, W. (2017) 'Allelic reprogramming of 3D chromatin architecture during early mammalian development', *Nature,* 547(7662), pp. 232-235.

Edgar, B. A., Weir, M. P., Schubiger, G. and Kornberg, T. (1986) 'Repression and turnover pattern fushi tarazu RNA in the early Drosophila embryo', *Cell,* 47(5), pp. 747-54.

Eils, R., Dietzel, S., Bertin, E., Schröck, E., Speicher, M. R., Ried, T., Robert-Nicoud, M., Cremer, C. and Cremer, T. (1996) 'Three-dimensional reconstruction of painted human interphase chromosomes: active and inactive X chromosome territories have similar volumes but differ in shape and surface structure', *J Cell Biol,* 135(6 Pt 1), pp. 1427-40.

Engreitz, J. M., Pandya-Jones, A., McDonel, P., Shishkin, A., Sirokman, K., Surka, C., Kadri, S., Xing, J., Goren, A., Lander, E. S., Plath, K. and Guttman, M. (2013) 'The Xist lncRNA exploits three-dimensional genome architecture to spread across the X chromosome', *Science,* 341(6147), pp. 1237973.

Fabre, P. J., Benke, A., Manley, S. and Duboule, D. (2015) 'Visualizing the HoxD Gene Cluster at the Nanoscale Level', *Cold Spring Harb Symp Quant Biol,* 80, pp. 9-16.

Fadloun, A., Le Gras, S., Jost, B., Ziegler-Birling, C., Takahashi, H., Gorab, E., Carninci, P. and Torres-Padilla, M. E. (2013) 'Chromatin signatures and retrotransposon profiling in mouse embryos reveal regulation of LINE-1 by RNA', *Nat Struct Mol Biol,* 20(3), pp. 332-8.

Ferrari, F., Alekseyenko, A. A., Park, P. J. and Kuroda, M. I. (2014) 'Transcriptional control of a whole chromosome: emerging models for dosage compensation', *Nat Struct Mol Biol,* 21(2), pp. 118-25.

Flach, G., Johnson, M. H., Braude, P. R., Taylor, R. A. and Bolton, V. N. (1982) 'The transition from maternal to embryonic control in the 2-cell mouse embryo', *EMBO J,* 1(6), pp. 681-6.

Flavahan, W. A., Drier, Y., Liau, B. B., Gillespie, S. M., Venteicher, A. S., Stemmer-Rachamimov, A. O., Suvà, M. L. and Bernstein, B. E. (2016) 'Insulator dysfunction and oncogene activation in IDH mutant gliomas', *Nature,* 529(7584), pp. 110-4.

Flyamer, I. M., Gassler, J., Imakaev, M., Brandão, H. B., Ulianov, S. V., Abdennur, N., Razin, S. V., Mirny, L. A. and Tachibana-Konwalski, K. (2017) 'Single-nucleus Hi-C reveals unique chromatin reorganization at oocyte-to-zygote transition', *Nature,* 544(7648), pp. 110-114.

Fortin, J. P. and Hansen, K. D. (2015) 'Reconstructing A/B compartments as revealed by Hi-C using long-range correlations in epigenetic data', *Genome Biol,* 16, pp. 180.

Foygel, K., Choi, B., Jun, S., Leong, D. E., Lee, A., Wong, C. C., Zuo, E., Eckart, M., Reijo Pera, R. A., Wong, W. H. and Yao, M. W. (2008) 'A novel and critical role for Oct4 as a regulator of the maternal-embryonic transition', *PLoS One,* 3(12), pp. e4109.

Franke, M., Ibrahim, D. M., Andrey, G., Schwarzer, W., Heinrich, V., Schöpflin, R., Kraft, K., Kempfer, R., Jerković, I., Chan, W. L., Spielmann, M., Timmermann, B., Wittler, L., Kurth, I., Cambiaso, P., Zuffardi, O., Houge, G., Lambie, L., Brancati, F., Pombo, A., Vingron, M., Spitz, F. and Mundlos, S. (2016) 'Formation of new chromatin domains determines pathogenicity of genomic duplications', *Nature,* 538(7624), pp. 265-269.

Fudenberg, G. and Imakaev, M. (2017) 'FISH-ing for captured contacts: towards reconciling FISH and 3C', *Nat Methods,* 14(7), pp. 673-678.

Fukuda, A., Mitani, A., Miyashita, T., Sado, T., Umezawa, A. and Akutsu, H. (2016) 'Maintenance of Xist Imprinting Depends on Chromatin Condensation State and Rnf12 Dosage in Mice', *PLoS Genet,* 12(10), pp. e1006375.

Fukuda, A., Tomikawa, J., Miura, T., Hata, K., Nakabayashi, K., Eggan, K., Akutsu, H. and Umezawa, A. (2014) 'The role of maternal-specific H3K9me3 modification in establishing imprinted X-chromosome inactivation and embryogenesis in mice', *Nat Commun,* 5, pp. 5464.

Fulka, H. and Langerova, A. (2014) 'The maternal nucleolus plays a key role in centromere satellite maintenance during the oocyte to embryo transition', *Development,* 141(8), pp. 1694-704.

Galupa, R. and Heard, E. (2015) 'X-chromosome inactivation: new insights into cis and trans regulation', *Curr Opin Genet Dev,* 31, pp. 57-66.

Gartler, S. M. and Riggs, A. D. (1983) 'Mammalian X-chromosome inactivation', *Annu Rev Genet,* 17, pp. 155-90.

Gendrel, A. V. and Heard, E. (2014) 'Noncoding RNAs and epigenetic mechanisms during X-chromosome inactivation', *Annu Rev Cell Dev Biol,* 30, pp. 561-80.

Giacalone, J., Friedes, J. and Francke, U. (1992) 'A novel GC-rich human macrosatellite VNTR in Xq24 is differentially methylated on active and inactive X chromosomes', *Nat Genet,* 1(2), pp. 137-43.

Giorgetti, L., Galupa, R., Nora, E. P., Piolot, T., Lam, F., Dekker, J., Tiana, G. and Heard, E. (2014) 'Predictive polymer modeling reveals coupled fluctuations in chromosome conformation and transcription', *Cell,* 157(4), pp. 950-63.

Giorgetti, L. and Heard, E. (2016) 'Closing the loop: 3C versus DNA FISH', *Genome Biol,* 17(1), pp. 215.

Giorgetti, L., Lajoie, B. R., Carter, A. C., Attia, M., Zhan, Y., Xu, J., Chen, C. J., Kaplan, N., Chang, H. Y., Heard, E. and Dekker, J. (2016) 'Structural organization of the inactive X chromosome in the mouse', *Nature,* 535(7613), pp. 575-9.

Giorgio, E., Robyr, D., Spielmann, M., Ferrero, E., Di Gregorio, E., Imperiale, D., Vaula, G., Stamoulis, G., Santoni, F., Atzori, C., Gasparini, L., Ferrera, D., Canale, C., Guipponi, M., Pennacchio, L. A., Antonarakis, S. E., Brussino, A. and Brusco, A. (2015) 'A large genomic deletion leads to enhancer adoption by the lamin B1 gene: a second path to autosomal dominant adult-onset demyelinating leukodystrophy (ADLD)', *Hum Mol Genet,* 24(11), pp. 3143-54.

Golbus, M. S., Calarco, P. G. and Epstein, C. J. (1973) 'The effects of inhibitors of RNA synthesis (alpha-amanitin and actinomycin D) on preimplantation mouse embryogenesis', *J Exp Zool,* 186(2), pp. 207-16.

Gontan, C., Achame, E. M., Demmers, J., Barakat, T. S., Rentmeester, E., van IJcken, W., Grootegoed, J. A. and Gribnau, J. (2012) 'RNF12 initiates X-chromosome inactivation by targeting REX1 for degradation', *Nature,* 485(7398), pp. 386-90.

Grant, J., Mahadevaiah, S. K., Khil, P., Sangrithi, M. N., Royo, H., Duckworth, J., McCarrey, J. R., VandeBerg, J. L., Renfree, M. B., Taylor, W., Elgar, G., Camerini-Otero, R. D., Gilchrist, M. J. and Turner, J. M. (2012) 'Rsx is a metatherian RNA with Xist-like properties in X-chromosome inactivation', *Nature,* 487(7406), pp. 254-8.

Gröschel, S., Sanders, M. A., Hoogenboezem, R., de Wit, E., Bouwman, B. A. M., Erpelinck, C., van der Velden, V. H. J., Havermans, M., Avellino, R., van Lom, K., Rombouts, E. J., van Duin, M., Döhner, K., Beverloo, H. B., Bradner, J. E., Döhner, H., Löwenberg, B., Valk, P. J. M., Bindels, E. M. J., de Laat, W. and Delwel, R. (2014) 'A single oncogenic enhancer rearrangement causes concomitant EVI1 and GATA2 deregulation in leukemia', *Cell,* 157(2), pp. 369-381.

Guo, F., Li, X., Liang, D., Li, T., Zhu, P., Guo, H., Wu, X., Wen, L., Gu, T. P., Hu, B., Walsh, C. P., Li, J., Tang, F. and Xu, G. L. (2014) 'Active and passive demethylation of male and female pronuclear DNA in the mammalian zygote', *Cell Stem Cell,* 15(4), pp. 447-459.

Gómez-Marín, C., Tena, J. J., Acemel, R. D., López-Mayorga, M., Naranjo, S., de la Calle-Mustienes, E., Maeso, I., Beccari, L., Aneas, I., Vielmas, E., Bovolenta, P., Nobrega, M. A., Carvajal, J. and Gómez-Skarmeta, J. L. (2015) 'Evolutionary comparison reveals that diverging CTCF sites are signatures of ancestral topological associating domains borders', *Proc Natl Acad Sci U S A,* 112(24), pp. 7542-7.

Haarhuis, J. H. I., van der Weide, R. H., Blomen, V. A., Yáñez-Cuna, J. O., Amendola, M., van Ruiten, M. S., Krijger, P. H. L., Teunissen, H., Medema, R. H., van Steensel, B., Brummelkamp, T. R., de Wit, E. and Rowland, B. D. (2017) 'The Cohesin Release Factor WAPL Restricts Chromatin Loop Extension', *Cell,* 169(4), pp. 693-707.e14.

Haberle, V., Li, N., Hadzhiev, Y., Plessy, C., Previti, C., Nepal, C., Gehrig, J., Dong, X., Akalin, A., Suzuki, A. M., van IJcken, W. F. J., Armant, O., Ferg, M., Strähle, U., Carninci, P., Müller, F. and Lenhard, B. (2014) 'Two independent transcription initiation codes overlap on vertebrate core promoters', *Nature,* 507(7492), pp. 381-385.

Hamatani, T., Carter, M. G., Sharov, A. A. and Ko, M. S. (2004) 'Dynamics of global gene expression changes during mouse preimplantation development', *Dev Cell,* 6(1), pp. 117-31.

Hasegawa, Y., Brockdorff, N., Kawano, S., Tsutui, K. and Nakagawa, S. (2010) 'The matrix protein hnRNP U is required for chromosomal localization of Xist RNA', *Dev Cell,* 19(3), pp. 469-76.

Heard, E., Rougeulle, C., Arnaud, D., Avner, P., Allis, C. D. and Spector, D. L. (2001) 'Methylation of histone H3 at Lys-9 is an early mark on the X chromosome during X inactivation', *Cell,* 107(6), pp. 727-38.

Hendrickson, P. G., Doráis, J. A., Grow, E. J., Whiddon, J. L., Lim, J. W., Wike, C. L., Weaver, B. D., Pflueger, C., Emery, B. R., Wilcox, A. L., Nix, D. A., Peterson, C. M., Tapscott, S. J., Carrell, D. T. and Cairns, B. R. (2017) 'Conserved roles of mouse DUX and human DUX4 in activating cleavage-stage genes and MERVL/HERVL retrotransposons', *Nat Genet,* 49(6), pp. 925-934.

Heyn, P., Kircher, M., Dahl, A., Kelso, J., Tomancak, P., Kalinka, A. T. and Neugebauer, K. M. (2014) 'The earliest transcribed zygotic genes are short, newly evolved, and different across species', *Cell Rep,* 6(2), pp. 285-92.

Hnisz, D., Weintraub, A. S., Day, D. S., Valton, A. L., Bak, R. O., Li, C. H., Goldmann, J., Lajoie, B. R., Fan, Z. P., Sigova, A. A., Reddy, J., Borges-Rivera, D., Lee, T. I., Jaenisch, R., Porteus, M. H., Dekker, J. and Young, R. A. (2016) 'Activation of proto-oncogenes by disruption of chromosome neighborhoods', *Science,* 351(6280), pp. 1454-1458.

Huang, J., Marco, E., Pinello, L. and Yuan, G. C. (2015) 'Predicting chromatin organization using histone marks', *Genome Biol,* 16, pp. 162.

Hug, C. B., Grimaldi, A. G., Kruse, K. and Vaquerizas, J. M. (2017) 'Chromatin Architecture Emerges during Zygotic Genome Activation Independent of Transcription', *Cell,* 169(2), pp. 216-228.e19.

Huynh, K. D. and Lee, J. T. (2003) 'Inheritance of a pre-inactivated paternal X chromosome in early mouse embryos', *Nature,* 426(6968), pp. 857-62.

Hwang, J. Y., Oh, J. N., Park, C. H., Lee, D. K. and Lee, C. K. (2015) 'Dosage compensation of X-chromosome inactivation center-linked genes in porcine preimplantation embryos: Non-chromosome-wide initiation of X-chromosome inactivation in blastocysts', *Mech Dev,* 138 Pt 3, pp. 246-55.

Ibn-Salem, J., Köhler, S., Love, M. I., Chung, H. R., Huang, N., Hurles, M. E., Haendel, M., Washington, N. L., Smedley, D., Mungall, C. J., Lewis, S. E., Ott, C. E., Bauer, S., Schofield, P. N., Mundlos, S., Spielmann, M. and Robinson, P. N. (2014) 'Deletions of chromosomal regulatory boundaries are associated with congenital disease', *Genome Biol,* 15(9), pp. 423.

Inoue, A., Jiang, L., Lu, F., Suzuki, T. and Zhang, Y. (2017) 'Maternal H3K27me3 controls DNA methylation-independent imprinting', *Nature,* 547(7664), pp. 419-424.

Ishiuchi, T., Enriquez-Gasca, R., Mizutani, E., Bošković, A., Ziegler-Birling, C., Rodriguez-Terrones, D., Wakayama, T., Vaquerizas, J. M. and Torres-Padilla, M. E. (2015) 'Early embryonic-like cells are induced by downregulating replication-dependent chromatin assembly', *Nat Struct Mol Biol,* 22(9), pp. 662-71.

Jachowicz, J. W., Bing, X., Pontabry, J., Bošković, A., Rando, O. J. and Torres-Padilla, M. E. (2017) 'LINE-1 activation after fertilization regulates global chromatin accessibility in the early mouse embryo', *Nat Genet,* 49(10), pp. 1502-1510.

John, S., Sabo, P. J., Canfield, T. K., Lee, K., Vong, S., Weaver, M., Wang, H., Vierstra, J., Reynolds, A. P., Thurman, R. E. and Stamatoyannopoulos, J. A. (2013) 'Genome-scale mapping of DNase I hypersensitivity', *Curr Protoc Mol Biol,* Chapter 27, pp. Unit 21.27.

Johnson, M. H., Maro, B. and Takeichi, M. (1986) 'The role of cell adhesion in the synchronization and orientation of polarization in 8-cell mouse blastomeres', *J Embryol Exp Morphol,* 93, pp. 239-55.

Jonkers, I., Barakat, T. S., Achame, E. M., Monkhorst, K., Kenter, A., Rentmeester, E., Grosveld, F., Grootegoed, J. A. and Gribnau, J. (2009) 'RNF12 is an X-Encoded dose-dependent activator of X chromosome inactivation', *Cell,* 139(5), pp. 999-1011.

Jukam, D., Shariati, S. A. M. and Skotheim, J. M. (2017) 'Zygotic Genome Activation in Vertebrates', *Dev Cell,* 42(4), pp. 316-332.

Jung, Y. H., Sauria, M. E. G., Lyu, X., Cheema, M. S., Ausio, J., Taylor, J. and Corces, V. G. (2017) 'Chromatin States in Mouse Sperm Correlate with Embryonic and Adult Regulatory Landscapes', *Cell Rep,* 18(6), pp. 1366-1382.

Kageyama, S., Nagata, M. and Aoki, F. (2004) 'Isolation of nascent messenger RNA from mouse preimplantation embryos', *Biol Reprod,* 71(6), pp. 1948-55.

Kaiser, V. B., Taylor, M. S. and Semple, C. A. (2016) 'Mutational Biases Drive Elevated Rates of Substitution at Regulatory Sites across Cancer Types', *PLoS Genet,* 12(8), pp. e1006207.

Kalantry, S., Purushothaman, S., Bowen, R. B., Starmer, J. and Magnuson, T. (2009) 'Evidence of Xist RNA-independent initiation of mouse imprinted X-chromosome inactivation', *Nature,* 460(7255), pp. 647-51.

Kane, D. A., Hammerschmidt, M., Mullins, M. C., Maischein, H. M., Brand, M., van Eeden, F. J., Furutani-Seiki, M., Granato, M., Haffter, P., Heisenberg, C. P., Jiang, Y. J., Kelsh, R. N., Odenthal, J., Warga, R. M. and Nüsslein-Volhard, C. (1996) 'The zebrafish epiboly mutants', *Development,* 123, pp. 47-55.

Kano, H., Godoy, I., Courtney, C., Vetter, M. R., Gerton, G. L., Ostertag, E. M. and Kazazian, H. H. (2009) 'L1 retrotransposition occurs mainly in embryogenesis and creates somatic mosaicism', *Genes Dev,* 23(11), pp. 1303-12.

Katainen, R., Dave, K., Pitkänen, E., Palin, K., Kivioja, T., Välimäki, N., Gylfe, A. E., Ristolainen, H., Hänninen, U. A., Cajuso, T., Kondelin, J., Tanskanen, T., Mecklin, J. P., Järvinen, H., Renkonen-Sinisalo, L., Lepistö, A., Kaasinen, E., Kilpivaara, O., Tuupanen, S., Enge, M., Taipale, J. and Aaltonen, L. A. (2015) 'CTCF/cohesin-binding sites are frequently mutated in cancer', *Nat Genet,* 47(7), pp. 818-21.

Kay, G. F., Barton, S. C., Surani, M. A. and Rastan, S. (1994) 'Imprinting and X chromosome counting mechanisms determine Xist expression in early mouse development', *Cell,* 77(5), pp. 639-50.

Kay, G. F., Penny, G. D., Patel, D., Ashworth, A., Brockdorff, N. and Rastan, S. (1993) 'Expression of Xist during mouse development suggests a role in the initiation of X chromosome inactivation', *Cell,* 72(2), pp. 171-82.

Ke, Y., Xu, Y., Chen, X., Feng, S., Liu, Z., Sun, Y., Yao, X., Li, F., Zhu, W., Gao, L., Chen, H., Du, Z., Xie, W., Xu, X., Huang, X. and Liu, J. (2017) '3D Chromatin Structures of Mature Gametes and Structural Reprogramming during Mammalian Embryogenesis', *Cell,* 170(2), pp. 367-381.e20.

Kelly, S. J. (1977) 'Studies of the developmental potential of 4- and 8-cell stage mouse blastomeres', *J Exp Zool,* 200(3), pp. 365-76.

Kelly, S. J., Mulnard, J. G. and Graham, C. F. (1978) 'Cell division and cell allocation in early mouse development', *J Embryol Exp Morphol,* 48, pp. 37-51.

Keohane, A. M., O'neill, L. P., Belyaev, N. D., Lavender, J. S. and Turner, B. M. (1996) 'X-Inactivation and histone H4 acetylation in embryonic stem cells', *Dev Biol,* 180(2), pp. 618-30.

Kidder, G. M. and McLachlin, J. R. (1985) 'Timing of transcription and protein synthesis underlying morphogenesis in preimplantation mouse embryos', *Dev Biol,* 112(2), pp. 265-75.

Kigami, D., Minami, N., Takayama, H. and Imai, H. (2003) 'MuERV-L is one of the earliest transcribed genes in mouse one-cell embryos', *Biol Reprod,* 68(2), pp. 651-4.

Kind, J., Pagie, L., de Vries, S. S., Nahidiazar, L., Dey, S. S., Bienko, M., Zhan, Y., Lajoie, B., de Graaf, C. A., Amendola, M., Fudenberg, G., Imakaev, M., Mirny, L. A., Jalink, K., Dekker, J., van Oudenaarden, A. and van Steensel, B. (2015) 'Genome-wide maps of nuclear lamina interactions in single human cells', *Cell,* 163(1), pp. 134-47.

KLINGER, H. P. (1958) 'The fine structure of the sex chromatin body', *Exp Cell Res,* 14(1), pp. 207-11.

Koehler, D., Zakhartchenko, V., Froenicke, L., Stone, G., Stanyon, R., Wolf, E., Cremer, T. and Brero, A. (2009) 'Changes of higher order chromatin arrangements during major genome activation in bovine preimplantation embryos', *Exp Cell Res,* 315(12), pp. 2053-63.

Koehler, D., Zakhartchenko, V., Ketterl, N., Wolf, E., Cremer, T. and Brero, A. (2010) 'FISH on 3D preserved bovine and murine preimplantation embryos', *Methods Mol Biol,* 659, pp. 437-45.

Kyogoku, H., Fulka, J., Wakayama, T. and Miyano, T. (2014) 'De novo formation of nucleoli in developing mouse embryos originating from enucleolated zygotes', *Development,* 141(11), pp. 2255-9.

Latham, K. E., Solter, D. and Schultz, R. M. (1992) 'Acquisition of a transcriptionally permissive state during the 1-cell stage of mouse embryogenesis', *Dev Biol,* 149(2), pp. 457-62.

Le Dily, F., Baù, D., Pohl, A., Vicent, G. P., Serra, F., Soronellas, D., Castellano, G., Wright, R. H., Ballare, C., Filion, G., Marti-Renom, M. A. and Beato, M. (2014) 'Distinct structural transitions of chromatin topological domains correlate with coordinated hormone-induced gene regulation', *Genes Dev,* 28(19), pp. 2151-62.

Le, T. B., Imakaev, M. V., Mirny, L. A. and Laub, M. T. (2013) 'High-resolution mapping of the spatial organization of a bacterial chromosome', *Science,* 342(6159), pp. 731-4.

Lee, J. T., Davidow, L. S. and Warshawsky, D. (1999) 'Tsix, a gene antisense to Xist at the X-inactivation centre', *Nat Genet,* 21(4), pp. 400-4.

Lee, J. T. and Lu, N. (1999) 'Targeted mutagenesis of Tsix leads to nonrandom X inactivation', *Cell,* 99(1), pp. 47-57.

Lee, M. T., Bonneau, A. R. and Giraldez, A. J. (2014) 'Zygotic genome activation during the maternal-to-zygotic transition', *Annu Rev Cell Dev Biol,* 30, pp. 581-613.

Lee, M. T., Bonneau, A. R., Takacs, C. M., Bazzini, A. A., DiVito, K. R., Fleming, E. S. and Giraldez, A. J. (2013) 'Nanog, Pou5f1 and SoxB1 activate zygotic gene expression during the maternal-to-zygotic transition', *Nature,* 503(7476), pp. 360-4.

Lepikhov, K. and Walter, J. (2004) 'Differential dynamics of histone H3 methylation at positions K4 and K9 in the mouse zygote', *BMC Dev Biol,* 4, pp. 12.

Lettice, L. A., Heaney, S. J., Purdie, L. A., Li, L., de Beer, P., Oostra, B. A., Goode, D., Elgar, G., Hill, R. E. and de Graaff, E. (2003) 'A long-range Shh enhancer regulates expression in the developing limb and fin and is associated with preaxial polydactyly', *Hum Mol Genet,* 12(14), pp. 1725-35.

Liang, H. L., Nien, C. Y., Liu, H. Y., Metzstein, M. M., Kirov, N. and Rushlow, C. (2008) 'The zinc-finger protein Zelda is a key activator of the early zygotic genome in Drosophila', *Nature,* 456(7220), pp. 400-3.

Lieberman-Aiden, E., van Berkum, N. L., Williams, L., Imakaev, M., Ragoczy, T., Telling, A., Amit, I., Lajoie, B. R., Sabo, P. J., Dorschner, M. O., Sandstrom, R., Bernstein, B., Bender, M. A., Groudine, M., Gnirke, A., Stamatoyannopoulos, J., Mirny, L. A., Lander, E. S. and Dekker, J. (2009) 'Comprehensive mapping of long-range interactions reveals folding principles of the human genome', *Science,* 326(5950), pp. 289-93.

Liu, X., Wang, C., Liu, W., Li, J., Li, C., Kou, X., Chen, J., Zhao, Y., Gao, H., Wang, H., Zhang, Y., Gao, Y. and Gao, S. (2016a) 'Distinct features of H3K4me3 and H3K27me3 chromatin domains in pre-implantation embryos', *Nature,* 537(7621), pp. 558-562.

Liu, Y., Lu, X., Shi, J., Yu, X., Zhang, X., Zhu, K., Yi, Z., Duan, E. and Li, L. (2016b) 'BTG4 is a key regulator for maternal mRNA clearance during mouse early embryogenesis', *J Mol Cell Biol,* 8(4), pp. 366-8.

Lonfat, N. and Duboule, D. (2015) 'Structure, function and evolution of topologically associating domains (TADs) at HOX loci', *FEBS Lett,* 589(20 Pt A), pp. 2869-76.

Lu, F., Liu, Y., Inoue, A., Suzuki, T., Zhao, K. and Zhang, Y. (2016) 'Establishing Chromatin Regulatory Landscape during Mouse Preimplantation Development', *Cell,* 165(6), pp. 1375-88.

Lupiáñez, D. G., Kraft, K., Heinrich, V., Krawitz, P., Brancati, F., Klopocki, E., Horn, D., Kayserili, H., Opitz, J. M., Laxova, R., Santos-Simarro, F., Gilbert-Dussardier, B., Wittler, L., Borschiwer, M., Haas, S. A., Osterwalder, M., Franke, M., Timmermann, B., Hecht, J., Spielmann, M., Visel, A. and Mundlos, S. (2015) 'Disruptions of

topological chromatin domains cause pathogenic rewiring of gene-enhancer interactions', *Cell,* 161(5), pp. 1012-1025.

LYON, M. F. (1961) 'Gene action in the X-chromosome of the mouse (Mus musculus L.)', *Nature,* 190, pp. 372-3.

Lyon, M. F. (2006) 'Do LINEs have a role in X-chromosome inactivation?', *J Biomed Biotechnol,* 2006(1), pp. 59746.

Macfarlan, T. S., Gifford, W. D., Driscoll, S., Lettieri, K., Rowe, H. M., Bonanomi, D., Firth, A., Singer, O., Trono, D. and Pfaff, S. L. (2012) 'Embryonic stem cell potency fluctuates with endogenous retrovirus activity', *Nature,* 487(7405), pp. 57-63.

Mak, W., Nesterova, T. B., de Napoles, M., Appanah, R., Yamanaka, S., Otte, A. P. and Brockdorff, N. (2004) 'Reactivation of the paternal X chromosome in early mouse embryos', *Science,* 303(5658), pp. 666-9.

Marahrens, Y., Panning, B., Dausman, J., Strauss, W. and Jaenisch, R. (1997) 'Xist-deficient mice are defective in dosage compensation but not spermatogenesis', *Genes Dev,* 11(2), pp. 156-66.

Martin, C., Beaujean, N., Brochard, V., Audouard, C., Zink, D. and Debey, P. (2006) 'Genome restructuring in mouse embryos during reprogramming and early development', *Dev Biol,* 292(2), pp. 317-32.

Mayer, W., Niveleau, A., Walter, J., Fundele, R. and Haaf, T. (2000) 'Demethylation of the zygotic paternal genome', *Nature,* 403(6769), pp. 501-2.

McHugh, C. A., Chen, C. K., Chow, A., Surka, C. F., Tran, C., McDonel, P., Pandya-Jones, A., Blanco, M., Burghard, C., Moradian, A., Sweredoski, M. J., Shishkin, A. A., Su, J., Lander, E. S., Hess, S., Plath, K. and Guttman, M. (2015) 'The Xist lncRNA interacts directly with SHARP to silence transcription through HDAC3', *Nature,* 521(7551), pp. 232-6.

Meissner, A., Mikkelsen, T. S., Gu, H., Wernig, M., Hanna, J., Sivachenko, A., Zhang, X., Bernstein, B. E., Nusbaum, C., Jaffe, D. B., Gnirke, A., Jaenisch, R. and Lander, E. S. (2008) 'Genome-scale DNA methylation maps of pluripotent and differentiated cells', *Nature,* 454(7205), pp. 766-70.

Merkenschlager, M. and Nora, E. P. (2016) 'CTCF and Cohesin in Genome Folding and Transcriptional Gene Regulation', *Annu Rev Genomics Hum Genet,* 17, pp. 17-43.

Meyer, B. J. (2010) 'Targeting X chromosomes for repression', *Curr Opin Genet Dev,* 20(2), pp. 179-89.

Minajigi, A., Froberg, J., Wei, C., Sunwoo, H., Kesner, B., Colognori, D., Lessing, D., Payer, B., Boukhali, M., Haas, W. and Lee, J. T. (2015) 'Chromosomes. A comprehensive Xist interactome reveals cohesin repulsion and an RNA-directed chromosome conformation', *Science,* 349(6245).

Mizuguchi, T., Fudenberg, G., Mehta, S., Belton, J. M., Taneja, N., Folco, H. D., FitzGerald, P., Dekker, J., Mirny, L., Barrowman, J. and Grewal, S. I. S. (2014) 'Cohesin-dependent globules and heterochromatin shape 3D genome architecture in S. pombe', *Nature,* 516(7531), pp. 432-435.

Mohammed, H., Hernando-Herraez, I., Savino, A., Scialdone, A., Macaulay, I., Mulas, C., Chandra, T., Voet, T., Dean, W., Nichols, J., Marioni, J. C. and Reik, W. (2017)

'Single-Cell Landscape of Transcriptional Heterogeneity and Cell Fate Decisions during Mouse Early Gastrulation', *Cell Rep,* 20(5), pp. 1215-1228.

Montavon, T., Soshnikova, N., Mascrez, B., Joye, E., Thevenet, L., Splinter, E., de Laat, W., Spitz, F. and Duboule, D. (2011) 'A regulatory archipelago controls Hox genes transcription in digits', *Cell,* 147(5), pp. 1132-45.

Moreira de Mello, J. C., Fernandes, G. R., Vibranovski, M. D. and Pereira, L. V. (2017) 'Early X chromosome inactivation during human preimplantation development revealed by single-cell RNA-sequencing', *Sci Rep,* 7(1), pp. 10794.

Murchison, E. P., Stein, P., Xuan, Z., Pan, H., Zhang, M. Q., Schultz, R. M. and Hannon, G. J. (2007) 'Critical roles for Dicer in the female germline', *Genes Dev,* 21(6), pp. 682-93.

Nagano, T., Lubling, Y., Stevens, T. J., Schoenfelder, S., Yaffe, E., Dean, W., Laue, E. D., Tanay, A. and Fraser, P. (2013) 'Single-cell Hi-C reveals cell-to-cell variability in chromosome structure', *Nature,* 502(7469), pp. 59-64.

Nagano, T., Lubling, Y., Várnai, C., Dudley, C., Leung, W., Baran, Y., Mendelson Cohen, N., Wingett, S., Fraser, P. and Tanay, A. (2017) 'Cell-cycle dynamics of chromosomal organization at single-cell resolution', *Nature,* 547(7661), pp. 61-67.

Naito, E., Dewa, K., Yamanouchi, H. and Kominami, R. (1994) 'Sex typing of forensic DNA samples using male- and female-specific probes', *J Forensic Sci,* 39(4), pp. 1009-17.

Naito, E., Dewa, K., Yamanouchi, H., Takagi, S. and Kominami, R. (1993) 'Sex determination using the hypomethylation of a human macro-satellite DXZ4 in female cells', *Nucleic Acids Res,* 21(10), pp. 2533-4.

Namekawa, S. H., Payer, B., Huynh, K. D., Jaenisch, R. and Lee, J. T. (2010) 'Two-step imprinted X inactivation: repeat versus genic silencing in the mouse', *Mol Cell Biol,* 30(13), pp. 3187-205.

Naumova, N., Imakaev, M., Fudenberg, G., Zhan, Y., Lajoie, B. R., Mirny, L. A. and Dekker, J. (2013) 'Organization of the mitotic chromosome', *Science,* 342(6161), pp. 948-53.

Nesterova, T. B., Slobodyanyuk, S. Y., Elisaphenko, E. A., Shevchenko, A. I., Johnston, C., Pavlova, M. E., Rogozin, I. B., Kolesnikov, N. N., Brockdorff, N. and Zakian, S. M. (2001) 'Characterization of the genomic Xist locus in rodents reveals conservation of overall gene structure and tandem repeats but rapid evolution of unique sequence', *Genome Res,* 11(5), pp. 833-49.

Ni, Y., Cao, B., Ma, T., Niu, G., Huo, Y., Huang, J., Chen, D., Liu, Y., Yu, B., Zhang, M. Q. and Niu, H. (2017) 'Super-resolution imaging of a 2.5 kb non-repetitive DNA in situ in the nuclear genome using molecular beacon probes', *Elife,* 6.

Noordermeer, D. and Duboule, D. (2013) 'Chromatin architectures and Hox gene collinearity', *Curr Top Dev Biol,* 104, pp. 113-48.

Nora, E. P., Dekker, J. and Heard, E. (2013) 'Segmental folding of chromosomes: a basis for structural and regulatory chromosomal neighborhoods?', *Bioessays,* 35(9), pp. 818-28.

Nora, E. P., Goloborodko, A., Valton, A. L., Gibcus, J. H., Uebersohn, A., Abdennur, N., Dekker, J., Mirny, L. A. and Bruneau, B. G. (2017) 'Targeted Degradation of CTCF

Decouples Local Insulation of Chromosome Domains from Genomic Compartmentalization', *Cell,* 169(5), pp. 930-944.e22.

Nora, E. P., Lajoie, B. R., Schulz, E. G., Giorgetti, L., Okamoto, I., Servant, N., Piolot, T., van Berkum, N. L., Meisig, J., Sedat, J., Gribnau, J., Barillot, E., Blüthgen, N., Dekker, J. and Heard, E. (2012) 'Spatial partitioning of the regulatory landscape of the X-inactivation centre', *Nature,* 485(7398), pp. 381-5.

Northcott, P. A., Lee, C., Zichner, T., Stütz, A. M., Erkek, S., Kawauchi, D., Shih, D. J., Hovestadt, V., Zapatka, M., Sturm, D., Jones, D. T., Kool, M., Remke, M., Cavalli, F. M., Zuyderduyn, S., Bader, G. D., VandenBerg, S., Esparza, L. A., Ryzhova, M., Wang, W., Wittmann, A., Stark, S., Sieber, L., Seker-Cin, H., Linke, L., Kratochwil, F., Jäger, N., Buchhalter, I., Imbusch, C. D., Zipprich, G., Raeder, B., Schmidt, S., Diessl, N., Wolf, S., Wiemann, S., Brors, B., Lawerenz, C., Eils, J., Warnatz, H. J., Risch, T., Yaspo, M. L., Weber, U. D., Bartholomae, C. C., von Kalle, C., Turányi, E., Hauser, P., Sanden, E., Darabi, A., Siesjö, P., Sterba, J., Zitterbart, K., Sumerauer, D., van Sluis, P., Versteeg, R., Volckmann, R., Koster, J., Schuhmann, M. U., Ebinger, M., Grimes, H. L., Robinson, G. W., Gajjar, A., Mynarek, M., von Hoff, K., Rutkowski, S., Pietsch, T., Scheurlen, W., Felsberg, J., Reifenberger, G., Kulozik, A. E., von Deimling, A., Witt, O., Eils, R., Gilbertson, R. J., Korshunov, A., Taylor, M. D., Lichter, P., Korbel, J. O., Wechsler-Reya, R. J. and Pfister, S. M. (2014) 'Enhancer hijacking activates GFI1 family oncogenes in medulloblastoma', *Nature,* 511(7510), pp. 428-34.

Ogushi, S., Palmieri, C., Fulka, H., Saitou, M., Miyano, T. and Fulka, J. (2008) 'The maternal nucleolus is essential for early embryonic development in mammals', *Science,* 319(5863), pp. 613-6.

OGUSHI, S. and SAITOU, M. (2010) 'The nucleolus in the mouse oocyte is required for the early step of both female and male pronucleus organization', *J Reprod Dev,* 56(5), pp. 495-501.

OHNO, S., KAPLAN, W. D. and KINOSITA, R. (1959) 'Formation of the sex chromatin by a single X-chromosome in liver cells of Rattus norvegicus', *Exp Cell Res,* 18, pp. 415-8.

Okamoto, I., Arnaud, D., Le Baccon, P., Otte, A. P., Disteche, C. M., Avner, P. and Heard, E. (2005) 'Evidence for de novo imprinted X-chromosome inactivation independent of meiotic inactivation in mice', *Nature,* 438(7066), pp. 369-73.

Okamoto, I., Otte, A. P., Allis, C. D., Reinberg, D. and Heard, E. (2004) 'Epigenetic dynamics of imprinted X inactivation during early mouse development', *Science,* 303(5658), pp. 644-9.

Okamoto, I., Patrat, C., Thépot, D., Peynot, N., Fauque, P., Daniel, N., Diabangouaya, P., Wolf, J. P., Renard, J. P., Duranthon, V. and Heard, E. (2011) 'Eutherian mammals use diverse strategies to initiate X-chromosome inactivation during development', *Nature,* 472(7343), pp. 370-4.

Orsztynowicz, M., Lechniak, D., Pawlak, P., Kociucka, B., Kubickova, S., Cernohorska, H. and Madeja, Z. E. (2017) 'Changes in chromosome territory position within the nucleus reflect alternations in gene expression related to embryonic lineage specification', *PLoS One,* 12(8), pp. e0182398.

Palmirotta, R., Verginelli, F., Cama, A., Mariani-Costantini, R., Frati, L. and Battista, P. (1998) 'Origin and gender determination of dried blood on a statue of the Virgin Mary', *J Forensic Sci,* 43(2), pp. 431-4.

Parelho, V., Hadjur, S., Spivakov, M., Leleu, M., Sauer, S., Gregson, H. C., Jarmuz, A., Canzonetta, C., Webster, Z., Nesterova, T., Cobb, B. S., Yokomori, K., Dillon, N., Aragon, L., Fisher, A. G. and Merkenschlager, M. (2008) 'Cohesins functionally associate with CTCF on mammalian chromosome arms', *Cell,* 132(3), pp. 422-33.

Park, S. J., Komata, M., Inoue, F., Yamada, K., Nakai, K., Ohsugi, M. and Shirahige, K. (2013) 'Inferring the choreography of parental genomes during fertilization from ultralarge-scale whole-transcriptome analysis', *Genes Dev,* 27(24), pp. 2736-48.

Patrat, C., Okamoto, I., Diabangouaya, P., Vialon, V., Le Baccon, P., Chow, J. and Heard, E. (2009) 'Dynamic changes in paternal X-chromosome activity during imprinted X-chromosome inactivation in mice', *Proc Natl Acad Sci U S A,* 106(13), pp. 5198-203.

Peaston, A. E., Evsikov, A. V., Graber, J. H., de Vries, W. N., Holbrook, A. E., Solter, D. and Knowles, B. B. (2004) 'Retrotransposons regulate host genes in mouse oocytes and preimplantation embryos', *Dev Cell,* 7(4), pp. 597-606.

Peat, J. R., Dean, W., Clark, S. J., Krueger, F., Smallwood, S. A., Ficz, G., Kim, J. K., Marioni, J. C., Hore, T. A. and Reik, W. (2014) 'Genome-wide bisulfite sequencing in zygotes identifies demethylation targets and maps the contribution of TET3 oxidation', *Cell Rep,* 9(6), pp. 1990-2000.

Petropoulos, S., Edsgärd, D., Reinius, B., Deng, Q., Panula, S. P., Codeluppi, S., Plaza Reyes, A., Linnarsson, S., Sandberg, R. and Lanner, F. (2016) 'Single-Cell RNA-Seq Reveals Lineage and X Chromosome Dynamics in Human Preimplantation Embryos', *Cell,* 165(4), pp. 1012-26.

Phillips, J. E. and Corces, V. G. (2009) 'CTCF: master weaver of the genome', *Cell,* 137(7), pp. 1194-211.

Phillips-Cremins, J. E., Sauria, M. E., Sanyal, A., Gerasimova, T. I., Lajoie, B. R., Bell, J. S., Ong, C. T., Hookway, T. A., Guo, C., Sun, Y., Bland, M. J., Wagstaff, W., Dalton, S., McDevitt, T. C., Sen, R., Dekker, J., Taylor, J. and Corces, V. G. (2013) 'Architectural protein subclasses shape 3D organization of genomes during lineage commitment', *Cell,* 153(6), pp. 1281-95.

Pickersgill, H., Kalverda, B., de Wit, E., Talhout, W., Fornerod, M. and van Steensel, B. (2006) 'Characterization of the Drosophila melanogaster genome at the nuclear lamina', *Nat Genet,* 38(9), pp. 1005-14.

Pikó, L. and Clegg, K. B. (1982) 'Quantitative changes in total RNA, total poly(A), and ribosomes in early mouse embryos', *Dev Biol,* 89(2), pp. 362-78.

Pinheiro, I. and Heard, E. (2017) 'X chromosome inactivation: new players in the initiation of gene silencing', *F1000Res,* 6.

Popken, J., Graf, A., Krebs, S., Blum, H., Schmid, V. J., Strauss, A., Guengoer, T., Zakhartchenko, V., Wolf, E. and Cremer, T. (2015) 'Remodeling of the Nuclear Envelope and Lamina during Bovine Preimplantation Development and Its Functional Implications', *PLoS One,* 10(5), pp. e0124619.

Probst, A. V., Santos, F., Reik, W., Almouzni, G. and Dean, W. (2007) 'Structural differences in centromeric heterochromatin are spatially reconciled on fertilisation in the mouse zygote', *Chromosoma,* 116(4), pp. 403-15.

Pálfy, M., Joseph, S. R. and Vastenhouw, N. L. (2017) 'The timing of zygotic genome activation', *Curr Opin Genet Dev,* 43, pp. 53-60.

, Über die Zelltheilung. .

Ram, P. T. and Schultz, R. M. (1993) 'Reporter gene expression in G2 of the 1-cell mouse embryo', *Dev Biol,* 156(2), pp. 552-6.

Ranisavljevic, N., Okamoto, I., Heard, E. and Ancelin, K. (2017) 'RNA FISH to Study Zygotic Genome Activation in Early Mouse Embryos', *Methods Mol Biol,* 1605, pp. 133-145.

Rao, S. S., Huntley, M. H., Durand, N. C., Stamenova, E. K., Bochkov, I. D., Robinson, J. T., Sanborn, A. L., Machol, I., Omer, A. D., Lander, E. S. and Aiden, E. L. (2014) 'A 3D map of the human genome at kilobase resolution reveals principles of chromatin looping', *Cell,* 159(7), pp. 1665-80.

Rastan, S. (1982) 'Timing of X-chromosome inactivation in postimplantation mouse embryos', *J Embryol Exp Morphol,* 71, pp. 11-24.

Rastan, S. (1983) 'Non-random X-chromosome inactivation in mouse X-autosome translocation embryos--location of the inactivation centre', *J Embryol Exp Morphol,* 78, pp. 1-22.

Rastan, S. and Brown, S. D. (1990) 'The search for the mouse X-chromosome inactivation centre', *Genet Res,* 56(2-3), pp. 99-106.

Rastan, S. and Robertson, E. J. (1985) 'X-chromosome deletions in embryo-derived (EK) cell lines associated with lack of X-chromosome inactivation', *J Embryol Exp Morphol,* 90, pp. 379-88.

Rego, A., Sinclair, P. B., Tao, W., Kireev, I. and Belmont, A. S. (2008) 'The facultative heterochromatin of the inactive X chromosome has a distinctive condensed ultrastructure', *J Cell Sci,* 121(Pt 7), pp. 1119-27.

Ricci, M. A., Cosma, M. P. and Lakadamyali, M. (2017) 'Super resolution imaging of chromatin in pluripotency, differentiation, and reprogramming', *Curr Opin Genet Dev,* 46, pp. 186-193.

Rossant, J. (1976) 'Postimplantation development of blastomeres isolated from 4- and 8-cell mouse eggs', *J Embryol Exp Morphol,* 36(2), pp. 283-90.

Rougier, N., Bourc'his, D., Gomes, D. M., Niveleau, A., Plachot, M., Pàldi, A. and Viegas-Péquignot, E. (1998) 'Chromosome methylation patterns during mammalian preimplantation development', *Genes Dev,* 12(14), pp. 2108-13.

Sagai, T., Hosoya, M., Mizushina, Y., Tamura, M. and Shiroishi, T. (2005) 'Elimination of a long-range cis-regulatory module causes complete loss of limb-specific Shh expression and truncation of the mouse limb', *Development,* 132(4), pp. 797-803.

Santenard, A., Ziegler-Birling, C., Koch, M., Tora, L., Bannister, A. J. and Torres-Padilla, M. E. (2010) 'Heterochromatin formation in the mouse embryo requires critical residues of the histone variant H3.3', *Nat Cell Biol,* 12(9), pp. 853-62.

Schmitt, A. D., Hu, M., Jung, I., Xu, Z., Qiu, Y., Tan, C. L., Li, Y., Lin, S., Lin, Y., Barr, C. L. and Ren, B. (2016a) 'A Compendium of Chromatin Contact Maps Reveals Spatially Active Regions in the Human Genome', *Cell Rep,* 17(8), pp. 2042-2059.

Schmitt, A. D., Hu, M. and Ren, B. (2016b) 'Genome-wide mapping and analysis of chromosome architecture', *Nat Rev Mol Cell Biol,* 17(12), pp. 743-755.

Sexton, T., Yaffe, E., Kenigsberg, E., Bantignies, F., Leblanc, B., Hoichman, M., Parrinello, H., Tanay, A. and Cavalli, G. (2012) 'Three-dimensional folding and functional organization principles of the Drosophila genome', *Cell,* 148(3), pp. 458-72.

Shen, L., Inoue, A., He, J., Liu, Y., Lu, F. and Zhang, Y. (2014) 'Tet3 and DNA replication mediate demethylation of both the maternal and paternal genomes in mouse zygotes', *Cell Stem Cell,* 15(4), pp. 459-471.

Simon, M. D., Pinter, S. F., Fang, R., Sarma, K., Rutenberg-Schoenberg, M., Bowman, S. K., Kesner, B. A., Maier, V. K., Kingston, R. E. and Lee, J. T. (2013) 'High-resolution Xist binding maps reveal two-step spreading during X-chromosome inactivation', *Nature,* 504(7480), pp. 465-469.

Smeets, D., Markaki, Y., Schmid, V. J., Kraus, F., Tattermusch, A., Cerase, A., Sterr, M., Fiedler, S., Demmerle, J., Popken, J., Leonhardt, H., Brockdorff, N., Cremer, T., Schermelleh, L. and Cremer, M. (2014) 'Three-dimensional super-resolution microscopy of the inactive X chromosome territory reveals a collapse of its active nuclear compartment harboring distinct Xist RNA foci', *Epigenetics Chromatin,* 7, pp. 8.

Spitz, F., Gonzalez, F. and Duboule, D. (2003) 'A global control region defines a chromosomal regulatory landscape containing the HoxD cluster', *Cell,* 113(3), pp. 405-17.

Splinter, E., de Wit, E., Nora, E. P., Klous, P., van de Werken, H. J., Zhu, Y., Kaaij, L. J., van Ijcken, W., Gribnau, J., Heard, E. and de Laat, W. (2011) 'The inactive X chromosome adopts a unique three-dimensional conformation that is dependent on Xist RNA', *Genes Dev,* 25(13), pp. 1371-83.

Stamatoyannopoulos, J. A., Snyder, M., Hardison, R., Ren, B., Gingeras, T., Gilbert, D. M., Groudine, M., Bender, M., Kaul, R., Canfield, T., Giste, E., Johnson, A., Zhang, M., Balasundaram, G., Byron, R., Roach, V., Sabo, P. J., Sandstrom, R., Stehling, A. S., Thurman, R. E., Weissman, S. M., Cayting, P., Hariharan, M., Lian, J., Cheng, Y., Landt, S. G., Ma, Z., Wold, B. J., Dekker, J., Crawford, G. E., Keller, C. A., Wu, W., Morrissey, C., Kumar, S. A., Mishra, T., Jain, D., Byrska-Bishop, M., Blankenberg, D., Lajoie, B. R., Jain, G., Sanyal, A., Chen, K. B., Denas, O., Taylor, J., Blobel, G. A., Weiss, M. J., Pimkin, M., Deng, W., Marinov, G. K., Williams, B. A., Fisher-Aylor, K. I., Desalvo, G., Kiralusha, A., Trout, D., Amrhein, H., Mortazavi, A., Edsall, L., McCleary, D., Kuan, S., Shen, Y., Yue, F., Ye, Z., Davis, C. A., Zaleski, C., Jha, S., Xue, C., Dobin, A., Lin, W., Fastuca, M., Wang, H., Guigo, R., Djebali, S., Lagarde, J., Ryba, T., Sasaki, T., Malladi, V. S., Cline, M. S., Kirkup, V. M., Learned, K., Rosenbloom, K. R., Kent, W. J., Feingold, E. A., Good, P. J., Pazin, M., Lowdon, R. F., Adams, L. B. and Consortium, M. E. (2012) 'An encyclopedia of mouse DNA elements (Mouse ENCODE)', *Genome Biol,* 13(8), pp. 418.

Stergachis, A. B., Neph, S., Reynolds, A., Humbert, R., Miller, B., Paige, S. L., Vernot, B., Cheng, J. B., Thurman, R. E., Sandstrom, R., Haugen, E., Heimfeld, S., Murry, C. E.,

Akey, J. M. and Stamatoyannopoulos, J. A. (2013) 'Developmental fate and cellular maturity encoded in human regulatory DNA landscapes', *Cell,* 154(4), pp. 888-903.

Stevens, T. J., Lando, D., Basu, S., Atkinson, L. P., Cao, Y., Lee, S. F., Leeb, M., Wohlfahrt, K. J., Boucher, W., O'Shaughnessy-Kirwan, A., Cramard, J., Faure, A. J., Ralser, M., Blanco, E., Morey, L., Sansó, M., Palayret, M. G. S., Lehner, B., Di Croce, L., Wutz, A., Hendrich, B., Klenerman, D. and Laue, E. D. (2017) '3D structures of individual mammalian genomes studied by single-cell Hi-C', *Nature,* 544(7648), pp. 59-64.

Storfer-Glazer, F. A. and Wood, W. B. (1994) 'Effects of chromosomal deficiencies on early cleavage patterning and terminal phenotype in Caenorhabditis elegans embryos', *Genetics,* 137(2), pp. 499-508.

Straub, T., Grimaud, C., Gilfillan, G. D., Mitterweger, A. and Becker, P. B. (2008) 'The chromosomal high-affinity binding sites for the Drosophila dosage compensation complex', *PLoS Genet,* 4(12), pp. e1000302.

Sun, S., Payer, B., Namekawa, S., An, J. Y., Press, W., Catalan-Dibene, J., Sunwoo, H. and Lee, J. T. (2015) 'Xist imprinting is promoted by the hemizygous (unpaired) state in the male germ line', *Proc Natl Acad Sci U S A,* 112(47), pp. 14415-22.

Symmons, O., Pan, L., Remeseiro, S., Aktas, T., Klein, F., Huber, W. and Spitz, F. (2016) 'The Shh Topological Domain Facilitates the Action of Remote Enhancers by Reducing the Effects of Genomic Distances', *Dev Cell,* 39(5), pp. 529-543.

Symmons, O., Uslu, V. V., Tsujimura, T., Ruf, S., Nassari, S., Schwarzer, W., Ettwiller, L. and Spitz, F. (2014) 'Functional and topological characteristics of mammalian regulatory domains', *Genome Res,* 24(3), pp. 390-400.

Tachibana, M., Ma, H., Sparman, M. L., Lee, H. S., Ramsey, C. M., Woodward, J. S., Sritanaudomchai, H., Masterson, K. R., Wolff, E. E., Jia, Y. and Mitalipov, S. M. (2012) 'X-chromosome inactivation in monkey embryos and pluripotent stem cells', *Dev Biol,* 371(2), pp. 146-55.

Tada, T., Obata, Y., Tada, M., Goto, Y., Nakatsuji, N., Tan, S., Kono, T. and Takagi, N. (2000) 'Imprint switching for non-random X-chromosome inactivation during mouse oocyte growth', *Development,* 127(14), pp. 3101-5.

Tadros, W. and Lipshitz, H. D. (2009) 'The maternal-to-zygotic transition: a play in two acts', *Development,* 136(18), pp. 3033-42.

Takagi, N. and Abe, K. (1990) 'Detrimental effects of two active X chromosomes on early mouse development', *Development,* 109(1), pp. 189-201.

Takagi, N. and Sasaki, M. (1975) 'Preferential inactivation of the paternally derived X chromosome in the extraembryonic membranes of the mouse', *Nature,* 256(5519), pp. 640-2.

Takagi, N., Sugawara, O. and Sasaki, M. (1982) 'Regional and temporal changes in the pattern of X-chromosome replication during the early post-implantation development of the female mouse', *Chromosoma,* 85(2), pp. 275-86.

Takizawa, T., Meaburn, K. J. and Misteli, T. (2008) 'The meaning of gene positioning', *Cell,* 135(1), pp. 9-13.

Tang, F., Barbacioru, C., Wang, Y., Nordman, E., Lee, C., Xu, N., Wang, X., Bodeau, J., Tuch, B. B., Siddiqui, A., Lao, K. and Surani, M. A. (2009) 'mRNA-Seq whole-transcriptome analysis of a single cell', *Nat Methods,* 6(5), pp. 377-82.

TARKOWSKI, A. K. (1959) 'Experiments on the development of isolated blastomers of mouse eggs', *Nature,* 184, pp. 1286-7.

Teklenburg, G., Weimar, C. H., Fauser, B. C., Macklon, N., Geijsen, N., Heijnen, C. J., Chuva de Sousa Lopes, S. M. and Kuijk, E. W. (2012) 'Cell lineage specific distribution of H3K27 trimethylation accumulation in an in vitro model for human implantation', *PLoS One,* 7(3), pp. e32701.

Tong, Z. B., Gold, L., Pfeifer, K. E., Dorward, H., Lee, E., Bondy, C. A., Dean, J. and Nelson, L. M. (2000) 'Mater, a maternal effect gene required for early embryonic development in mice', *Nat Genet,* 26(3), pp. 267-8.

Torres-Padilla, M. E. and Zernicka-Goetz, M. (2006) 'Role of TIF1alpha as a modulator of embryonic transcription in the mouse zygote', *J Cell Biol,* 174(3), pp. 329-38.

Tsujimura, T., Klein, F. A., Langenfeld, K., Glaser, J., Huber, W. and Spitz, F. (2015) 'A discrete transition zone organizes the topological and regulatory autonomy of the adjacent tfap2c and bmp7 genes', *PLoS Genet,* 11(1), pp. e1004897.

Tukiainen, T., Villani, A. C., Yen, A., Rivas, M. A., Marshall, J. L., Satija, R., Aguirre, M., Gauthier, L., Fleharty, M., Kirby, A., Cummings, B. B., Castel, S. E., Karczewski, K. J., Aguet, F., Byrnes, A., Lappalainen, T., Regev, A., Ardlie, K. G., Hacohen, N., MacArthur, D. G., Consortium, G., Laboratory, D. t. A. C. C. L. A. W. G., Group, S. M. g. A. W., groups, E. G. e., Fund, N. C., NIH/NCI, NIH/NHGRI, NIH/NIMH, NIH/NIDA, Site—NDRI, B. C. S., Site—RPCI, B. C. S., Resource—VARI, B. C., Bank, B. B. R. U. o. M. B. E., Management, L. B. P., Study, E., &Visualization—EBI, G. B. D. I. and Genome Browser Data Integration &Visualization—UCSC Genomics Institute, U. i. o. C. S. C. (2017) 'Landscape of X chromosome inactivation across human tissues', *Nature,* 550(7675), pp. 244-248.

Uh, K. and Lee, K. (2017) 'Use of Chemicals to Inhibit DNA Replication, Transcription, and Protein Synthesis to Study Zygotic Genome Activation', *Methods Mol Biol,* 1605, pp. 191-205.

Ulianov, S. V., Tachibana-Konwalski, K. and Razin, S. V. (2017) 'Single-cell Hi-C bridges microscopy and genome-wide sequencing approaches to study 3D chromatin organization', *Bioessays,* 39(10).

Ulitsky, I., Shkumatava, A., Jan, C. H., Subtelny, A. O., Koppstein, D., Bell, G. W., Sive, H. and Bartel, D. P. (2012) 'Extensive alternative polyadenylation during zebrafish development', *Genome Res,* 22(10), pp. 2054-66.

Valton, A. L. and Dekker, J. (2016) 'TAD disruption as oncogenic driver', *Curr Opin Genet Dev,* 36, pp. 34-40.

Van de Vosse, D. W., Wan, Y., Wozniak, R. W. and Aitchison, J. D. (2011) 'Role of the nuclear envelope in genome organization and gene expression', *Wiley Interdiscip Rev Syst Biol Med,* 3(2), pp. 147-66.

van Steensel, B. and Belmont, A. S. (2017) 'Lamina-Associated Domains: Links with Chromosome Architecture, Heterochromatin, and Gene Repression', *Cell,* 169(5), pp. 780-791.

van Steensel, B. and Henikoff, S. (2000) 'Identification of in vivo DNA targets of chromatin proteins using tethered dam methyltransferase', *Nat Biotechnol,* 18(4), pp. 424-8.

Vicente-García, C., Villarejo-Balcells, B., Irastorza-Azcárate, I., Naranjo, S., Acemel, R. D., Tena, J. J., Rigby, P. W. J., Devos, D. P., Gómez-Skarmeta, J. L. and Carvajal, J. J. (2017) 'Regulatory landscape fusion in rhabdomyosarcoma through interactions between the PAX3 promoter and FOXO1 regulatory elements', *Genome Biol,* 18(1), pp. 106.

Wan, L. B., Pan, H., Hannenhalli, S., Cheng, Y., Ma, J., Fedoriw, A., Lobanenkov, V., Latham, K. E., Schultz, R. M. and Bartolomei, M. S. (2008) 'Maternal depletion of CTCF reveals multiple functions during oocyte and preimplantation embryo development', *Development,* 135(16), pp. 2729-38.

Wang, F., Shin, J., Shea, J. M., Yu, J., Bošković, A., Byron, M., Zhu, X., Shalek, A. K., Regev, A., Lawrence, J. B., Torres, E. M., Zhu, L. J., Rando, O. J. and Bach, I. (2016a) 'Regulation of X-linked gene expression during early mouse development by Rlim', *Elife,* 5.

Wang, H. and Dey, S. K. (2006) 'Roadmap to embryo implantation: clues from mouse models', *Nat Rev Genet,* 7(3), pp. 185-99.

Wang, J., Mager, J., Chen, Y., Schneider, E., Cross, J. C., Nagy, A. and Magnuson, T. (2001) 'Imprinted X inactivation maintained by a mouse Polycomb group gene', *Nat Genet,* 28(4), pp. 371-5.

Wang, L., Zhang, J., Duan, J., Gao, X., Zhu, W., Lu, X., Yang, L., Li, G., Ci, W., Li, W., Zhou, Q., Aluru, N., Tang, F., He, C., Huang, X. and Liu, J. (2014) 'Programming and inheritance of parental DNA methylomes in mammals', *Cell,* 157(4), pp. 979-991.

Wang, S., Su, J. H., Beliveau, B. J., Bintu, B., Moffitt, J. R., Wu, C. T. and Zhuang, X. (2016b) 'Spatial organization of chromatin domains and compartments in single chromosomes', *Science,* 353(6299), pp. 598-602.

Wang, X., Miller, D. C., Clark, A. G. and Antczak, D. F. (2012) 'Random X inactivation in the mule and horse placenta', *Genome Res,* 22(10), pp. 1855-63.

Warner, C. M. and Versteegh, L. R. (1974) 'In vivo and in vitro effect of alpha-amanitin on preimplantation mouse embryo RNA polymerase', *Nature,* 248(5450), pp. 678-80.

Waterston, R. H. and Lindblad-Toh, K. and Birney, E. and Rogers, J. and Abril, J. F. and Agarwal, P. and Agarwala, R. and Ainscough, R. and Alexandersson, M. and An, P. and Antonarakis, S. E. and Attwood, J. and Baertsch, R. and Bailey, J. and Barlow, K. and Beck, S. and Berry, E. and Birren, B. and Bloom, T. and Bork, P. and Botcherby, M. and Bray, N. and Brent, M. R. and Brown, D. G. and Brown, S. D. and Bult, C. and Burton, J. and Butler, J. and Campbell, R. D. and Carninci, P. and Cawley, S. and Chiaromonte, F. and Chinwalla, A. T. and Church, D. M. and Clamp, M. and Clee, C. and Collins, F. S. and Cook, L. L. and Copley, R. R. and Coulson, A. and Couronne, O. and Cuff, J. and Curwen, V. and Cutts, T. and Daly, M. and David, R. and Davies, J. and Delehaunty, K. D. and Deri, J. and Dermitzakis, E. T. and Dewey, C. and Dickens, N. J. and Diekhans, M. and Dodge, S. and Dubchak, I. and Dunn, D. M. and Eddy, S. R. and Elnitski, L. and Emes, R. D. and Eswara, P. and Eyras, E. and Felsenfeld, A. and Fewell, G. A. and Flicek, P. and Foley, K. and

Frankel, W. N. and Fulton, L. A. and Fulton, R. S. and Furey, T. S. and Gage, D. and Gibbs, R. A. and Glusman, G. and Gnerre, S. and Goldman, N. and Goodstadt, L. and Grafham, D. and Graves, T. A. and Green, E. D. and Gregory, S. and Guigó, R. and Guyer, M. and Hardison, R. C. and Haussler, D. and Hayashizaki, Y. and Hillier, L. W. and Hinrichs, A. and Hlavina, W. and Holzer, T. and Hsu, F. and Hua, A. and Hubbard, T. and Hunt, A. and Jackson, I. and Jaffe, D. B. and Johnson, L. S. and Jones, M. and Jones, T. A. and Joy, A. and Kamal, M. and Karlsson, E. K. and Karolchik, D. and Kasprzyk, A. and Kawai, J. and Keibler, E. and Kells, C. and Kent, W. J. and Kirby, A. and Kolbe, D. L. and Korf, I. and Kucherlapati, R. S. and Kulbokas, E. J. and Kulp, D. and Landers, T. and Leger, J. P. and Leonard, S. and Letunic, I. and Levine, R. and Li, J. and Li, M. and Lloyd, C. and Lucas, S. and Ma, B. and Maglott, D. R. and Mardis, E. R. and Matthews, L. and Mauceli, E. and Mayer, J. H. and McCarthy, M. and McCombie, W. R. and McLaren, S. and McLay, K. and McPherson, J. D. and Meldrim, J. and Meredith, B. and Mesirov, J. P. and Miller, W. and Miner, T. L. and Mongin, E. and Montgomery, K. T. and Morgan, M. and Mott, R. and Mullikin, J. C. and Muzny, D. M. and Nash, W. E. and Nelson, J. O. and Nhan, M. N. and Nicol, R. and Ning, Z. and Nusbaum, C. and O'Connor, M. J. and Okazaki, Y. and Oliver, K. and Overton-Larty, E. and Pachter, L. and Parra, G. and Pepin, K. H. and Peterson, J. and Pevzner, P. and Plumb, R. and Pohl, C. S. and Poliakov, A. and Ponce, T. C. and Ponting, C. P. and Potter, S. and Quail, M. and Reymond, A. and Roe, B. A. and Roskin, K. M. and Rubin, E. M. and Rust, A. G. and Santos, R. and Sapojnikov, V. and Schultz, B. and Schultz, J. and Schwartz, M. S. and Schwartz, S. and Scott, C. and Seaman, S. and Searle, S. and Sharpe, T. and Sheridan, A. and Shownkeen, R. and Sims, S. and Singer, J. B. and Slater, G. and Smit, A. and Smith, D. R. and Spencer, B. and Stabenau, A. and Stange-Thomann, N. and Sugnet, C. and Suyama, M. and Tesler, G. and Thompson, J. and Torrents, D. and Trevaskis, E. and Tromp, J. and Ucla, C. and Ureta-Vidal, A. and Vinson, J. P. and Von Niederhausern, A. C. and Wade, C. M. and Wall, M. and Weber, R. J. and Weiss, R. B. and Wendl, M. C. and West, A. P. and Wetterstrand, K. and Wheeler, R. and Whelan, S. and Wierzbowski, J. and Willey, D. and Williams, S. and Wilson, R. K. and Winter, E. and Worley, K. C. and Wyman, D. and Yang, S. and Yang, S. P. and Zdobnov, E. M. and Zody, M. C. and Lander, E. S. and Consortium, M. G. S. (2002) 'Initial sequencing and comparative analysis of the mouse genome', *Nature,* 420(6915), pp. 520-62.

Weischenfeldt, J., Dubash, T., Drainas, A. P., Mardin, B. R., Chen, Y., Stütz, A. M., Waszak, S. M., Bosco, G., Halvorsen, A. R., Raeder, B., Efthymiopoulos, T., Erkek, S., Siegl, C., Brenner, H., Brustugun, O. T., Dieter, S. M., Northcott, P. A., Petersen, I., Pfister, S. M., Schneider, M., Solberg, S. K., Thunissen, E., Weichert, W., Zichner, T., Thomas, R., Peifer, M., Helland, A., Ball, C. R., Jechlinger, M., Sotillo, R., Glimm, H. and Korbel, J. O. (2017) 'Pan-cancer analysis of somatic copy-number alterations implicates IRS4 and IGF2 in enhancer hijacking', *Nat Genet,* 49(1), pp. 65-74.

West, J. D., Frels, W. I., Chapman, V. M. and Papaioannou, V. E. (1977) 'Preferential expression of the maternally derived X chromosome in the mouse yolk sac', *Cell,* 12(4), pp. 873-82.

Whiddon, J. L., Langford, A. T., Wong, C. J., Zhong, J. W. and Tapscott, S. J. (2017) 'Conservation and innovation in the DUX4-family gene network', *Nat Genet,* 49(6), pp. 935-940.

Wiekowski, M., Miranda, M. and DePamphilis, M. L. (1991) 'Regulation of gene expression in preimplantation mouse embryos: effects of the zygotic clock and the first mitosis on promoter and enhancer activities', *Dev Biol,* 147(2), pp. 403-14.

Wiellette, E. L., Harding, K. W., Mace, K. A., Ronshaugen, M. R., Wang, F. Y. and McGinnis, W. (1999) 'spen encodes an RNP motif protein that interacts with Hox pathways to repress the development of head-like sclerites in the Drosophila trunk', *Development,* 126(23), pp. 5373-85.

Williamson, I., Berlivet, S., Eskeland, R., Boyle, S., Illingworth, R. S., Paquette, D., Dostie, J. and Bickmore, W. A. (2014) 'Spatial genome organization: contrasting views from chromosome conformation capture and fluorescence in situ hybridization', *Genes Dev,* 28(24), pp. 2778-91.

Woltering, J. M., Noordermeer, D., Leleu, M. and Duboule, D. (2014) 'Conservation and divergence of regulatory strategies at Hox Loci and the origin of tetrapod digits', *PLoS Biol,* 12(1), pp. e1001773.

Wu, J., Huang, B., Chen, H., Yin, Q., Liu, Y., Xiang, Y., Zhang, B., Liu, B., Wang, Q., Xia, W., Li, W., Li, Y., Ma, J., Peng, X., Zheng, H., Ming, J., Zhang, W., Zhang, J., Tian, G., Xu, F., Chang, Z., Na, J., Yang, X. and Xie, W. (2016) 'The landscape of accessible chromatin in mammalian preimplantation embryos', *Nature,* 534(7609), pp. 652-7.

Wutz, A. and Jaenisch, R. (2000) 'A shift from reversible to irreversible X inactivation is triggered during ES cell differentiation', *Mol Cell,* 5(4), pp. 695-705.

Wutz, A., Rasmussen, T. P. and Jaenisch, R. (2002) 'Chromosomal silencing and localization are mediated by different domains of Xist RNA', *Nat Genet,* 30(2), pp. 167-74.

Xue, F., Tian, X. C., Du, F., Kubota, C., Taneja, M., Dinnyes, A., Dai, Y., Levine, H., Pereira, L. V. and Yang, X. (2002) 'Aberrant patterns of X chromosome inactivation in bovine clones', *Nat Genet,* 31(2), pp. 216-20.

Xue, Z., Huang, K., Cai, C., Cai, L., Jiang, C. Y., Feng, Y., Liu, Z., Zeng, Q., Cheng, L., Sun, Y. E., Liu, J. Y., Horvath, S. and Fan, G. (2013) 'Genetic programs in human and mouse early embryos revealed by single-cell RNA sequencing', *Nature,* 500(7464), pp. 593-7.

Yang, F., Babak, T., Shendure, J. and Disteche, C. M. (2010) 'Global survey of escape from X inactivation by RNA-sequencing in mouse', *Genome Res,* 20(5), pp. 614-22.

Yu, C., Ji, S. Y., Sha, Q. Q., Dang, Y., Zhou, J. J., Zhang, Y. L., Liu, Y., Wang, Z. W., Hu, B., Sun, Q. Y., Sun, S. C., Tang, F. and Fan, H. Y. (2016) 'BTG4 is a meiotic cell cycle-coupled maternal-zygotic-transition licensing factor in oocytes', *Nat Struct Mol Biol,* 23(5), pp. 387-94.

Zaret, K. S. and Mango, S. E. (2016) 'Pioneer transcription factors, chromatin dynamics, and cell fate control', *Curr Opin Genet Dev,* 37, pp. 76-81.

Zeng, F., Baldwin, D. A. and Schultz, R. M. (2004) 'Transcript profiling during preimplantation mouse development', *Dev Biol,* 272(2), pp. 483-96.

Zeng, F. and Schultz, R. M. (2003) 'Gene expression in mouse oocytes and preimplantation embryos: use of suppression subtractive hybridization to identify oocyte- and embryo-specific genes', *Biol Reprod,* 68(1), pp. 31-9.

Zhan, Y., Mariani, L., Barozzi, I., Schulz, E. G., Blüthgen, N., Stadler, M., Tiana, G. and Giorgetti, L. (2017) 'Reciprocal insulation analysis of Hi-C data shows that TADs represent a functionally but not structurally privileged scale in the hierarchical folding of chromosomes', *Genome Res,* 27(3), pp. 479-490.

Zhang, B., Zheng, H., Huang, B., Li, W., Xiang, Y., Peng, X., Ming, J., Wu, X., Zhang, Y., Xu, Q., Liu, W., Kou, X., Zhao, Y., He, W., Li, C., Chen, B., Li, Y., Wang, Q., Ma, J., Yin, Q., Kee, K., Meng, A., Gao, S., Xu, F., Na, J. and Xie, W. (2016) 'Allelic reprogramming of the histone modification H3K4me3 in early mammalian development', *Nature,* 537(7621), pp. 553-557.

Zhang, L. F., Huynh, K. D. and Lee, J. T. (2007) 'Perinucleolar targeting of the inactive X during S phase: evidence for a role in the maintenance of silencing', *Cell,* 129(4), pp. 693-706.

Zheng, H., Huang, B., Zhang, B., Xiang, Y., Du, Z., Xu, Q., Li, Y., Wang, Q., Ma, J., Peng, X., Xu, F. and Xie, W. (2016) 'Resetting Epigenetic Memory by Reprogramming of Histone Modifications in Mammals', *Mol Cell,* 63(6), pp. 1066-79.

Zuccotti, M., Boiani, M., Ponce, R., Guizzardi, S., Scandroglio, R., Garagna, S. and Redi, C. A. (2002) 'Mouse Xist expression begins at zygotic genome activation and is timed by a zygotic clock', *Mol Reprod Dev,* 61(1), pp. 14-20.

Zuin, J., Dixon, J. R., van der Reijden, M. I., Ye, Z., Kolovos, P., Brouwer, R. W., van de Corput, M. P., van de Werken, H. J., Knoch, T. A., van IJcken, W. F., Grosveld, F. G., Ren, B. and Wendt, K. S. (2014) 'Cohesin and CTCF differentially affect chromatin architecture and gene expression in human cells', *Proc Natl Acad Sci U S A,* 111(3), pp. 996-1001.

université PARIS-SACLAY | ÉCOLE DOCTORALE Structure et dynamique des systèmes vivants (SDSV)

Title: Description de l'architecture du chromosome X pendant le développement préimplantatoire de souris

Mots-clés: Inactivation du chromosome X, conformation chromosomique, embryon preimplantatoire, HiC sur cellule unique

Résumé: La structure tridimensionnelle du génome semble avoir un rôle important dans la régulation de l'expression des gènes. Récemment, l'essor de nouvelles et nombreuses techniques permettant de capturer et séquencer les interactions entre différentes régions du génome (voire du génome entier) a révolutionné notre vision de l'organisation du génome. Plusieurs niveaux d'organisation ont été décrits et plus particulièrement les TADs (Topologically Associating Domains) à l'échelle du mégabase. Ces derniers représentent des domaines d'interactions préférentielles au sein du chromosome à l'échelle du mégabase et pourraient opérer en tant qu'unité régulatrice de l'expression des gènes contenus dans ces domaines. Bien qu'ils soient très conservés, par exemple entre l'homme et la souris, mais également au cours de la différentiation, des modifications majeures de conformation ont lieu lors de certains évènements tels que l'inactivation du chromosome X. Ce phénomène épigénétique permet la compensation de dose chez les femelles mammifères, où l'un des deux chromosomes X est rendu silencieux. La structure du X inactif est extrêmement différente de celle du X actif avec une perte globale de la structure locale en TADs et la formation de deux larges domaines, appelés mégadomaines. L'objectif de ma thèse a été d'explorer l'architecture du génome après la fécondation, et plus particulièrement la structure du chromosome X, au moment où l'embryon nouvellement formé reprogramme sa chromatine, devient totipotent et active son propre génome. Chez la souris, cette réorganisation structurelle et fonctionnelle coïncide avec l'inactivation soumise à l'empreinte du chromosome X chez les femelles. Grâce à deux techniques complémentaires, le DNA FISH 3D avec imagerie à haute résolution et le HiC sur cellule unique et allèle-spécifique, j'ai décrit la dynamique de la ré-organisation du génome en embryon pré implantatoire, à cette période d'activation du génome embryonnaire. Par ailleurs, j'ai caractérisé les changements de structure du chromosome X paternel au cours de son inactivation. Cette étude détaille la dynamique spatio-temporelle du génome, et plus spécifiquement du chromosome X au cours de son inactivation, dans l'embryon précoce et élargit ainsi notre compréhension du lien entre la structure et la régulation transcriptionnelle au cours des premières étapes du développement embryonnaire suivant la fécondation.

Title: Deciphering X chromosome architecture during mouse preimplantation development

Keywords: X chromosome inactivation, chromosome conformation, preimplantation embryo, single cell HiC

Abstract: 3D folding of the genome is thought to play an important role in gene regulation. Recently, a new era in our understanding of genome organization has been opened up thanks to the plethora of new techniques enabling interactions between loci to be captured and sequenced in depth. Several layers of chromosome organization have been identified. In particular topologically associating domains (TADs) have been uncovered as a level of folding at the megabase scale. TADs represent preferential cis-interactions within domains across chromosomes and are thought to sometimes operate as regulatory units in coordinating gene expression. Although TADs are largely constant during cellular differentiation and are conserved between man and mouse, drastic changes in conformation can occur in some biological processes such as X-chromosome inactivation (XCI). XCI achieves dosage compensation in mammalian females, be rendering one X chromosome silent. The conformation of the inactive X is strikingly different from its active counterpart: with a global loss of local structure and formation of two large domains. The aim of my PhD was to explore genome architecture - and more specifically X-chromosome structure after fertilization - when the newly formed embryo reprograms its chromatin toward totipotency, and activates its own genome. In mouse, this structural and functional reorganization coincides with the onset of imprinted XCI in female embryos. Using two complementary techniques, 3D DNA FISH with super resolution microscopy and allele-specific, single-cell HiC, I examined the dynamics of genome reorganization in mouse pre-implantation embryos during and after genome activation. I also characterized the structural changes of the paternal X chromosome while it is inactivated. This study describes the conformation dynamics of the genome in the early embryo and in particular of the X chromosome as it undergoes XCI, thus contributing to our understanding of the intricate interplay between structure and function at the onset of development.